LRRK2 Mutations in Parkinson's disease: The Role in Autophagy and Lysosomal Function

Orientador – Doctor Richard Wade-Martins

Categoria – Professor Catedrático

Afiliação – Oxford Parkinson's Disease Centre, University of Oxford

Coorientador – Doutor Jorge Azevedo

Categoria – Professor Catedrático

Afiliação – Instituto de Ciências Biomédicas Abel Salazar, Universidade do Porto

MARTA NEVES MADUREIRA

Tese de Candidatura ao grau de Doutor em Biologia Básica e Aplicada submetida ao Instituto de Ciências Biomédicas Abel Salazar da Universidade do Porto.

Publications and Conference Presentations

Williamson MG*, **Madureira M***, McGuinness W, Heon-Roberts R, Mock ED, Naidoo K, Cramb KML, Caiazza MC, Malpartida AB, Lavelle M, Savory K, Humble SW, Patterson R, Davis JB, Connor-Robson N, Ryan BJ, Wade-Martins R. Mitochondrial dysfunction and mitophagy defects in LRRK2-R1441C Parkinson's disease models. *Hum Mol Genet.* 2023 Sep 5;32(18):2808-2821. doi: 10.1093/hmg/ddad102. PMID: 37384414; PMCID: PMC10481106.

Madureira M, Connor-Robson N, Wade-Martins R. "LRRK2: Autophagy and Lysosomal Activity". *Front Neurosci*. 2020 May 25;14:498. doi: 10.3389/fnins.2020.00498.

Almeida AC, Drpic D, Okada N, Bravo J, **Madureira M**, Maiato H. Functional Dissection of Mitosis Using Immortalized Fibroblasts from the Indian Muntjac, a Placental Mammal with Only Three Chromosomes. Methods Mol Biol. 2020;2101:247-266. doi: 10.1007/978-1-0716-0219-5_16.

* - Shared first co-authorship

Selected for Talk - **AD/PD Conference 2022. Barcelona, Spain (March 2022)**

“LRRK2 in Parkinson’s Disease: the role in lysosomal and mitochondrial function”, on the “*Glucocerebrosidase, LRRK2-PD and Alpha-synuclein*” Panel.

Selected for Poster Talk **– EMBO Workshop Autophagy 2019: From Molecular Principles to Human Diseases. Scotland, UK (August 2019)**

“LRRK2 and vATPase a1 interaction in Parkinson’s Disease: the role in lysosomal function”

This work was supported by a Ph.D. scholarship awarded to Marta Neves Madureira by Fundação para a Ciência e Tecnologia (FCT, Portugal) throughout the Graduate Program in Areas of Basic and Applied Biology (GABBA), Universidade do Porto, Portugal. The research conducted at the Wade-Martins laboratory (University of Oxford) was funded by the Monument Trust Discovery Award from Parkinson's United Kingdom (Grant J-1403), the Michael J. Fox Foundation and MRC Dementias Platform UK Stem Cell Network equipment grant (MC_EX_MR/N50192X/1).

Acknowledgements

This journey to achieve a doctoral degree has been as rewarding as it has been difficult. There are many people involved in this massive phase of my life and I want to thank you all for supporting me, sparing words of encouragement and also telling me off when I needed to!

To my supervisor Prof Richard Wade-Martins, thank you for offering me the opportunity to carry out lab work necessary for my research project. I have learned so much from you and from all the wonderful colleagues at the Wade-Martins group. Oxford provided an exciting work environment, with all the equipment I could dream of and then some! I can remember many highlights from seminars and departmental talks, which all enriched my experience. I also want to thank you for financially supporting my PhD, I can only hope I have managed to be a good student and colleague in return!

To my co-supervisor Prof Jorge Azevedo, thank you so much for your support throughout the years and for always making yourself available for any questions I might have had. It has been very valuable to me to have a healthy relationship with you and therefore, the University of Porto.

Thank you to Fundacao para a Ciencia e Tecnologia for funding my PhD and for providing me the opportunity to achieve this, travel to conferences and become a better researcher.

To Natalie, thank you for guiding me through the first years of my PhD and making sure I gained more confidence and knowledge as the weeks went by. I will take all the sage advice I have received with me, which certainly made me more resilient for whatever the future holds. I will fondly remember our Zoom meetings over lockdown, and of course your continued support even from Cardiff. On a more personal note, thank you for being supportive in the more desperate times and for celebrating the small successes. It has meant the world. To Becky, my cutie patootie, you have taught me so much and it is a joy to still have you in my life, even separated by a whole ocean! Thank you for allowing me to listen to T-Pain in labs, I feel like it was at times as needed as any other lab reagent ahah. You are the reason why I became so interested in LRRK2.

To my GABBA family, we met in a cold rainy December in 2016 and I have since held each of you in my heart. Anaisa, Ana Maria, Catarina, Filipa, Joana, Manuel, Maria Ines and Silvia, what a great pleasure it was to immerse myself in science discussions and often late nights finishing up project ideas and presentations with you all. We went to battle together and came out stronger and sharper for it! Organising a Symposium with you all has been

one of the biggest challenges of this Program, and it perfectly showcased all our strengths. We surely put on a show!

To my Wade-Martins colleagues and fellow PhD students Bryan, Pete, Quyen and Billy, and my gals Maria-Claudia, Naroa, Rachel and Fe, thank you for the many drinks at the pub, sharing our frustrations with growing neurons and dealing with so many problems at once. I truly believe it was all meant to prepare us for the big challenges of life, with more grace and ease. Thank you to the “non-students” Nora, Pip, Ben, Kalina, Sandor, Martha, Charmaine, Dayne, Siv, Saba, Milena, Gabriele, Gabi, Mel, Deepak, Sarah Pierce and Lorraine. Matt, my duuude, thanks for all the pub lunches, many delicious restaurant-quality meals over at yours and of course the birth of our paper. I am fully aware I owe my PhD partly to the fruits of your labour as well. Brent, thank you for letting me vent my frustrations with data and for always having good advice that drove me to do better. I will miss your epic Easter egg hunts, your wonderful sense of humour and Christmas playlists (I still think Fairytale of New York doesn’t gather the requisites necessary to be a Christmas song ahah).

I would like to thank all my Portuguese friends for all the support and comraderie Ana, Goncalo, Clara, Miguel, Cristovao, Ines, Andre, Luz, Alex, all their babies who became my nieces and nephews. Thank you to “the cousin of my cousin” aka “prima das primas” Teresa for many fun days/nights together supporting each other. Kaitlyn, my bbg, thank you for all the support. We went from sharing an office to sharing the most delicate and deepest parts of our lives. I am very happy to have you in my life, and I can’t even believe we are about to finish this huge, long journey that is a PhD. It took a lot from us, but it also gave us lots of opportunities for growth and personal development in almost every angle. I have no doubt we will continue to lean on each other for all the good and bad life throws at us. Thanks for all the chats and MHW, and then when distance did not allow for that, thank you for all the vns.

To my parents, Mom and Dad thank you for providing some of the best education one can get, while urging me to keep working and studying hard. It undoubtedly nurtured the curiosity I displayed as a child and helped to turn me into a researcher... still can’t quite believe that is my profession. Any successes I will achieve will always be connected to you both in that way and I am very grateful for all that your sacrifices have brought. Thank you to my brother for bringing us all a light of youth and fresh perspectives, seeing you grow up into a funny and bright mind has been such a joy. To my aunt Alice and uncle Ricardo, thank you for welcoming me into your home for the first 7 months of this journey. I appreciate you so much for this and hope to one day repay you all the kindness and support you have shown me. I am very blessed to have had your hospitality, that provided such a safe and familiar

start to this PhD journey. Thank you for your patience with me when I had to work hard and late into the night to meet some tight deadlines. Finally, thank you for allowing me into your family trio, some of my sweetest memories of that time are with you and Kika, who is so kind-hearted and mature beyond her years. Thank you to my long-time best friend Carlota, you have been such an inspiration, ever since that trip to Soltroia back in 2010. Our bond only grew stronger, even at a distance. I know we may not see each other as much as we'd like but everytime we do we just snap back to being the same two best friends, doing lengthy study nights plus late-night cinema combos, with 50% comedy 40% wisdom 10% life drama. You got me through some difficult times, and I am so lucky to have you.

To my sister, where do I even begin. Thank you for being my strongest supporter, what I am today I also owe to you. You show a grace, wisdom, mental maturity and kindness I have never seen anyone display. You are funny and so strong, and you know the lyrics to every song we like and we sing at the top of our lungs during all those 3-hour car trips to Porto. You are such a bright light in my life, and you make me want to do better and be a better person. You have taught me so much and part of the reason why I keep going is for you. Thank you for everything you have done for me, I am so so happy and grateful to have you in my life, and I feel lucky I got you as my younger sister. If it's you and me against the world, then so be it. Love you like XO.

Finally, to my partner Arron. Thank you for putting up with me when I was at my most frustrated, annoyed and stressed. We have made it through some tough times together and came back stronger for it. In parallel to dealing with your own challenges, you were available for me to share my burdens too. We have shared so many joyous moments (I am pretty sure we saw 90% of the west end together) and I cherish our time together now more so than ever. I am very lucky to have you in my life, fighting my corner, telling me off when I need to, and always being ever so loving and caring. Love you!

“The beginning of knowledge is the discovery of something we do not understand.”

Frank Herbert

Abstract

Parkinson's disease (PD) is a neurodegenerative disorder currently affecting 2% of individuals over 60 years old. The *Leucine-rich repeat kinase 2* (*LRRK2*) gene has been identified as the most common genetic cause for PD. The two most frequent mutations are *LRRK2-G2019S* and *LRRK2-R1441C*, located in the kinase domain and in the ROC-COR domain, respectively. Although autophagic-lysosomal dysfunction and many mitochondria related pathways have been implicated in PD, our understanding is still limited. Here, we aim to further our understanding of autophagy-lysosomal pathways, mitochondrial health and mitophagy using *LRRK2-R1441C* rat primary cortical and human induced pluripotent stem cell-derived dopaminergic (iPSC-DA) cultures as models of PD.

Even though there was an increase in proteolytic degradation levels in *LRRK2-R1441C* iPSC-derived dopaminergic cultures, there were no changes in autophagosomal and lysosomal markers, compared to healthy controls. Using co-immunoprecipitation in human culture models, it was demonstrated the novel interaction between LRRK2 and lysosomal proton pump vATPase-a1 subunit occurs at the LRRK2-COR domain. vATPase-a1 cellular localisation was investigated in LRRK2-related PD models but there was no evidence of abnormal accumulation of vATPase-a1 in the ER, Golgi or lysosomes.

However, we found *LRRK2-R1441C* neurons exhibit decreased mitochondrial membrane potential, impaired mitochondrial function and decreased basal mitophagy levels. Mitochondrial morphology was altered in *LRRK2-R1441C* iPSC-DA but not in cortical neuronal cultures or aged striatal tissue, indicating a cell type-specific phenotype. Additionally, *LRRK2-R1441C* but not *LRRK2-G2019S* neurons demonstrated decreased levels of the mitophagy marker pS65Ub in response to mitochondrial damage, which could disrupt degradation of damaged mitochondria. This impaired mitophagy activation and mitochondrial function were not corrected by the LRRK2 inhibitor MLi-2 in *LRRK2-R1441C* iPSC-DA neuronal cultures.

Furthermore, we demonstrate LRRK2 interaction with MIRO1, a protein necessary to stabilise and to anchor mitochondria for transport, occurs at mitochondria, in a genotype-independent manner. Despite this, we found that degradation of MIRO1 was impaired in *LRRK2-R1441C* cultures upon induced mitochondrial damage, suggesting a divergent mechanism from the *LRRK2-G2019S* mutation.

These results demonstrate the importance of LRRK2 in mitochondrial biology, as well as the critical role of the mitophagy in PD and the potential of mitochondria-targeting compounds as a therapeutic for the disease.

Resumo

A doença de Parkinson (PD) é uma doença neurodegenerativa que afeta atualmente 2% dos indivíduos com mais de 60 anos de idade. O *Leucine-rich repeat kinase 2* (LRRK2) foi identificado como a causa genética mais comum em PD. As duas mutações mais frequentes são *LRRK2-G2019S* e *LRRK2-R1441C*, localizadas no domínio quinase e no domínio ROC-COR, respectivamente. Embora disfunção em autofagia e balanço em mitocôndria tenham sido implicadas em PD, o conhecimento exacto dos mecanismos ainda é limitado. No presente estudo, pretendemos aprofundar a compreensão do processo de autofagia e lisosomas, saúde mitocondrial e mitofagia usando culturas dopaminérgicas derivadas de células-estaminais pluripotentes (iPSC-DA) e culturas primárias de *LRRK2-G2019S* e *LRRK2-R1441C* como modelos de PD.

Embora tenha havido um aumento nos níveis de degradação proteolítica em culturas dopaminérgicas derivadas de *LRRK2-R1441C* iPSC, não houve alterações nos marcadores de autofagia ou lisosomas, em comparação com controlos saudáveis. Usando co-imunoprecipitação em modelos de cultura celular (humana), foi demonstrado que a nova interação entre LRRK2 e a subunidade da bomba de prótons vATPase-a1 localizada em regiões acídicas tais como os lisosomas, ocorre no domínio LRRK2-COR. A localização celular de vATPase-a1 foi investigada em modelos de LRRK2-PD, mas não houve evidência de acumulação anormal no Retículo Endoplasmático, Golgi ou lisossomas.

No entanto, modelos neuronais de *LRRK2-R1441C* exibiram diminuição do potencial de membrana mitocondrial, função mitocondrial prejudicada e diminuição dos níveis basais de mitofagia. A morfologia mitocondrial em *LRRK2-R1441C* iPSC-DA encontra-se alterada, mas não em culturas neuronais corticais ou tecido estriatal envelhecido, indicando um fenótipo específico dependente do tipo de célula. Além disso, os neurónios *LRRK2-R1441C*, mas não os neurónios *LRRK2-G2019S*, demonstraram níveis reduzidos do marcador de mitofagia pS65Ub em resposta ao dano mitocondrial, o que poderia interromper a degradação de mitocôndrias danificadas. Essa ativação mitofágica prejudicada e a função mitocondrial não foram corrigidas pelo inibidor de kinase de LRRK2 (MLi-2) em culturas neuronais *LRRK2-R1441C* iPSC-DA.

Além disso, demonstramos que a interação de LRRK2 com MIRO1, uma proteína necessária para estabilizar e ancorar mitocôndrias para transporte, ocorre na mitocôndria de maneira independente do genótipo. Apesar disso, descobrimos que a degradação de MIRO1 encontra-se alterada em culturas *LRRK2-R1441C* após dano mitocondrial induzido, sugerindo um mecanismo divergente da mutação *LRRK2-G2019S*.

Estes resultados demonstram a importância de LRRK2 na biologia mitocondrial, bem como o papel crítico da mitofagia em PD e o potencial de compostos direcionados à mitocôndria como terapêutica para a doença de Parkinson.

List of Abbreviations

	Abbreviation	Definition
1	AD	Alzheimer's Disease
2	ALS/FTD	Amyotrophic Lateral Sclerosis/Frontotemporal Dementia
3	ANK	Ankyrin Repeat
4	ARM	Armadillo Repeat Motif
5	ATP	Adenosine Triphosphate
6	BAC	Bacterial Artificial Chromosome
7	CMA	Chaperone-Mediated Autophagy
8	COMT	Catechol-O-Methyltransferase
9	COR	C-Terminal of ROC
10	DAn	Dopaminergic Neurons
11	DAT	Dopamine Transporter
12	DJ-1	Parkinson Protein 7
13	DNA	Deoxyribonucleic Acid
14	DRP1	Dynamin-Related Protein 1
15	ETC	Electron Transport Chain
16	ESCRT	Endosomal Sorting Complexes Required for Transport
17	FADH	Flavin Adenine Dinucleotide (Reduced Form)
18	GBA	Glucocerebrosidase
19	GTPase	Guanosine Triphosphatase
20	GWAS	Genome-Wide Association Studies
21	KD	Knock-Down
22	KO	Knock-Out
23	LC3	Microtubule-Associated Protein 1A/1B-Light Chain 3
24	LBs	Lewy Bodies
25	LRR	Leucine-Rich Repeat
26	LRRK2	Leucine-Rich Repeat Kinase 2
27	MAO-B	Monoamine Oxidase-B
28	MAPT	Microtubule-Associated Protein Tau

29	MAM	Mitochondria-Associated ER Membrane
30	Mbp	Megabase Pairs (a unit of DNA length)
31	MEF	Mouse Embryonic Fibroblasts
32	MPP+	1-Methyl-4-Phenylpyridinium
33	MPTP	1-Methyl-4-Phenyl-1,2,5,6-Tetrahydropyridine
34	mtDNA	Mitochondrial DNA
35	NADH	Nicotinamide Adenine Dinucleotide (Reduced Form)
36	NIX	NIP3-Like Protein X
37	OMM	Outer Mitochondrial Membrane
38	OPTN	Optineurin
39	OPA1	Optic Atrophy 1
40	OxPhos	Oxidative Phosphorylation
41	PD	Parkinson's Disease
42	PDD	Parkinson's Disease with Dementia
43	PINK1	PTEN-Induced Putative Kinase 1
44	PNS	Peripheral Nervous System
45	RBD	Resting Eye Movement (REM) Sleep Behavior Disorder
46	RRF	Retrorubral Field
47	ROS	Reactive Oxygen Species
48	ROC	Ras of Complex
49	SNPc	Substantia Nigra Pars Compacta
50	STN	Subthalamic Nucleus
51	TCA	Tricarboxylic Acid
52	TG	Transgenic
53	UPDRS	Unified Parkinson's Disease Rating Scale
54	UPS	Ubiquitin-Proteasome System
55	VPS35	Vacuolar Protein Sorting 35
56	vATPase	Vacuolar-Type ATPase
57	vATPase-a1	Vacuolar ATPase Subunit a1
58	VTA	Ventral Tegmental Area
59	WD40	WD-40 Repeat Motif
60	XPDS	X-Linked Parkinsonism with Spasticity

Table of Contents

Chapter 1 – Introduction

1.1. Parkinson's disease

1.1.1. Introduction

Parkinson's disease (PD) is the second most common neurodegenerative disorder worldwide, with more than 4 million people over 50 affected by the disease, with a projection for the number of individuals with PD to double by 2030 (Dorsey et al. 2007). Parkinson's disease was first characterised over 200 years ago by James Parkinson, who reported similar involuntary tremors of the limbs and bradykinesia in six different patients, with no apparent loss of sense and intellect in his essay entitled "An essay in the shaking palsy" (Parkinson 1817). Parkinson's disease is characterised by a loss of dopaminergic neurons (DAn) in the *Substantia Nigra pars compacta* (SNpc) region of the midbrain as well as their projections to the striatum. This specific dopaminergic neurodegeneration within an important regulator of voluntary movements results in the hallmark clinical symptoms of PD such as bradykinesia, resting tremor, and muscle rigidity (Antony et al. 2013). Moreover, *post-mortem* analysis reveals the presence of α-synuclein protein aggregates, known as Lewy bodies (LBs), throughout the brain (Spillantini et al. 1997). Alpha-synuclein forms the main component of LBs and is thought to spread to interconnected brain regions in a prion-like manner, a process that is currently not fully understood (Wang and Hay 2015).

1.1.2. Clinical characterisation

Patients diagnosed with Parkinson's disease often present motor symptoms which include resting tremors, muscle rigidity, postural instability, bradykinesia (slowness of movement) and gait, as well as non-motor symptoms such as dementia, pain, fatigue, mild-cognitive impairment and urinary symptoms (Kalia and Lang 2015; Jankovic and Tan 2020). These motor symptoms are heterogeneous in patients, further dividing into subtypes of the disease, including tremor-dominant (with absence of other motor symptoms) and non-tremor dominant. Non-tremor dominant can be further divided into akinetic-rigid syndrome and postural instability gait disorder (Marras and Lang 2013).

Non-motor symptoms can also precede PD hallmark motor symptoms by as much as two decades, referred to as prodromal symptoms. Prodromal PD refers to a phase during

which clinical signs of disease are not evident but underlying neurodegeneration has started and progressed. These prodromal markers can manifest as RBD (Resting Eye Movement (REM) Sleep Behaviour Disorder) and preparation of individuals that have RBD and convert to PD acts as one of the best early markers of PD. Other prodromal markers include hyposmia, constipation, hypotension, diabetes mellitus, urinary and erectile dysfunction, anxiety and depression (Mantri, Morley, and Siderowf 2019; Jankovic and Tan 2020). Current diagnosis of PD involves identification of genetic causes, confirming parkinsonism (bradykinesia, plus one other cardinal motor symptom), excluding atypical parkinsonism (other neurodegenerative conditions presenting similar symptoms) but can only be confirmed in *post-mortem* examination (Bloem, Okun, and Klein 2021).

1.1.3. Pathophysiologic mechanisms

Studies investigating human *post-mortem* samples from PD patients demonstrated a neuronal loss in the SNPc, locus coeruleus and other neuronal populations (Ehringer and Hornykiewicz 1960). The accumulation of Lewy bodies and loss of dopaminergic neurons, which present a distinct dark colour due to the dopamine synthesis by-product neuromelanin, leads to reduced striatal dopamine levels (Fig. 1.1 A) (Kordower et al. 2008a). Midbrain DAn are located in three major nuclei including the SNpc (A9), the ventral tegmental area (VTA; A10), and the retrorubral field (RRF; A8). DAn in the SNpc project to the dorsal striatum via the nigrostriatal pathway releasing dopamine to modulate corticostriatal transmission in medium spiny neurons (MSN) expressing dopamine D1 or D2 receptors, which leads to movement activation or suppression, respectively. It is the preferential loss of A9 ventral midbrain DAn (vmDAn) that results in the hallmark motor symptoms of PD. Currently, the main hypothesis to explain this susceptibility of A9 vmDAns to neurogeneration highlights how DAn of the SNpc have highly branched, long, unmyelinated axons that put a high energetic burden on the cell (Pissadaki and Bolam 2013) which may lead them to become more susceptible to cellular stress. Furthermore, SNpc neurons use L-type calcium channels for pacemaking activity (Surmeier, Guzman, and Sanchez-Padilla 2010) and the maintenance of calcium gradients will place high energy demands on the cell, therefore exacerbating the already increased burden on these DAn.

Disease progression can be quantified using alpha-synuclein pathology as proposed by the Braak hypothesis which suggests that early pathological changes occur in the medulla oblongata and olfactory bulb (Braak stages 1 and 2) before advancing rostrally

to the substantia nigra and midbrain when clinical motor symptoms are likely to be present (Braak stages 3 and 4) and lastly the cortical regions eventually become affected in late stages (Braak stages 5 and 6). At a late stage of PD mesocortical, mesolimbic and tubero-infundibular regions of the brain are affected, impairing brain functions such as cognition and memory, emotion and reward, and sensory processing and hormonal regulation, respectively (Fig. 1.1 B) (Braak et al. 2003). Certain species of α-synuclein can activate neuroinflammatory response and more importantly can 'seed' and progressively spread α-synuclein pathology from cell to cell, as demonstrated by the surprising presence of Lewy bodies in the young neural grafts of transplanted PD patients, more than a decade after surgery (Kordower et al. 2008a; Kordower et al. 2008b; Li et al. 2008).

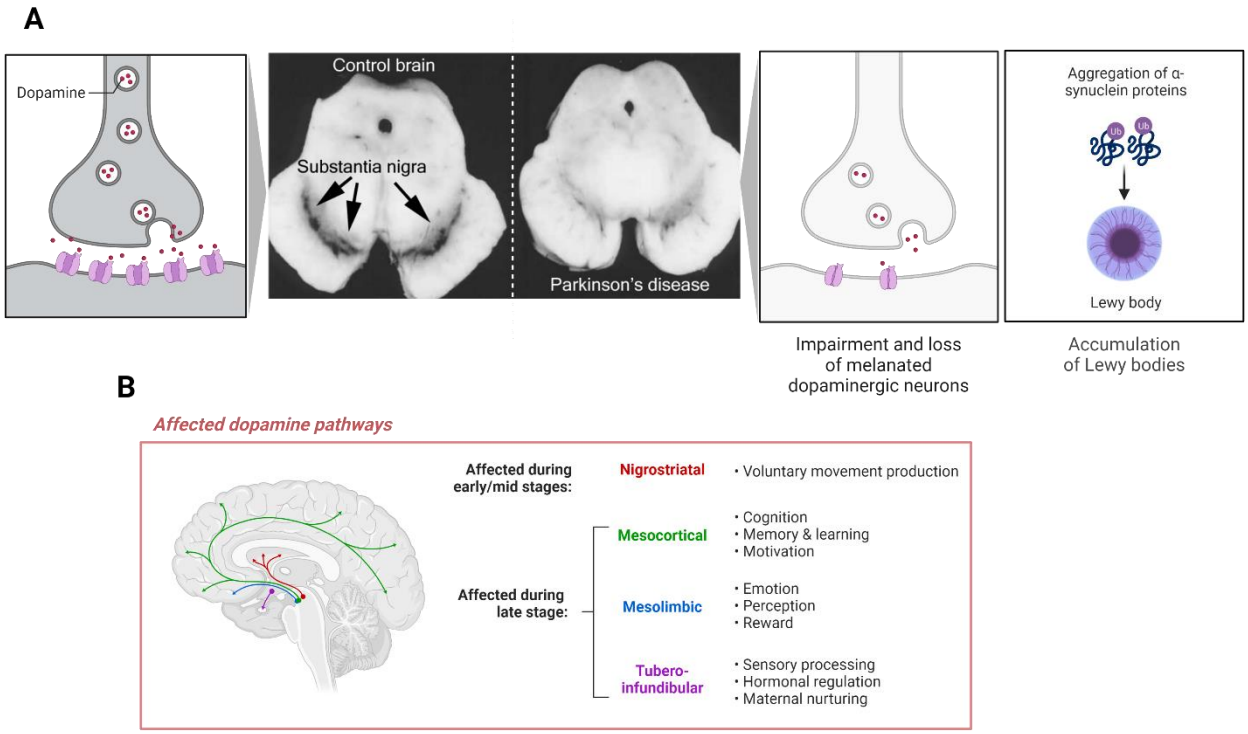

***Figure 1.1. – Parkinson's disease pathology*. (A)** Horizontal human brain sections from a healthy control and PD patient (Mackenzie, 2001). Arrows indicate the pigmented cells of the SNpc. Neurodegeneration in the nigrostriatal regions leads to impairment and loss of melanated dopaminergic neurons, caused by accumulation of α-synuclein aggregates into Lewy Bodies. **(B)** Disruption of the dopaminergic circuits affects nigrostriatal projections during early/mid stages of PD, and then as disease progresses, it affects mesocortical, mesolimbic and tubero-infundibular regions of the brain, affecting different brain functions such as motor function, cognition and memory.

The role of LBs is not yet completely understood since not all familial PD showed LBs at *post-mortem* examination (Doherty and Hardy 2013; Gaig et al. 2007). The presence of LBs and Lewy neurites (LN) are also histopathologic features of Parkinson's disease with dementia (PDD), dementia with Lewy bodies (DLB), and the mixed form of Alzheimer's disease (AD) and DLB. On the other hand, LBs have even been observed in neurologically normal *post-mortem* brains (Markesbery et al. 2009). LB load in patients also correlates poorly with the severity of symptoms (Colosimo et al. 2003; Parkkinen, Pirttilä, and Alafuzoff 2008). However, it is known that the oligomeric form of α-synuclein, which is a precursor to the fibrillary α-synuclein found in LBs, is highly neurotoxic (Winner et al. 2011; Näsström et al. 2011) and α-synuclein oligomers have been observed in *post-mortem* brains (Tofaris et al. 2003; Roberts, Wade-Martins, and Alegre-Abarrategui 2015). Therefore, it has been hypothesised that oligomeric species of α-synuclein would cause neuronal degeneration in PD (Helwig et al. 2016; Winner et al. 2011; Bengoa-Vergniory et al. 2017; Roberts, Bengoa-Vergniory, and Alegre-Abarrategui 2019). Importantly, other proteins such as ubiquitin (Spillantini et al. 1997), 14-3-3 proteins (Kawamoto et al. 2002), heat shock cognate 71 kDa protein (HSC70) (Leverenz et al. 2007) and tau (Ishizawa et al. 2003) have also been found in LBs.

Many different cellular dysfunctions have been implicated in human *post-mortem* tissues, in vitro human cell lines, human brain organoids and animal models of PD (Fig. 1.2.). These include oxidative stress induced by reactive oxygen species (ROS) and metals (Trist, Hare, and Double 2019), mitochondrial dysfunction (Malpartida et al. 2021), disruption of calcium homeostasis, synaptic dysfunction (Nguyen et al. 2019), impairment of protein clearance (involving key ubiquitin-proteasome and autophagy-lysosomal systems) (Lu, Wu, and Yue 2020; Madureira, Connor-Robson, and Wade-Martins 2020), neuroinflammation, protein misfolding and aggregation (mainly α-synuclein and tau) (Mehra, Sahay, and Maji 2019; Pan et al. 2021) and apoptosis (Antony et al. 2013). This body of work will focus mainly in the lysosomal and mitochondrial dysfunction in a subset of PD.

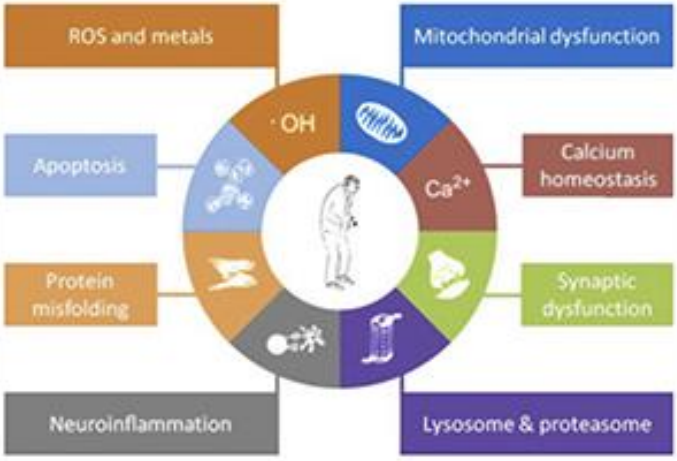

Figure 1.2. – Cellular hallmarks of Parkinson's disease. All subtypes of PD may share common cellular phenotypes. Correlations between the represented cellular phenotypes and disease progression are well established, even though the chronology and cell-specific dysfunction remains to be elucidated. Taken from (Antony et al. 2013).

1.1.4. Aetiology of Parkinson's disease

Causes of Parkinson's disease are still not entirely understood, with the main relevant factors being genetics, the environment and interactions between them.

1.1.4.1. Genetics

1.1.4.1.1. Familial PD genes

Currently, 5-10% of patients present with a familial form of PD, illustrating how research into these genes and their neuropathological pathways is vital. Familial mutations have been described in a number of genes including *SNCA* and *LRRK2* which are responsible for autosomal dominant PD forms, while mutations in *Parkin*, *PINK1*, *DJ-1* and *ATP13A2* are accountable for autosomal recessive PD (Klein and Westenberger 2012).

The first familial mutation to be linked to PD was the *A53T* mutation in the *α-synuclein* (*SNCA*) gene which was identified in an Italian family (Hardy 2010; Polymeropoulos et al. 1997). The A53T mutation in α-synuclein has been associated with altered autophagy and mitochondrial dysfunction (Pupyshev et al. 2018; Smith et al. 2005). Since then, multiple rare genetic alterations such as duplication, triplication and other point-mutations such as *A30P*, *E46K*, *H50Q* and *G51D*, have been reported in the *SNCA* gene. *SNCA*-related PD is usually associated with early onset disease with a more rapid

progression and with dose dependent effects on both of these outcomes (Zeng et al. 2018; Schneider and Alcalay 2017; Wang and Hay 2015). Although the exact role of α-synuclein remains elusive, numerous pathological mechanisms, such as synaptic dysfunction, ER-Golgi trafficking disruption, endoplasmic reticulum (ER) stress, Golgi fragmentation and perturbation of the autophagy-lysosomal pathway have been associated with α-synuclein mutations (Zambon et al. 2019; Ryan et al. 2013; Chung et al. 2013; Colla et al. 2012; Wang and Hay 2015).

Mutations in the *Leucine-Rich Repeat Kinase 2* (*LRRK2*) gene, located in the *PARK8* loci, are the most common mutations found in familial autosomal dominant PD (Singleton, Farrer, and Bonifati 2013; Paisán-Ruíz et al. 2004; Zimprich et al. 2004). Due to their similar age of onset, symptom progression and neuropathology *LRRK2*-PD patients cannot be clinicopathologically distinguished from idiopathic patients. LRRK2 is mainly considered to be a cytoplasmic protein, but it can also be found on organelle membranes, such as the mitochondria and lysosomes (Orenstein et al. 2013). Mutations in the *LRRK2* gene account for 2% to 40% of PD cases, depending on populations (Klein and Westenberger 2012). The two most common mutations, *G2019S* and *R1441C*, account for up to 10% and 2.5% of sporadic PD cases, respectively, depending on population group. The difference in frequency between the two mutations may be explained by incomplete, age-dependent penetrance. The *G2019S* mutation presents a penetrance ranging from 17% at 50 years old to 85% at 70 years old, and the R1441C mutation presents with more severe phenotypes (Healy, Wood, and Schapira 2008; Kluss, Mamais, and Cookson 2019). These findings along with the evidence from GWAS, showing *LRRK2* variants impact on the risk of developing PD, show how understanding the role of LRRK2 in PD pathology will be critical to fully comprehend both familial and sporadic forms of disease.

The heterozygous *glucocerebrosidase* (*GBA)* variants are one of the most common PD risk factors, found in 3–20% of PD and Lewy Body Dementia (LBD) patients, depending on the population (Gan-Or, Dion, and Rouleau 2015; Blauwendraat et al. 2020). Some of the most common variants are the *E326K*, *T369M*, *N370S* and *L444P* mutations. Interestingly, homozygous or compound heterozygous state *GBA* mutations may cause autosomal recessive Gaucher's disease, a lysosomal storage disorder (Futerman et al. 2004). The *GBA* gene encodes for glucocerebrosidase (GCase), the lysosomal membrane enzyme that cleaves the glycolipid glucosylceramide. However, the majority of GBA variant carriers will not develop PD, suggesting other genetic and/or environmental factors that affect the penetrance of these variants (Blauwendraat et al.

2020). Two recent studies independently showed that *GBA* mutation carriers can also carry the *LRRK2-G2019S* mutation, with no impact on age of onset (Yahalom et al. 2019; Blauwendraat et al. 2020). However, when compared to non-carriers, *LRRK2-G2019S* carriers displayed higher activity levels of GCase. Since *GBA* mutations are linked to reduced GCase activity and more aggressive PD pathology, it was hypothesised *LRRK2* mutations could have a protective effect on *GBA* mutation carriers through a mechanism that remains unknown (Alcalay et al. 2015). Contrary to this observation, and importantly in induced pluripotent stem cell (iPSC) derived dopaminergic neurons, *LRRK2-G2019S* and *LRRK2-R1441C* patients showed lower GCase activity, which was then increased after treatment with the LRRK2 inhibitor MLi-2, in neurons with either *LRRK2* or *GBA* mutations (Ysselstein et al. 2019). It is hypothesised that reduced GCase activity leads to impaired lysosomal function and therefore accumulation of insoluble α-synuclein (Beavan and Schapira 2013). Moreover, a recent report showed that LRRK2 inhibitor MLi-2 rescued lysosomal pH levels and corrected cathepsin B activity in *GBA* mutant knock-in (KI) astrocytes (Sanyal et al. 2020). Taken together, these results suggest an interplay between GBA and LRRK2, albeit still not fully understood, that paves the way for more research to be conducted on this subject.

1.1.4.1.2. GWAS loci

Genome wide association studies (GWAS) have uncovered numerous low-risk susceptibility variants for sporadic PD, namely in the *LRRK2*, *GBA*, *MAPT*, *Parkin*, *PINK1*, *DJ-1* and *VPS35* loci (Nalls et al. 2014; Singleton, Farrer, and Bonifati 2013; Hardy 2010). Moreover, the study identified a *LRRK2* variant in a non-coding region (rs76904798h), which confers around 15% increased risk of developing sporadic PD (Nalls et al. 2014). A recent meta-analysis of GWAS has reported a list of 17 additional loci associated with disease, altogether implicating pathways such as neuronal survival, neuroinflammation, vesicle trafficking, mitochondria metabolism, autophagy and lysosomal function with PD (Fig. 1.3) (Chang et al. 2017). Other PD associated genes have also been implicated in the autophagy and mitophagy pathways including *GBA, VPS35, ATP13A2, PINK1* and *Parkin* (Ramirez et al. 2006; Vives-Bauza et al. 2010; Zavodszky et al. 2014; Fernandes et al. 2016; Taguchi et al. 2017).

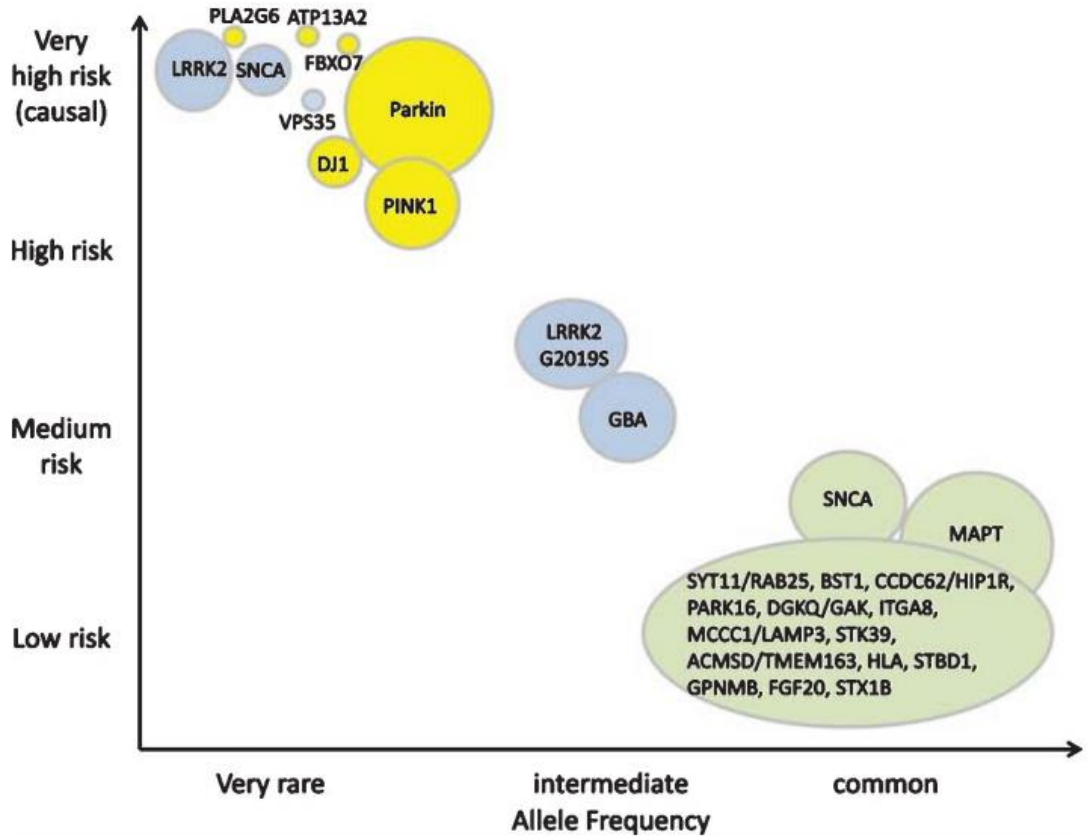

Figure 1.3. – Genetic risk burden in Parkinson's disease. Continuum of variants of different effect strengths and allele frequencies. The size of the bubbles roughly corresponds to population allele frequencies. Colours symbolize modes of inheritance: dominant (blue), recessive (yellow), risk loci (green). Taken from (Gasser 2015).

1.1.4.2. Environment

There has been some debate about the genetic and environmental factors contribution in pathogenesis of PD. Some risk factors implicated in PD have been identified, such as pesticides (paraquat, organochlorine, and carbamate derivatives) and heavy metal exposure (manganese) (Yan et al. 2018; Dutheil et al. 2010). Neurotoxic models using chemical toxins such as 6-Hydroxydopamine (6-OHDA), 1-methyl-4-phenyl-1,2,3,6-tetrahydropyridine (MPTP), paraquat and rotenone lead to severe striatal DA depletion that mirrors an advanced stage of PD (Di Monte, Lavasani, and Manning-Bog 2002). Whilst toxin-induced models allow to investigate the consequences and mechanisms of DA dysfunction, LBs are not commonly observed and models fail to recapitulate the progressive, age dependent effects of PD.

On the other hand, tobacco and caffeine consumption could be potential environmental neuroprotective agents, reducing the risk of PD (Di Monte, Lavasani, and Manning-Bog

2002). Although the analysis of various environmental exposures from epidemiological studies shows a lack of robustness and consistency in some associations, for example traumatic head injury (Huang et al. 2018).

1.1.5. Treatment strategies

"But although, at present, uninformed as to the precise nature of the disease, still it ought not to be considered as one against which there exists no countervailing remedy. On the contrary, there appears to be sufficient reason for hoping that some remedial process may ere long be discovered, by which, at least, the progress of the disease may be stopped."

James Parkinson (Parkinson 1817)

This quote can still be applied today and summarises, in part, what drives research into Parkinson's disease. More than 200 years ago, Dr. Parkinson's prediction of a treatment that would slow the progress of the disease is yet to be found, as the currently approved treatments focus on alleviating symptoms and maintaining quality of life. A recent review of the guidelines for the treatment of Parkinson's disease recommends the administration of medication to patients to increase striatal DA levels and ameliorate motor deficits associated with the disease. This pharmaceutical therapy is usually complemented with rehabilitative therapies such as physiotherapy and exercise (Armstrong and Okun 2020). The main types of pharmacologic agents used include dopamine precursors and agonists, monoamine oxidase-B (MAO-B) and catechol-O-methyltransferase (COMT) inhibitors, glutamatergic and anticholinergic agents, administered according to symptoms and progression of the disease (Ellis and Fell 2017; Armstrong and Okun 2020).

The use of the dopamine precursor levodopa (or L-Dopa) is still the "gold standard" for the treatment of Parkinson's disease, as dopamine is a positively charged molecule that does not cross the blood-brain barrier (BBB) (Jodko-Piorecka and Litwinienko 2013; Lewitt 2015). Once this precursor has entered the central nervous system, it is converted into DA by the aromatic l-amino acid decarboxylase enzyme (or DOPA decarboxylase). Furthermore, Carbidopa is often prescribed in combination to inhibit peripheral metabolism of levodopa and increasing the availability in the central nervous system (CNS) (Ellis and Fell 2017). L-Dopa is the most cost-effective agent for improvement of quality of life and symptom relief in the current therapeutic panorama. A study showing levodopa could rapidly reverse hypokinesia in rabbits treated with reserpine, a drug used

to treat high blood pressure, catapulted the hypothesis that levodopa could be used to treat Parkinson's disease by enhancing striatal dopaminergic neurotransmission (Oster and Sorkin 1942; Lewitt 2015). However, it has been reported that patients commonly exhibit inconsistent response to levodopa over time, causing motor fluctuations and dyskinesia respectively designated as L-DOPA induced dyskinesia (LID) (Calabresi et al. 2010). Pre-clinical and clinical trials indicate LID symptoms such as chorea and dystonia can be reduced with pulsatile stimulation of striatal postsynaptic receptors (Olanow, Obeso, and Stocchi 2006).

The monoamine oxidase-B enzyme oxidises amines such as dopamine, converting it to 3,4-dihydroxyphenylacetic acid (DOPAC) which is in turn converted to homovanillic acid (HVA) by catechol-O-methyltransferase (Edmondson, Binda, and Mattevi 2007). In a parallel metabolic pathway, COMT converts DA into 3-methoxytyramine (3-MT), that is in turn oxidised and converted to HVA by MAO-B. Both MAO-B and COMT inhibitors can be used in combination with other drugs or alone to alleviate motor symptoms by decreasing dopamine metabolism and consequently increasing dopamine concentrations in the brain (Ellis and Fell 2017; Edmondson, Binda, and Mattevi 2007). Some examples of MAO-B and COMT inhibitors approved for standard PD care are selegiline and rasagiline, and entacapone and tolcapone, respectively.

Dopamine agonists include apomorphine, bromocriptine, ropinirole, pramipexole, and rotigotine. These drugs act on dopamine receptors to amplify the effects of dopamine, the most potent being agonists of D2-like receptors. DA agonists are another safe and effective alternative to L-DOPA, especially in younger patients, and is associated with a lower incidence of motor complications at the 5-year mark (Alonso-Cánovas et al. 2014). A 2010 meta-analysis of all the controlled trials performed with DA agonists found a significant reduction in 'off' time, Unified Parkinson's Disease Rating Scale (UPDRS) score and incidence of dyskinesia (Stowe et al. 2011). However, it has been demonstrated that DA agonists play a role in the pathogenesis of Impulse Control Disorder (ICD); particularly pathological gambling, hypersexuality and compulsive shopping and eating (Alonso-Cánovas et al. 2014).

Anticholinergic agents antagonise the effects of acetylcholine at muscarinic receptors postsynaptic to striatal interneurons. However, antagonism of acetylcholine can be associated with a variety of adverse effects such as cognitive impairment, confusion, hallucination, blurred vision, dry mouth, constipation, and urinary retention. Even though anticholinergics are used to reduce tremor they also have no effect on bradykinesia. The

limited symptom management and number of side effects hinder the usefulness of anticholinergics in the treatment of PD (Jankovic and Tan 2020).

In parallel to the symptomatic treatment for the motor symptoms experienced by PD patients, there are also some surgical treatments such as Deep Brain Stimulation (DBS), focused ultrasound and cell replacement therapies. It is important to highlight how DBS can be used in patients with moderate to advanced PD presenting with fluctuating response, troublesome dyskinesia or levodopa-unresponsive symptoms. Thalamic DBS is most frequently used to control high-amplitude tremor in patients with essential tremor, but STN or globus pallidus interna (GPi) are the most frequent targets for DBS treatment of patients with PD with disabling tremor and/or levodopa-related motor complications.

Deep brain stimulation is used to treat the effects of wearing off that involve motor symptoms, tremor, and dyskinesia and it involves surgical placement of unilateral or bilateral electrodes transcranially in the subthalamic nucleus or the globus pallidus interna. These electrodes are attached to a battery in the chest, similar to a pacemaker, which stimulate these brain regions to mitigate the unbalanced neuronal activity underlying motor symptoms (Schuepbach et al. 2013). Patients undergoing DBS can have a higher risk of infection at the surgery site, and it is important to clarify this method still does not halt the progression of neuronal degeneration (Pepper et al. 2013; Shulman, De Jager, and Feany 2011).

1.2. LRRK2

LRRK2 can be found ubiquitously in the human body although expression levels are mainly detected in kidneys, lung, granulocytes in the blood and the brain (Miklossy et al. 2006; Paisán-Ruíz et al. 2004; Zimprich et al. 2004). Relatively high levels of LRRK2 mRNA measured by in situ hybridisation have been detected in areas innervated by the mesencephalic dopamine system, such as the caudatus and putamen regions of the human brain, but not in dopamine neurons per se. Similar findings are reported in adult mouse and rat brains, where expression of LRRK2 mRNA was specifically located in the striatum and parts of the cortex, yet no significant levels in dopamine neurons (Galter et al. 2006). These findings are recapitulated when analysing endogenous LRRK2 protein expression levels in rodent models (West et al. 2014). A study of a large sample cohort using a dense genotyping array technique revealed that LRRK2 mRNA levels were highest in the occipital cortex and lowest in the cerebellum and white matter. As for the substantia nigra and putamen, the regions most implicated in the PD pathology, LRRK2

expression levels were not significant (Trabzuni et al. 2013). LRRK2 expression levels have also been detected in astrocytes, oligodendrocytes, microglia and in different immune cell subsets, such as monocytes, B cells and T cells (Cook et al. 2017; Miklossy et al. 2006). Furthermore, LRRK2 expression levels differ between primary cultures of astrocytes (Giesert et al. 2013), macrophages (Schapansky et al. 2014) and microglia (Gillardon, Schmid, and Draheim 2012) that present relatively high levels compared to neuronal cultures where endogenous expression levels are low (Schapansky et al. 2014).

1.2.1. Structure

LRRK2 comprises a large homodimeric protein (285 kDa) and has several functional domains including an armadillo repeat (ARM) region, an ankyrin repeat region (ANK) and a leucine-rich repeat (LRR) domain, which are important for mediating protein-protein interactions. There is also a ROC-COR domain which consists of a GTPase of the ROCO family. The C-terminal of LRRK2 contains a functional kinase MAPKKK-like domain, regulated by the GTPase activity of LRRK2, and also a WD-40 domain that regulates protein-protein interactions (Fig. 1.4) (Myasnikov et al. 2021; Guaitoli et al. 2016). Therefore, LRRK2 has both kinase and GTPase function and can also operate as a scaffolding unit in signalling pathways (Paisán-Ruíz et al. 2004; Outeiro et al. 2019). However, the biological role of LRRK2 is not yet completely understood.

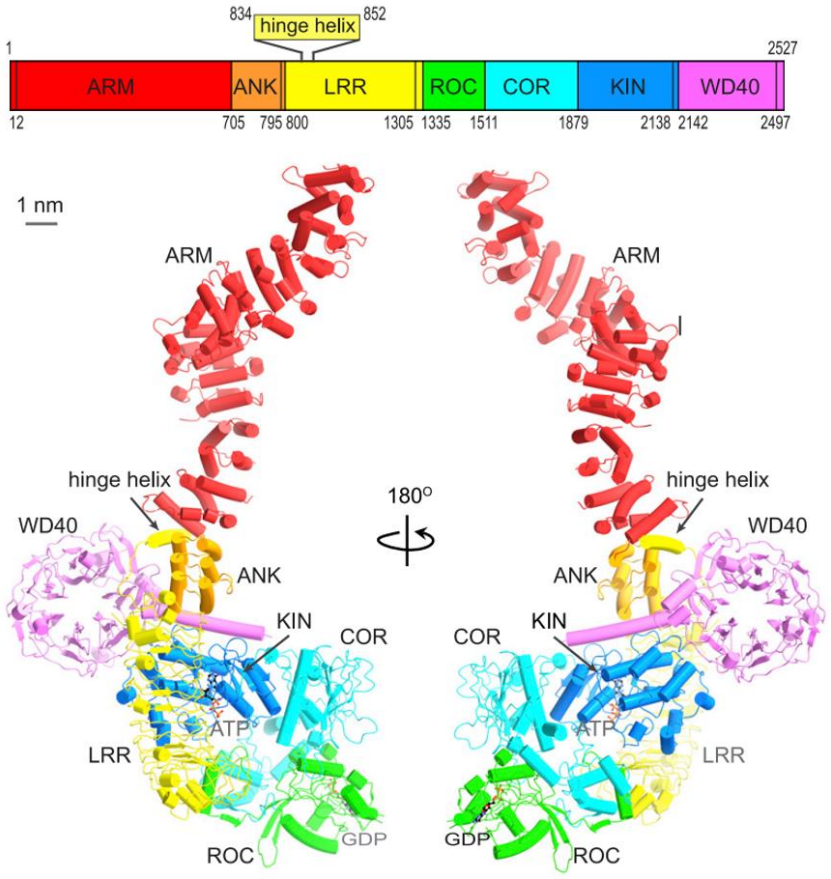

***Figure 1.4. – LRRK2 structure*.** Top: domain scheme of LRRK2. The domain boundary is mapped based on its cryo-EM structure. The domain boundary is labelled. Bottom: cylinder model of the full-length LRRK2 at two views. ARM, ANK, LRR, ROC, COR, KIN, and WD40 domains (red, orange, yellow, green, cyan, blue, and violet, respectively). The linkers connecting adjacent domains are coloured using the same colour as the previous domain. Abbreviations: ARM, armadillo repeat motif; ANK, ankyrin repeat; LRR, leucine-rich repeat; ROC, ras of complex; COR, C-terminal of ROC; KIN, kinase. Taken from (Myasnikov et al. 2021).

1.2.2. Physiological role

LRRK2 has been reported to phosphorylate several substrates, including GTPases of the Rab superfamily Rab3, Rab5, Rab7L1, Rab8, Rab10, Rab12, Rab29 and Rab32, indicating a role in endosomal and vesicle trafficking pathways (Dodson et al. 2012; MacLeod et al. 2013; Beilina et al. 2014; Cho et al. 2014; Yun et al. 2015; Steger et al. 2016; Connor-Robson et al. 2019). LRRK2 also interacts with microtubules, suggesting a role in cytoskeleton dynamics and neurite outgrowth (Godena et al. 2014; Parisiadou et al. 2014). Studies in LRRK2 mutant models also implicate a role in mitochondria morphology, homeostasis and mitophagy (Malpartida et al. 2021; Yue et al. 2015).

LRRK2 regulates pathways in immune cells, such as cytokine release and phagocytosis (Wallings and Tansey 2019). More recently, LRRK2 has been described to regulate nuclear envelope integrity by interacting with lamin A/C (Shani et al. 2019).

1.2.3. LRRK2 mutations

Over the last few decades, many *LRRK2* mutations have been identified in monogenic PD. In 2002, the *I2020T* mutation in a Japanese family in which the *PARK8* locus was first described as associated with PD (Funayama et al. 2002). Later in 2004, *Y1699C*, *R1441G* and *R1441C* were identified (Paisán-Ruíz et al. 2004; Zimprich et al. 2004), followed by the *G2019S* mutation found in multiple kindreds across North America and Europe (Nichols et al. 2005; Kachergus et al. 2005) and the *R1441H* mutation, identified in a patient of European ancestry (Deng et al. 2006). In 2006, the *I2012T* mutation was also identified in a familial case of PD in Taiwan (Deng et al. 2006) and in 2010 the *N1437H* mutation was detected in a large Norwegian family (Ross et al. 2008). Moreover, other mutations are considered as risk factors for sporadic PD, such as the *R1628P* (Ross et al. 2008) and *G2385R* mutations (Di Fonzo et al. 2006), which confer a two-fold increased risk of disease. LRRK2 mutations associated with PD are mainly located in the kinase, Roc, and COR domains, thus highlighting the importance of these functional domains. The G2019S and I2020T mutations occur in the kinase domain, R1441C/G/H in Roc domain, and Y1699C and N1437H, which are significantly more penetrant, occur in COR domains (Lee and Cannon 2015).

Interestingly, PD patients with *LRRK2* mutations are typically clinically and pathologically indistinguishable from sporadic PD (Healy et al. 2008) with similar age of onset, nigrostriatal neuronal loss and responsiveness to DA replacement therapy (Singleton, Farrer, and Bonifati 2013). This cohort of PD patients usually does not present with Lewy body pathology (except for G2019S), but sometimes exhibit neurofibrillary tau tangles (Kett and Dauer 2012). However, mutant LRRK2 carriers demonstrated reduced incidences of cognitive impairment and sleep disturbances, despite similar motor and non-motor symptoms (Healy et al. 2008).

1.2.4. LRRK2 cellular dysfunctions

The G2019S mutation, located in the kinase domain, increases the kinase activity of LRRK2 whereas the R1441C mutation, located in the GTPase domain, decreases GTPase activity (Chen and Wu 2018; Lewis et al. 2007; West et al. 2005). There is evidence suggesting LRRK2-R1441C increases kinase activity (West et al. 2005), yet other reports suggest it does not directly enhance kinase activity (Steger et al. 2016;

Nichols et al. 2010; Lewis et al. 2007), thus indicating this effect is still unclear. As discussed above, LRRK2 likely has numerous functions and disruption to its normal physiological roles would result in a broad array of phenotypes within cellular structures (Fig. 1.5) (Usmani, Shavarebi, and Hiniker 2021). For instance, pathogenic LRRK2 leads to impairment of late stages of endocytosis, trafficking to lysosomes and synaptic vesicle endocytosis (Gómez-Suaga et al. 2012; Rivero-Ríos et al. 2016; Connor-Robson et al. 2019). LRRK2-G2019S models present increased sensitivity to mitochondrial toxins and accumulation of damaged mitochondria while both LRRK2-G2019S and LRRK2-R1441C cause increased mitochondrial fragmentation, suggesting a toxic gain-of-function phenotypic alteration (Karuppagounder et al. 2016; Mortiboys et al. 2010; Ramonet et al. 2011; Wang et al. 2012). Both LRRK2-G2019S and LRRK2-R1441C seem to alter actin cytoskeleton stability and LRRK2-R1441C shows disruption of microtubule-dependent organelle and vesicle transport (Godena et al. 2014; Parisiadou et al. 2014; Caesar et al. 2015). LRRK2-G2019S has reduced interaction with lamin A/C, causing nuclear lamina disorganisation and leakage of nuclear proteins in a loss-of-function manner (Shani et al. 2019). Considering the many potential roles of LRRK2 it is important to understand how it plays a role in each pathway. Studies focused on specific cellular contexts will help uncover the full extent of mutant LRRK2 effects.

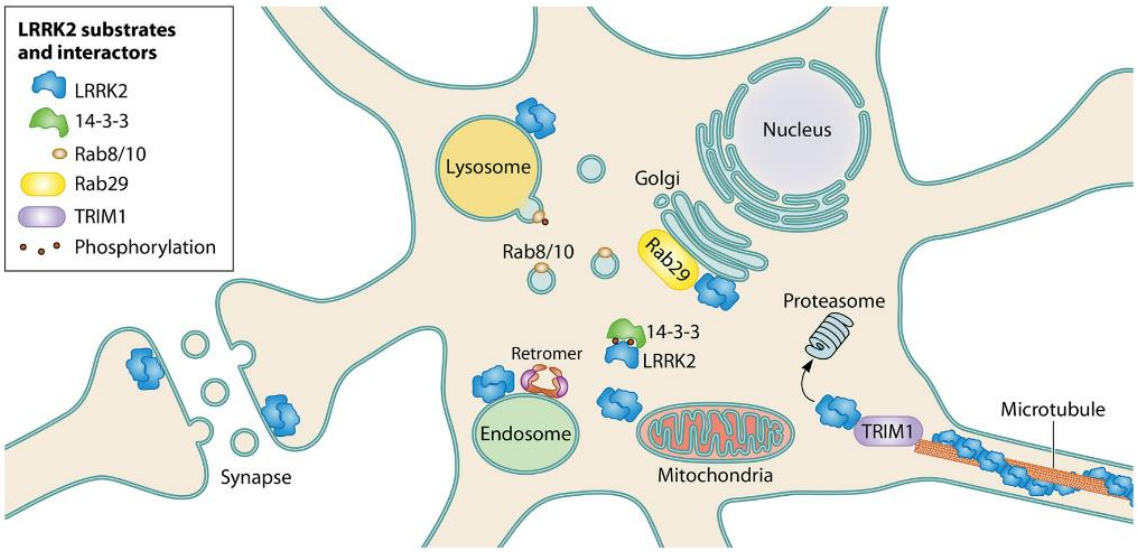

***Figure 1.5. – LRRK2 subcellular localisation*.** LRRK2 is found in the cytoplasm, where it binds to 14-3-3 proteins in a phosphorylation-dependent manner, and at cell membranes, where it forms a homodimer. LRRK2 function appears particularly important to the endolysosomal system and trans-Golgi network. Here, LRRK2 is activated by and phosphorylates Rab29 and also recruits and phosphorylates Rab8A/10 (as well as other Rab proteins) to initiate downstream pathways. In overexpression, LRRK2 binds the

microtubule in an ordered helix, and LRRK2 proteasomal degradation is regulated by TRIM1. LRRK2 also appears to have important roles in normal retromer and mitochondrial function and mitophagy. Taken from (Usmani, Shavarebi, and Hiniker 2021).

1.2.5. Models to study LRRK2-related Parkinson's disease

There are several models available to study LRRK2-related PD, providing both *in vitro* and *in vivo* assays to understand the underlying molecular mechanisms driving LRRK2 induced dopaminergic neurodegeneration. The essential features of an animal model of PD include age-dependent, progressive degeneration of DAn of the SNpc, motor dysfunction that is responsive to DA replacement therapy (resembling the hallmark PD motor symptoms), α-synuclein positive LBs and neurodegeneration levels elsewhere in the brain less severe than DAn loss in the midbrain (Dawson, Ko, and Dawson 2010). Animal models to study LRRK2-PD *in vivo* can be divided into invertebrate models, which include *Caenorhabditis elegans* and *Drosophila melanogaster*, and vertebrate models which include zebrafish and mammalian models (rodent models).

1.2.5.1. Invertebrate animal models

The main advantage to using the *C. elegans* nematode invertebrate model is a well-defined and genetically tractable nervous system. However, *C. elegans* contains only one *lrrk-1* gene encoding a LRRK-like protein. Nonetheless, there have been important loss of function studies linking LRRK2 function to ER stress and Golgi network (Xiong et al. 2012; Yuan et al. 2011). Overexpression of LRRK2 in *C. elegans* recapitulates some of the key features of PD, such as age dependent DAn neurodegeneration, behavioural deficits, and locomotor dysfunction that are accompanied by a reduction of dopamine levels. Furthermore, it also establishes a link to mitochondrial dysfunction, autophagy impairment and ER stress and supports a role for LRRK2 kinase and GTPase activity in LRRK2-mediated neurotoxicity *in vivo* (Saha et al. 2009; Yao et al. 2010). *Drosophila* have one human LRRK2 homolog dLRRK and residues affected by PD-causing mutations in *Lrrk2* are conserved, have well-defined nervous systems with neurotransmitters similar to mammals, can undergo complex behavioural tests and present clusters of DAn, making it an important tool to study LRRK2-PD. These tools include LRRK2 knock-out (KO), which show dLRRK2 is not essential for survival of DAn (Xiong and Yu 2018), and transgenic (TG) models, which have demonstrated reduced axonal transport rates may contribute to the formation of Lewy bodies or lewy neurites in

some PD cases carrying *R1441C* or *Y1669C* mutation (Saha et al. 2004) and that different *LRRK2* pathogenic mutations act at distinct pathways and cause varied neuropathology in the DA neurodegeneration (Xiong and Yu 2018).

1.2.5.2. Vertebrate animal models

As for LRRK2 zebrafish models, there has been limited development despite zebrafish homolog zLRRK2 presenting high conservation with human *LRRK2* and neurodegenerative and locomotion defects being rescued with L-dopa or by over-expressing zLRRK2 or human *LRRK2* mRNA (Sheng et al. 2010). However, a similar study showed opposite results and therefore loss of function zLRRK2 models requires further evaluation (Ren et al. 2011).

Rodent models of mouse and rat are widely used due to similar neuronal networks and basal ganglia circuitry with high conservation of homologs with the human disease-causing genes. Mouse LRRK2 KO models show neurodegeneration in the peripheral nervous system (PNS), but not in the midbrain DAn, even in aged mice (up to 2 years old). Furthermore, LRRK2 KO mice develop kidney pathology and impaired autophagy lysosomal function (Tong et al. 2012). The role of LRRK2 in α-synuclein pathology has also been investigated in LRRK2 KO mice, with one study showing rescue of α-synuclein aggregation whilst another study showed accumulation and aggregation of α-synuclein. Although these contrary findings could be due to different levels of α-synuclein expression, there is still a debate on whether LRRK2 inhibition could be a therapeutic avenue to attenuate α-synuclein-related neurodegeneration. Many LRRK2 transgenic mouse models have been generated, varying widely with regards to the strain, the promoters used for transgene expression, the *LRRK2* mutations studied, the use of human or endogenous genes, use of cDNA or complete human genetic sequence and the methodology to characterise each model. While most LRRK2 TG mice manifest deficits in DA transmission and DA-responsive behaviour (Sloan et al. 2016; Yue et al. 2015; Chou et al. 2014; Li et al. 2010; Li et al. 2009), only two LRRK2-G2019S transgenic models exhibit age-dependent SNpc DAn neurodegeneration (Chen et al. 2012; Ramonet et al. 2011). Using rat models offers advantages in studying late onset disorders, as these animals are physiologically easier to monitor, and complex behaviour studies are easier to set up. LRRK2-KO rat models show consistent phenotypes with LRRK2-KO mouse models, presenting abnormal phenotypes in peripheral organs such as kidney, spleen, lung, and liver but no significant loss of SNpc neurons (Baptista et al. 2013; Ness et al. 2013). The first rat LRRK2 transgenic model used a Doxycycline (dox)-inducible system to achieve temporal overexpression of LRRK2-G2019S, showing

enhanced locomotor activity with age and impaired dopamine reuptake by the dopamine transporter (DAT), but no DAn neurodegeneration (Zhou et al. 2011). Human BAC LRRK2-G2019S or R1441G rats were developed but showed no age-dependent neurodegeneration nor motor/cognitive deficits. However, LRRK2-G2019S induced oxidative stress in nigrostriatal regions, and increased inducible nitric oxide synthase expression and abnormal morphology SNpc DA neurons (Lee et al. 2015; Shaikh et al. 2015; Walker et al. 2014). Furthermore, G2019S- and R1441C BAC TG rats develop age dependent decrease in striatal DA release and L-DOPA-responsive impairments in motor coordination (Sloan et al. 2016). Regarding transgenic technique strategies, it is crucial to recognise that BAC and KI models express mutant LRRK2 during development and could potentially exhibit compensatory mechanisms that prevent loss of DAn. Viral-mediated animal models of LRRK2 can be useful to bypass the development of compensatory effects as well as targeting SNpc DA neuronal populations specifically, while controlling the dosage and transgene copy number. Recombinant adenoviral vector expressing LRRK2-G2019S was injected in rats and presented robust degeneration of SNpc DAn. However, these animals display a non-significant increase in monomeric α-synuclein (Tsika et al. 2015) or a strong LRRK2 protein destabilization (Nguyen et al. 2020).

1.2.5.3. Human induced pluripotent stem cell models

Since 2006, disease models have been revolutionised by the generation of induced pluripotent stem cell (iPSC), accomplished by overexpressing four major transcription factors in adult fibroblast cells (Oct3/4, c-Myc, Sox2, and Klf4) (Takahashi and Yamanaka 2006). iPSC-derived PD models provide a highly physiologically relevant model, using fibroblast cells isolated directly from patients which are differentiated into dopaminergic neurons, among other neuronal types, without exceedingly invasive interventions. *LRRK2-G2019S* iPSC-derived dopaminergic neurons display reduced neurite length, accumulation of α-synuclein and tau, increased vulnerability to cellular stress, and impaired autophagy and mitochondrial function (Sánchez-Danés et al. 2012; Orenstein et al. 2013; Reinhardt et al. 2013; Su and Qi 2013; di Domenico et al. 2019). Since much less is known about the second most common *LRRK2* mutation R1441C, one of the main aims of the current project is to investigate autophagy and mitochondrial function in *LRRK2-R1441C* iPSC-derived dopaminergic cultures. One caveat of the current two-dimensional neuronal cultures is the lack of complete physiological networks and cell types that mimic brain physiology and PD-related phenotypes. To tackle this, microfluidic cultures and *in vitro* midbrain organoids have been generated and are

currently still being characterised and established (Kim et al. 2019; Chlebanowska et al. 2020).

1.3. vATPase

Vacuolar-type ATPases (vATPase) are ATP-dependent proton pumps, essential to acidification-dependent processes such as endocytic trafficking, autophagy and lysosomal protein degradation. Mutations in the genes encoding for vATPase or its known interactors are associated with cancer cell survival and metastasis (Stransky, Cotter, and Forgac 2016), osteopetrosis (Frattini et al. 2000), cutis laxa (Kornak et al. 2008), renal tubular acidosis (Karet et al. 1999; Smith et al. 2000) and neurodegenerative diseases such as Alzheimer's disease (AD) (Lee et al. 2010; Majumdar et al. 2011) and PD (Chang et al. 2017). However, the mechanisms that lead vATPase dysfunction to increase risk of developing PD are still largely unknown.

1.3.1. Structure

Recently, Wang and colleagues resolved the structure of the human vATPase proton pump using cryo-electron microscopy (EM) and reported two domains, V_1 and V_0, consistent with previously reported structures for yeast, rat and bovine vATPase (Wang et al. 2020; Roh et al. 2018; Abbas et al. 2020; Wang et al. 2020). The membrane extrinsic V_1 domain is composed of 8 subunits (top A_3B_3 head, central stalk of D and F subunits, three peripheral stalks of E and G subunits, bottom of subunits H and C and the N-terminal domain of a from the V_0 complex), whereas the membrane integral V_0 domain is composed of 8 subunits (c- and c''-ring and ATP6AP1 and ATP6AP2 subunits inside the c-ring; the adjacent CTD of subunit a, e1, and RNaseK and subunit d1 at the cytosolic side of the c-ring to connect to the central stalk of the V_1 complex) (Fig. 1.6) (Wang et al. 2020).

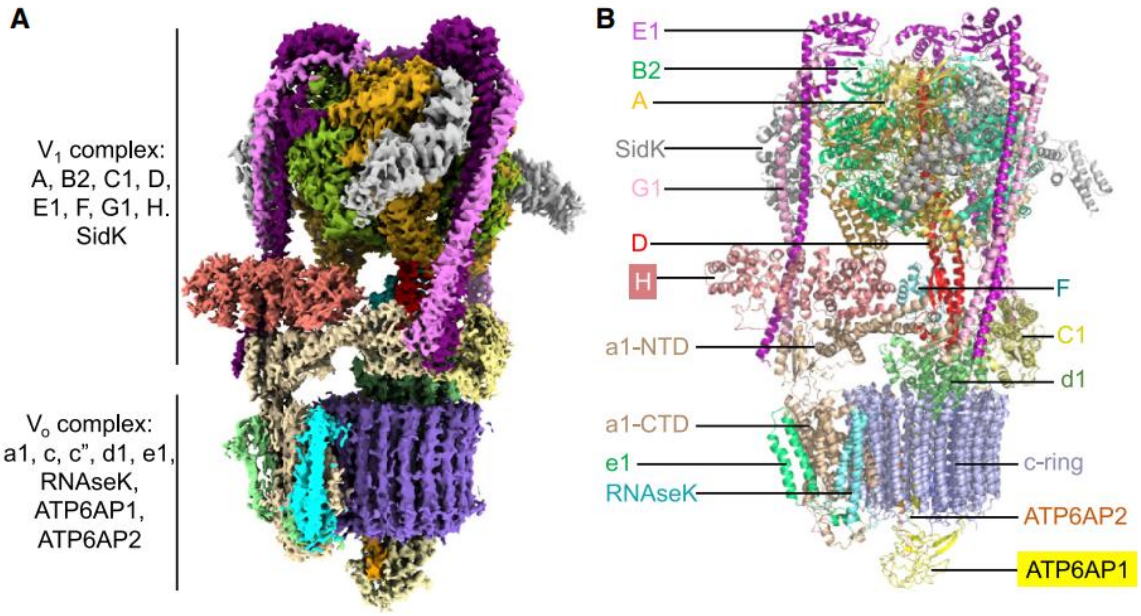

***Figure 1.6. – Human vATPase structure*. (A)** Cryo-EM density of human vATPase (state 1) with subunits colour coded. **(B)** Ribbon diagram of the human vATPase structure (state 1) with subunits colour coded and labelled. Subunits H and ATP6AP1, which are absent or not fully traced in the rat vATPase structure, are highlighted. Taken from (Wang et al. 2020).

1.3.2. Physiological role and disease

Vacuolar-type ATPases are important for many aspects of endocytic-lysosomal pathway and intracellular trafficking as they are the primary proton pumps responsible for acidifying and maintaining the pH of intracellular compartments within cells, regulating pH gradients in the Golgi apparatus, ER, late endosomes and lysosomes (Vasanthakumar and Rubinstein 2020; Collins and Forgac 2020). Briefly, vATPases are responsible for acidifying from *cis* Golgi (pH ~ 6.7) to the *trans* Golgi (pH ~ 6.0), allowing newly synthesized proteins to traverse along the Golgi apparatus and undergo post-translational modifications, and subsequently targeted to their cellular destination in a pH-dependent manner (Vasanthakumar and Rubinstein 2020). Retrograde transport of ER-resident proteins, mediated by the KDEL receptor, is also facilitated by the pH gradient created between ER (pH ~7) and Golgi (Bräuer et al. 2019). vATPases generate the acidic pH of late endosomes (pH < 6.0), which is required for cargo release followed by recycling of the receptor back to the Golgi apparatus. Hydrolytic enzymes, which are crucial to lysosomal protein degradation, are delivered to lysosomes through late endosomes, where they are activated by a more acidic pH (pH 4.5 – 5.0) (Vasanthakumar and Rubinstein 2020; Coutinho, Prata, and Alves 2012). In neuronal

cells, vATPases generate the pH gradient and membrane potential required for loading neurotransmitters into synaptic vesicles and fusion of synaptic vesicles at the presynaptic membrane requires dissociation of the V_1 and V_0 regions, which subsequently reassemble during clathrin-mediated endocytosis (Hnasko and Edwards 2012; Bodzęta, Kahms, and Klingauf 2017). Other functions involve receptor-mediated endocytosis of internalised ligands, allowing the receptor to be recycled back to the cell surface (Naslavsky and Caplan 2018), processing peptide prohormones and the subsequent secretion of mature hormones (Schoonderwoert et al. 2000) as well as virus entry through late endosomes (White and Whittaker 2016).

In 2017, a meta-analysis of GWAS identified a novel risk association between PD and the *ATP6V0A1* gene, which encodes the a1 subunit (V_0 domain) of vATPase (Chang et al. 2017). Another link between vATPase and neurodegeneration was found, with ATP6AP2 variants causing X-linked Parkinsonism with spasticity (XPDS), an early-onset form of Parkinsonism showing defective lysosomal acidification (Korvatska et al. 2013). Furthermore, a novel interaction between LRRK2 and vATPase-a1 subunit was discovered, which was severely decreased in *LRRK2-R1441C* primary cortical neurons exhibiting lysosomal degradation impairment (Wallings, Connor-Robson, and Wade-Martins 2019). Since this novel interaction was discovered, there has not been any new reports about how LRRK2 interacts with vATPase-a1 and how the R1441C mutation disrupts lysosomal biology. As such, one of the main aims of the current project is to investigate and characterise the LRRK2/vATPase-a1 interaction and its cellular localisation, using primary cortical and iPSC-derived dopaminergic cultures as PD models.

1.4. Autophagy

The term autophagy (from ancient Greek meaning “self-eating”) refers to a cellular feature involving cytoplasmic materials and the culmination of these in lysosomal degradation, a highly conserved process through evolution. These two key characteristics allow discrimination between autophagy, which operates on entities that are freely accessible to cytosolic proteins, and vesicular trafficking and other endocytic processes (such as phagocytosis), which operate on entities that originate at the plasma membrane (Galluzzi et al. 2017).

1.4.1. Autophagy mechanisms

Focused investigation into *LRRK2* mutations revealed the first evidence for impaired autophagy and lysosomal dysfunction in cells (Alegre-Abarrategui and Wade-Martins 2009; Gómez-Suaga et al. 2012; Plowey et al. 2008). Autophagy can be defined as the process that regulates recycling of cellular components by degrading dysfunctional or damaged proteins and organelles. There are several types of autophagy, macroautophagy, microautophagy, chaperone-mediated autophagy (CMA) and the recently discovered precision autophagy (Cuervo et al. 2004; Kimura et al. 2015; Manzoni and Lewis 2017). Here we focus on macroautophagy, CMA and microautophagy, as these mechanisms have undergone the most research (Fig 1.7).

1.3.1.1. Macroautophagy

In this project we focused on macroautophagy (henceforth referred to as autophagy). Briefly, cells will respond to certain conditions, such as starvation, through signalling pathways to initiate autophagy. This triggers the formation of the phagophore around the cargo to be degraded, and when the encapsulation is complete it forms an autophagosome. The autophagosome will then fuse with a lysosome (autolysosome) where the cargo will be degraded by lysosomal enzymes (as summarised in Fig. 1.7 A). The main regulators of autophagy are mammalian/mechanistic target of rapamycin complex 1 (mTORC1), adenosine monophosphate-activated protein kinase (AMPK) and phosphoinositol 3 kinase (PI3K)/Beclin-1 that act to activate or repress the formation of autophagic vesicles in response to cellular conditions (Alers et al. 2012; Meley et al. 2006; Chan, Kir, and Tooze 2007; Noda and Ohsumi 1998). To initiate autophagy, mTORC1 is inhibited, thus reducing mTORC1-dependent phosphorylation of ULK1 which consecutively switches to an active state. Subsequently, ULK1 activation stimulates phagophore formation (Kamada et al. 2000). Beclin-1 and the vacuolar sorting protein 34 (VPS34), together with other proteins, form a complex that is recruited to the phagophore to stabilise ULK. VPS34 converts phosphoinositol into phosphoinositol-3-phosphate (PI(3)P) which in turn binds to WD repeat domain phosphoinositide-interacting (WIPI) proteins, to recruit autophagy-related proteins (Atg) (Dikic and Elazar 2018; Behrends et al. 2010). The ubiquitin signal in tagged proteins binds to p62 (also known as sequestosome 1, SQSTM1) which interacts with microtubule-associated proteins 1A/1B light chain 3A (LC3) to target cargo to be enveloped by the newly forming phagophore (Mizushima, Ohsumi, and Yoshimori 2002; Gan-Or, Dion, and Rouleau 2015; Manzoni and Lewis 2017). As such, p62 is a receptor for cargo destined to be degraded by autophagy, including ubiquitinated protein aggregates destined for

clearance, and therefore has been widely used as a marker for early autophagy events. Moreover, pro-LC3 cytosolic is cleaved by Atg-4 to LC3-I, which then covalently conjugates to phosphatidylethanolamine (PE) to LC3-II before being incorporated into the autophagosome membrane. Notably, p62 and LC3 conversion are widely used as markers of autophagosome formation (Yoshii and Mizushima 2017; Mizushima and Yoshimori 2007). Once the phagophore completely engulfs its cargo, it forms an autophagosome, which in turn fuses with the lysosome to form the autolysosome.

The final step in autophagy is the lysosomal degradation of proteins or organelles, such as the mitochondria (designated as mitophagy), mediated by acidic lysosomal hydrolases (Mizushima, Ohsumi, and Yoshimori 2002; Manzoni and Lewis 2017). Maintenance of acidic pH within the range of 4.5-5.0 in lysosomes is essential to activate hydrolytic enzymes and to degrade targeted cellular content (Hu et al. 2015). The low pH in lysosomes is regulated by the vacuolar type H^+-ATPase (vATPase) that pumps protons to the lysosomal lumen against their electrochemical gradient, using the energy obtained from ATP hydrolysis. A counterion flux is established to prevent the lysosome from over-acidifying, by coupling the movement of cations to the cytosol or entry of anions to dissipate the transmembrane voltage generated by the vATPase (Mindell 2012). The TRPML1 cation channel (transient receptor potential cation channel, mucolipin subfamily, member 1) is expressed in lysosomes and late-endosomes and it releases local calcium by transporting Ca^{2+} from the lumen to the cytosol (Ghislat and Knecht 2013; Li et al. 2017). The luminal pore structure of TRPML1 seems to be important for the Ca^{2+} and pH mediated regulation of the channel, where increased pH in lysosomes leads to decreased TRPML1 activity (Li et al. 2017). Additionally, high levels of lysosomal Ca^{2+}, sustained through the maintenance of an acidic pH, are necessary for the Ca^{2+} release that precedes the fusion of lysosomes with autophagosomes or endosomes (Ghislat and Knecht 2013; Li et al. 2017).

1.3.1.2. Chaperone-mediated autophagy

Contrary to macroautophagy, CMA requires chaperone protein Hsc70 to recognise the target substrate through KFERQ-like motifs. Subsequently, Hsc70 binds to lysosomal protein LAMP2A to internalise substrates, which are then degraded by cathepsins (Fig. 1.7 B). CMA is largely responsible for α-synuclein clearance, since α-synuclein contains a recognition motif and is translocated into lysosomes for degradation (Cuervo et al. 2004). The physiological role of LRRK2 and dysfunction in CMA have been recently reviewed by Berwick and colleagues (Berwick et al. 2019). It is reported that LRRK2-G2019S acts on LAMP2A and blocks CMA, affecting lysosomal degradation of proteins

and precipitating the accumulation of α-synuclein in neuronal cells (Orenstein et al. 2013). In concordance, both *LRRK2-G2019S* iPSC-derived astrocyte cultures and *LRRK2-R1441C* knock-in mouse embryonic fibroblasts showed decreased CMA levels (di Domenico et al. 2019; Ho et al. 2019). In parallel to macroautophagy, these effects will undoubtedly contribute to PD pathology through lysosomal damage.

1.3.1.3. Microautophagy

Microautophagy is the least studied form of autophagy, and it occurs when cytoplasmic entities to be degraded are engulfed via direct membrane invagination at the surface of the lysosome or vacuole in a non-specific manner (Farré and Subramani 2004). The underlying molecular mechanism of the cargo delivery process remains largely unclear. A similar mechanism involving late endosomes, designated endosomal microautophagy, requires multiple endosomal sorting complexes required for transport (ESCRT) systems for lysosome or endosome delivery (Sahu et al. 2011; Uytterhoeven et al. 2015; Mukherjee et al. 2016; Galluzzi et al. 2017) (Fig. 1.7 C).

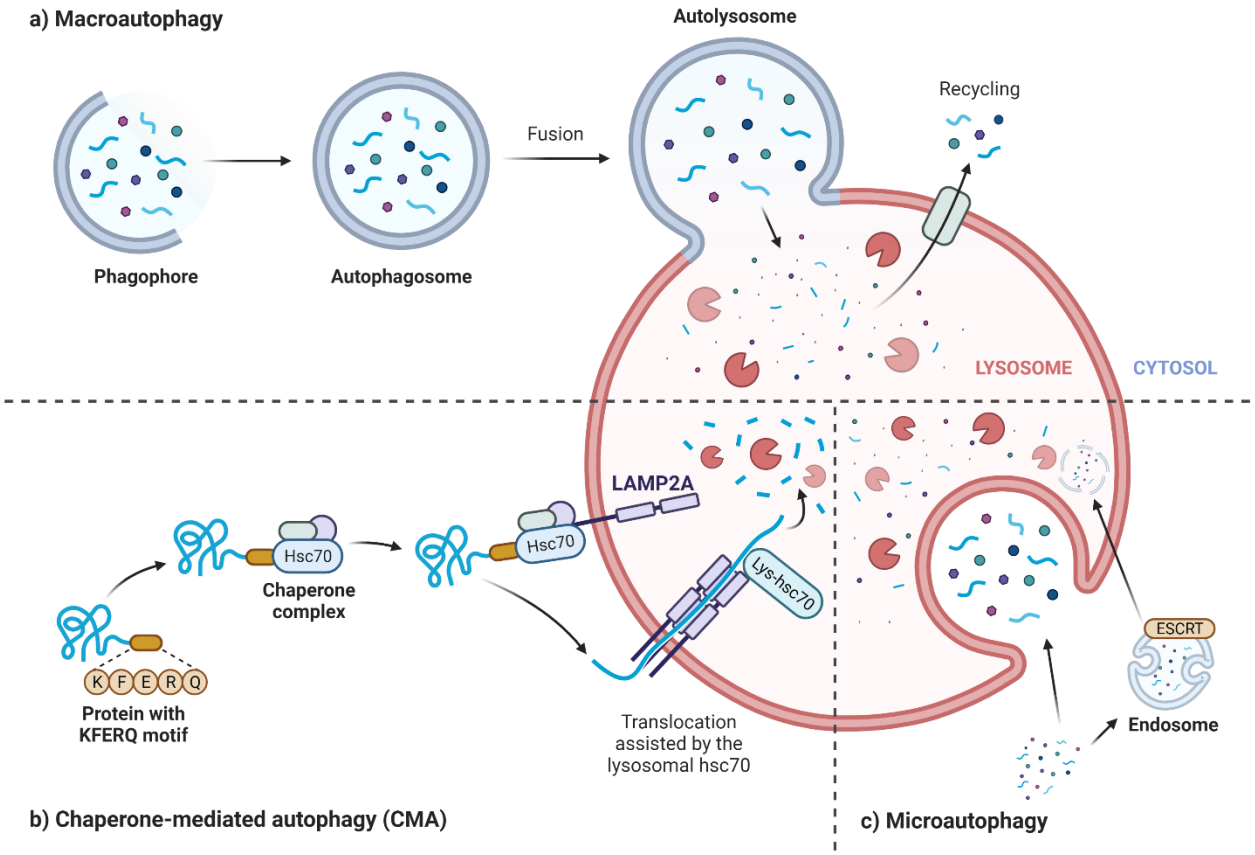

***Figure 1.7. – Main types of autophagy*. (A)** Macroautophagy involves the sequestration of cellular material, the formation of autophagosomes, their fusion with lysosomes, and

lysosomal degradation of the autophagolysosomal content. **(B)** In Chaperone-mediated autophagy (CMA), proteins containing the KFERQ motif are identified in the cytosol by Hsc70 chaperon complexes and taken to the lysosomal surface. Then, these complexes bind to the receptor protein LAMP2A, forming a translocation complex, the protein substrates unfold and cross the lysosomal membrane to be degraded. **(C)** Microautophagy in which material is degraded "in bulk" and endosomal microautophagy in which endosomes engulf cytosolic materials within multivesicular bodies that contain other cytosolic components and degrade these materials upon fusion with lysosomes. The endosomal invagination relies on the ESCRT family of proteins. Adapted from Biorender template.

1.4.2. Autophagy in Parkinson's disease

Considering neuronal cells are in a post-mitotic state, it is crucial that protein recycling is well maintained to ensure normal cellular and synaptic function. Furthermore, α-synuclein can be degraded via proteasome, chaperone-mediated autophagy and autophagy in neurons (Cuervo et al. 2004; Vogiatzi et al. 2008; Webb et al. 2003). Hence, impaired autophagy could cause decreased lysosomal protein degradation and lead to accumulation of aggregated α-synuclein in Lewy bodies. This proposed pathology model has been demonstrated in studies where *in vitro* treatment of neuronal cells with the inhibitor of autophagy initiation 3-MA (3-methyladenine) or knocking out autophagy genes precipitated α-synuclein aggregates to accumulate in vesicle fractions, increased exocytosis of α-synuclein and transcellular transfer of α-synuclein, apoptotic cell death in the recipient cells to rise and dopaminergic axonal and dendritic degeneration to increase (Lee et al. 2013; Ahmed et al. 2012; Friedman et al. 2012). The intricate relation between LRRK2 and α-synuclein will be further addressed in the context of lysosomal function in this chapter.

The complexity of the autophagy-lysosomal pathway (ALP), combined with a broad spectrum of LRRK2 functions and the variety of PD models used, ultimately contribute to LRRK2-associated phenotypes that appear to be conflicting and seemingly difficult to integrate (Manzoni and Lewis 2017). Carefully reviewing the current field of LRRK2 biology, dissecting different models and *LRRK2* mutations will provide a clearer insight into the interplay of LRRK2, autophagy and lysosomal function in fibroblasts, neurons, microglia and astrocytes.

1.5. LRRK2 in the autophagy-lysosome pathway

The LRRK2 literature on autophagy is extensive and, although it is clear LRRK2 has a role in this pathway, the exact point and the direction in which mutations in *LRRK2* affect the pathway have been referred to as uncertain or contradictory (Manzoni 2017; Cookson 2016; Wallings, Manzoni, and Bandopadhyay 2015; Cookson 2017; Madureira, Connor-Robson and Wade-Martins 2020). Nevertheless, multiple studies have concluded that this complex protein is implicated in PD and linked to impaired autophagy and dysfunctional lysosomal activity (Cherubini and Wade-Martins 2018; Wallings, Manzoni, and Bandopadhyay 2015; Cookson 2017; Manzoni and Lewis 2017; Wallings, Connor-Robson, and Wade-Martins 2019; Schapansky et al. 2018; Henry et al. 2015; di Domenico et al. 2019; Manzoni et al. 2013). Therefore, it is crucial to understand the role of LRRK2 in autophagy to allow the development of new therapies.

1.5.1. Phagophore biogenesis

Once autophagy is initiated through canonical mTORC1, AMPK or PI3K/Beclin-1 signalling pathways, the phagophore starts to encapsulate the cargo for degradation. In this early stage of autophagy, increased phosphorylation of p62 selectively binds to both ubiquitinated proteins and LC3, recruiting them to the nascent phagophore.

Treatment of mouse astrocyte primary cultures with LRRK2 kinase inhibitor LRRK2-in-1 has been reported to activate autophagy and increase LC3-II levels through an active Beclin-1 complex non-canonical pathway that is mTORC1 and ULK1 independent (Manzoni et al. 2016). In parallel, *LRRK2-G2019S* iPSC-derived astrocyte cultures showed increased autophagic vacuoles, decreased autophagosome-lysosome fusion and scattered, rather than perinuclear, distribution of lysosomes (di Domenico et al. 2019). Taken together, these findings imply that LRRK2 kinase activity represses autophagy in astrocytes (Fig. 1.9).

Interestingly, prolonged inhibition of LRRK2 kinase activity in primary astrocyte cultures also showed an altered phosphorylation state of ULK1, in a mTORC1 independent manner. This uncovers a non-canonical ULK1 pathway, independent from mTORC1, that is still poorly characterised and raises the possibility that LRRK2 inhibitors for PD treatment could ultimately have the undesired effect of astrocyte autophagy dysregulation (Manzoni et al. 2018). Kalogeropulou and colleagues showed the cargo sequestration protein p62 has been reported to be a novel phosphorylation substrate of LRRK2 *in vitro* in human embryonic kidney 293 (HEK) cells and rat neuronal cultures.

The N-terminus of LRRK2, the Ser910/935 phosphorylated residues of LRRK2 and the C-terminus of p62 are all necessary for this interaction, at which LRRK2 phosphorylates the Thr138 residue in the ZZ domain of p62. Moreover, *LRRK2* mutations (*N1437H, R1441C/G/H, Y1699C, G2019S*) all increase phosphorylation of p62 (Table 1.1). Phosphorylation of p62 was blocked when treating cells with LRRK2 kinase inhibitors MLi-2, PF745 and GNE1023. Co-expression of LRRK2-G2019S with p62 exhibited an increased neurotoxicity compared to LRRK2-G2019S with unphosphorylatable p62 (Kalogeropulou et al. 2018). However, previous work in overexpressing *LRRK2-WT* HEK models has also demonstrated that both *LRRK2-WT* and mutant *LRRK2-G2019S* indirectly reduce phosphorylation of p62, which in turn decreases its affinity to ubiquitinated cargo, thus decreasing autophagic protein degradation (Table 1.1). Notably, two different sites of p62 demonstrated increased phosphorylation in *LRRK2* knock-down (KD) cells, using a lentivirus-mediated shRNA *Lrrk2* KD in rat primary cortical neurons (Park et al. 2016). This is supported by the fact that p62 phosphorylation is associated with initiation of autophagy (Liu et al. 2016). Additionally, the relationship between LRRK2 and p62 seems to be bidirectional, where LRRK2 phosphorylates p62 (Fig. 1.8) and p62 overexpression leads to LRRK2 degradation through the autophagy-lysosomal pathway. LRRK2 indirectly regulates the phosphorylation of two different residues in the SMIR domain of p62 (Ser351 and Ser403), leading to p62-mediated autophagy that degrades ubiquitinated LRRK2 (Park et al. 2016). As is apparent from the above, the interplay between LRRK2 and p62 is not fully understood and examining this will be vital to characterise its role in autophagy initiation.

Leucyl-tRNA synthetase (LRS) is a modulator of autophagy as it is responsible for the attachment of leucine to $tRNA^{Leu}$, followed by activation of mTORC1 which blocks autophagy (Han et al. 2012). LRRK2 has been reported to regulate LRS by phosphorylating its conserved editing domain at residue T293, which increases the amount of misfolded proteins that accumulate, leading to ER stress and induced autophagy. Introducing the *LRRK2-G2019S* mutation increased kinase activity causing LRS to be phosphorylated, culminating in exacerbated autophagy (Fig. 1.8) (Ho et al. 2018). This unveils a new pathological pathway for LRRK2 in PD and investigation of other *LRRK2* mutations should be pursued in the future to corroborate this model. Nevertheless, it seems that LRRK2 is involved in regulating autophagy for auto-degradation through interaction with p62 and could contribute to phagophore biogenesis in ER stress conditions.

1.5.2. Autophagosome formation

Following the formation of the phagophore and respective closing around the cargo, a vacuole composed of a lipidic bilayer membrane is formed, designated as the autophagosome. LC3-I and LC3-II are present in phagophores and autophagosomes, so it is difficult to discern between these two autophagic components (Mizushima and Yoshimori 2007; Yoshii and Mizushima 2017; Klionsky et al. 2016). Moreover, the LC3-II/LC3-I ratio is used as an autophagy marker, however this ratio alone does not provide sufficient data to distinguish between increased autophagosome biogenesis and reduced autophagosome clearance, therefore requiring additional immunohistochemistry techniques to properly measure this phase of autophagy (Cookson 2016; Mizushima and Yoshimori 2007; Klionsky et al. 2016).

A transgenic mouse model of human WT and mutant *LRRK2* overexpression, showed *LRRK2-G2019S* cultured dopaminergic neurons (DAn) demonstrate age-dependent degeneration and also manifest an increased number of autophagic vacuoles, which reduced neurite complexity. *LRRK2-G2019S* transgenic mice also showed enlarged autophagic vacuoles *in vivo* (Ramonet et al. 2011). Yet, in neuronal cultures treated with LRRK2 kinase inhibitor LRRK2-in-1, there was an increase in LC3-II and p62 levels (Manzoni et al., 2013). Combining LRRK2-in-1 treatment with bafilomycin A1, which blocks autophagosome-lysosome fusion by inhibiting vATPase activity, resulted in increased LC3-II levels. This suggests LRRK2 acts to block autophagosome formation (Manzoni et al., 2013). Since then, a new generation of more specific LRRK2 kinase inhibitors have been developed, such as MLi-2, PF-06447475 and GSK2578215A (Atashrazm and Dzamko 2016). Concomitantly, an increase in LC3B and p62 protein levels in *LRRK2-G2019S* 12–19-month-old mice brain lysate corroborates this observation *in vivo* (Ho et al., 2018). This finding was also confirmed *in vitro* using primary astrocytes cultured from a *Lrrk2* knock-out (*Lrrk2*-KO) mouse model (Manzoni et al. 2016) and by treating SH-SY5Y neurons and astrocyte cultures with the potent GSK2578215A inhibitor (Saez-Atienzar et al. 2014; Manzoni et al. 2016) (Table 1.1). In concordance with these findings, a study in human induced pluripotent stem cell derived dopaminergic neurons differentiated from idiopathic or *LRRK2-G2019S*-PD patients, reported increased p62 and LC3-II levels after treatment with leupeptin and NH_4Cl to inhibit lysosomal degradation, when compared to control DAn, indicating a blockage of autophagosome clearance (Sánchez-Danés et al. 2012). Similarly, a recent characterisation of the autophagic pathway in rat cortical primary cultures expressing human wildtype *LRRK2* (*LRRK2-hWT*) or human *LRRK2-G2019S* detected decreased

levels of LC3 puncta compared to non-transgenic cultures (nTG) after treatment with trehalose, a compound to induce lysosomal biogenesis, but no changes in LAMP1, which is a well-established lysosomal marker. Hence, these data suggested that *LRRK2-hWT* and *LRRK2-G2019S* inhibit autophagosome biogenesis.

Taken together, these results demonstrate that overexpressing *LRRK2-hWT* or *LRRK2-G2019S* blocks autophagosome formation in neuronal cells (Wallings, Connor-Robson, and Wade-Martins 2019; Manzoni et al. 2016; Saez-Atienzar et al. 2014; Manzoni et al. 2013; Sánchez-Danés et al. 2012; Ramonet et al. 2011), which is ameliorated by LRRK2 kinase inhibition (Saez-Atienzar et al. 2014; Manzoni et al. 2013) (Fig. 1.9). Even though the reports mentioned in this section take advantage of different models and conditions, they consistently show increased levels of LC3-II. Thus, it is possible to speculate that both overexpression of LRRK2-WT or LRRK2-G2019S would act to block autophagosome biogenesis and clearance, giving rise to non-processed autophagic vacuoles.

1.5.3. Autophagosome and lysosome fusion

The next step in the autophagy process is the fusion of the autophagosome with a lysosome to form the autolysosome. Recent efforts to characterise the autophagic pathway in rat cortical primary cultures expressing human *LRRK2* demonstrated an increased co-localisation of *LRRK2-R1441C* puncta to LAMP1, placing mutated LRRK2 at the lysosome. Furthermore, decreased co-localisation of LC3 and LAMP1 puncta in *LRRK2-R1441C* cultures indicates decreased autolysosome count. Hence, this suggested a deficient autophagosome-lysosome fusion in *LRRK2-R1441C* neuronal primary cultures (Fig. 1.9) (Wallings, Connor-Robson, and Wade-Martins 2019). Contrastingly, work using a mouse conditional transgenic model under the ROSA26 promoter in a Cre-recombinase-dependent system to selectively express *LRRK2-R1441C* in midbrain dopaminergic neurons did not show any abnormality in autophagic markers p62 and LC3 *in vivo* (Tsika et al. 2014). However, the authors do not reference any lysosomal markers to assess autophagic flux and this conditional transgenic model did not present any motor deficits or nigral dopaminergic neurodegeneration, contrary to other LRRK2 transgenic models (Li et al. 2009; Ramonet et al. 2011; Sloan et al. 2016). In parallel, in a culture of iPSC-derived *LRRK2-G2019S* astrocytes, there was a decreased co-localisation of LC3 and LAMP1 in astrocytes, suggesting the autophagosome-lysosome fusion step was repressed (di Domenico et al. 2019). Together this work demonstrates that mutations in *LRRK2* can affect the autophagy

pathway in both neurons and astrocytes in the same way (Table 1.1). When exposing SH-SY5Y neuronal cultures to the LRRK2 kinase inhibitor GSK2578215A for a prolonged period, autolysosome count was also reduced (Saez-Atienzar et al. 2014). Furthermore, the impaired autophagosome-lysosome fusion reported in *LRRK2-G2019S* models might result in the presence of enlarged, dysfunctional autophagic vacuoles (Fig. 1.8) (Plowey et al. 2008). These structures could be interpreted either as abnormal large autophagosomes (Sánchez-Danés et al. 2012) or as enlarged lysosomes (MacLeod et al. 2006), which could lead to confounding conclusions on G2019S-related autophagy phenotypes. It is noteworthy to state these two reports were carried out in human iPSC-derived DAns and rat primary cortical cultures, respectively, thus this role of LRRK2 appears to be conserved across the two species and cell types.

Work by Manzoni and colleagues concluded that a LRRK2-dependent increase in autophagosomes was not caused by a decline in autophagosome-lysosome fusion but by an increase in autophagosome biogenesis (Manzoni et al. 2016). Although, a caveat of that study was that measurement of autophagosomes (LC3-II/LC3-I) and lysosomal function was conducted in H4 neuroglioma cell cultures. Caution should be taken given that autophagy has been reported to be upregulated in H4 neuroglioma cancer cells to overcome stress induced apoptosis (Zhou et al. 2016), unlike in PD neuronal models where autophagy is deficient. On the other hand, a study by Obergasteiger and colleagues using SH-SY5Y cells overexpressing *LRRK2-WT* or *LRRK2-G2019S* shows that *LRRK2-G2019S* neurons present with increased LC3-II protein levels and LC3B puncta, indicating an autophagosome accumulation. Measurement of autolysosome production using a double-tagged GFP-LC3-mCherry construct in this model showed autolysosomes were reduced in *LRRK2-G2019S* when compared to *LRRK2-WT*, suggesting a defective autophagosome-lysosome fusion (Fig. 1.8). Proteolytic activity of lysosomes assessed with DQ-Red-BSA assay demonstrated LRRK2-G2019S induced a defect in lysosomal activity, culminating in an accumulation of endogenous α-synuclein inclusions. Defects in autophagosome-lysosomal fusion, proteolytic impairment and α-synuclein accumulation phenotypes were rescued after treatment with the PF-475 LRRK2 kinase inhibitor, highlighting the importance of LRRK2 in autophagy-mediated α-synuclein degradation (Obergasteiger et al. 2020). Hence, there is robust evidence that demonstrates the two most common *LRRK2* mutations, G2019S and R1441C, lead to an obstruction of the fusion between autophagosomes and lysosomes and result in the presence of large dysfunctional autophagic vacuoles.

1.5.4. Lysosomal function

After the autolysosome is formed, the maintenance and regulation of lysosomal function, including correct lysosomal acidity, is crucial for protein degradation and recycling. It is important to maintain the lysosomal pH at around 4.5-5.0 as hydrolytic enzymes in the lysosome are only active at a narrow acidic pH interval (Hu et al. 2015). Investigation of *LRRK2-R1441C* cortical primary cultures demonstrated lysosomal pH was significantly less acidic in these neurons and consequently autophagosome-lysosome fusion and lysosomal protein degradation were decreased (Wallings, Connor-Robson, and Wade-Martins 2019). Furthermore, *LRRK2-R1441C* neuronal cultures also demonstrated significantly increased intracellular calcium stores driven specifically by increased lysosomal calcium levels. In addition, *LRRK2-R1441C* cultures were shown to have significantly reduced lysosomal calcium release through TRPML1 channels in the lysosomal membrane (Table 1.1). Calcium release from lysosomes is a key step for the autophagosome-lysosomal fusion and also for the late endosomal-lysosomal fusion (Ghislat and Knecht 2013). This work also revealed a novel interaction between LRRK2 and subunit a1 of the proton pump vATPase, for which the encoding gene *ATP6V0A1* is also a GWAS hit for increased risk in PD (Chang et al. 2017). This interaction was severely decreased in the *LRRK2-R1441C* neurons (Wallings, Connor-Robson, and Wade-Martins 2019).

Several authors have reported enlarged lysosomes in different *LRRK2-G2019S* models, including SH-SY5Y neurons, transgenic mice models, primary cortical neurons, primary astrocytes and human *post-mortem* tissue (Bang et al. 2016; Hockey et al. 2015; Henry et al. 2015; Dodson et al. 2014; MacLeod et al. 2006; MacLeod et al. 2013; Higashi et al. 2009; Ramonet et al. 2011) as well as in *LRRK2-R1441C* and *LRRK2-Y1699C* mouse primary astrocytes (Henry et al. 2015). Enlarged lysosomes also appeared to be perinuclear and aggregated in *LRRK2-G2019S* derived fibroblasts and were normalised after treatment with LRRK2 kinase inhibitors. This abnormal lysosomal morphology was also rescued by blocking TPC2, an endo-lysosomal ion channel implicated in Ca^{2+} signalling from acidic organelles (Hockey et al. 2015).

Primary cortical neurons from a *LRRK2-G2019S* knock-in mouse model also described similar lysosomal phenotypes as *LRRK2-R1441C* rat primary cortical neurons described above, where lysosomal pH was aberrantly increased exceeding physiological values (Wallings, Connor-Robson, and Wade-Martins 2019; Schapansky et al. 2018). In addition, perinuclear and distal lysosomal count was increased while lysosomal size was decreased in *LRRK2-G2019S* neurons, reflecting altered lysosomal function. Reported

lysosomal dysfunction was associated with accumulation of endogenous, detergent-insoluble α-synuclein and increased neuronal α-synuclein release into the media (Schapansky et al. 2018) (Table 1.1). In parallel, a model of *LRRK2* overexpression in HEK cells has demonstrated that LRRK2-G2019S inhibits the activity of lysosomal enzymes Cathepsin B and L that play a vital part in lysosomal α-synuclein degradation (McGlinchey and Lee 2015). This debilitated lysosomal function led to inhibition of the lysosomal degradation of α-synuclein, promoting its aggregation. This mechanism could underlie LRRK2 and α-synuclein pathology, characteristic of PD. Given the *LRRK2-G2019S* induced inhibitory effect on Cathepsins B and L was not dependent on kinase activity (Hu et al. 2018), it would be interesting to verify this finding in other *LRRK2* mutations, in addition to confirming it in neuronal cell models. A transcriptomic analysis of autophagy related genes in SH-SY5Y cells overexpressing *LRRK2-WT* or *LRRK2-G2019S* also found altered mRNA levels of *CTSB*, which encodes for Cathepsin B (Obergasteiger et al. 2020). Overexpression of *LRRK2-G2019S* in cultured neurons and dopaminergic neurons in the rat SNpc exhibited an accumulation of α-synuclein inclusions after exposure to sonicated α-synuclein fibrils, when compared to nTG and to *LRRK2-WT*. These α-synuclein inclusions decreased after treatment with two separate LRRK2 kinase inhibitors, rescuing the accumulation of α-synuclein in the *LRRK2-G2019S* neurons and implicating LRRK2 kinase activity in the observed phenotype. Additionally, Volpicelli-Daley and colleagues have demonstrated that *LRRK2-WT* overexpression did not induce α-synuclein inclusions (Volpicelli-Daley et al. 2016). Collectively, these studies suggest a putative role of LRRK2 in α-synuclein accumulation.

Nonetheless, the interaction between LRRK2 and α-synuclein remains unresolved, with some reports being inconsistent. For instance, while one study concluded that inhibiting endogenous LRRK2 kinase activity by incorporating MLi-2 into the diet of an α-synuclein PFF PD mouse model did not protect neurons from α-synuclein pathology or motor deficits (Henderson et al. 2019), another study showed that administering the HG-10-102-01 LRRK2 kinase inhibitor intraperitoneally to transgenic mice overexpressing human WT α-synuclein significantly reduced trans-axonal α-synuclein aggregates and phosphorylated α-synuclein in different brain regions of transgenic mice (Bae et al. 2018). However, the results presented by Henderson et al. and Volpicelli-Daley et al. taken together could suggest that it is mutated *LRRK2* that increases the progression of pathological α-synuclein inclusions by increasing a pool of α-synuclein that is more susceptible to forming inclusions. These observations along with studies demonstrating α-synuclein is processed by lysosomes in cell models overexpressing LRRK2 (Hu et al.

2018; Obergasteiger et al. 2020), underline the prospects of targeting lysosomal function as novel drug-developing avenues worth pursuing for LRRK2-related PD.

To summarise, evidence has been accumulating for the key role of LRRK2 and lysosomal function in PD. The studies discussed above indicate that the *LRRK2* mutations G2019S and R1441C present altered lysosomal pH and consequently affect lysosomal activity and protein degradation (Bang et al. 2016; Hockey et al. 2015; Henry et al. 2015; Dodson et al. 2014; MacLeod et al. 2013; Higashi et al. 2009; Ramonet et al. 2011; Schapansky et al. 2018; Hu et al. 2018; Wallings, Connor-Robson, and Wade-Martins 2019). Indeed, lysosomal markers LAMP1, Cathepsin D and HSP73 are decreased in PD nigral tissue, as well as increased α-synuclein aggregates, when compared to age-matched controls (Chu et al. 2009). A recent report described how repurposing clioquinol, an anti-parasitic drug, could be used to revert autophagic impairment and lysosomal dysfunction phenotypes in a neuronal *LRRK2-R1441C* model, demonstrating the ability to modulate such phenotypes (Wallings, Connor-Robson, and Wade-Martins 2019). Therefore, it will be important to further investigate the role of mutated *LRRK2* in lysosomal maturation, maintenance of lysosomal pH and lysosomal calcium homeostasis in the future.

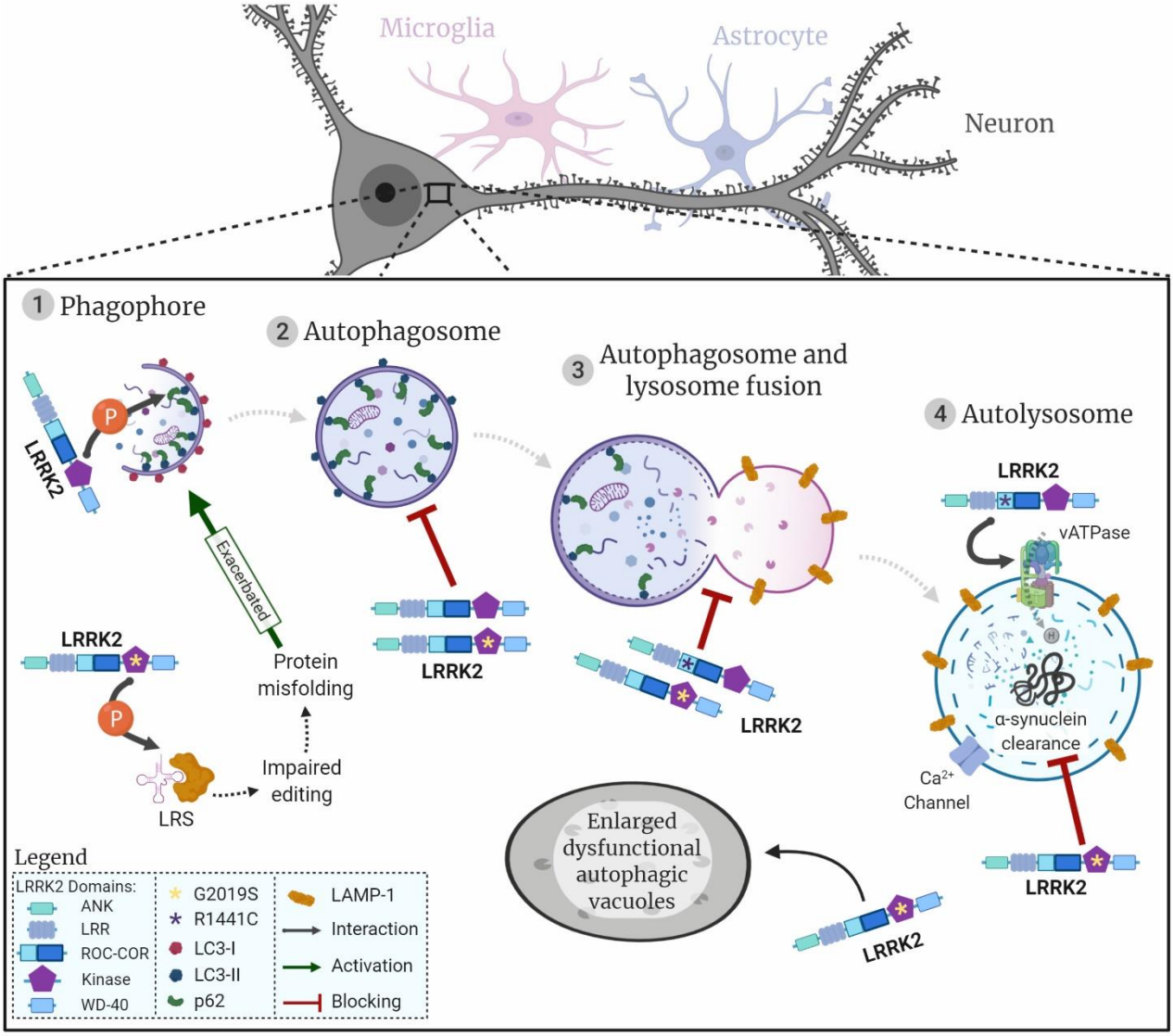

Figure 1.8 – LRRK2 and the neuronal autophagy-lysosomal pathway. Representation of the autophagic process in neuronal cells, initiated with the generation of the phagophore surrounding the cargo to be degraded (1). Once the cargo is fully encapsulated by a bi-layered membrane the autophagosome (2) fuses with the lysosome (3) to produce the autolysosome (4). Proteins/organelles are degraded via lysosomal enzymes. The diagram shows how LRRK2 wildtype and the two most common LRRK2 mutations are likely to impact autophagic flow and lysosomal protein degradation. LRRK2 is represented by its respective domains (ANK, LRR, ROC, COR, Kinase and WD-40). LRRK2 mutations are represented by asterisks in the respective domains where they are located. G2019S: yellow asterisk in kinase domain; R1441C: purple asterisk in ROC domain; interactions represented by arrows; flow of autophagic phases represented by dashed arrows.

1.5.5. Regulation of the autophagic flux

In this section we will focus on several LRRK2 models that strongly suggest both excessive and diminished LRRK2 activity can lead to impaired autophagic flux (Schapansky et al. 2014). In turn, either an exacerbated or insufficient autophagic flux could lead to neurodegeneration which is observed in PD pathology (Chu 2006). Specifically, disturbances in autophagy impose downstream effects on neurons, such as accumulation of non-degraded α-synuclein and its respective release into extracellular media (di Domenico et al. 2019; Schapansky et al. 2018; Obergasteiger et al. 2018; Henry et al. 2015), reduced neurite outgrowth (MacLeod et al. 2006) and impaired mitophagy (Su, Guo, and Qi 2015; Su and Qi 2013). These PD phenotypes caused by dysfunctional ALP indicate autophagy and lysosomal activity could, in part, be underlying the molecular basis for this neurodegenerative disorder. Abnormal LRRK2 function can lead to impaired autophagy and lysosomal function due to a disruption in the cellular autophagic flux, yet different cell types present with distinct cellular bioenergetic needs and protein turnover rates. Accordingly, in efforts to create a clear picture of the role of LRRK2 in autophagic flux, we individually review the autophagic flux in fibroblasts, neurons and microglia/astrocyte LRRK2 models (Fig. 1.9).

Currently, one of the main challenges in the LRRK2 autophagy field is the measurement of autophagic flux. Since autophagic flux is a dynamic process occurring within cells, it is crucial to utilise a combination of methods that would enable an interpretation of the several different stages of autophagy, from phagophore biogenesis to lysosomal degradation of cargo. Techniques such as measurement of autophagic markers by western blot have limitations. For instance, the autophagic marker LC3 is expressed throughout different stages of autophagy, making it difficult to interpret autophagic alterations by analysing LC3 changes alone. Thus, autophagic marker measurement would normally represent a single time point in the autophagic flux. By combining these approaches with immunofluorescence, co-localisation and pH sensitive dyes, it is possible to obtain a more accurate picture of the autophagic flux.

1.5.5.1. Fibroblasts

Fibroblasts can be obtained from patients in a safe, non-invasive and inexpensive manner and have been widely used in reprogramming techniques to obtain iPSCs, which in turn can be differentiated into iPSC-derived neurons (Bahmad et al. 2017). Despite

being a non-neuronal model, fibroblasts are useful cellular models to investigate and predict PD pathology.

In fibroblasts isolated from patients with *LRRK2-R1441C* and *LRRK2-Y1699C* mutations (located in the ROC-COR domains) undergoing starvation, there was a decrease in WIPI2 and p62 puncta and a decrease in LC3-II/LC3-I ratio, suggesting a decreased autophagic flux (Fig. 1.9). In the case of *LRRK2-G2019S* isolated fibroblasts under starvation conditions, cells showed a decrease in LC3-II/LC3-I ratio while WIPI2 and p62 levels were not significantly altered compared to wildtype fibroblasts. It is important to add that immunoblot (IB) for LAMP1 did not show differences in any of the mutations studied, indicating a disruption of autophagy upstream of the lysosomes. However, this finding was not confirmed with immunocytochemistry techniques (Manzoni et al., 2013). When comparing fibroblasts from skin biopsies of *LRRK2-G2019S* individuals not manifesting PD symptoms, *LRRK2-G2019S* PD patients and healthy controls, non-manifesting *G2019S* demonstrated upregulated autophagy and preserved mitochondrial function while fibroblasts from *LRRK2-G2019S* PD patients presented with elevated p62 levels, reduced LC3-II ratios and mitochondrial dysfunction. Thus, implicating exhaustion of mitochondrial bioenergetic and autophagic reserve in the development of PD (Juárez-Flores et al. 2018). Collectively, these studies indicate decreased autophagic flux in *LRRK2-G2019S* fibroblasts (Fig. 1.9) (Juárez-Flores et al. 2018; Manzoni et al., 2013).

On the other hand, in a separate study PD *LRRK2-G2019S* fibroblasts had decreased p62, but showed an increase in Beclin-1, LC3, LAMP1 and Cathepsin B, culminating in an increase of autophagic flux and lysosomal activity, in basal conditions (Fig. 1.9, Table 1.1) (Bravo-San Pedro et al. 2013). The authors use LAMP2 as a lysosomal marker and levels were reported to be increased (Bravo-San Pedro et al. 2013). However, LAMP2A has been implicated in CMA (Bandyopadhyay et al. 2008), and since LAMP1 was not measured it could be hypothesised that the increase in autophagic flux can represent an increase in CMA specifically, rather than macroautophagy.

A similar model reported excessive autophagic flux in the context of increased mitophagy in primary fibroblasts from *LRRK2-G2019S* PD patients, as a consequence of mitochondrial depolarization and dysfunction (Su, Guo, and Qi 2015; Su and Qi 2013). It is important to note the studies had different autophagy cellular contexts (basal *vs.* starvation) and fibroblasts were cultured in slightly different conditions. Mutated *LRRK2* autophagic phenotypes have been described as contradictory (Manzoni and Lewis 2017; Manzoni 2017; Cookson 2016). However, since LRRK2 physiological function in fibroblasts is not completely understood, perhaps it is not entirely unexpected that

LRRK2-G2019S would display different results under distinct conditions, once again highlighting the importance of comparing between similar cell types and culture conditions, for instance basal *vs.* starvation.

It is equally important to adopt a consistent method for autophagic flux analysis. If the same markers and conditions were to be applied across the field in a more conventional and consistent manner, it would become easier to compare and interpret the literature. Other cell types, for instance HEK and PC12 (rat pheochromocytoma cells from the adrenal medulla) overexpressing human LRRK2, have shown an increased autophagic flux in the presence of *LRRK2-WT* and *LRRK2-G2019S*, through Ca^{2+}-dependent activation of a CaMKK/adenosine monophosphate (AMP)-activated protein kinase pathway (Gómez-Suaga et al. 2012). Nonetheless, these cellular models do not entirely recapitulate neurodegeneration and would need further confirmation.

1.5.5.2. Neurons

Given the clear loss of SNpc dopaminergic neurons in PD, research has focused on understanding the neuronal role of LRRK2 through numerous models. Analysis of autophagic markers in *Lrrk2*-KO primary cortical neurons demonstrated no significant changes in p62 and LAMP1 levels, yet showed increased LC3-II conversion and importantly, increased lysosomal protein degradation, when compared to WT using the pulse chase assay (Wallings, Connor-Robson, and Wade-Martins 2019). Contrary to previous *Lrrk2-KO* literature conveying there were autophagic changes in the kidney but not in the brain (Tong et al. 2012), this indicates an increase in autophagic flux in *Lrrk2*-KO neurons (Fig. 1.9) (Wallings, Connor-Robson, and Wade-Martins 2019). However, a novel double *Lrrk* knock-out (DKO) mouse model in which both *Lrrk1* and *Lrrk2* are deleted, meaning LRRK1 does not compensate for the lack of LRRK2*,* reported a decrease in autophagic flux in neurons (Fig. 1.9). This was evidenced by increased p62, decreased LC3-I and increased LC3-II levels in different sub-regions of the *Lrrk*-DKO mouse brain, including SNpc and striatum. Quantitative electron microscopy (EM) analysis also demonstrated age-dependent accumulation of autophagosomes and autolysosomes in the SNpc of *Lrrk*-DKO mouse, and consequent autophagy impairment. Interestingly, autophagic dysfunction was observed at 10 months and preceded accumulation of α-synuclein and dopaminergic neurodegeneration (seen at 15 months), indicating disrupted autophagy can lead to PD pathology (Giaime et al. 2017). When comparing *Lrrk2*-KO mouse model phenotypes with *LRRK2* mutant models some similarities emerge, with the autophagosome processing stages of autophagy being

particularly affected (Table 1.1). While *Lrrk2*-KO shows blocked autophagosome biogenesis, *Lrrk*-DKO, *LRRK2-G2019S* and *LRRK2-R1441C* show blocked clearance of autophagosomes into autolysosomes (Manzoni et al. 2016; Giaime et al. 2017; Wallings, Connor-Robson, and Wade-Martins 2019; di Domenico et al. 2019; Ramonet et al. 2011; Sánchez-Danés et al. 2012; Ho et al. 2018; Obergasteiger et al. 2020). Given LRRK2 is a complex protein involved in several different functional processes in the cell, considering mutations in *LRRK2* in a strict binary loss or gain of its normal function might not reflect the full scope of the *LRRK2* mutant effects in its downstream pathways.

As discussed above, *Lrrk2* knock-down in rat primary cortical neurons exhibit increased p62 phosphorylation (Park et al. 2016), which in turn promotes phagophore biogenesis and is associated with autophagy initiation. Nevertheless, this study did not measure other important autophagic markers such as LC3 and LAMP1.

Early evidence in cultured HEK cells where *LRRK2* was knocked-down with siRNA showed increased turnover of lipidated LC3, measured by the LC3-I and LC3-II ratio, which reflected an increased autophagic activity (Alegre-Abarrategui et al. 2009). However, the lack of evidence on the effects of neuronal LRRK2-KD in autophagy means further validation is necessary to conclude whether it induces an increase in autophagic flux. Comprehensive characterisation of autophagy and lysosomal function in rat primary cortical neurons expressing human *LRRK2-G2019S* and *LRRK2-R1441C* has revealed this pathway is compromised whereas those from *Lrrk2*-KO rats demonstrate an upregulation of autophagic flux. In the case of *LRRK2-hWT* and *LRRK2-G2019S* neurons, there was an inhibited autophagosome production, while in *LRRK2-R1441C* expressing neurons there was a decreased autophagosome-lysosome fusion and lysosomal dysfunction (Wallings, Connor-Robson, and Wade-Martins 2019). In agreement with these findings, a non-neuronal model overexpressing *LRRK2-R1441C* in HEK cultures also described accumulation of large autophagic vacuoles, increased p62 and decreased protein degradation, which translated into an impaired autophagic balance (Alegre-Abarrategui et al. 2009). This shows similar phenotypic alterations in autophagy in two separate studies and cell types. Measuring lysosomal protein degradation using the pulse-chase assay, arguably the most accurate method for measuring true autophagic flux, uncovered an overall decreased lysosomal degradation across the LRRK2 genotypes, with the *LRRK2-R1441C* resulting in the most significant alteration. In parallel, there was also an increase in LC3 puncta *in vivo*, in *LRRK2-R1441C* dopaminergic neurons of the SNpc of 22-month-old animals, when compared to nTG. Consequently, neuronal autophagic flux was decreased in *G2019S* and *R1441C*

mutations (Wallings, Connor-Robson, and Wade-Martins 2019). Equally, mouse primary neuronal cortical cultures overexpressing *LRRK2-G2019S* showed decreased LC3-I and LAMP1 levels and increased basal levels of LC3-II. The decreased LC3-I and LAMP1 levels were also confirmed *in vivo*, in 20-month-old *LRRK2-G2019S* knock-in mouse cortical tissue. *LRRK2-G2019S* neurons had increased number yet smaller lysosomes that were mis-localised and had less acidic pH. This points to poor lysosomal activity and decreased autophagosome turnover in *LRRK2-G2019S* neurons and consequently, a significantly decreased autophagic flux. ALP disruption increased α-synuclein accumulation and release from neurons, which were rescued with the LRRK2 kinase inhibitor GSK2578215A (Schapansky et al. 2018).

Research into dopaminergic neurons derived from iPSCs of familial PD patients with the *LRRK2-G2019S* mutation and of idiopathic PD patients, cultured during a prolonged period (up to 75 days) induces stress conditions that mimicked *in vivo* aging in patients. These iPSC-derived DAns showed decreased LC3 flux and co-localisation of LC3/LAMP1, accumulated autophagic vesicles and decreased lysosomal function when compared to healthy controls, thus indicating a reduced autophagic flux (Fig. 1.9). *LRRK2-G2019S* neurons also showed a decreased number and length of neurites (Sánchez-Danés et al. 2012). Similarly, analysis of autophagic markers in the basal ganglia of *LRRK2-G2019S* patient *post-mortem* tissue showed a decrease in p62 and LAMP1 in comparison to matched idiopathic PD patients, assessed both by immunohistochemistry and immunoblotting (Mamais et al. 2018). Furthermore, overexpression of human *LRRK2-WT* in *C. elegans* dopaminergic neurons improved autophagy throughout their life span whereas *LRRK2-G2019S* and *LRRK2-R1441C* expression inhibited autophagy (Fig. 1.9). *LRRK2-G2019S* expression accelerated age-related loss of autophagic function and co-expression of either mutant or WT LRRK2 with α-synuclein further accentuated inhibition of autophagy and DA neuronal death (Saha et al. 2015). In agreement, various other models have indicated *LRRK2-G2019S* leads to impaired autophagy and lysosomal function, such as follicle cells in Drosophila Melanogaster (Dodson et al. 2012; 2014), human neuroepithelial stem cells (Walter et al. 2019) and HEK cells (Hu et al. 2018). Induced protein quality control-associated autophagy was also impaired in both SH-SY5Y neurons and transgenic mice overexpressing LRRK2-G2019S (Bang et al. 2016).

Attempting to draw conclusions from LRRK2 and its role in ALP has resulted in conflicting reports. Analysing both *LRRK2-G2019S* patient derived iPSC models and models overexpressing *LRRK2-G2019S* there is consensus that the G2019S mutation leads to

a decrease in autophagic flux (Juárez-Flores et al. 2018; Manzoni et al. 2013; Wallings, Connor-Robson, and Wade-Martins 2019; Schapansky et al. 2018; Saha et al. 2015; Sánchez-Danés et al. 2012; di Domenico et al. 2019) (Table 1.1). This change is likely attributed to an increase in kinase activity as evidenced by rescue of autophagic flux when using LRRK2 kinase inhibitors (Saez-Atienzar et al. 2014; Manzoni et al. 2013; Wallings, Connor-Robson, and Wade-Martins 2019).

Since LRRK2 function is not yet fully understood, it is important to investigate the role of wildtype LRRK2 in autophagy under physiological conditions in neuronal cell systems. To this effect, knock-down and knock-out studies of LRRK2 revealed an increased autophagic flux (Wallings, Connor-Robson, and Wade-Martins 2019; Park et al. 2016). Interestingly, contrary to *Lrrk2*-KD in neuronal cells, *Lrrk2*-KD in microglia suggested deficits in the induction of autophagy, although only one autophagy marker was analysed along with protein clearance, as discussed below in this chapter (Schapansky et al. 2014). This highlights once more the degree of LRRK2 phenotypic cellular heterogeneity. Furthermore, a *Lrrk2*-KO mouse model detected phenotypic alterations in the kidneys and lungs but not in the brain (Tong et al. 2012; 2010). This could be due to a compensating mechanism in the brain, as suggested by the decrease in the flux of autophagy present in the *Lrrk*-DKO mouse model (Giaime et al. 2017). Moreover, a decreased autophagic flux was also reported in LRRK2 knock-in or transgenic models (Wallings, Connor-Robson, and Wade-Martins 2019; Saha et al. 2015; Schapansky et al. 2018) (Table 1.1). Considering LRRK2 regulates several functions in the cell, it is important to investigate LRRK2-mediated alterations in autophagic flux in the context of other cellular organelles and even other cell types, as any processes depending on autophagy will likely be perturbed. These processes could include lysosomal function as well as synaptic vesicle trafficking and recycling, mitophagy and the endo-lysosomal pathway (Connor-Robson et al. 2019; Wang 2017; Pan et al. 2017).

It seems LRRK2 acts as a brake in the autophagy-lysosomal pathway in neuronal cells, which is supported by an increase in autophagic flux when LRRK2 is knocked-out (Park et al. 2016; Wallings, Connor-Robson, and Wade-Martins 2019). However, when *LRRK1* and *LRRK2* are simultaneously knocked-out, or when *LRRK2* is mutated, there is a reduced autophagic flux (Sánchez-Danés et al. 2012; Saha et al. 2015; Giaime et al. 2017; Schapansky et al. 2018; Wallings, Connor-Robson, and Wade-Martins 2019), which points to the conclusion that LRRK2 function is also required for normal autophagic function to some extent. This argument suggests associating LRRK2 with loss-of-function in autophagy might be contradictory and unclear. Other authors have also

discussed the issue of gain vs. loss of function in LRRK2-associated PD and concluded that it is not a straightforward concept in LRRK2 literature (Cookson 2017; Gan-Or, Dion, and Rouleau 2015). Thus, LRRK2 function and potential regulation of autophagy remain unclear. Future studies will be necessary to validate this hypothesis and to elucidate the role of LRRK2 in neuronal autophagy.

1.5.5.3. Microglia and Astrocytes

Investigating neuronal models exclusively does not recapitulate the intricacies of the human brain environment. Neurons are surrounded and supported by microglia, astrocytes and oligodendrocytes (collectively referred to as glial cells) and form a complex network that likely play a role in any phenotypic outcome.

In non-neuronal models such as microglia BV2 cultures and through staining of glial cells in mouse brain tissue, endogenous LRRK2 expression increases upon microglia activation (Fig. 1.9) (Lee, James, and Cowley 2017; Schapansky et al. 2014; Moehle et al. 2012). This leads to LRRK2 phosphorylation, translocation and recruitment to autophagosomal membranes, which drives an increase in autophagy. Upon stimulation of microglia with Toll-like-Receptor 4, increasing autophagy and phagocytosis could be an anti-inflammatory defence mechanism in the context of neuroinflammation (Schapansky et al. 2014; Deretic 2011). On the other hand, knock-down of LRRK2 in microglia shows deficits in the induction of autophagy, a direct effect of a decreased LC3-II conversion ability in these cells, and in autophagic protein clearance after rapamycin treatment (Fig. 1.9) (Schapansky et al. 2014). However, this study did not measure multiple autophagy markers, such as p62 or LAMP1 to confirm altered autophagic flux. Still, this supports a model of PD pathology where LRRK2 regulates autophagy in microglia differently to its role in neurons.

Research into neuron-astrocyte co-culturing systems has also contributed to our understanding of LRRK2 PD pathology. By generating co-cultures of iPSC-derived astrocytes and ventral midbrain dopaminergic neurons from either familial *LRRK2-G2019S* patients or healthy individuals, it was revealed that *LRRK2-G2019S*-derived astrocytes accumulate α-synuclein and co-cultured control vmDAns display shortened neurites and neurodegeneration (di Domenico et al. 2019). Additionally, *LRRK2-G2019S* vmDAns co-cultured with control-derived astrocytes showed less severe neurite shortening, a more complex neurite arborization and decreased α-synuclein accumulation in neurons, when compared to co-cultures with *LRRK2-G2019S*

astrocytes. This effect was independent of direct neuron-astrocyte contact. However, the authors do not show autophagy characterisation in co-cultured neurons or astrocytes (di Domenico et al. 2019).

Turnover of α-synuclein is processed by both CMA and autophagy (Xilouri, Brekk, and Stefanis 2013), which were both impaired in *LRRK2-G2019S* astrocytes. *LRRK2-G2019S* derived astrocytes revealed an increased number of autophagosomes (LC3-positive puncta) that were localised in both distal and perinuclear regions, opposed to a preferable mainly perinuclear distribution. However, a decreased LC3/LAMP1 co-localisation, higher p62 and reduced LC3-II levels revealed an autophagosome-lysosome fusion blockage, resulting in deteriorated autophagic flux in *LRRK2-G2019S* astrocytes (Fig. 1.9) (di Domenico et al. 2019). In agreement to the findings described in microglia models, astrocyte models unveil a key role for glial cells in non-cell autonomous PD pathogenesis. In this scenario, a non-cell autonomous LRRK2-mediated increase in lysosomal secretion may increase α-synuclein release and aggregation, augmenting PD pathology. This is supported by observing the release of lysosomal contents into the cytosol when exposing cells to lysosomal overload stress, where Rab7L1, LRRK2, and phosphorylated Rab8/10 are sequentially accumulated onto the stressed lysosomes (Eguchi et al. 2018). However, primary astrocyte cultures from *Lrrk2*-KO mouse showed no difference in lysosomal size compared to nTG, whilst lysosomal count almost doubled. Thus, it could indicate autophagic flux is increased in *Lrrk2*-KO, concomitant with lysosomal dysfunction and in agreement with studies of *Lrrk2*-KO neuronal cultures (Fig. 1.9). The authors report variable effects of LRRK2 manipulations in autophagy when examining LC3 and p62 levels but data was not shown in the report (Henry et al. 2015). As discussed above, measurement of autophagic markers would be fundamental to determine whether LRRK2-KO induces autophagic flux alterations in astrocytes. Complementary to this, characterisation of an array of autophagic-lysosomal markers in WT and *Lrrk2*-KO mouse bone marrow-derived macrophages, after infection with *Mycobacterium tuberculosis*, revealed an increase in autophagic flux wherein LAMP1-positive phagosome as well as Cathepsin L-positive phagosome count is increased, but there are no differences in p62 and LC3B (Härtlova et al. 2018).

As evidenced in the sections above, focusing only on measuring markers of autophagosome formation might not be sufficient to infer on the dynamics of autophagic flux, since altered levels of autophagosomes and autolysosomes do not necessarily implicate impaired lysosomal activity or protein degradation (Cookson 2017; Giménez-Xavier et al. 2008). Hence, it would be extremely valuable to combine the measurement

of an array of proteins to assess autophagic flow in future research, including autophagosome, autolysosome and lysosomal markers as well as treatment with autophagy modulators such as 3-MA, bafilomycin and chloroquine (Yoshii and Mizushima 2017; Klionsky et al. 2016). Investigating the late phases of autophagy is also a crucial part of monitoring autophagy, including lysosomal function and protein degradation assays to measure degradation of autophagic substrates, such as pH-sensitive tagged proteins, Lysotracker dye to analyse lysosomal morphology, LysoSensor dye to measure lysosomal pH and pulse-chase assay to measure protein degradation (Yoshii and Mizushima 2017; Klionsky et al. 2016).

Nevertheless, the *LRRK2-G2019S* mutation seems to have a similar impact in activated microglia when compared to fibroblasts and neurons, resulting in a decreased autophagic flux (Table 1.1). By partially reducing LRRK2 expression and function using siRNA/shRNA, there is an increased induction of autophagy, except in activated microglia where autophagy decreases. In activated microglia cultures, endogenous LRRK2 expression increases and there is an increase in autophagic flux. Therefore, it is possible that LRRK2 positively regulates the autophagy machinery in the context of neuro-inflammation. However, the mechanism underlying this regulation in glial populations is still unknown and more research should be focused to resolve LRRK2 and its contribution to autophagy in PD.

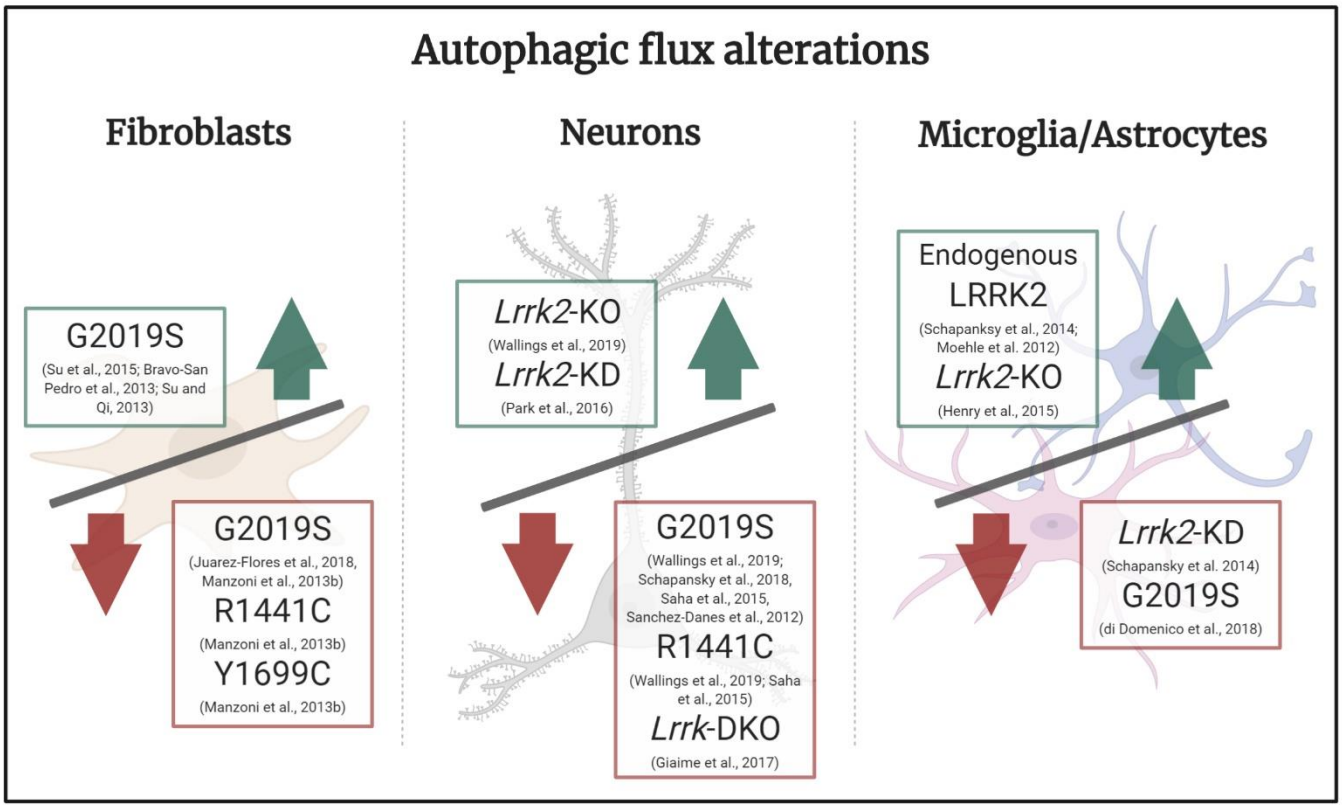

Figure 1.9 – Autophagic flux alterations in different cell types and LRRK2 models. In LRRK2-G2019S fibroblasts under basal culture conditions there is an increase in autophagic flux, whereas in starvation conditions LRRK2-G2019S, R1441C and Y1699C all show a decrease in autophagic flux. In neuronal Lrrk2-KO and KD models there is an increase in autophagic flux, whilst in LRRK2-G2019S, R1441C and Lrrk-DKO it is decreased. In microglia or astrocyte cultures, there was an increase in autophagic flux mediated by endogenous LRRK2 and in Lrrk2-KO models. On the other hand, Lrrk2-KD and LRRK2-G2019S overexpression cultures presented a decrease in flux. Green upwards arrow (Increase in autophagic flux), Red downwards arrow (decrease in autophagic flux).

Table 1.1 - *LRRK2 Models and alterations in different stages of the autophagy-lysosomal pathway.*

	LRRK2 Models					
Stage	***LRRK2-WT***	***LRRK2-G2019S***	***LRRK2-R1441C***	***Lrrk2-* KD**	***Lrrk2-* KO**	***Lrrk*-DKO**
Phagophore Biogenesis	Increased phosphorylation of p62 (Kalogeropoulou et al 2018)	Increased phosphorylation of p62 (Kalogeropoulou et al 2018)	Increased phosphorylation of p62 (Kalogeropoulou et al. 2018)	Increased phosphorylation of p62 (Park et al. 2016)		
	Indirectly reduce phosphorylation of p62 (Park et al. 2016)	Indirectly reduce phosphorylation of p62 (Park et al. 2016)				
	LRRK2 phosphorylates LRS, increasing misfolded proteins and inducing autophagy (Ho et al. 2018)	Increased kinase activity phosphorylates LRS, exacerbating autophagy (Ho et al. 2018)				
Autophagosome Formation	Blocked autophagosome formation (Ramonet et al. 2011; Manzoni et al. 2013; Saez-Atienzar et al. 2014; Manzoni et al. 2016)	Blocked clearance of autophagosomes, increased non-processed autophagic vacuoles (Ramonet et al. 2011; Sánchez-Danés et al. 2012; Ho et al. 2018; Wallings et al. 2019)			Blocked autophagosome formation (Manzoni et al. 2016)	Blocked clearance of autophagosomes, enlarged non-processed autophagic vacuoles (Giaime et al. 2017)

Autophagosome and lysosome Fusion		Deficient autophagosome-lysosome fusion (Saez-Atienzar et al. 2014; di Domenico et al. 2019; Obergasteiger et al. 2019)	Deficient autophagosome-lysosome fusion (Wallings et al. 2019)			
Lysosomal Function		Abnormal lysosomal morphology (MacLeod et al. 2006; Higashi et al. 2009; Ramonet et al. 2011; MacLeod et al. 2013; Dodson et al. 2014; Bang et al. 2016; Hockey et al. 2015; Henry et al. 2015; Schapansky et al. 2018) Abnormal lysosomal cellular localisation (Hockey et al. 2015; Schapansky et al. 2018) Increased lysosomal pH (Schapansky et al. 2018) Inhibition of lysosomal enzymatic	Increased lysosomal pH, reduced lysosomal calcium release through TRPML1 channels leading to increased lysosomal calcium levels (Wallings et al. 2019)			

			activity (McGlinchey and Lee 2015; Hu et al. 2018)				
			Lysosomal dysfunction culminated in α-synuclein accumulation (Volpicelli-Daley et al. 2016; Hu et al. 2018)				
Flux	**Fibroblasts**		↑ (Su and Qi 2013; Bravo San-Pedro et al. 2013; Su et al. 2015)	↓ (Manzoni et al. 2013)			
			↓ (Manzoni et al. 2013; Juarez-Flores et al. 2018)				
	Neurons	Not altered (Wallings et al. 2019)	↓ (Sanchez-Danes et al. 2012; Saha et al. 2015; Schapansky et al. 2018; Wallings et al. 2019)	↓ (Saha et al. 2015; Wallings et al. 2019)	↑ (Park et al. 2016)	↑ (Wallings et al. 2019)	↓ (Giaime et al. 2017)
	Microglia/ Astrocytes	↑ (Moehle et al. 2012; Schapansky et al. 2014)	↓ (di Domenico et al. 2019)		↓ (Schapansky et al. 2014)	↑ (Henry et al. 2015)	

LRS, Leucyl-tRNA synthetase; ↑ increased autophagic flux; ↓ reduced autophagic flux.

As discussed above, different PD models have informed on the different mechanisms whereby *LRRK2* mutations impact on its functional activity and can lead to disease (Cherubini and Wade-Martins 2018; Cookson 2016; Wallings, Manzoni, and Bandopadhyay 2015; Cookson 2017; Manzoni and Lewis 2017; Connor-Robson et al. 2019). Therefore, the use of different PD models and systems has firstly revealed that LRRK2 phenotypes display cellular heterogeneity, which is an important consideration for future studies of LRRK2 function (Schapansky, Nardozzi, and Lavoie 2015). Indeed, *LRRK2* mutations manifest different pathogenesis depending on the cell type (Zeng et al. 2018). Therefore, some caution should be exercised when selecting cultural conditions (basal *vs.* starvation) and comparing LRRK2 models to study autophagy in PD, as well as considering human *versus* non-human LRRK2 expression, as it is paramount to confirm any phenotypes in biologically relevant contexts of disease. Hence, it is important to individually assess autophagic flux in fibroblasts, neurons and microglia/astrocytes. Concurrently, it will be crucial to combine neuronal and non-cell autonomous methods, for instance by utilising 3D midbrain cultures or co-cultures of neuronal and neuroimmune cells, in the efforts to completely understand LRRK2 pathology in PD.

Moreover, it is essential to point out that accurate measurement of autophagic flux is crucial when comparing LRRK2 phenotypic effects in the autophagy-lysosomal pathway. Analysing LC3-I and LC3-II could provide insights into the rates of autophagosome formation, however LC3 is present in phagophores, autophagosomes and autolysosomes and measurement would often only represent a single time point, rather than the flow of autophagy. Another widely used marker of autophagy is LAMP1, which is expressed in lysosomes and autolysosomes but also in late endosomes of the endocytic pathway. This could introduce confounding factors in studies relying solely on one specific marker.

When analysing LRRK2 phenotypes relating to autophagic flux, it is evident that *LRRK2* mutations, specifically the G2019S and R1441C, act in a different manner and at different stages of the autophagy pathway (Table 1.1). This observation may not be surprising given these mutations are situated in different enzymatic domains of LRRK2, the kinase domain and GTPase domain respectively (Fig. 1.9). The most common LRRK2 mutation, G2019S, is consistently associated with an increase in kinase activity and a decrease in autophagic flux (Juárez-Flores et al. 2018; Manzoni et al. 2013; Wallings, Connor-Robson, and Wade-Martins 2019; Schapansky et al. 2018; Saha et al. 2015; Sánchez-Danés et al. 2012; di Domenico et al. 2019) whereas the second most common mutation, R1441C, exhibits decreased autophagic flux, with lysosomal activity being particularly impaired (Wallings,

Connor-Robson, and Wade-Martins 2019; Saha et al. 2015). Conceivably, impaired lysosomal function could lead to deficient protein clearance and could fit the model of Lewy body pathology wherein there is an accumulation of aggregated α-synuclein (Schapansky, Nardozzi, and Lavoie 2015; Orenstein et al. 2013; Schapansky et al. 2018; Hu et al. 2018). Indeed, impaired autophagy has been recently proposed to be an aggravator of PD (Johnson et al. 2019). Consequently, different LRRK2 mutations located in different domains will have distinct cellular effects downstream and alongside of autophagic impairment, such as dysregulated mitophagy, endocytosis and vesicular trafficking (Connor-Robson et al. 2019; Chen and Wu 2018; Manzoni et al. 2013).

1.6. Mitochondria

Mitochondria are crucial organelles for generation of aerobic energy, synthesis of key macromolecules, calcium homeostasis, and regulation of apoptosis. Mitochondria contain their own circular, double-stranded mitochondrial DNA (mtDNA), distinct from nuclear DNA, and are highly dynamic organelles with an inner membrane with cristae to increase surface area, an outer membrane, an intermembrane space and the mitochondrial matrix. Whilst nuclear DNA encodes subunits of the mitochondrial respiratory chain (MRC), as well as assembly factors, transport proteins, or unidentified proteins that are crucial for mitochondrial function, mtDNA encodes for two ribosomal RNAs, 22 tRNAs, and 12 subunits of the electron transport chain (ETC) (Van Der Bliek, Sedensky, and Morgan 2017).

1.6.1. Mitochondrial function

The main function of mitochondria in cells is to generate energy in the form of ATP through the tricarboxylic acid (TCA) cycle (or Krebs cycle) and oxidative phosphorylation (OxPhos). Within the mitochondrial matrix, the TCA cycle oxidises acetyl CoA to produce the reducing agents NADH and FADH, which ultimately enter the oxidative phosphorylation process as electron donors. Importantly, precursors to certain amino acids are also generated within the TCA cycle. Within the inner mitochondrial membrane, oxidative phosphorylation is the process of synthesizing ATP, by transferring electrons through a series of large protein complexes (Complex I to IV), establishing an electro-chemical gradient until oxygen is consumed as the final electron acceptor, forming water as a by-product. The inner-membrane electrochemical potential generated by OxPhos is essential to mitochondrial functions, such as mitochondrial protein import (Neupert and Herrmann 2007; Nunnari and

Suomalainen 2012) and is used to trigger changes on the molecular level that alter mitochondrial behaviours in response to mitochondrial dysfunction. The mitochondria-associated ER membrane (MAM) plays a critical role in lipid biosynthesis and calcium signalling. Neuronal axons and dendrites and muscle fibers utilise physical tethers to stably position mitochondria at specific locations for efficient bioenergetics exertion (Nunnari and Suomalainen 2012). It is possible to measure mitochondrial respiration of cultured cells to determine mitochondrial function, by using a series of inhibitors of respiration, assessing both the rates of disappearance of oxygen (oxygen consumption rate, OCR) and the acidification of the medium (extracellular acidification rate, ECAR) with different substrates and uncouplers, a technique developed with the Seahorse Metabolic Analyzer (Van Der Bliek, Sedensky, and Morgan 2017).

1.6.2. Mitochondria quality control

When mitochondria are damaged and become defective or dysfunctional, it is important cells efficiently clear them to maintain mitochondrial homeostasis. The presence of dysfunctional mitochondria within cells leads to bioenergetic deficits, less efficient calcium buffering and accumulation of oxygen reactive species (ROS) (Court and Coleman 2012; Sheng and Cai 2012). Mitochondrial oxidative stress triggers caspase activation, DNA damage, and apoptosis (Mishra and Chan 2014). Many mutations in PD genes have been implicated in mitochondrial-related pathways such as *PTEN-induced putative kinase 1* (*PINK1)* and *Parkin*, which cause familial autosomal recessive, *DJ-1*, *LRRK2* and *SNCA*. Mitochondria quality control is regulated through three main mechanisms: ubiquitination and proteosome, fission/fusion and mitophagy.

1.6.2.1. Proteasome degradation

Key effector mitochondrial proteins located in the OMM like MIRO1 and Mitofusins (MFN), display their domains at the cytosolic side of the membrane, which become accessible to be degraded by the ubiquitin-proteasome system (UPS). Selectively removing fusion or fission components, the UPS allows effective regulation of damaged mitochondria, supporting the effective separation of dysfunctional mitochondria (Fig. 1.10 A) (Tanaka et al. 2010; Bragoszewski, Turek, and Chacinska 2017).

1.6.2.2. Fission and fusion

Mitochondria constantly undergo changes in their morphology, either by fusing with other mitochondria or by fission of one mitochondrion into two separate organelles. Mitochondrial

fission is regulated by cytosolic protein dynamin-related protein 1 (DRP1) (Detmer and Chan 2007; Reddy et al. 2011; Kandimalla and Reddy 2016). DRP1 is recruited to the outer mitochondrial membrane (OMM) by specific receptors (MiD49, MiD51, Fis1, and MFF) and forms a ring-like structure so that one mitochondrion structure contracts into two daughter mitochondria, via GTP hydrolysis (Kalia et al. 2018; Palmer et al. 2011). Mitochondrial fusion is mainly regulated by OPA1, mitofusin 1 (MFN1) and mitofusin 2 (MFN2) (Mishra and Chan 2014; Roy et al. 2015). During fusion, OMM proteins MFN1 and MFN2 bind to MFNs of neighbouring mitochondria, which brings the two organelles together (Meeusen et al. 2006; Song et al. 2009). OPA1 is involved in inner membrane fusion, crating one continuous membrane (Fig. 1.10 B).

Mitochondrial fission can help to control the mitochondrial quality by segregating damaged or unhealthy mitochondria away from the healthy mitochondria, and which would then be singled out for degradation via the mitophagy pathways (Fig. 1.10 B).

1.6.2.3. Mitophagy

Mitophagy, the autophagic degradation of defective mitochondria, is regulated by PINK1 and Parkin activation upon mitochondrial membrane depolarisation, accumulation of unfolded proteins in the mitochondrial matrix or oxidative stress (Jin and Youle 2013; Pimenta De Castro et al. 2012; Xiao et al. 2017). PINK1 is stabilised at the OMM, phosphorylating ubiquitin (Ub) at the serine 65 residue. For this reason, phospho-serine65 Ub (pSer65Ub) is currently considered as a marker of PINK1-induced mitophagy activation. Contrastingly, in healthy mitochondria, PINK1 is imported through translocase of the outer mitochondrial membrane (TOM) and translocase of the inner membrane (TIM) complexes, and then subsequently cleaved by PARL and MPP, released back to the cytosol and targeted for proteasome-mediated degradation (Rossmann et al. 2021; Malpartida et al. 2021). Cytosolic Parkin is auto inhibited, but once recruited to active PINK1 sites, RING1 of the Parkin domain binds pSer65Ub, initiating a series of conformational changes that culminates in Parkin activation by PINK1-mediated phosphorylation of Parkin Ub-like domain. Active Parkin synthesises Ub chains on OMM proteins, which are substrates for PINK1 Ub phosphorylation, recruiting more Parkin in a feed-forward mechanism, assembling Ub chains recognised by autophagy adaptors Optineurin (OPTN), NDP52, p62 and LC3 at maximal activation (~4400-fold activation) (Fig. 1.10 A) (Swatek et al. 2019; Wauer et al. 2015; Gladkova et al. 2018; Malpartida et al. 2021). This activation of the mitophagy pathway is balanced by several deubiquitylases (DUBs), such as USP30, USP8, USP14, USP15 and USP35, antagonising Parkin activity either directly or through its substrates. Located at the OMM, USP30 negatively regulates PINK1/parkin-dependent

mitophagy through deubiquitylation of several OMM substrates, including RHOTs, VDACs and MFNs, establishing a threshold for initiating mitophagy. Furthermore, PTEN-Long (PTEN-L) and PPEF2 phosphatases have been demonstrated to regulate pSer65Ub phosphorylation, negatively regulating mitophagy in neurons and astrocytes *in vitro* and *in vivo* (Liming Wang et al. 2018; Wall et al. 2019; Li et al. 2018).

Mitophagy can also occur in a PINK1/Parkin-independent manner, mediated by various OMM proteins, including the autophagy receptor proteins NIP3-like protein X (NIX; BNIP3L), BNIP3 and FUNDC1, which directly interact with LC3 to mediate formation of the autophagosome. Phosphorylation of NIX and BNIP3 associate with LC3, whereas under hypoxia conditions both CK2 and Sc kinases and PGAM5 phosphatase influence FUNDC1 phosphorylation status, ensuring specificity of the process in different tissues in response to different stimuli. Interestingly, NIX and BNIP3 can be ubiquitinated by parkin, reflecting an intricate crosstalk between PINK1/parkin-dependent and -independent regulation of mitochondrial dynamics (Fig. 1.10 B) (Palikaras, Lionaki, and Tavernarakis 2018).

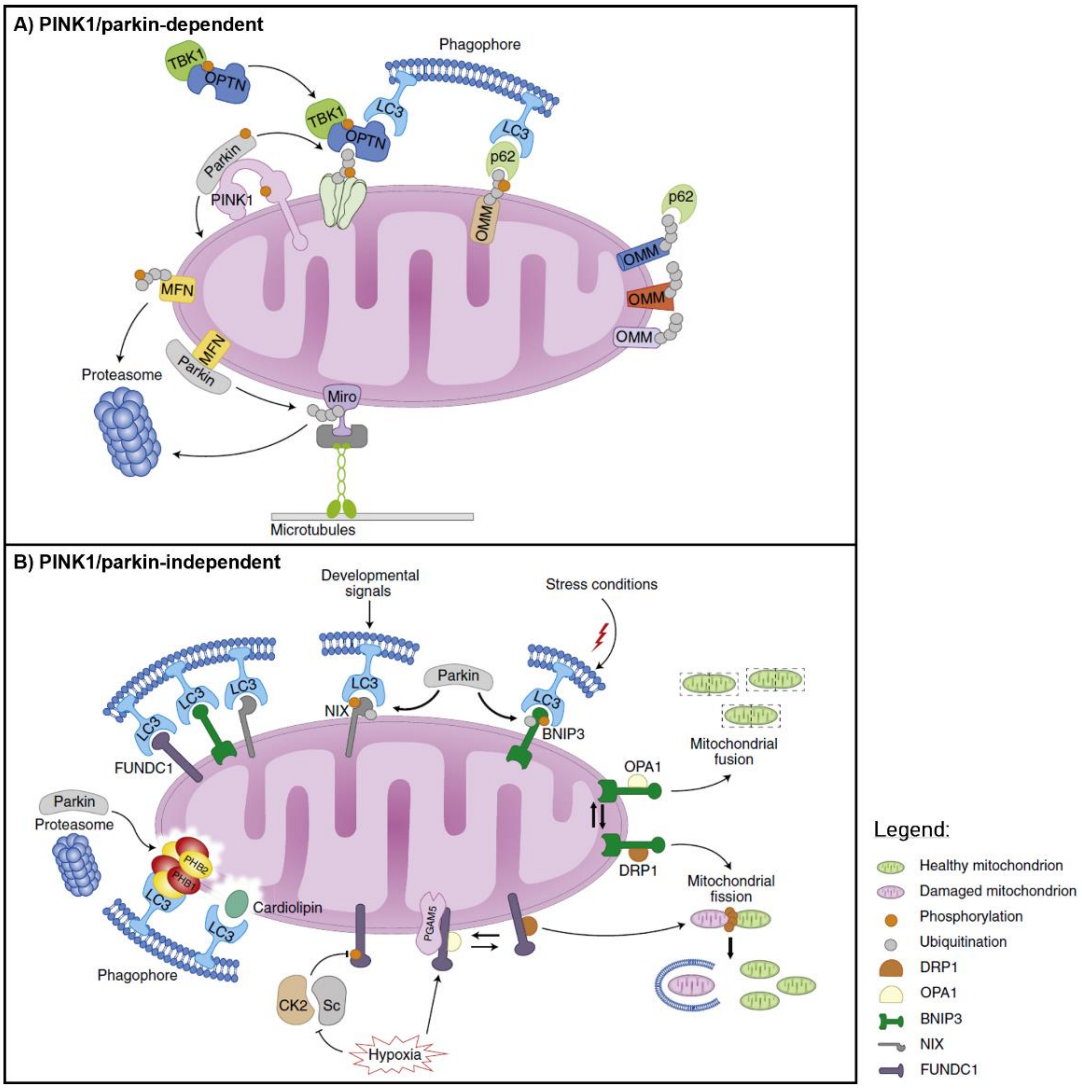

***Figure 1.10. – Mitochondrial quality control dynamics*. (A)** PINK1/parkin-dependent mitophagy occurs upon mitochondrial damage. **(B)** PINK1/parkin-independent mitophagy and mitochondrial fission and fusion help maintain healthy mitochondrial networks. Adapted from (Palikaras, Lionaki, and Tavernarakis 2018).

1.6.3. Mitochondrial dysfunction in PD

Mitochondrial dysfunction has been linked to PD through environmental exposure and genetic factors. A distinct form of parkinsonism with a rapid onset has been linked to the toxic cation 1-methyl-4-phenylpyridinium (MPP+), generated by MAO-B enzyme processing of 1-methyl-4-phenyl-1,2,5,6-tetrahydropyridine (MPTP) from environmental exposure, and is selectively taken up by dopaminergic neurons, causing inhibition of Complex I, III, and IV of the respiratory chain (Langston et al. 1983; Heikkila et al. 1984; Langston et al. 1984; Desai et al. 1996). Mitochondrial dysfunction as a central mechanism with PD was also supported by *post-mortem* brain sections of PD patients exhibiting complex I deficiency (Schapira et al. 1989). Furthermore, a subset of sporadic PD patients' fibroblasts demonstrated mitochondrial or lysosomal dysfunction, and differentiation into dopaminergic neurons exacerbated the decrease of complex I and IV expression levels (Carling et al. 2020). Impaired Complex I and III function leads to reduced levels of ATP generation, altered mitochondrial membrane potential and production of ROS, including oxygen radicals and hydrogen peroxide, which can damage cells and have been suggested to contribute to neurodegeneration through mitochondrial dysfunction (Muller, Liu, and Van Remmen 2004; Murphy 2009; Nunnari and Suomalainen 2012). Oxidative damage also affects mtDNA, and a single rotenone dose was sufficient to induce mtDNA damage in rat midbrain neurons, but not in cortical neurons. Additionally, midbrain neurons produced more mitochondrial H_2O_2 than cortical neurons, in response to rotenone-induced complex I inhibition. The same study showed *post-mortem* nigral neurons, but not cortical neurons, from PD patients displayed mtDNA damage (Sanders et al. 2014). Increases in somatic point mutations, deletions and mtDNA copy number have been reported in brain regions of PD patients, including the SNpc (Dölle et al. 2016; Bender et al. 2006; Nido et al. 2018; Reeve et al. 2008; Bury et al. 2017; Coxhead et al. 2016).

There have been many genetic associations between mitochondrial quality control related genes and PD. Mutations in *PINK1* and *PRKN* genes, which encode PINK1 and Parkin, lead to mitophagy defects and cause familial autosomal recessive forms of early-onset PD (Kitada et al. 1998; Valente et al. 2001; Narendra et al. 2010). Moreover, increased pSer65Ub formation has been observed in *post-mortem* PD brain, significantly correlating

with LBs and neurofibrillary tangle levels, and diminished in patients with *PINK1/PRKN* mutations, highlighting the importance of mitophagy (Hou et al. 2018; Fiesel et al. 2015). Assessing *post-mortem* brain tissue from PD patients carrying heterozygous mutations in the *GBA* gene, identified increased mitochondrial content, increased mitochondrial oxidative stress, and impaired autophagy, consistent with iPSC-derived dopaminergic neuronal cultures from patients with *GBA-L444P* mutations and *GBA-KO* neurons (Li et al. 2019; Schöndorf et al. 2018). In 2015, *CHCHD2*, which encodes a protein that modulates mitochondrial function in conjunction with the ALS/FTD-associated gene *CHCHD10*, was identified as a novel familial PD gene (Funayama et al. 2015; Liu et al. 2020). Mutations in *CHCHD2* culminate in altered mitochondrial structure, cytochrome C destabilisation, impaired respiration, increased mitochondrial ROS, and have been linked to α-synuclein aggregation and oligomerisation in human *post-mortem* brain tissues and iPSC-derived DAn (Meng et al. 2017; Ikeda et al. 2019). Mutations in *DJ-1*, a deglycase protein that acts as a redox sensor and chaperone, are associated with impaired mitochondrial quality control, causing autosomal recessive PD (Strobbe et al. 2018; Kojima et al. 2016). Interestingly, a mutation in *VPS35* induces mitochondrial fragmentation and dysfunction through interaction with dynamin-like protein (DLP) 1 and enhances turnover of the mitochondrial DLP1 complexes via the mitochondria-derived vesicle-dependent trafficking towards lysosomal degradation. Notably, VPS35-DLP1 interaction was increased in the brains of sporadic PD cases (Wang et al. 2016). PD-causing point mutations in α-synuclein, such as *A53T*, *E46K*, *H50Q*, lead to various mitochondrial alterations (Appel-Cresswell et al. 2013; Khalaf et al. 2014; Cannon et al. 2013; Ryan et al. 2015). In turn, α-synuclein has been shown to accumulate in mitochondria, interfering with complex I function and increasing mitophagy (Chinta et al. 2010). All these key interactors highlight the crosstalk between mitochondria homeostasis and lysosomal activity and how its impairment leads to neurodegeneration.

1.7. LRRK2 and mitochondrial network dynamics

1.7.1. LRRK2 and mitochondrial function

In LRRK2-related PD different cellular pathways are impaired and contribute to molecular pathology. These have been extensively reviewed and include autophagy (Madureira, Connor-Robson, and Wade-Martins 2020), vesicular trafficking (Singh and Muqit 2020), endolysosomal system (Erb and Moore 2020) and the mitochondrial network (Malpartida et al. 2021). Animal models have shown reduced rate of OXPHOS, decreased intracellular basal ATP production and mitochondrial fragmentation in LRRK2-G2019S mouse

embryonic fibroblasts (MEF) (Toyofuku et al. 2020). In human *LRRK2-G2019S* fibroblasts, mitochondria show reduced mitochondrial membrane potential, decreased OXPHOS activity and decreased basal ATP production (Mortiboys et al. 2010). A study in *LRRK2-R1441G* transgenic mice showed altered mitochondria morphology and dysfunction with decreased mitophagy in MEFs and mouse brain (Liu et al. 2021). On the other hand, not many studies have investigated mitochondrial function in LRRK2-R1441C.

1.7.2. LRRK2 regulation of mitophagy

It is vital for cells to clear damaged mitochondria to prevent further stress and cell death. Therefore, mitochondrial autophagy (mitophagy) is a crucial cellular process and its disruption has been associated with PD (Malpartida et al. 2021; Singh and Ganley 2021). Basal mitophagy inversely correlates with LRRK2 kinase activity *in vivo* and LRRK2-G2019S impairs basal mitophagy in reporter mouse models (Singh et al. 2021). In human patient-specific neuroepithelial stem cells and primary fibroblasts, LRRK2-G2019S exhibits abnormal mitochondrial function and morphology and decreased mitophagy (Bonello et al. 2019; Korecka et al. 2019; Walter et al. 2019; Wauters et al. 2020). In LRRK2-R1441C, depolarization-induced mitophagy and mitochondrial function are impaired in primary fibroblasts (Wauters et al. 2020). However, the effect of *LRRK2-R1441C* mutation on mitochondrial network, function, and clearance in dopaminergic neurons, which are the most important neuronal subtypes in PD, is still poorly understood. Recently, independent studies have identified three main mechanisms linking LRRK2 and regulation of mitophagy. In iPSC-derived dopaminergic neurons, LRRK2-G2019S exhibits decreased interaction with OMM protein MIRO1, which leads to MIRO1 decreased degradation in depolarised mitochondria and consequent decrease in mitophagy levels (Hsieh et al. 2016). Also in depolarised mitochondria, *LRRK2* mutations G2019S and R1441C block PINK1/parkin-dependent mitophagy through increased phosphorylation of RAB10, which inhibits its interaction with the autophagy receptor OPTN in primary fibroblasts (Wauters et al. 2020). In parallel, LRRK2-G2019S interferes with protein–protein interactions involving Parkin and fission protein DRP1 on the OMM, resulting in decreased mitophagy in primary fibroblasts (Bonello et al. 2019).

Ultimately, research into the relation of LRRK2, mitochondrial pathways and lysosomal activity could have an impact on new drug screening approaches to potentially find novel compounds to treat LRRK2 related PD.

1.8. Aims of the project

Mitochondrial health and autophagy-lysosomal pathways have been linked to LRRK2-PD pathophysiology, therefore this research project will focus on these two cellular pathways to characterise disease mechanisms in PD using animal and human models.

- **Aim 1: LRRK2 and vATPase-a1 interaction**

The first aim of our study is to further characterise this interaction in human cellular models and assess the effects of anti-malaria drug Clioquinol in LRRK2-vATPase-a1 interaction using human cellular models. Recent evidence has shown that expression of *LRRK2-G2019S* or *LRRK2-WT* inhibited autophagosome production, whereas *LRRK2-R1441C* shows impaired autolysosome fusion and increased lysosomal pH. A novel interaction has been described in rat primary cultures between LRRK2 and the a1 subunit of the lysosomal H+-pump vATPase. This interaction was abolished in the *LRRK2-R1441C* mutation, leading to a decrease in a1 protein levels and cellular mislocalisation.

- **Aim 2: LRRK2 and Autophagy**

The second aim is to characterise the impact of *LRRK2-R1441C* and *LRRK2-G2019S* mutations on autophagy and lysosomal function using LRRK2 rat cortical primary cultures and LRRK2 human model of iPSC-derived dopaminergic cultures.

- **Aim 3: LRRK2 and Mitochondria**

The third aim is to investigate mitochondrial health and mitophagy, both under basal and stress conditions, using *in vivo* and *in vitro* LRRK2 models of Parkinson's disease. With a focus specifically on *LRRK2-R1441C* using rat primary cortical neurons and iPSC-derived dopaminergic neuronal models characterise mitochondrial health, morphology and function. We assess PINK1/parkin-dependent mitophagy and uncover the molecular mechanism underlying the phenotypic alterations observed. Finally, we explore the role of LRRK2 kinase activity by treating neuronal cultures with LRRK2 kinase inhibitor MLi-2.

Chapter 2 - Materials and Methods

2.1. Cell culture and transfection

2.1.1. Human embryonic kidneys 293T cell culture

Human embryonic kidneys 293T (HEK293T) cells were cultured in Dulbecco's modified Eagle's medium, high glucose, GlutaMAX™ Supplement (Gibco), containing 10% fetal bovine serum and penicillin (100 U/ml)/streptomycin (100 µg/ml). Cells were kept in the incubator at 37°C, 5% CO_2, 95% relative humidity, trypsinised with 0.25% Trypsin-EDTA solution (Sigma Aldrich) and passaged every third/fourth day in the culture.

Freezing Medium

Full medium with 20% FBS and 10% DMSO (Sigma)

Freshly prepared when required

2.1.2. Transfection

HEK293T cells were seeded at 80% confluency in poly-l-lysine coated plates (1 x 10^6 cells/ml for 6-well plates, 4 x 10^5 cells/ml for 12 well-plates and 1 x 10^6 cells/ml for 96-well plates). The following day, cells were changed to Opti-MEM® Reduced-Serum Medium (Gibco) before transfection. Plasmid DNA constructs were mixed with Lipofectamine 2000 and incubated at room temperature for a maximum of 25 minutes to allow formation of complexes before being added to the corresponding well. Cells were incubated for 5 hours and then changed to DMEM medium. Cells were incubated to undergo transient transfection for 48 hours and then were lysed and collected as described. Cell lysates were accessed by SDS-PAGE.

2.1.3. Treatment with compounds

For some experiments, HEK293T cultures were treated with compounds before cells were lysed and collected (see Table 2.1).

Table. 2.1. *Compounds used for cell culture treatment*

Compound	Supplier	Catalogue Number	Concentration	Incubation Time
MLi-2	Tocris	5756	100 nM	2h or 48h
PF-06447475	MedChem Express	HY-12477	50 nM	2h
Clioquinol	Abcam	ab120355	1 µM	48h

Chloroquine	Merck	C6628	100 nM	24 h
CCCP	Merck	215911	10 µM	6h or 24h

2.2. Construct library

2.2.1. LRRK2 and vATPase a1 constructs

All LRRK2 construct plasmids are in a pCMV-Tag 3B vector background, with two myc-tag cassettes in the N-terminal region. LRRK2 plasmids were a gift from Dr. Mark Cookson and were purchased from Addgene (https://www.addgene.org/Mark_Cookson/), except for 2xMyc-LRRK2-ROC that was built *in-house* (see Table 2.2). Both vATPase-a1 construct plasmids contain two flag-tag cassettes in the C-terminal region and were a kind gift from Prof. Morris Manolson (Esmail et al. 2018) (see Table 2.2).

Table. 2.2. *Construct Library*

	Construct	**Plasmid Number**	**Insert Sequence (aminoacids)**
LRRK2	2xMyc-LRRK2-WT	25361	Full length (1-2527)
	2xMyc-LRRK2-LRR	25072	879-1278
	2xMyc-LRRK2-RCK	25065	1329-2219
	2xMyc-LRRK2-COR	25069	1408-1850
	2xMyc-LRRK2-Kinase	25071	1863-2218
	2xMyc-LRRK2-WD-40	25073	2155-2527
	2xMyc-LRRK2-3xKD	25366	Full length, "Kinase Dead" construct. Lysine 1906 mutated to Alanine. Aspartate 1994 mutated to Alanine. Aspartate 2017 mutated to Alanine
	2xMyc-LRRK2-G2019S	25362	Full length, Glycine 2019 mutated to Serine
	2xMyc-LRRK2-R1441C	25363	Full length, Arginine 1441 mutated to Cysteine
	2xMyc-LRRK2-ROC	Built *in-house*	1388-1515

vATPase	2xFlag-vATPase-a1	Gift from *Manolson*	Full length (1-858)
	2xFlag-vATPase-a1 Mutated (N495Q)	Gift from *Manolson*	Full length, Asparagine 495 mutated to Glutamine

2.2.2. LRRK2-ROC construct

To build a construct containing the LRRK2-ROC domain only, a gBlock gene fragment was ordered from Integrated DNA Technologies, Inc. (IDT) (https://eu.idtdna.com/site/order/gblockentry). *LRRK2-ROC* sequence was obtained from *LRRK2* gene reference sequence available from NCBI (GenBank: AY792511.1).

LRRK2-ROC gBlock (IDT):

5'-
GATCTGAGCCCGGGATCCGAGCAGAAACTCATCTCCGAGGAAGCATTGCTGCAAGA
GTTCGATATCACTAGCCTCTACAAAAAGGCAGGGTCCGAGTTTGCGCTCAGGATGAA
ACTTATGATAGTTGGCAATACTGGTAGCGGGAAAACTCTTCTGCAACAACTTATGAAG
ACCAAAAAGTCCGATCTTGGCATGCAATCTGCTACGGTGGGAATAGATGTCAAGGAC
TGGCCTATTCAAATCCGGGACAAGCGGAAGCGAGACCTCGTGCTCAATGTGTGGGA
TTTCGCTGGGCGCGAGGAATTCTATTCTACCCATCCACACTTTATGACCCAACGGGC
GCTGTATTTGGCAGTTTATGATTTGAGCAAAGGTCAAGCGGAGGTAGACGCGATGAA
ACCTTGGCTGTTTAATATCAAAGCTCGCGCTTCAAGCTCACCTGTCATCCTTGTCGG
GACGCATCTCGACGTGAGTGATGAAAAGCAGCGGAAAGCGTGCATGAGCAAGATCA
CAAAGGAACTGCTCAACAAGCGGGGTTTCCCCGCTATCCGAGATTACCATTTTGTGA
ACGCCACTGAAGAGTCCGACGCCCTTGCAAAATTGAGGAAAACCATTATCAACGAAT
CTCTGAATTTTAAGATTCGGGATCAGGAACGACGCGCAAACAGTACCCAATTGTCCT
GCACTAAGTGGTAATCAGTGCCATAGTTGATAAAGGTCCCCGGTAAGTGTACCCAAT
TCGCCCTATAGTGAGTCGTATTACAATTCACTCGATCGCCCTTCCCAACAGTTGCG-3'

2.2.3. Restriction enzyme digestion

LRRK2 constructs were digested with BamHI and PvuI whereas vATPase-a1 constructs were digested with SacI and SacII. Restriction enzymes were purchased from New England Biolabs (NEB) and used according to protocol provided by the manufacturers. A mastermix containing DNA, the respective enzymes at 1 unit/µg of DNA, 5 µl CutSmart buffer and MilliQ H_2O up to a 50 µl total volume was incubated at 37°C for a minimum of one hour. The reaction was then run on an agarose gel to assess fragment size (Table 2.3).

Table 2.3. *Colony screening with restriction enzymes for LRRK2 and vATPase-a1 constructs.*

LRRK2 Construct	Restriction Enzymes	Expected bands (base pairs)
LRRK2-WT	BamHI and PvuI	8515 and 3470
LRRK2-LRR		3979 and 1768
LRRK2-RCK		3797 and 3240
LRRK2-ROC		4188 and 767
LRRK2-COR		3797 and 3240
LRRK2-Kinase		3797 and 1635
LRRK2-WD-40		3979 and 1689
LRRK2-G2019S		7797 and 4188
LRRK2-R1441C		7797 and 4188
vATPase-a1-WT	SacI and SacII	4600 and 2635
vATPase-a1-Mut		4600 and 2635

2.2.4. DNA fragment purification from agarose gel

Following the digestion of approximately 10 µg of 2xMyc-LRRK2-WT DNA with restriction enzymes BamHI and PvuI, the resultant DNA was run on an agarose gel and visualised on the UV lamp at 312 nm. Using a clean scalpel, the correct sized fragment was excised from the gel. The selected portion of the gel was then weighed, and the DNA purified from it using the QIAquick gel extraction kit (Qiagen). This was done following the supplied manufacturer instructions. This method was required for excising the pCMV-Tag 3B vector backbone after enzymatic digestion. The resulting fragments were purified before ligating the LRRK2-ROC gBlock gene fragment.

2.2.5. Ligation reactions

To ligate the pCMV-Tag 3B vector backbone and LRRK2-ROC gBlock, the vector/insert ratio was calculated using New England Biolabs Ligation Calculator online tool (http://nebiocalculator.neb.com/#!/ligation). A ligation mastermix was prepared containing vector and insert at the estimated molar ratio of 1:5, ligase buffer and T4 DNA ligase. The mix was incubated at 37°C for 2 hours. Following this, 2µl of the reaction were used for transformation of high efficiency competent cells.

2.2.6. Transformation of competent cells

For transformation, One Shot Stbl3 chemically competent *E. coli* (Invitrogen) or DH5αTH high efficiency cells (New England Biolabs) were thawed on ice. Plasmid DNA (1-5 µl) of the appropriate plasmid were added and mixed gently, followed by incubation on ice for 30 minutes. The cells then underwent heat shock at 42°C for 30 seconds to allow the bacterial membranes to become permeable, allowing the entrance of plasmid DNA. The cells were then placed back on ice for 2 minutes to allow the membranes to recover. Warmed SOC medium was then added to the competent cells and incubated for 1 hour at 37°C, with shaking to allow the expression of antibiotic resistance genes. Then, 150 µl of cell suspension was plated and spread on appropriate selective agar plates, followed by incubation overnight at 37°C.

2.2.7. Preparation of Agar Plates and Luria Broth

For Luria Broth (LB) medium, 25g of Luria Broth Base (Invitrogen) were added per 1L of RO H_2O. For agar plates, LB mixed with agar (Invitrogen) was added to 1L of RO H_2O, for a final concentration of 2%. These were then autoclaved. LB medium was stored at room temperature until required. Selective antibiotics were added to LB + agar at a concentration of 50µg/ml (Ampicillin for vATPase a1 constructs and Kanamycin for LRRK2 constructs), then the solution was poured into 6-cm Petri dishes and plates stored at 4°C until required.

2.2.8. Selection of bacterial colonies

After plates were incubated at 37°C overnight they were then used to select single bacterial colonies in order to further amplify recombinant plasmid DNA. Single colonies were picked from plates using sterile pipette tips and placed in 6 ml selective LB medium with the respective selective antibiotic, overnight at 37°C with shaking to aerate the suspension. For growing positively selected bacteria from glycerol stocks, a similar process was used, picking colonies from glycerol stocks with sterile pipette tips.

2.2.9. DNA extraction from bacterial suspension

Glycerol stocks were made by collecting 300 µl from overnight inoculations, mixing with 50% glycerol solution and storing at -80°C. Overnight inoculations were centrifuged at 10,000 rpm for 5 minutes and the resulting suspension discarded to obtain a pellet. The bacterial pellet was then resuspended and purified using mini prep columns from the QIAprep Spin Miniprep Kit (Qiagen). This system relies on alkaline lysis of the bacterial cells followed by adsorption of the DNA onto a silica membrane under high salt conditions. The resulting DNA was eluted in 30 µl Elution Buffer (Qiagen) and used for further analysis of the clone. All DNA samples were stored at -20°C until needed.

2.2.10. DNA Quantification

DNA concentration was estimated by measuring solution absorbance at 260nm on the Nanodrop CellDrop™ (DeNovix).

2.2.11. Sanger Sequencing

DNA sequence verification of plasmids was performed by SourceBioscience, using PCR primers Forward Reverse obtained from IDT or universal primers from SourceBioscience (see Table 2.4). Alternatively, samples were first processed with Big Dye sequencing reaction in a 96-well plate (see Table 2.5 for sequencing reaction and Table 2.6 for PCR conditions), using the same primers Forward and Reverse mentioned above. Then, samples were purified by adding 4µl of Precipitating Master Mix (125Mm EDTA, 3M NaAc) and 50µl of 100% Ethanol per sample and vortexed briefly. DNA was separated by centrifugation at 3,000 x g for 30 minutes, at 4°C. Supernatant was discarded and plate was centrifuged at 185 x g for 10 seconds, in an inverted position to discard remaining supernatant. To precipitate DNA, 70µl of 70% Ethanol were added to each sample followed by centrifugation at 1650 x g for 15 minutes, at 4°C. Supernatant was discarded and plate was centrifuged at 185 x g for 10 seconds, in an inverted position to discard remaining supernatant. Plate was aired for 5 minutes to eliminate remaining Ethanol. Sequencing was then carried out by the University of Oxford - Department of Zoology sequencing core. Analysis of the sequences was carried out using BioEdit (v7.2) software and SnapGene 5 (v5.0.7), GSL Biotech LLC. The sequenced constructs were aligned to the *LRRK2* gene reference sequence available from NCBI (NCBI Reference Sequence: NG_011709.2). Additionally, a *blastx* query was performed to confirm whether the generated *LRRK2* construct aligned with the *LRRK2* sequence in an unbiased search through a nucleotide database (https://blast.ncbi.nlm.nih.gov/Blast.cgi?LINK_LOC=blasthome&PAGE_TYPE=BlastSearch&PROGRAM=blastx), where the first hits found were positive for human *LRRK2* sequence, with 100% identity.

Table. 2.4. *Sequencing primers*

Primer	Target	Source	Sense Oligo Sequence (5' to 3')
Forward	*Human CMV immediate early promoter*	IDT	CGCAAATGGGCGGTAGGCGTG
Reverse	*SV40 polyA*	IDT	GAAATTTGTGATGCTATTGC

Forward	*M13F*	SourceBioscience	TGTAAAACGACGGCCAGT
Reverse	*M13R*	SourceBioscience	CAGGAAACAGCTATGACC

Table. 2.5. *Big Dye Sequencing reaction*

	1x (µl)
BigDye	0.5
5x sequencing buffer	1.75
Primer (either F or R, 10µM)	1.0
DNA (10ng/µl)	1.0
MilliQ H_2O	6.75
Total	10

Table. 2.6. *Big Dye Sequencing PCR conditions*

Temperature	**Duration**	**Cycles**
96°C	1 minute	
96°C	10 seconds	x30
50°C	5 seconds	
60°C	4 minutes	
4°C	∞	

2.3. Animal husbandry

Sprague Dawley (SD) rats were maintained in accordance with UK Home Office regulations, under the Animals (Scientific Procedures) Act of 1986. Animals were grouped in (55 x 40 cm) cages with bedding, with *ad libitum* access to food and water. Animals were fed RM1 diet (special Diets Services). Room atmosphere was maintained at 22°C at 60-70% humidity and animals were kept in a 12-hour light/dark cycle. Schedule 1 culling was

performed via rising concentrations of CO_2 and confirmed via cervical dislocation. All experiments were conducted in the light cycle.

2.4. Genotyping

2.4.1. DNA extraction from tail clippings

Tail clips were collected from animals and incubated in 450 µl lysis buffer (50 mM KCl, 1.5 mM MgCl2, 10 mM Tris, 0.45% NP40, 0.45% Tween-20 and 0.5 mg/ml proteinase K, pH 8.5) for 2 hours at 55°C and then at 95°C for 20 minutes to inactivate proteinase K, with brief vortexing throughout.

2.4.2. Genotyping PCR

To genotype extracted DNA, Polymerase chain reaction (PCR) was performed using reagents from Phire Green Hot Start II PCR Master Mix (ThermoScientific, F126L) (see Table. 2.7 and Table. 2.8 for genotyping PCR components and programme, respectively). Human specific primers were designed for exons 8, 20 and 38 of the *LRRK2* transgene and one primer set specific for the rat *Prolactin* gene was used as positive control (see Table 2.9).

Table. 2.7. *Genotyping PCR reaction*

Reaction components	**Volume (µl)**
Genomic DNA	2
Primer pair (10 mM forward and reverse)	1.5
2X Phire Green HS II Master Mix	10
MilliQ H_2O	6.5
Total Volume	20

Table. 2.8. *Genotyping PCR conditions*

Temperature	**Duration**	**Cycles**
98°C	30 seconds	
98°C	5 seconds	x34

58°C	5 seconds	
72°C	2 minutes	
72°C	1 minute	
4°C	∞	

Table. 2.9. *Genotyping PCR primers*

Target	Sense Oligo Sequence (5' to 3')	Anti-Sense Oligo Sequence (5' to 3')
Rat *Prolactin*	GCTTCTGAGCAATGACACCA	ATTCCAGGAGTGCACCAAAC
***LRRK2* Exon 08**	AAAGCTGTGCAGCAGTACCC	CACAGGACAGAAAAGGCATTG
***LRRK2* Exon 20**	GCTGTGGAAGAAGGAACAGC	CAGATGATTTAGGTCAGGTTTTTG
***LRRK2* Exon 38**	CTCAGATTGCCCCTGACTTG	GGCTGCTTCACTTAACTCACC

2.4.3. Agarose Gel Electrophoresis

PCR products were prepared by mixing 10 µl of sample and 1x loading buffer. Samples were loaded alongside 5 µl of DNA ladder and ran to visualise fragment size. PCR products were separated using an agarose gel (1% agarose, 0.005% ethidium bromide in TBE (Tris/Borate/ethylenediaminetetraacetic acid (EDTA)) buffer at 90 V. Gels were imaged using the Chemidoc™ Touch Imaging System (BioRad).

PCR Loading Buffer

100 mM Tris-Cl
4 % (w/v) SDS
0.2 % (w/v) Bromophenol Blue
20% (v/v) Glycerol

2.5. Generation of cortical primary cultures

TG male rats were bred with a SD female to produce transgenic and non-transgenic offspring litters. P1 rats were tail clipped and marked for genotyping. A minimum of 3 animals per genotype were pooled for each experiment. Tail clips were lysed to extract DNA and genotyped as described above. Genotyped pups were culled (P2-P5) in accordance

with UK Home Office regulations, under the Animals (Scientific Procedures) Act of 1986. Brains were extracted and placed in fresh, ice cold Neurobasal(A) media for transportation. Meninges were removed and cortical areas were dissected and shredded into ~0.5 mm pieces in a sterile petri dish with sterile scalpels and collected in ice cold, fresh Neurobasal(A) media. Tissue was incubated in water bath at 37°C in Neurobasal(A) medium (Life Technologies) plus 0.1% trypsin, for 20 minutes. Trypsin was inactivated with Neurobasal(A) containing 20% foetal bovine serum (FBS) and samples were then centrifuged at 1000 x g at 37°C for 5 minutes. FBS containing media was then replaced with Neurobasal(A) wash media and centrifuged at 1000 x g at 37°C for 3 minutes. The wash step was repeated one more time. Wash media was removed and replaced with growth media (Neurobasal(A) media, 2 mM L-glutamine, 1X B27, 1ml MycoZap™ (Lonza)). Tissue was triturated using a P1000 pipette (15x) and then with a P200 pipette (~30x). Processed tissue was stained for dead cells using Solution 18 (Chemotec) containing 80 µg/ml Acridine Orange and 40 µg/ml DAPI, counted using NucleoCounter® NC-250™ (ChemoMetec, Denmark). and seeded accordingly (see Table. 2.10 for cell densities). Cells were kept in the incubator at 37°C, 5% CO_2, 95% relative humidity and 50% of medium was replaced every 2 days. All assays were completed at DIV 14-15.

Table. 2.10. *Seeding cell densities*

Plate type	Cell density	Volume
24-well	8 x 10^5 / ml	500 µl
24-well; coverslip	1.875 x 10^6 / ml	80 µl
96-well	7.5 x 10^5 / ml	100 µl
T75	1 x 10^6 / ml	10 ml

2.6. iPSC-derived dopaminergic neurons

Participant recruitment and LRRK2 *mutation* screening, culture and reprogramming of primary fibroblasts, genotyping of iPSC lines and maintenance of iPSC lines were all carried out by Sally Cowley's group. The generation and characterization of the iPSC lines from healthy individuals and from PD patients carrying the *LRRK2-R1441C* or *LRRK2-G2019S* mutation have been previously described (Connor-Robson et al. 2019; Lang et al. 2019). Cells were replated at DIV 20 and seeded at 5 x 10^5 cells/ml, followed by 15 days of maturation. All experiments were carried out at 35 DIV and data was gathered from 2-3 independent differentiations.

2.6.1. Modified Kriks Protocol

iPSCs were patterned for 11 days to become ventral midbrain precursors cells with LDN193189 (100nM, Merck), SB431542 (10 mM, Tocris), SHH C24II N-terminus (100 ng ml-1, Bio-Techne), Purmorphamine (2 mM, Millipore), FGF8a (100 ng ml-1, Bio-Techne) and CHIR99021 (3 mM, Tocris). Two days prior neuronal induction, iPSCs were dissociated to single cells and plated at a density of 150,000 cells/cm^2 on Geltrex (Life Technologies) and cultured until sub-confluent. Cells were then grown 11 days in knockout serum replacement medium (KSR) containing KO DMEM (Life Technologies), 15% knockout serum replacement (Life Technologies), 2 mM L-glutamine (Life Technologies) and 10 mM β-mercaptoethanol (Merck). KSR medium was gradually shifted to NNB medium containing Neurobasal medium, 0.5X N2, 0.5X B27 and 2 mM L-glutamine (Life Technologies) starting on day 5 of differentiation as described previously. On day 11, media was changed to NB medium containing Neurobasal medium, B27 and 2 mM L-glutamine (Life Technologies) supplemented with CHIR (until day 13) and with BDNF (brain-derived neurotrophic factor, 20n ml-1; Peprotech), ascorbic acid (0.2 mM, Merck), GDNF (glial cell line-derived neurotrophic factor, 20 ng ml-1; Peprotech), TGFβ3 (transforming growth factor type β3, 1 ng ml-1; Peprotech), dibutyryl cAMP (0.5mM; Merck), and DAPT (10mM; Abcam) for 9 days. On day 20, cells were dissociated using Accutase (Life Technologies) and replated at the cell density of 300,000 cells/cm2 in dishes pre-coated with Geltrex in final differentiation medium (NB supplemented with BDNF, GDNF, TGFb3, DAPT, dbcAMP and ascorbic acid). On day 22, cells were treated for an hour with 1 µg ml-1 of Mitomycin C (Life Technologies) in NB medium. Cells were then cultured in final differentiation medium for two weeks until DIV35 before any given experiment.

2.6.2. Expansion Protocol

Feeder-free iPSC lines were routinely cultured on Matrigel (BD Biosciences) in mTeSR1 (StemCell Technologies). Differentiation of dopaminergic neurons was based on previously described protocols (Williamson et al. 2023).

Briefly, two days prior to neuronal induction, iPSCs were dissociated to single cells and plated at a density of 1.5 x 10^5 cells/cm^2 on Geltrex (Life Technologies). iPSCs were patterned for 10 days to become ventral midbrain precursor cells (Zambon et al. 2019). After patterning (DIV 10), cells were expanded for 19 days in KSR and NNB medium (1:3) supplemented with LDN193189 (100nM, Merck) and CHIR99021 (3 µM, Tocris) (Fedele et al., 2017). Cells were passaged four times 1:2 with Accutase on days 10+1, 10+7, 10+13 and 10+18 and plated with 10 µM Y-27632 onto Geltrex coated plates. Cells were frozen at DIV 10+18 in 1:3 of KSR:NNB medium supplemented with 10 % (v/v) DMSO.

Following the expansion of ventral midbrain precursor cells (DIV 11), media was changed to NB medium containing Neurobasal medium, B27 and 2 mM L-glutamine (Life Technologies) and differentiated into dopaminergic neuronal cultures (Zambon et al. 2019). Cells were replated at DIV 20 and seeded at 2.5 x 10^5 cells/cm^2, followed by 15 days of maturation. All experiments were carried out at DIV 35 and data was gathered from 2-3 independent differentiations.

2.7. Fixation and immunocytochemistry staining

Cells were washed with DPBS+/+, fixed with 4% paraformaldehyde solution for 20 minutes and then washed twice with DPBS+/+. Fixed cells were incubated for 1 hour at room temperature in Blocking Solution (0.1% Triton-X, 10% normal goat serum, in DPBS+/+) to block non-specific binding, and then incubated with primary antibodies diluted in Blocking Solution for 1 hour (see Table 2.11). Cells were washed 3x DPBS+/+ and incubated with secondary antibodies in diluted in Blocking Solution for 2/3 hours. Secondary antibodies were donkey anti-mouse and anti-rabbit Alexa Fluor-488 and −555 (Thermo Fisher, a21202, a31570, a21206, a31572), donkey anti-rabbit Alexa Fluor 647 (Invitrogen, a31573), goat anti-chicken Alexa Fluor-555 (Invitrogen a32932), donkey anti-rat Alexa Fluor 594 (Invitrogen, a21209) and donkey anti-mouse Alexa Fluor-647 (Thermo Fisher, a31571). Cells were then washed twice in DPBS+/+, then incubated in 1 µg/ml DAPI (Life Technologies) for 10 minutes at room temperature and washed once with DPBS+/+. Coverslips were mounted onto Superfrost® plus (VWR) microscope slides using Fluorosave reagent (Millipore) and stored in the dark at 4°C. Cells were imaged using the Invitrogen™ EVOS™ FL Auto cell imaging system at 20 x magnification and the Opera Phenix™ High Content Screening System at 63 x magnification.

2.7.1. Antibodies

Table. 2.11. *Antibodies for immunocytochemistry staining*

Antibody	Manufacturer	Catalogue Number	Species	Dilution
58-k Golgi	Abcam	ab27043	Mouse	1:500
Calnexin	Abcam	ab192439	Goat	1:500

Calreticulin	Abcam	ab22683	Mouse	1:500
C-Myc	Cell Signalling	#2276	Mouse	1:500
EEA1	Abcam	Ab70521	Mouse	1:500
Flag-tag	Abcam	Ab1162	Rabbit	1:500
GFAP	Dako	Z0334	Rabbit	1:500
GFP	Invitrogen	A11122	Rabbit	1:500
LAMP1	Santa Cruz Biot.	sc-20011	Mouse	1:100
LC3	Sigma	SAB1305552	Mouse	1:200
LRRK2	Antibodies Inc.	73-253	Mouse	1:500
LRRK2	Abcam	ab133474	Rabbit	1:500
MAP2	Abcam	ab92434	Chicken	1:1000
MIRO1 (RHOT1)	Merck	HPA010687	Rabbit	1:100
NucBlue	Thermo Scientific	R37605	-	1:1000
Phosphorylated S65 Ubiquitin	Merck	ABS1513-I-AF488	Rabbit	1:500
Rab7	Abcam	ab50533	Mouse	1:500
TH	Millipore	AB152	Rabbit	1:250
TOM20	Santa Cruz Biot.	sc-17764	Mouse	1:500
TOM20	Abcam	ab289670	Rat	1:250
vATPase-a1	Abcam	ab176858	Rabbit	1:500, 1:250

2.8. Electron Microscopy

Electron microscopy (EM) was performed by Dr. Natalie Connor-Robson as previously described (Connor-Robson et al. 2019; Janezic et al. 2013). Briefly, rats were terminally anesthetized and perfused with 4% PFA and 0.1% glutaraldehyde. Free-floating coronal brain sections were cut to 60 µm using a vibratome and then incubated with tyrosine

hydroxylase primary antibody (anti-TH, IHC 1:1000; Chemicon AB152). Dopaminergic terminals were revealed by silver-intensified immunogold conjugated secondary antibodies (Nanoprobes) and samples were dehydrated and embedded in Durcapan ACM resin (Fluka). Serial sections of dorsal striatum ~50 nm were cut and collected onto copper grids. Using ImageJ, a circumference was drawn around individual mitochondria and area and roundness measurements were recorded (50-100 mitochondria were analysed per animal). The formula for circularity is 4π(area/perimeter^2), with a value of 1.0 indicating a perfect circle (Takashimizu & Iiyoshi, 2016). ImageJ analysis performed by Dr. Matthew Williamson and statistical analysis performed by Marta Madureira.

2.9. Protein biochemistry

2.9.1. Cellular lysis

For *in vitro* cellular lysis, cells were washed with DPBS+/+ and lysed using either radio-immunoprecipitation (RIPA) buffer (50 mM Tris, 150 mM NaCl, 0.1% sodium dodecyl sulphate (SDS), 0.5.% Na deoxycholate, 1% Igepal (pH 7.4)) or Co-Immunoprecipitation (Co-IP) Lysis Buffer (50 mM Tris-HCl, 150 mM NaCl, 0.5 mM EDTA, 1% Igepal (pH 7.4)), both containing protease (cOmplete EDTA-free, Roche) and phosphatase (PhosSTOP, Roche) inhibitors (see Table 2.11 for lysis details). Cells were detached using a cell scraper (Falcon®) and collected to Eppendorf tubes. Lysates were centrifuged at 10,000 x g at 4°C for 10 minutes. Supernatants were retained and stored at -20°C or -80°C until needed.

Table. 2.12. *Cellular lysis details*

Plate type	Cell type	Lysis Buffer	Volume
24-well	HEK 293T	Co-IP Lysis Buffer	40 µl
12-well	HEK 293T	Co-IP Lysis Buffer	40 µl
6-well	HEK 293T	Co-IP Lysis Buffer	50 µl
6-well	iPSC-derived neurons	RIPA Buffer/Co-IP Lysis Buffer	50 µl
T75	Cortical Primary Cultures	RIPA Buffer	500 µl

2.9.2. Post-mortem tissue homogenisation

Samples were thawed on ice for 15 minutes followed by incubation with Co-IP Lysis Buffer containing protease and phosphatase inhibitors, for another 15 minutes on ice. Tissue was then homogenised on ice using a tissue tearer (Biospec Products), in Co-IP Lysis Buffer. Tissue homogenates were then centrifuged at 10,000 x g at 4°C. The supernatant and the pellet were separated, and both stored at -20°C.

2.9.3. Protein quantification (BCA Assay)

Bicinchonic acid solution was combined with Copper (II) Sulfate Pentahydrate 4% Solution (50:1) to make BCA solution. Protein sample was diluted in lysis buffer and 10 µl was added to a well of a 96-well plate. Then, 100 µl BCA solution was added to each well and incubated at 37°C for 30 minutes. Absorbance was read at 562 nm and the concentration of protein calculated from a bovine serum albumin standard curve.

2.9.4. Western blotting

Cells were lysed in the respective lysis buffer (see Table 2.12) and diluted to 5 µg/µl and 5 x Laemmli sample buffer added (12% SDS, 30% β-mercaptoethanol, 60% Glycerol, 0.012% Bromophenol blue and 375 mM Tris pH 6.8). Samples were reduced and denatured at 95°C for 5 minutes. Samples were loaded into 4-15% Criterion Tris-HCl polyacrylamide gels (BioRad) alongside BLUeye Prestained Protein Ladder (Geneflow) and Magic Mark XP (Invitrogen) to determine target protein molecular weight. Electrophoresis was performed at 200 V for ~60 minutes and proteins transferred to a polyvinylidene difluoride (PVDF) membrane using a Trans-Blot Turbo Transfer System (BioRad) which utilises Trans-Blot Turbo Midi PVDF transfer packs (BioRad) in accordance to manufacturer's instructions. Membranes were incubated in Blocking Solution (5% non-fat milk (Sigma) in PBS/0.1% Tween-20 (PBS-T)) for 1 hour at room temperate and subsequently incubated with primary antibody (see Table 2.13) in Blocking Solution overnight at 4°C. Membranes were washed with PBS-T (3x, 10 minutes) and incubated in horseradish peroxidase (HRP)-conjugated secondary antibody (1:1000) (BioRad) in blocking solution for 1 hour. Peroxidase-linked secondary antibodies used for WB were Goat anti-mouse IgG (H + L)-HRP Conjugate (1706516) and Goat anti-rabbit IgG (H + L)-HRP Conjugate (1706515) (Biorad). Membranes were washed in PBS-T (3x, 10 minutes) and developed using ECL solution (Millipore). Membranes were imaged using the Chemidoc^{TM}Touch Imaging System (BioRad) and quantified using ImageLab (BioRad).

10x Running Buffer (10x)

144g glycine

30.3g Tris Base

10g SDS

MilliQ H_2O up to 1L

PBS-T

PBS (Sigma) dissolved in 999 ml MilliQ H_2O

0.01% Tween-20 (VWR) 1 ml

2.9.5. Co-Immunoprecipitation of cultured cells

Dynabeads™ Protein G (Invitrogen) were washed in PBS+/+ using a magnetic rack (BioRad), using 1.5 mg/sample. Beads were incubated with 40 µg of antibody/sample overnight at 4°C, with rotation. Beads were washed 3 x in PBS+/+ and were then incubated with cell lysates (100 µg of protein for HEK 293T cultured cells, 2.4 mg for cortical primary cultures and at least 1mg for iPSC-DAn cultures) for 5 hours at room temperature, with rocking. Flowthrough was removed for analysis and beads washed 3 x in PBS+/+. Samples were eluted and boiled at 95°C (or 70°C for iPSC-DAn lysates) in 5 x Laemmli sample buffer for 5 minutes and assessed via SDS-PAGE. A mouse *anti*-IgG2a antibody was included as an isotype control to measure the level of nonspecific background signal caused by primary antibodies, corresponding to the isotype source from *anti*-Myc-tag antibody.

2.9.6. Co-Immunoprecipitation of *post-mortem* tissue

Lysates (6 mg of protein) were pre-cleared by incubation with 40 µl of Dynabeads™ Protein G (Invitrogen), for 1 hour at 4°C with rotation. Supernatants were recovered using a magnetic rack (BioRad) and incubated with 40 µg of antibody/sample overnight at 4°C, with rotation. The following day, 40 µl of Dynabeads™ Protein G were added and incubated for 5 hours at room temperature, with rocking. Flowthrough was removed for analysis and beads washed 5 x in PBS+/+ using a magnetic rack. Samples were eluted and boiled at 95°C in 5 x Laemmli sample buffer for 5 minutes and assessed via SDS-PAGE.

2.9.7. Antibodies

Table. 2.13. *Antibodies for Western Blotting*

Antibody	Manufacturer	Catalogue Number	Species	Dilution
β-actin	Biolegend	643807	Mouse	1:50,000
c-Myc	Cell Signalling	#2276	Mouse	1:500
Flag-tag	Abcam	Ab1162	Rabbit	1:500
GFP	Invitrogen	A11122	Rabbit	1:100
HSP60	Cell Signalling	12165	Rabbit	1:500
LAMP1	Santa Cruz Biot.	sc-20011	Mouse	1:1000
LC3B	Cell Signalling	2775	Rabbit	1:1000
LRRK2	Abcam	ab133474	Rabbit	1:500
LRRK2	Antibodies Inc	75-253	Mouse	1:100
MFN2	Abcam	ab56889	Mouse	1:500
MIRO1 (RHOT1)	Merck	WH0055288M1	Mouse	1:700
OPA1	BD Bioscience	612607	Mouse	1:500
OxPhos Human WB Antibody Cocktail	Thermo Scientific	45-8199	Mouse	1:500
OxPhos Rodent WB Antibody Cocktail	Thermo Scientific	45-8099	Mouse	1:500
p62	Abcam	ab109012	Rabbit	1:500
Phosphorylated S106 Rab12	Abcam	ab256487	Rabbit	1:250
Phosphorylated Ser1292 LRRK2	Abcam	ab203181	Rabbit	1:500
Phosphorylated Ser935 LRRK2	Abcam	ab133450	Rabbit	1:500
Phosphorylated T72 Rab8A	Abcam	ab230260	Rabbit	1:100
Phosphorylated T73 Rab10	Abcam	ab230261	Rabbit	1:250

Rab10	Cell Signalling	8127S	Rabbit	1:1000
Rab12	Proteintech	18843-1-AP	Rabbit	1:1000
Rab8A	DB Bioscience	610844	Mouse	1:100
TH	Millipore	AB152	Rabbit	1:500
TOM20	Proteintech	11802-1-AP	Rabbit	1:500
vATPase-a1 (v0a1)	Abcam	ab176858	Rabbit	1:500
vATPase-a1 (v0a1)	Santa Cruz Biot.	sc-293336	Mouse	1:500
vATPase-A1 (v1A1)	Santa Cruz Biot.	sc-374475	Mouse	1:500

2.10. Opera Phenix/Harmony image analyses

For quantitative analysis of immunocytochemistry staining, images were analysed using Harmony High-Content Imaging and Analysis Software (v. 9.3.1.471, Opera Phenix, Perkin Elmer). Pipelines were created to characterise neuronal-astrocytic populations in cortical primary cultures with MAP2, GFAP and DAPI antibody staining (Fig. 3.10). Similar pipelines were created to identify cellular distributions of LRRK2 and vATPase-a1 individually and for co-localised puncta of both protein complexes in neuronal populations of cortical primary cultures with Y-Pet/LRRK2, vATPase-a1, MAP2, organelle markers and DAPI antibody staining. Pipelines were also created to identify cellular distributions of LRRK2 and vATPase-a1 individually and for co-localised puncta of both protein complexes in HEK293T cultures with myc-tag LRRK2, vATPase-a1, organelle markers and DAPI antibody staining. Pipelines were created to characterise and quantify neuronal populations and determine spot number, spot area and relative spot intensity (corrected), average mean per well. To analyse mitochondrial morphology, we created a pipeline to identify nuclei and *Mito-QC* transduced neuronal cells, then applied the proprietary SER ridge filter to analyse mitochondrial spots (mCherry-positive puncta) and extracted the morphology measurements for area, roundness, width, length and width:length ratio which are automatically calculated.

2.11. Assessing proteolytic degradation

2.11.1. DQ-BSA assay

Primary cortical cultures or iPSC-derived DA neuronal cultures were plated in 96-well plates, treated with DMSO, Chloroquine (50 nM, 24 hours) or Clioquinol (100 nM, 48 hours) and incubated with 30 µg/ml DQ Red BSA (Invitrogen, D12051) and 0.1 µM NeuroFluor™ NeuO (StemCell Technologies, 01801) for 2 hours at 37°C with 5% CO_2. Then, cells were washed with DPBS once and incubated in Hanks' Balanced Salt Solution (HBSS). Cells were imaged live on an Opera Phenix™ High Content Screening System (Perkin Elmer) using the following channels: DAPI (excitation/emission, 360 nm⁄460 nm), DQ Red BSA (excitation/emission, 590 nm/620 nm) and NeuO (excitation/emission, 468 nm/557 nm). Lysosomal flux was measured as DQ-BSA number of spots multiplied by relative spot intensity in NeuO+ cells, referred to as DQ-BSA Index.

2.12. Assessing mitochondrial health and function

2.12.1. Seahorse assay

Primary cortical cultures or iPSC-derived DA neuronal cultures were plated in a XF96 Polystyrene Cell Culture Microplate (Seahorse Bioscience) on day 20 and further matured until day 35 before analysis. On the day of the assay, the assay medium was prepared fresh using the XF Base Medium (Agilent Technologies) supplemented with 10 mM Glucose (Merck), 1 mM Sodium Pyruvate (Merck) and 2 mM L-Glutamine (Thermo Fisher Scientific). At least 1 hour before the assay, the cells were washed once with the assay medium and then incubated at 37°C in a non-CO_2 incubator. Three baseline recordings were made, followed by sequential injection of the ATP synthase inhibitor oligomycin (Oligo; Merck, 1 µM), the mitochondrial uncoupler p-triflouromethoxyphenylhydrazone (FCCP; Merck, 1 µM), the Complex I and III inhibitors Rotenone and Antimycin A (R/A; Merck, 5 µM) and the glucose analog 2-deoxyglucose (2-DG; Merck, 50 mM). Mitochondrial respiration and glycolytic activity of DA cultures were measured using a Seahorse XFe96 Analyzer (Agilent Technologies) and normalized to total well protein content.

2.12.2. ATP Production measurement

Media was removed from plates and cells were mixed with CellTiter-Glo® 3D Cell Viability Assay (Promega). Then, 100µL of substrate medium were transferred to a 96-white plate and incubated for 25 minutes at room temperature, shielded from light. To measure ATP

production, luminescence was measured using the multi-mode plate reader PHERAstar FSX (BMG Labtech) and measurements were normalised to cell number. Cell number was measured prior to the start of the assay by adding Hoechst nuclear marker (NucBlue™ Live ReadyProbes™ Reagent, R37605, Invitrogen) to cells and imaging live (Opera Phenix™ High Content Screening System, Perkin Elmer).

2.12.3. Mitochondrial Reactive Oxygen Species

To detect mitochondrial ROS, cells were incubated with 2.5 µM MitoSOX Red Mitochondrial Superoxide Indicator (Life Technologies, M36008) and nuclear marker Hoechst (NucBlue™ Live ReadyProbes™ Reagent, R37605, Invitrogen) for 10 minutes at 37°C with 5% CO_2. Following a wash with growth media, Cells were immediately imaged and MitoSOX fluorescence was measured at excitation/emission maxima: 488/650-760 nm, using a confocal microscope (Opera Phenix™ High Content Screening System, Perkin Elmer).

2.12.4. Mitochondrial Membrane Potential

To detect changes in mitochondrial membrane potential (ΔΨm), cells were incubated with 5 µM JC-10 (AAT Bioquest, Inc.) at 37°C for 1h. The fluorescence intensities were measured using the multi-mode plate reader PHERAstar FSX (BMG Labtech) by fluorescence excitation/emission maxima: 514/529 nm, monomer form, and 585/590 nm, aggregate form. To establish that the JC-10 signal was indicative of ΔΨm, experiments were terminated inducing a maximal mitochondrial depolarization by addition of 10µm carbonyl cyanide 3-chlorophenylhydrazone (CCCP; Merck).

2.13. Assessing mitophagy flux

Imaging and analysis of the Mito-QC reporter to assess mitophagy was performed as previousy described (Allen et al., 2013). In brief, cells were imaged on an Opera Phenix™ High Content Screening System (Perkin Elmer) using the following channels: DAPI, eGFP and mCherry. Images were then processed and analysed using Harmony™ software (Perkin Elmer). In brief, the Harmony™ analysis pipeline consisted of the following building blocks: Find Nuclei, Find Cytoplasm, Image calculation: GFP/mCherry ratio, Find Spots (Red only), Calculate spot properties/cell.

2.14. Statistics

Graphs and statistical significance for all data was generated using Prism GraphPad (v. 9.3.1.471) software. The results are expressed as mean ± SEM. Statistical tests use were one- or two-way analysis of variance test to evaluate the differences between groups. One sample t-test or multiple t tests were used to compare between genotypes. Values of $P < 0.05$ were considered statistically significant. Details of statistical tests used for each graph are described in figure legends.

Chapter 3 – Characterising LRRK2 and vATPase-a1 interaction

3.1. Introduction and aims

As mentioned previously (section 1.5), *LRRK2* mutations affect the autophagy-lysosomal pathway. *LRRK2-hWT* and *LRRK2-G2019S* cultures have blocked clearance of autophagosomes whereas *LRRK2-R1441C* shows impaired autolysosome fusion and lysosomal degradation that is subsequently rescued by treatment with clioquinol, a zinc ionophore that restores physiologically acidic pH levels. A novel interaction between LRRK2 and the a1 subunit of vATPase has also been reported in rat primary cortical cultures, that is severely reduced in *LRRK2-R1441C* neuronal cultures (Wallings, Connor-Robson, and Wade-Martins 2019). This interaction has yet to be demonstrated in human cellular models, which will be crucial for the relevance of targeting vATPase and lysosomal function as a LRRK2-related PD therapeutic approach. Furthermore, the molecular features of this novel interaction between LRRK2 and lysosomal vATPase-a1 (v0a1) have not yet been characterised. Detailed investigation into the binding sites between LRRK2 and vATPase will determine the key interacting domains and advance strategies for potential therapies. We set out to recapitulate the interaction between LRRK2 and vATPase-a1 in a human cellular context, more specifically in HEK293T cells, human *post-mortem* tissue homogenates from a healthy donor and *LRRK2* iPSC-derived dopaminergic neurons. As discussed, LRRK2 effects and phenotypes are also dependent on cellular context (Zeng et al. 2018), so it is important to include various cell types and models. Using a LRRK2 and vATPase library of constructs, we also aim to determine which LRRK2 domains are necessary for the interaction between these two protein complexes to occur effectively.

It has also been described that vATPase-a1 is N-glycosylated in the ER and trafficked to the lysosome, where the V_0 and V_1 domains of the proton pump assemble to form the functional complex. When *presenilin 1 (PS-1)*, a genetic risk factor for Alzheimer's Disease, is knocked-out in mice blastocysts, the a1 subunit is retained in the ER and is not trafficked to the lysosome, leading to lysosomal defects and indicating PS-1 chaperones a1 subunit to its correct cellular coordinates (Lee et al. 2010). Following the impaired interaction between LRRK2-R1441C and v0a1 subunit in primary cortical cultures, we hypothesised that LRRK2 could also be involved in chaperoning a1, trafficking it from the ER to the lysosome, and that the *LRRK2-R1441C* mutation, located in the ROC domain, would disrupt this interaction. This could then result in reduced levels of vATPase-a1 in its respective functional site and consequent dysfunction of lysosomal degradation. To investigate this, we propose to visualise LRRK2 and vATPase-a1 in cells and analyse their co-localisation with various cellular organelles to assess its distribution, for instance in ER,

autophagosomes, lysosomes, early and late endosomes, mitochondria and Golgi-Apparatus.

Chapter aims:

- To characterise interaction between LRRK2 and vATPase-a1 in human models.
- To investigate the role of LRRK2 and vATPAse-a1 interaction in cellular biology.

3.2. Results

3.2.1. LRRK2 and v0a1 interaction occurs at the LRRK2 ROC domain

Assessing endogenous expression of v0a1 in HEK cells shows the a1 subunit can be found ubiquitously in cellular organelles as a1 co-localised with ER marker calreticulin, late endosome marker Rab7, early endosome marker EEA1, mitochondrial marker TOM20, lysosomal marker LAMP1, autophagosome marker LC3, Golgi-Apparatus marker 58-k Golgi, nuclei marker DAPI and LRRK2 (percentage of co-localised v0a1 spots with organelles/protein spots between 25-40%) (Fig. 3.1).

Further characterisation of the interaction between LRRK2 and vATPase-a1 has not yet been studied. To investigate this interaction in more detail, we sought to understand which LRRK2 domains were involved in binding to the a1 subunit of vATPase, and whether LRRK2 kinase enzymatic activity was necessary for this interaction. To tackle this, first we acquired a library of plasmid DNA constructs containing *hLRRK2* full sequence, *LRRK2-R1441C* mutation and constructs containing each *LRRK2* domain individually including *LRR*, *COR*, *ROC-COR-Kinase* (*RCK*), *Kinase* and *WD-40*. An additional construct containing 3 mutations that render LRRK2 kinase-dead (*LRRK2-KD*), namely Lysine 1906 mutated to Alanine, Aspartate 1994 mutated to Alanine and Aspartate 2017 mutated to Alanine was also acquired. *LRRK2* sequences were tagged with two *Myc-tag* cassettes in the N-terminus region, allowing the detection of transfected LRRK2 expression in cultures using an *anti-*Myc-tag antibody. Thus, a LRRK2 library was assembled containing the following constructs: *LRRK2-WT*, *LRRK2-LRR*, *LRRK2-RCK*, *LRRK2-ROC*, *LRRK2-COR*, *LRRK2-Kinase*, *LRRK2-WD-4*0, *LRRK2-R1441C* and *LRRK2-KD* (Fig. 3.2 A-B).

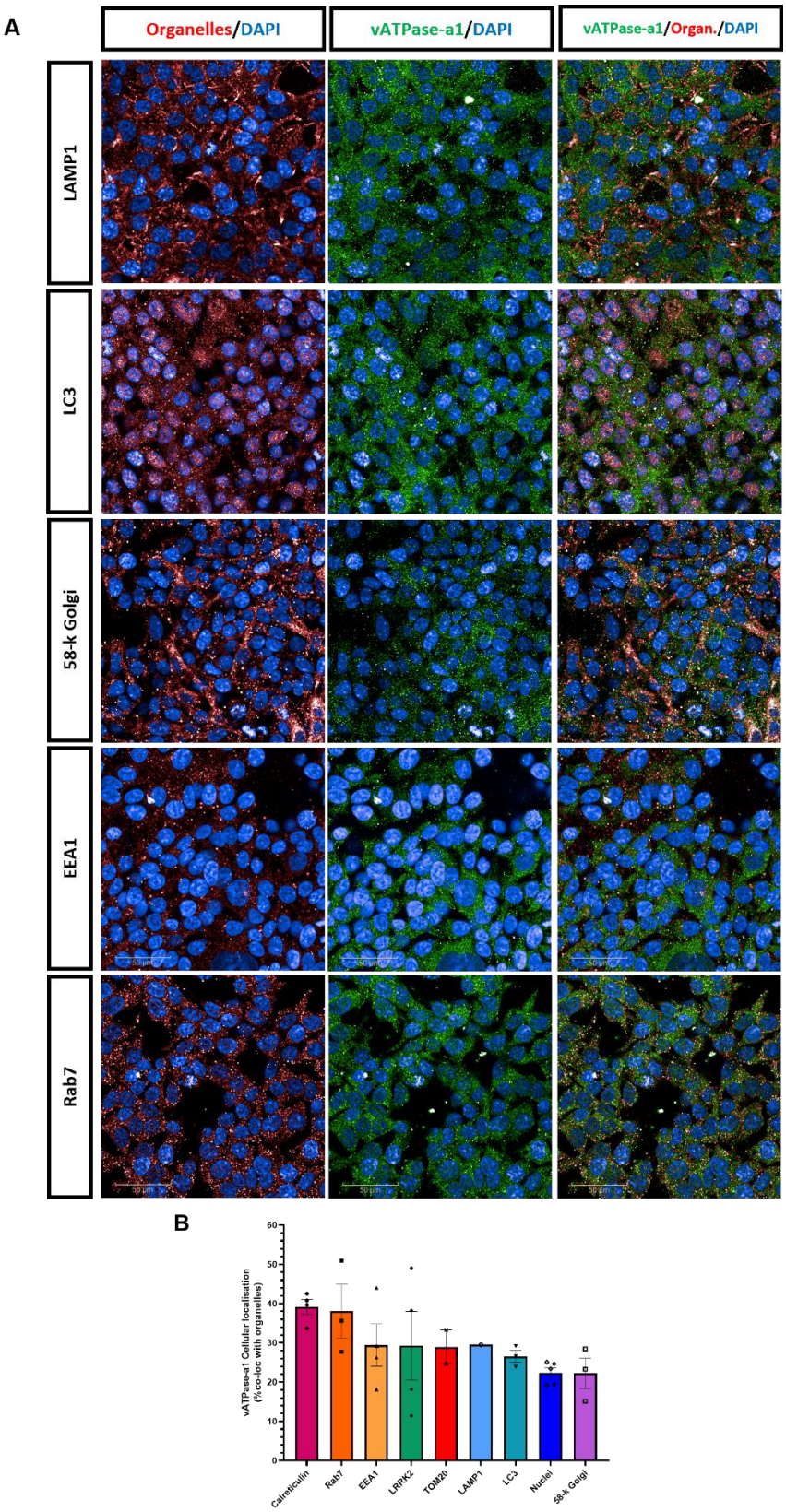

***Figure 3.1. – vATPase-a1 endogenous expression in HEK293T cells*. (A)** HEK293T cells were fixed and immunostained for vATPase-a1 and organelle markers corresponding to lysosomes (LAMP1), autophagosomes (LC3), trans-Golgi network (58-k Golgi), early

endosomes (EEA1) and late endosomes (Rab7). **(B)** Co-localisation between vATPase-a1 and organelle markers was quantified. (Bars represent mean +/- SEM; (N = 3 independent cultures; ∗P <0.05; non-significant (not represented); Ordinary one-way ANOVA. Scale bar = 50 µm).

We acquired a construct containing *vATPase-a1* wildtype sequence and another containing *vATPase-a1*, with the N-glycosylation recognition site mutated (N495Q), therefore rendering the site not glycosylated, henceforth referred to as *vATPase-a1-Mut*. The *vATPase-a1* constructs express a1 tagged with two Flag-tag cassettes in the C-terminus region, allowing for detection of transfected a1 expression in cultures. Also, these constructs contained an ampicillin antibiotic resistance cassette to allow for bacterial colony selection (Fig. 3.2 C). All plasmids were validated by restriction enzyme digestion followed by 2% agarose gel electrophoresis to resolve DNA fragments (Fig. 3.3 A) and Sanger-sequencing was performed to verify the correct nucleotide sequence of all plasmids (data not shown). Next, *LRRK2* and *vATPase-a1* plasmids were transfected into HEK293T cells to assess expression of transgenes and validate constructs. Lysates were collected and immunoblotted for *anti*-Myc-tag antibody to assess expression of myc-LRRK2 constructs, where all constructs showed bands corresponding to the expected sizes of LRRK2 transgenic protein (Fig. 3.3 B). Full length tagged LRRK2 and vATPase-a1 were transfected into HEK cells and co-localisation between myc-tag and LRRK2 or flag-tag and a1 subunit was assessed using immunostaining and immunoblotting to confirm successful transfection (Fig. 3.4). However, the myc antibody used to assess transfection of myc-LRRK2 showed high levels of fluorescence in non-transfected HEK cells, suggesting it lacks specificity as assessed by immunostaining. Then, the effect of ATPase-a1 mutation (N495Q) at the glycosylation site (vATPase-a1-Mut) on a1 subunit cellular trafficking was investigated, using transfected HEK cells and immunostaining to identify a1 subunit spots co-localising with different organelle markers for ER, Golgi-Apparatus, mitochondria, early and late endosomes (calreticulin, 58-k Golgi, TOM20, EEA1 and Rab7, respectively). Interestingly, mutated vATPase-a1 spots accumulated in the Golgi-Apparatus and were significantly decreased in mitochondria, downstream of the cellular trafficking cascade (Fig. 3.5). These results confirm the previous reports that a1 subunit mutation altered cellular trafficking (Lee et al. 2010)**.**

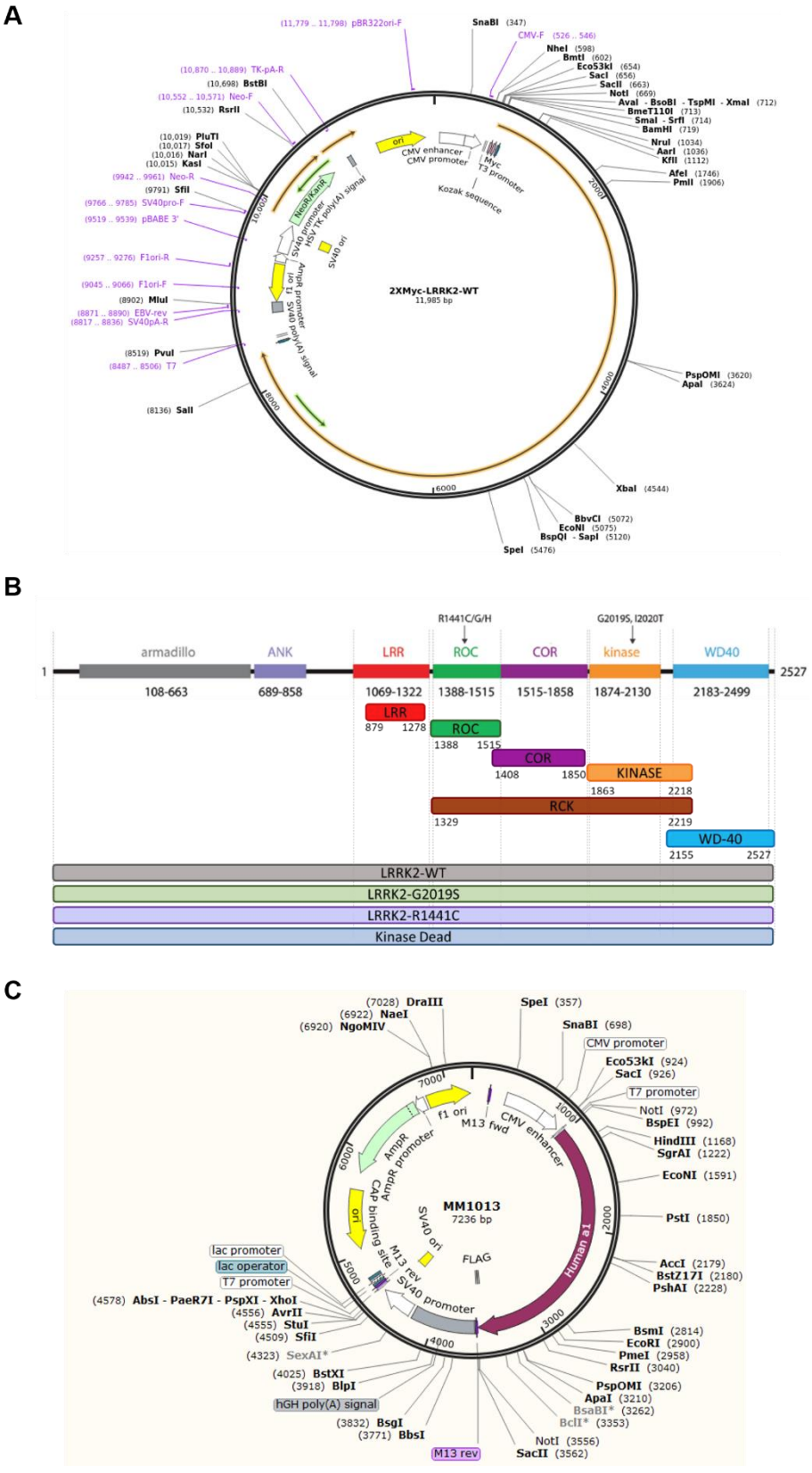

Figure 3.2 – LRRK2 and vATPase-a1 Bacterial Plasmids. **(A)** Example of a LRRK2 plasmid constructs used in this study (2xMyc-LRRK2-WT). The plasmid vector has a pCMV background. Contains a CMV promoter, 2 Myc-tag cassettes, LRRK2 sequence, poly(A)

signal and Kanamycin resistance gene cassette. **(B)** LRRK2 construct library showing LRRK2 protein and respective 2xMyc-tagged LRRK2 constructs available. **(C)** Example of 2xFlag-vTPase-a1-WT, one of the vATPase-a1 plasmid constructs. The plasmid contains a CMV promoter, vATPase-a1 sequence, 2 flag-tag cassettes, poly(A) signal and Ampicillin resistance gene cassette.

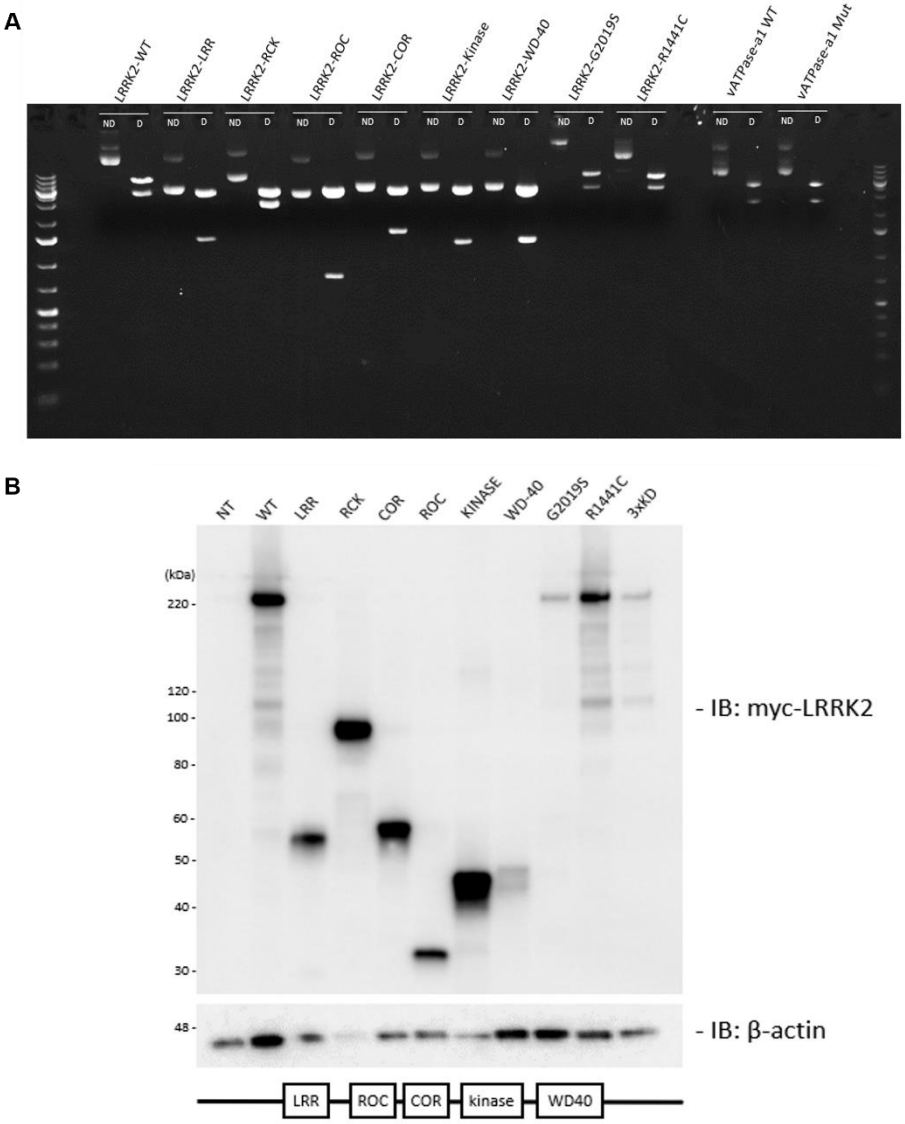

Figure 3.3 – Validation of Myc-LRRK2 and flag-vATPase constructs. **(A)** Restriction enzyme digestion was performed to verify LRRK2 and vATPase-a1 construct library. **(B)** Immunoblots of 2xMyc-LRRK2 constructs transiently transfected into HEK293T cells. Western Blot was probed using anti-Myc-tag antibody to identify LRRK2 and anti-β-actin. IB: immunoblot.

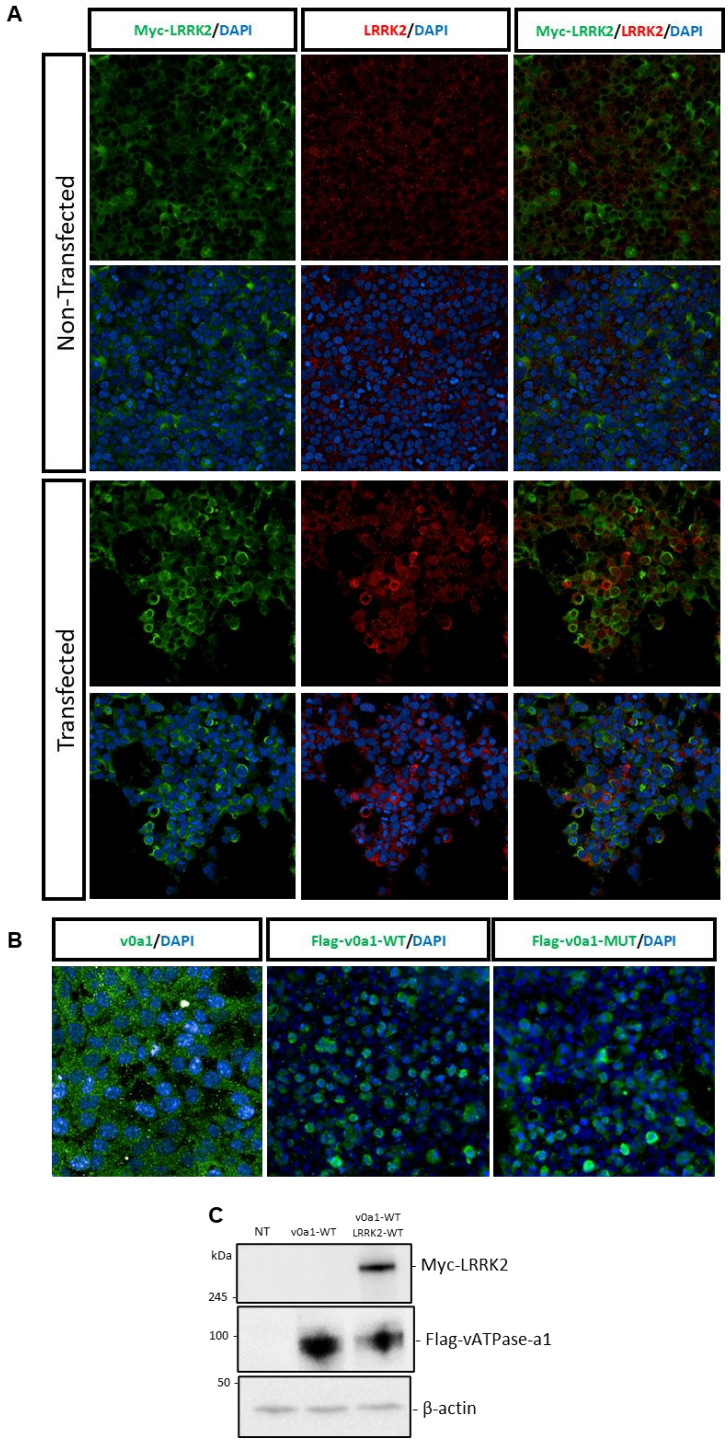

Figure 3.4 – Transfection of Myc-LRRK2 and flag-vATPase constructs. HEK293T cells were transiently co-transfected with 2xMyc-LRRK2-WT and 2xFlag-vATPase-a1 WT constructs and immunostained for **(A)** anti-Myc and anti-LRRK2 antibodies or **(B)** anti-Flag and anti-vATPase-a1 antibodies to observe plasmid expression. **(C)** Immunoblots of HEK293T cells transiently transfected with 2xMyc-LRRK2 and flag-vATPase constructs. Western Blot was probed using anti-Myc-tag antibody to identify LRRK2, anti-flag antibody to identify vATPase-a1 and anti-β-actin. N = 3 wells per condition.

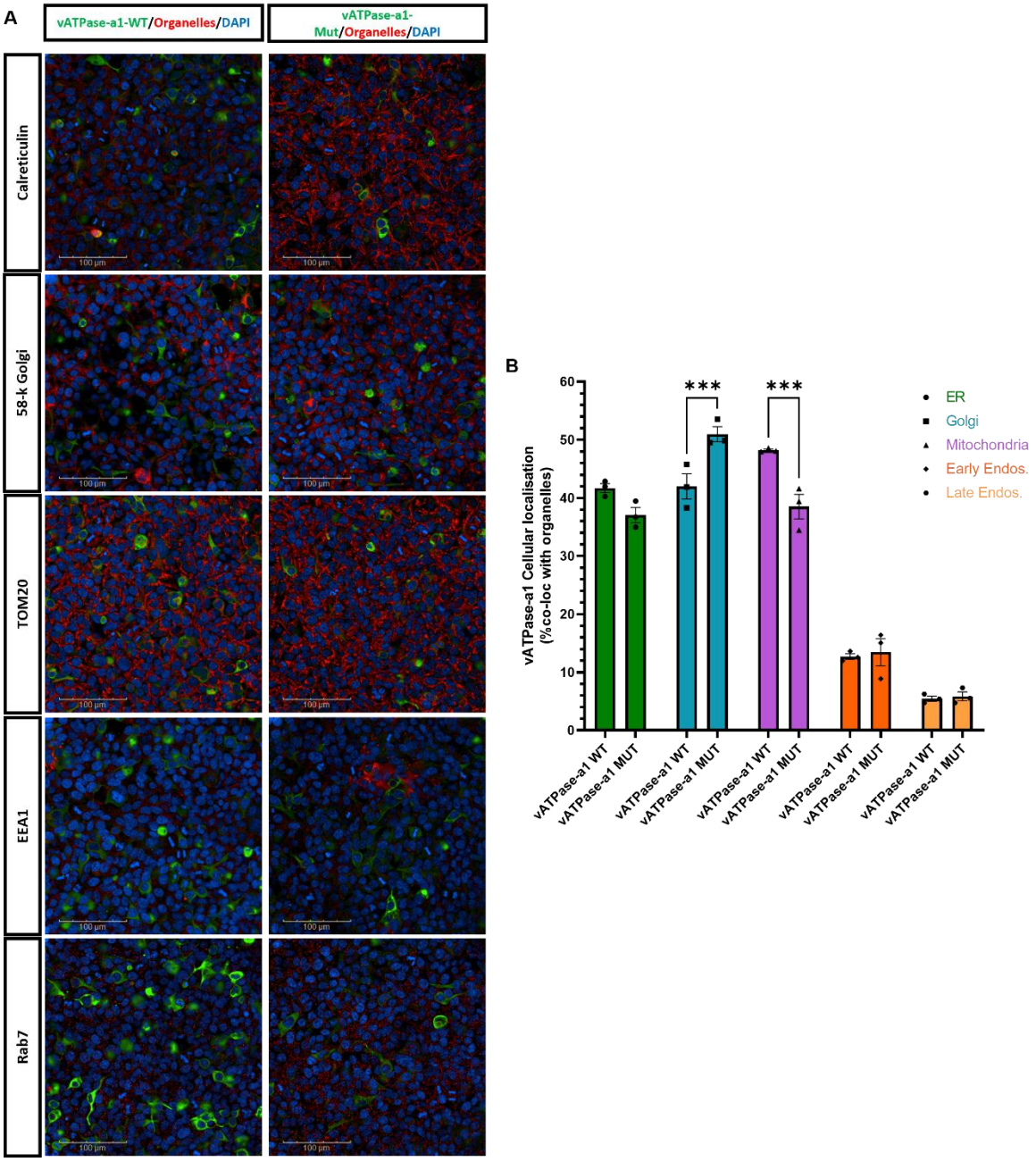

Figure 3.5 – vATPase-a1 cellular localisation in transfected HEK293T cells. HEK293T cells were transiently transfected with 2xFlag-vATPase-a1 WT or 2xFlag-vATPase-a1 MUT constructs. **(A)** Cells were fixed and stained for vATPase-a1 and organelle markers corresponding to endoplasmic reticulum (Calreticulin), trans-Golgi network (58-k Golgi), mitochondria (TOM20), early endosomes (EEA1) and late endosomes (Rab7). **(B)** Co-localisation between vATPase-a1 and organelle markers was quantified as a percentage of vATPase-a1 puncta co-localised with respective organelle marker puncta, over the total

vATPase-a1 population. (Bars represent mean +/- SEM; (N = 3 independent cultures; ***P <0.001; non-significant (not represented); Two-way ANOVA. Scale bar = 100 µm).

Recently, the interaction of LRRK2 and vATPase-a1 was discovered in LRRK2 transgenic rat primary cortical cultures, which is impaired by *LRRK2-R1441C* mutation but not *LRRK2-G2019S* (Wallings, Connor-Robson, and Wade-Martins 2019). This interaction was investigated in human cells (HEK) co-transfected with full length vATPase-a1 WT and LRRK2 constructs. By transfecting each *LRRK2* construct separately, while concomitantly co-transfecting *vATPase-a1-WT*, and then performing individual co-immunoprecipitation experiments, the LRRK2 binding site for vATPase-a1 can be determined. To this effect, LRRK2 was immunoprecipitated with anti-Myc-tag antibody and pulled-down v0a1 subunit was detected by immunoblotting. A band for a1 was also visible in the input (~130 kDa) and a band for LRRK2 was visible in the co-immunoprecipitated sample (285 kDa), which reflects the presence of both protein complexes, confirming the LRRK2/v0a1 interaction also occurs in human cellular models (Fig. 3.6 A-B). Contrary to LRRK2-WT, co-immunoprecipitated isotype control did not show a band for a1, while it showed a band for LRRK2 (285 kDa) and the presence of a1 in the input (~130 kDa) thereby confirming assay specificity (data not shown). An additional negative control was used consisting of co-immunoprecipitation performed without the pull-down antibody (anti-Myc antibody), which also showed absence of a1 subunit band but presence of myc-LRRK2 (data not shown). Analysis of the western blot revealed that a bright band was present in the co-immunoprecipitated sample corresponding to LRRK2-WT, but not for LRR, COR, Kinase or WD-40 domains (Fig. 3.6 A-B)**.** There were no differences between LRRK2 inputs, except an observed increase in LRRK2-RCK construct, when compared to LRRK2 full length construct (Fig. 3.6 C). Therefore, the interaction of the a1 subunit is likely occurring at the ROC domain of LRRK2, since all other domains showed a significant loss of LRRK2/v0a1 co-immunoprecipitation, compared to full length LRRK2 (Fig. 3.6 B, Fig. 3.6 D).

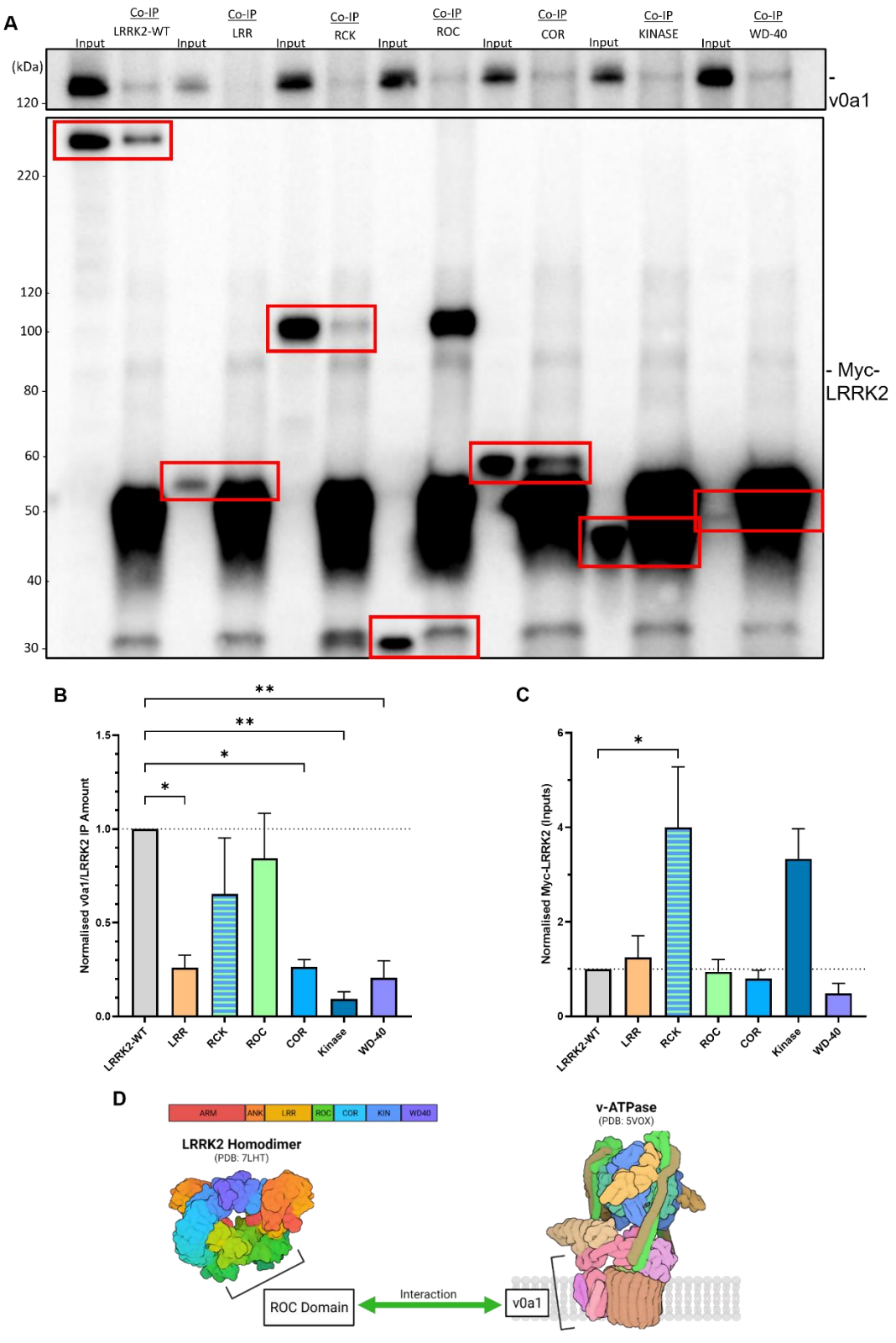

Figure 3.6 – LRRK2 and vATPase-a1 interact through the ROC domain region. **(A)** Using lysate from HEK293T transiently co-transfected with 2xMyc-LRRK2 library of constructs and 2xflag-vATPase-a1-WT constructs, the vATPase-a1 subunit was immunoprecipitated with anti-Myc-tag antibody and detected by anti-v0a1 antibody. **(B)** For

quantification, the intensity of v0a1 band is divided by the total LRRK2 intensity, expressed as a fraction of the mean of the 2xMyc-LRRK2-WT construct. **(C)** Myc-LRRK2 transfection efficiency was calculated as the input band for LRRK2 constructs, normalised to LRRK2-WT band intensity **(D)** Schematic representation to model the interaction between LRRK2 and vATPase. (Bars represent mean +/- SEM; (N = 3 independent cultures; ∗P <0.05; ∗∗P <0.01; non-significant (not represented); Ordinary one-way ANOVA.

Given that LRRK2 contains a MAPKKK-like domain that functions as a kinase, HEK293T cells transfected with full-length constructs containing the kinase domain (*LRRK2-WT*, *LRRK2-R1441C* and *LRRK2-KD*) were investigated further. To study the effects of LRRK2 kinase inhibitor in this interaction, a dose response experiment was performed with two different inhibitors (MLi-2 and PF-06447475), to establish the appropriate concentration significantly decreasing LRRK2 phosphorylation, as measured by LRRK2 autophosphorylation site pSer935 in transfected HEK cells. The 48 hours treatment showed a good inhibition of MLi-2 and PF-06447475 at 100nM, henceforth used experimentally (Fig. 3.7). Then, to establish whether kinase activity was required for LRRK2/v0a1 interaction, the effect of MLi-2 and PF-06447475 LRRK2 kinase inhibitors and clioquinol in the LRRK2/v0a1 interaction was assessed, using immunoprecipitation and immunoblotting of co-transfected HEK cells. As before**,** LRRK2/v0a1 interaction was confirmed in WT constructs, and there was an increase in *LRRK2-KD* and a decrease in *LRRK2-R1441C* constructs, albeit non-significant (Fig. 3.8). Kinase inhibitors and clioquinol did not show any significant changes in LRRK2/v0a1 interaction of co-transfected HEK cells and there were no significant differences in LRRK2 inputs (Fig. 3.8 B-C). Next, the vATPase-a1 glycosylation state and its role in LRRK2 interaction was assessed, by performing immunoprecipitation and immunoblotting of co-transfected HEK cells with full length LRRK2 constructs along with full length vATPase-a1 wildtype or mutant (N495Q) constructs (Fig. 3.9). The LRRK2/v0a1 interaction was confirmed in the *LRRK2-WT* construct, and there was significant increase in the *LRRK2-KD* construct (Fig. 3.9 B). However, no significant differences were observed in the *vATPase-a1-Mut* construct when co-transfected with full length LRRK2 constructs and there were no significant differences in LRRK2 inputs (Fig. 3.9 B-C).

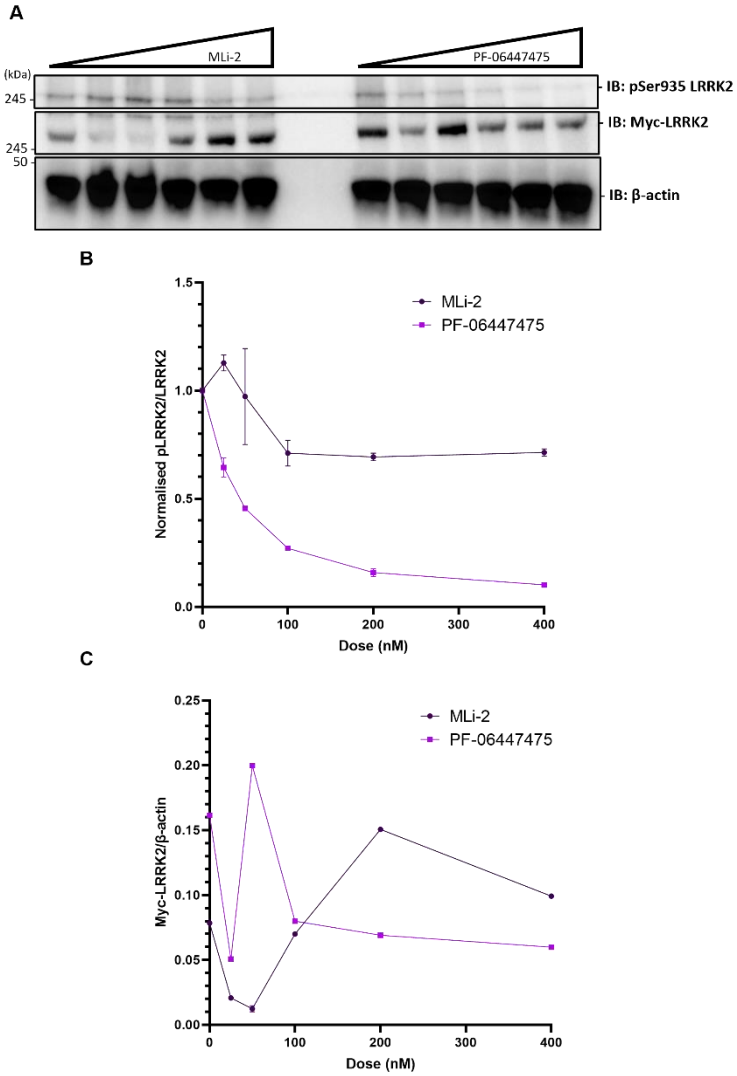

Figure 3.7 – LRRK2 kinase inhibition using MLi-2 and PF-06447475 in transfected HEK293T cells. **(A)** HEK293T cells were transiently transfected with 2xMyc-LRRK2-WT construct and treated with MLi-2 or PF-06447475 (0, 25, 50, 100, 200, 400nM) for 2h, prior to cell lysis. **(B)** For quantification, the ratio of phosphorylated LRRK2 (Ser935) over Myc-LRRK2 was calculated, normalised to the fraction of the non-treated 2xMyc-LRRK2-WT construct. **(C)** Myc-LRRK2 transfection efficiency was calculated as the intensity of the input band for LRRK2 constructs, normalised to LRRK2-WT band intensity. IB: immunoblot. Bars represent mean +/- SEM; (N = 3 wells per condition).

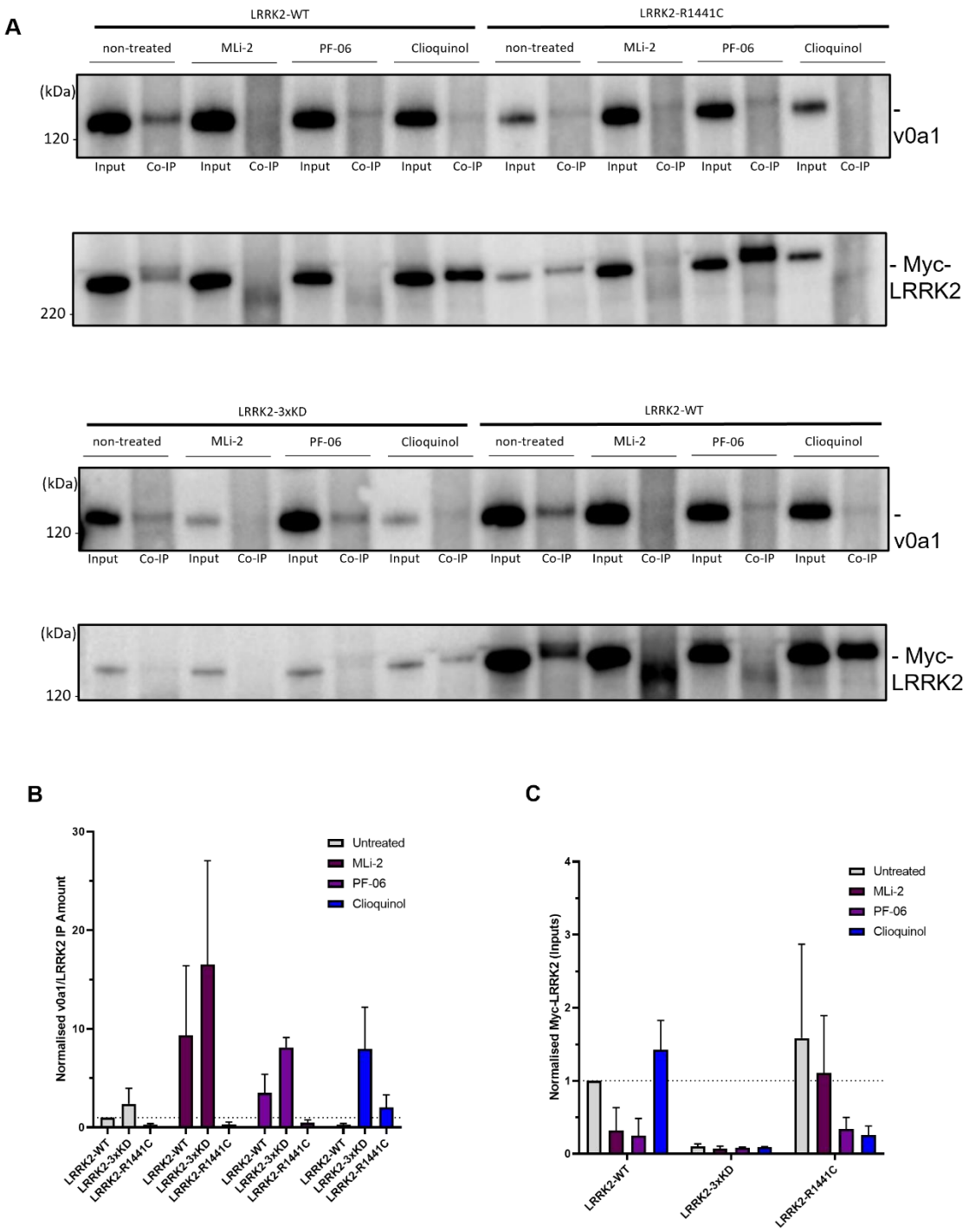

Figure 3.8 – Effect of LRRK2 kinase inhibitors and Clioquinol in LRRK2 interaction with vATPase-a1. **(A)** Using lysate from HEK293T transiently co-transfected with full length 2xMyc-LRRK2 constructs and 2xflag-vATPase-a1-WT constructs and treated with either MLi-2 (100nM, 2h), PF-06647475 (50nM, 2h) or Clioquinol (1µM, 48h), the vATPase-a1 subunit was immunoprecipitated with anti-Myc-tag antibody and detected by anti-flag tag antibody. **(B)** For quantification, the intensity of v0a1 band is divided by the total LRRK2 intensity, expressed as a fraction of the mean of the 2xMyc-LRRK2-WT construct. **(C)** Myc-

LRRK2 transfection efficiency was calculated as the input band for LRRK2 constructs, normalised to LRRK2-WT band intensity. (Bars represent mean +/- SEM; (N = 3 independent cultures; ∗P <0.05; non-significant (not represented); Two-way ANOVA.

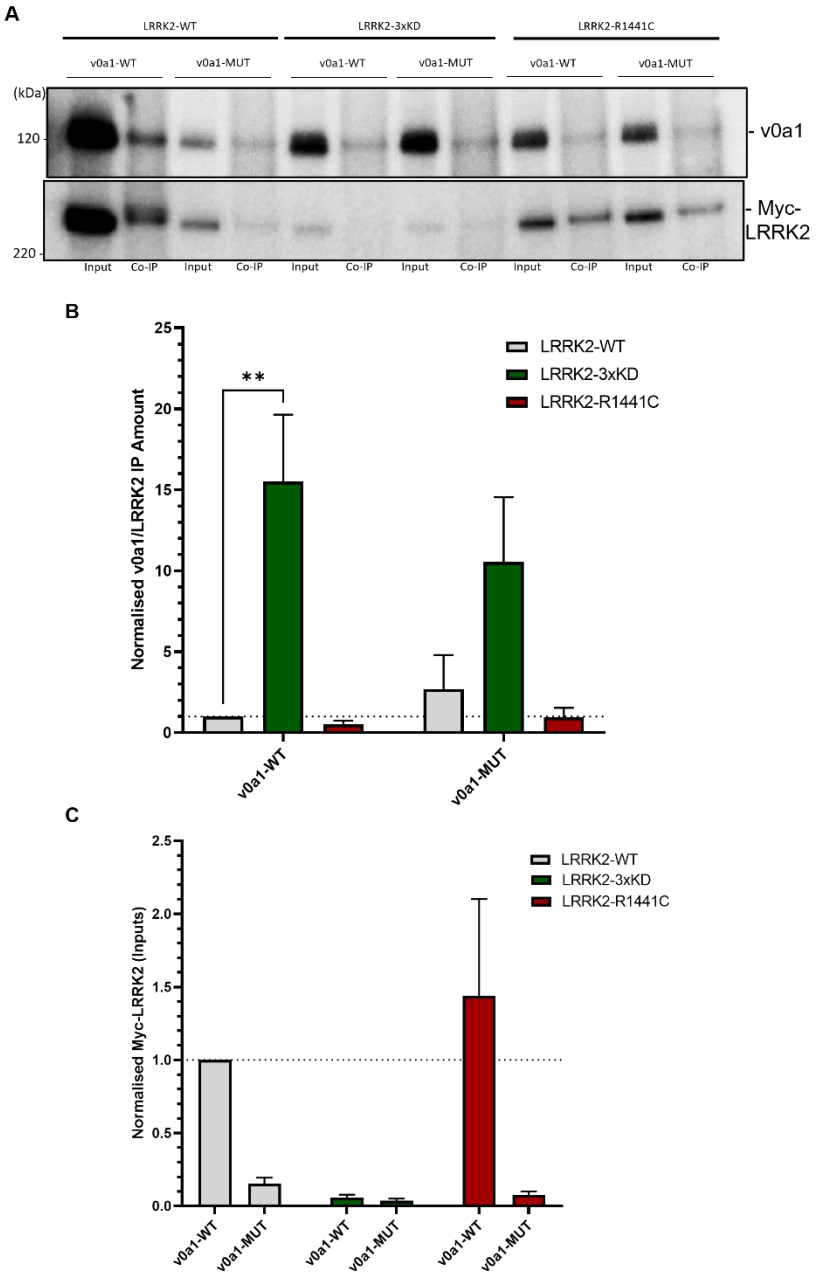

Figure 3.9 – Effect of vATPse-a1 glycosylation state in the interaction with LRRK2. **(A)** Using lysate from HEK293T transiently co-transfected with full length 2xMyc-LRRK2 constructs and 2xflag-vATPase-a1-WT or 2xflag-vATPase-a1-MUT constructs, the vATPase-a1 (v0a1) subunit was immunoprecipitated with anti-Myc-tag antibody and detected by anti-flag tag antibody. **(B)** For quantification, the intensity of v0a1 band is divided by the total LRRK2 intensity, expressed as a fraction of the mean of the 2xMyc-

LRRK2-WT construct. **(C)** Myc-LRRK2 transfection efficiency was calculated as the input band for LRRK2 constructs, normalised to LRRK2-WT band intensity. (Bars represent mean +/- SEM; (N = 3 independent cultures; ∗P <0.05; ∗∗P <0.01; non-significant (not represented); Two-way ANOVA.

Taken together, these results confirm the LRRK2/v0a1 interaction occurs in human cells, mainly within the ROC domain. LRRK2-R1441C impairment was not replicated, however it is likely kinase activity of LRRK2 plays a role, as a LRRK2 kinase-dead construct seemed to increase the LRRK2/v0a1 interaction. Concomitantly, MLi-2 and PF-06447475 LRRK2 kinase inhibitors and clioquinol do not show any changes in the LRRK2/v0a1 interaction. Finally, glycosylation status of 1 subunit does not seem to determine LRRK2/v0a1 interaction.

3.2.2. *LRRK2-R1441C* does not alter v0a1 cellular localisation in primary cortical cultures

Since LRRK2 levels vary between cell types it is possible LRRK2 plays different roles within different cell types, and it is important to include models more adequately recapitulate PD. First, *LRRK2-hWT*, *LRRK2-R1441C* and *LRRK2-G2019S* primary cortical cultures of BAC transgenic P1-P5 rat pups containing human LRRK2 sequence tagged with N-terminal YPet protein (26.8 kDa) were generated and characterised. DIV 14 cultures were fixed and stained for neuronal marker MAP2, astrocytic marker GFAP and DAPI. Primary cultures were characterised using Harmony software to create a pipeline to identify neuronal populations (cells positive for neuronal marker MAP2) and astrocytic populations (cells positive for astrocytic marker GFAP)**.** The pipeline consisted of building blocks to identify nuclei, cell body regions, cytoplasm regions for both neurons and astrocytes, and calculate the percentage of $MAP2^+$ and $GFAP^+$ cells relative to total cell number (Fig. 3.10). This allowed for the quantification of consistent populations of cells in all cultures, with 30-40% of cells identified as neuronal and 25-30% identified as astrocytic (Fig. 3.11 B). The remaining percentage of cellular populations present in these cultures were identified as “remaining nuclei” from other cell types present within culture.

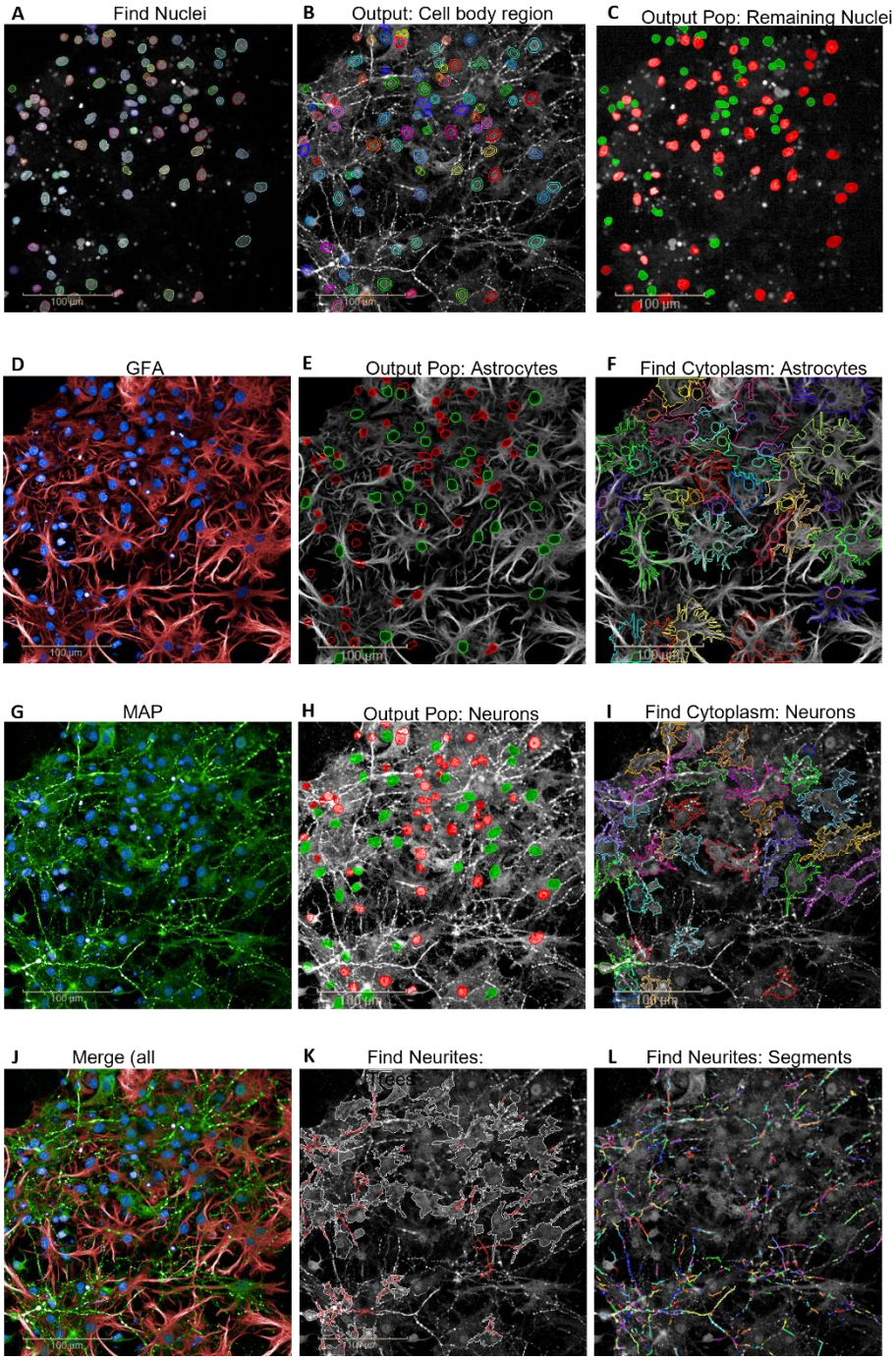

Figure 3.10. – Pipeline for identifying neuron and astrocyte populations in cortical cultures. Example for the building blocks used to create the pipeline for analysing primary culture populations, using Harmony 4.9 software (PerkinElmer). The pipeline starts by identifying nuclei and selecting by size and shape (A), and then creates a new population of cells by defining a ring around selected nuclei (B). Other nuclei are labelled as "Remaining Nuclei" (C). Based on GFAP staining (D), cells are selected as astrocytes from the pool of selected nuclei (E) and cell bodies, cytoplasm and cell membranes identified (F). The same process is repeated for MAP2 staining to select cells as neurons (G, H, I) and

additional building blocks were created to find and measure neurite trees and neurite segments (K, L). Harmony was also used to calculate number of objects, areas and length of cells. (Scale bar = 100 µm).

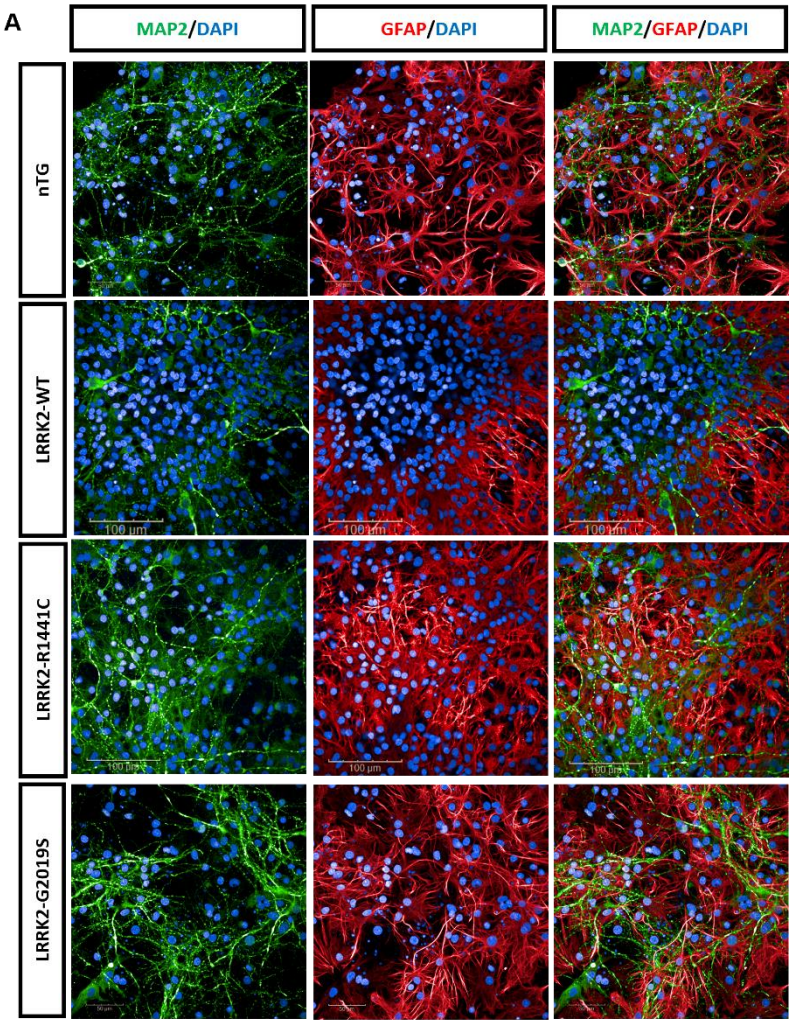

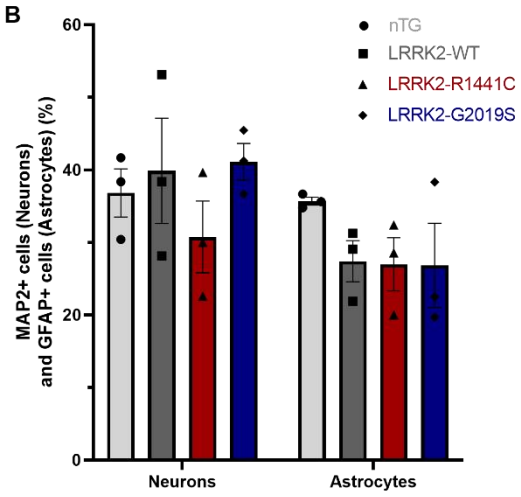

Figure 3.11. – Characterisation of neuronal and astrocytic populations in primary cortical cultures. Primary cortical cultures from P1-P5 pups were generated and characterised. (A) Cultures at DIV 14 were immunostained for neuronal marker MAP2 and astrocytic marker GFAP in order to assess cellular populations. (B) Neuronal and astrocytic populations were calculated as a percentage of total nuclei count and compared between non-transgenic and transgenic animals. Data points in graphs represent independent litters. (Bars represent mean +/- SEM; (N = 3 independent litters, per genotype; non-significant (not represented); Two-way ANOVA). Scale bar = 100 μm).

As part of the characterisation of cortical cultures, YPet-LRRK2 and a1 subunit expression were also confirmed in transgenic *LRRK2* cultures using immunoblotting, showing no expression of YPet-LRRK2 in non-transgenic littermates as expected. Additionally, quantification of YPet-LRRK2 expression showed no significant differences between genotypes (Fig. 3.12 A-B). At an initial stage, presence of LRRK2 and v0a1 was also assessed by immunostaining in *LRRK2-R1441C* cortical cultures and respective nTG littermates, to validate the antibodies and experimental protocols (Fig. 3.12 C). Unfortunately, these immunostaining experiments could not be carried out to completion as the commercial v0a1 antibody utilised was discontinued. Therefore, LRRK2 co-localisation with v0a1 could not be statistically assessed in *LRRK2-R1441C* cortical cultures.

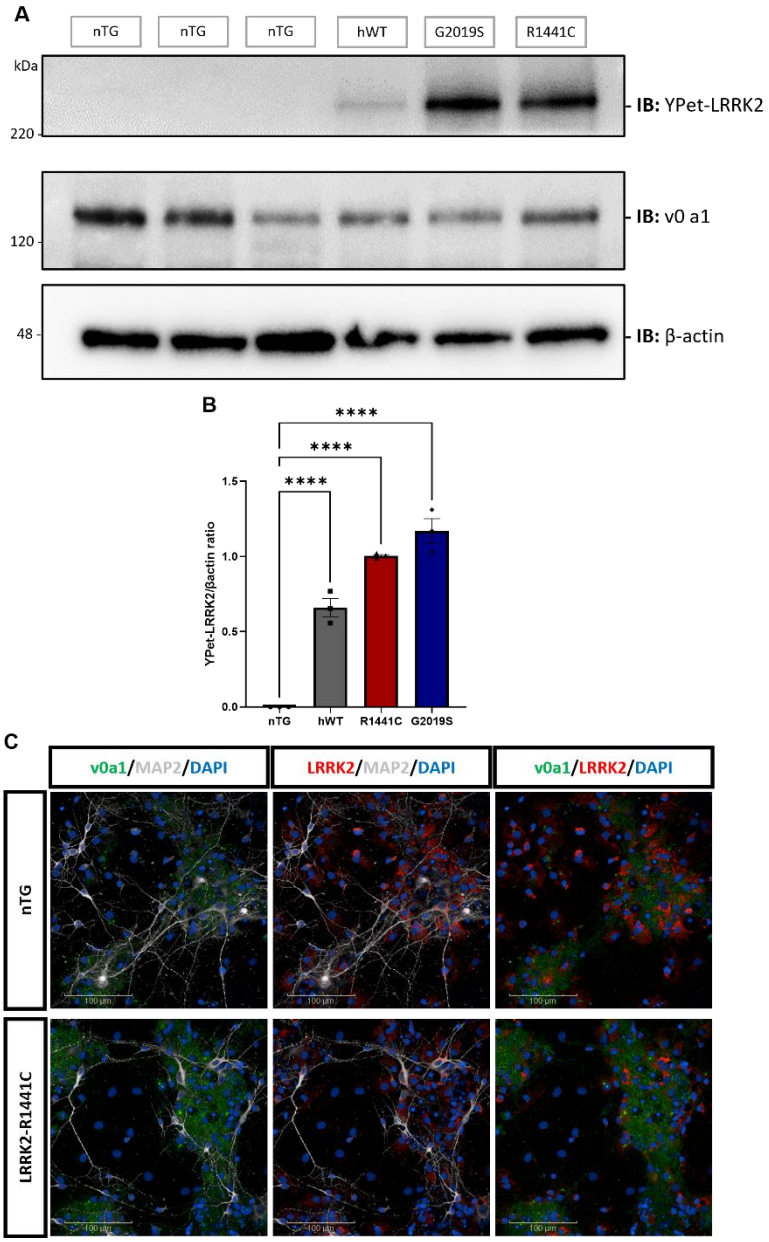

Figure 3.12 – LRRK2 and vATPase-a1 expression in primary cortical cultures. Primary cortical cultures from P1-P5 pups were generated, cultured and cells were fixed or lysates collected at DIV 14. (A) Lysates were immunoblotted for YPet-LRRK2 and vATPase-a1 (v0a1). (B) YPet-LRRK2 expression was calculated as a ratio to β-actin, and compared between genotypes. (C) Cells were fixed and immunostained for neuronal marker MAP2, LRRK2 and vATPase-a1 to observe presence of respective protein expression in culture. IB: immunoblot. Bars represent mean +/- SEM; (N = 3 independent litters, per genotype; ∗P <0.05; ∗∗∗∗P<0.0001; non-significant (not represented); Ordinary one-way ANOVA). Scale bar = 100 μm.

It has been previously shown *LRRK2-R1441C* cortical primary neuronal cultures show impaired LRRK2/a1 subunit interaction, and that impaired a1 trafficking leads to mis-localisation within cellular compartments in murine models. LRRK2 interaction with vATPase-a1 was confirmed in co-transfected HEK cells, likely occurring at the ROC domain of LRRK2. Since the LRRK2-R1441C mutation is located in the ROC domain, it was hypothesised that LRRK2 chaperones a1 from synthesis in the ER, through modification at the Golgi-Apparatus and finally to the lysosome, and this mechanism was dysregulated in LRRK2-R1441C. To address this question, we examined v0a1 expression within ER, Golgi and lysosomes, performing immunocytochemistry staining for these organelles in *LRRK2-R1441C* primary cortical cultures. Co-localisation of vATPase-a1 spots with organelle markers such as calreticulin, 58-k Golgi and LAMP1 (ER, Golgi and lysosomes, respectively) was quantified (Fig. 3.13-3.15). Interestingly, there is a slight, but not significant, increase in v0a1 spots co-localising with ER and Golgi markers in LRRK2-R1441C cortical neurons, specifically in $MAP2^{+}$ cells, when compared to non-transgenic littermates (Fig. 3.13 A-B, Fig. 3.14 A-B). Furthermore, there was a significant clioquinol-induced decrease in v0a1 spots co-localised with ER and Golgi markers in LRRK2-R1441C cultures, restoring percentages of v0a1/ER and v0a1/Golgi to percentages observed in non-transgenic littermates (Fig. 3.13 A-C, Fig. 3.14 A-C). There were no significant changes in v0a1 spots co-localising with LAMP1 spots, when comparing between *LRRK2-R1441C* and nTG littermate cortical neurons, or in clioquinol treated cultures (Fig. 3.15).

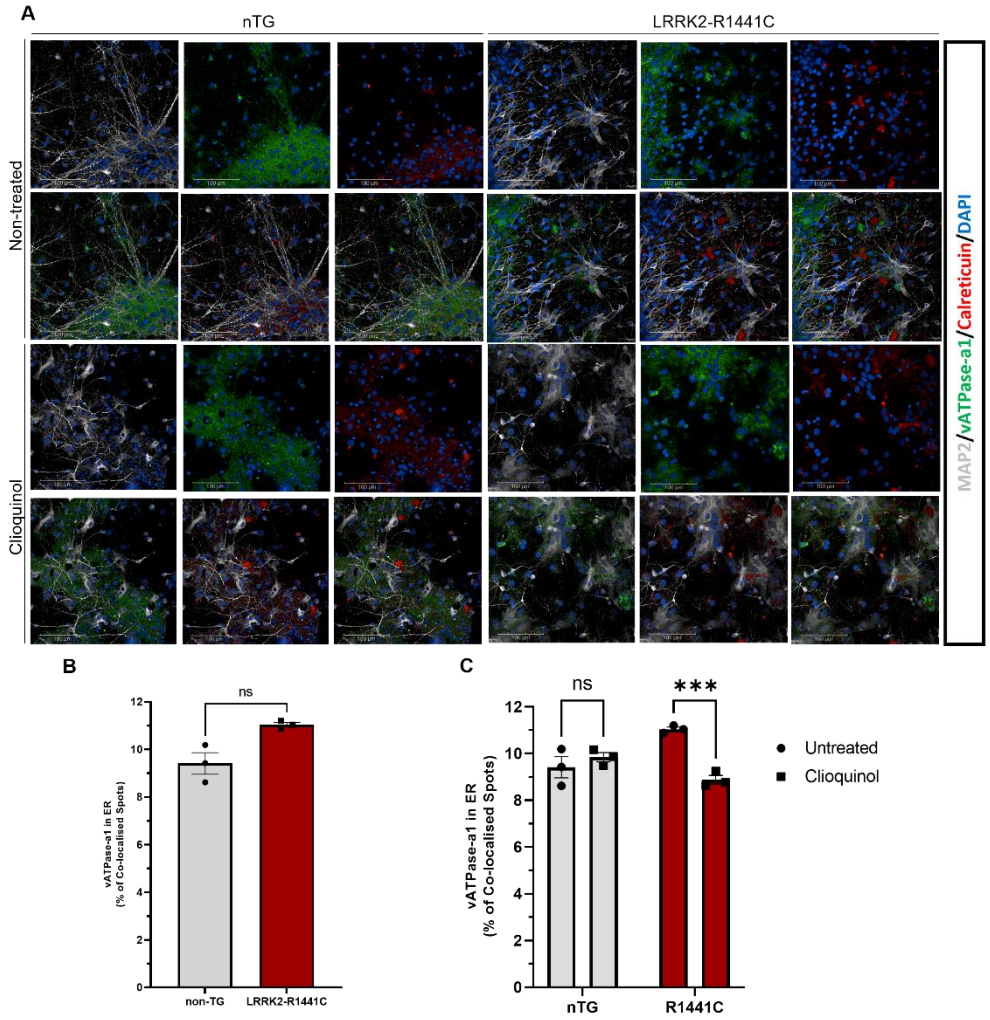

Figure 3.13 – vATPase-a1 expression in Endoplasmic Reticulum, in LRRK2-R1441C. Primary cortical cultures from P1-P5 pups were generated and treated with Clioquinol (1µM, 48h) prior to assays at DIV 14. **(A)** Cells were fixed and immunostained for neuronal marker MAP2, ER marker Calreticulin and vATPase-a1 (v0a1). Cellular expression was calculated as vATPase-a1 spots co-localised with ER marker Calreticulin measured in MAP2+ cells as a fraction of the total v0a1 population, and LRRK2-R1441C were compared to non-transgenic littermates **(B)** or between non-treated and Clioquinol treated conditions **(C)**. (Bars represent mean +/- SEM; (N = 3 independent litters, per genotype; ∗P <0.05; ∗∗∗P<0.001; non-significant (ns); Mann-Whitney non-parametric test, Two-way ANOVA). Scale bar = 100 µm).

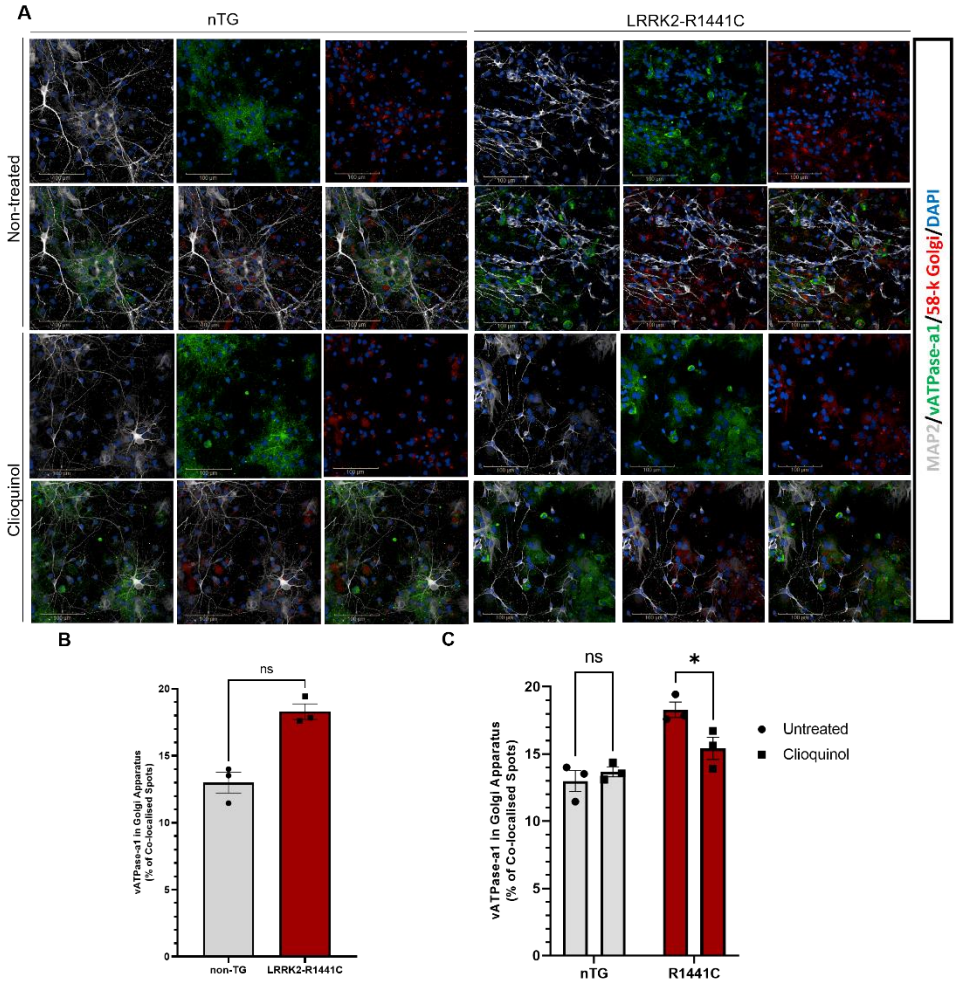

Figure 3.14 – vATPase-a1 expression in Golgi Apparatus, in LRRK2-R1441C. Primary cortical cultures from P1-P5 pups were generated, treated with Clioquinol (1µM, 48h) prior to assays. **(A)** Cells were fixed and immunostained for neuronal marker MAP2, Golgi Apparatus marker 58-k Golgi and vATPase-a1. Cellular expression was calculated as vATPase-a1 spots co-localised with Golgi Apparatus marker 58-k Golgi were measured in MAP2+ cells as a fraction of the total v0a1 population, and LRRK2-R1441C were compared to non-transgenic littermates **(B)** or between non-treated and Clioquinol treated conditions **(C)**. (Bars represent mean +/- SEM; (N = 3 independent litters, per genotype; ∗P <0.05; non-significant (ns); Mann-Whitney non-parametric test, Two-way ANOVA). Scale bar = 100 µm).

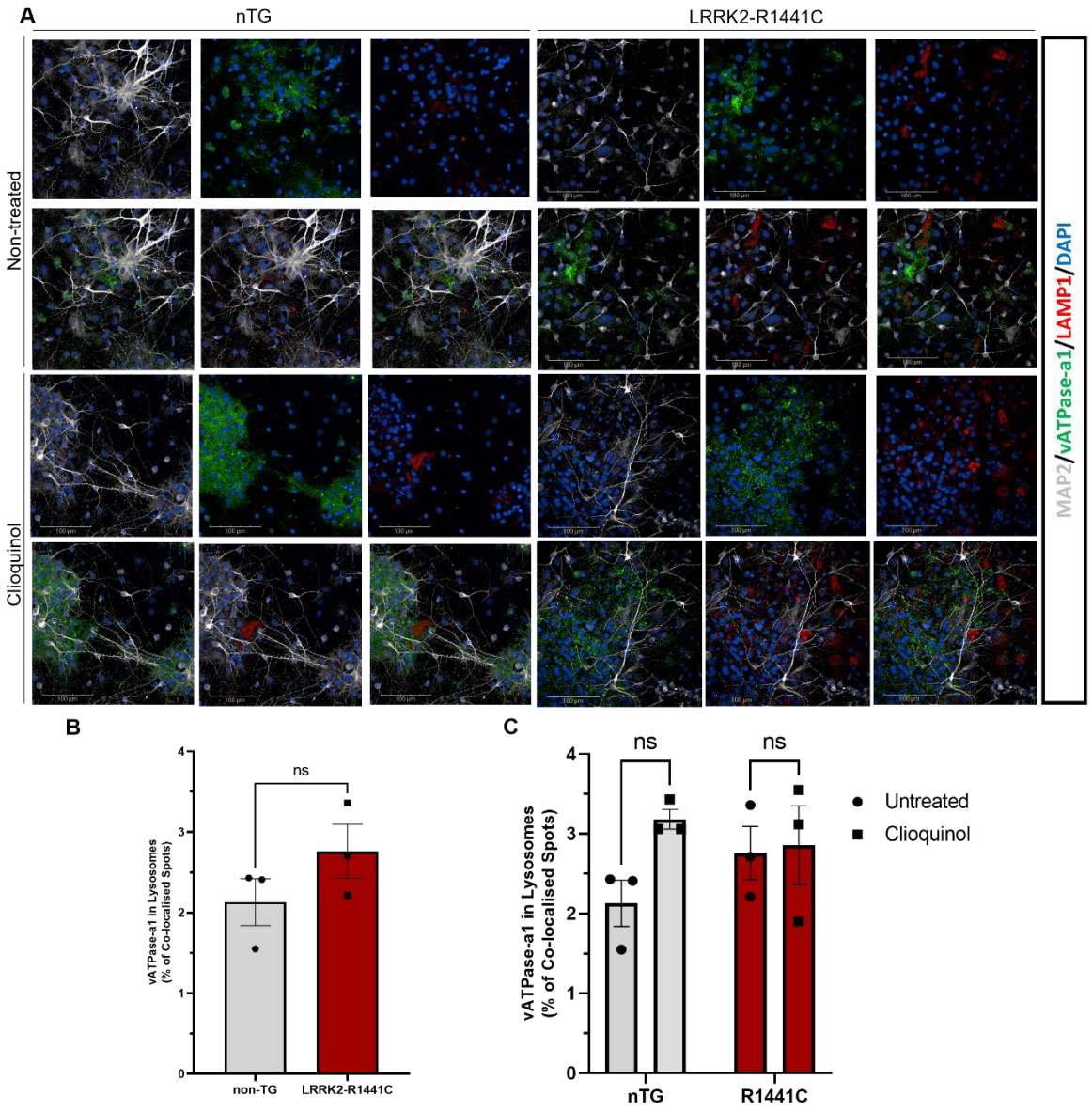

Figure 3.15 – Lysosomal vATPase-a1 expression, in LRRK2-R1441C. Primary cortical cultures from P1-P5 pups were generated, treated with Clioquinol (1µM, 48h) prior to assays. **(A)** Cells were fixed and immunostained for neuronal marker MAP2, lysosomal marker LAMP1 and vATPase-a1. Cellular expression was calculated as vATPase-a1 spots co-localised with lysosomal marker LAMP1 were measured in MAP2+ cells as a fraction of the total v0a1 population, and LRRK2-R1441C were compared to non-transgenic littermates **(B)** or between non-treated and Clioquinol treated conditions **(C)**. (Bars represent mean +/- SEM; (N = 3 independent litters, per genotype; non-significant (ns); Mann-Whitney non-parametric test, Two-way ANOVA). Scale bar = 100 µm).

This evidence could suggest that *LRRK2-R1441C* mutation, which affects the ROC domain of LRRK2, does not significantly alter a1 subunit cellular localisation in cortical primary cultures. On the other hand, clioquinol treatment showed no effect in v0a1 presence in lysosomes, but significantly decreased v0a1 co-localisation in ER and Golgi spots.

3.2.3. Characterising LRRK2 and v0a1 in *LRRK2* iPSC-derived dopaminergic cultures

Given the mis-localisation of a1 subunit towards the ER and Golgi organelles observed in *LRRK2-R1441C* rat cortical neuronal cultures, we assessed if this dysfunction was present in iPSC-derived dopaminergic (DA) neuronal cultures from Parkinson's patients with *LRRK2* mutations, as an independent model of PD. iPSCs derived from three patients with PD carrying the *LRRK2-R1441C* mutation, four patients with PD carrying the *LRRK2-G2019S* mutation, five healthy Controls, one isogenic Control for *LRRK2-R1441C* and one for *LRRK2-G2019S*, were differentiated to midbrain dopaminergic neurons using a Modified Kriks protocol (Kriks et al. 2011) (Materials and Methods 2.6.1., Fig. 3.16). The presence of mature neurons ($MAP2^+$) and the percentage of tyrosine hydroxylase-positive (TH^+) dopamine neurons was consistent across multiple differentiations (Fig. 3.17). Interestingly, both *LRRK2-R1441C* and *LRRK2-G2019S* iPSC-derived dopaminergic cultures showed a decrease in percentage of TH^+ dopamine neurons when compared to Control iPSC-DAn cultures (Fig. 3.17 A, D). This decrease in TH^+ neurons was confirmed with decreased TH expression when compared to iPSC-DAn culture lysates, using immunoblotting (Fig. 3.17 C, E). Due to this difference in TH content between genotypes, mature neuron marker MAP2 was used in subsequent experiments to assess expression per neuronal cell. LRRK2 kinase activity was decreased in *LRRK2-R1441C* and *LRRK2-G2019S*, compared to control iPSC-DA neuronal cultures, as assessed by western blotting of phosphorylated LRRK2 (Fig. 3.18 A-C). However, the immunoblotting signal from LRRK2 bands was not clear throughout all samples. Quantifications and statistical analysis are therefore limited and would benefit from further repeats, which did not happen due to time constraints on the current project. LRRK2 phosphorylation substrate Rab10 did not show any differences between LRRK2 and control iPSC-DA neuronal cultures (Fig. 3.18 D-F). Notably, in these iPSC-DA cultures MLi-2 and chloroquine treatment did not have any effect on LRRK2 phosphorylation or Rab10 phosphorylation levels. The former suggests MLi-2 treatment at 50nM for 48 h was not sufficient to inhibit LRRK2 kinase activity in iPSC-DA cultures.

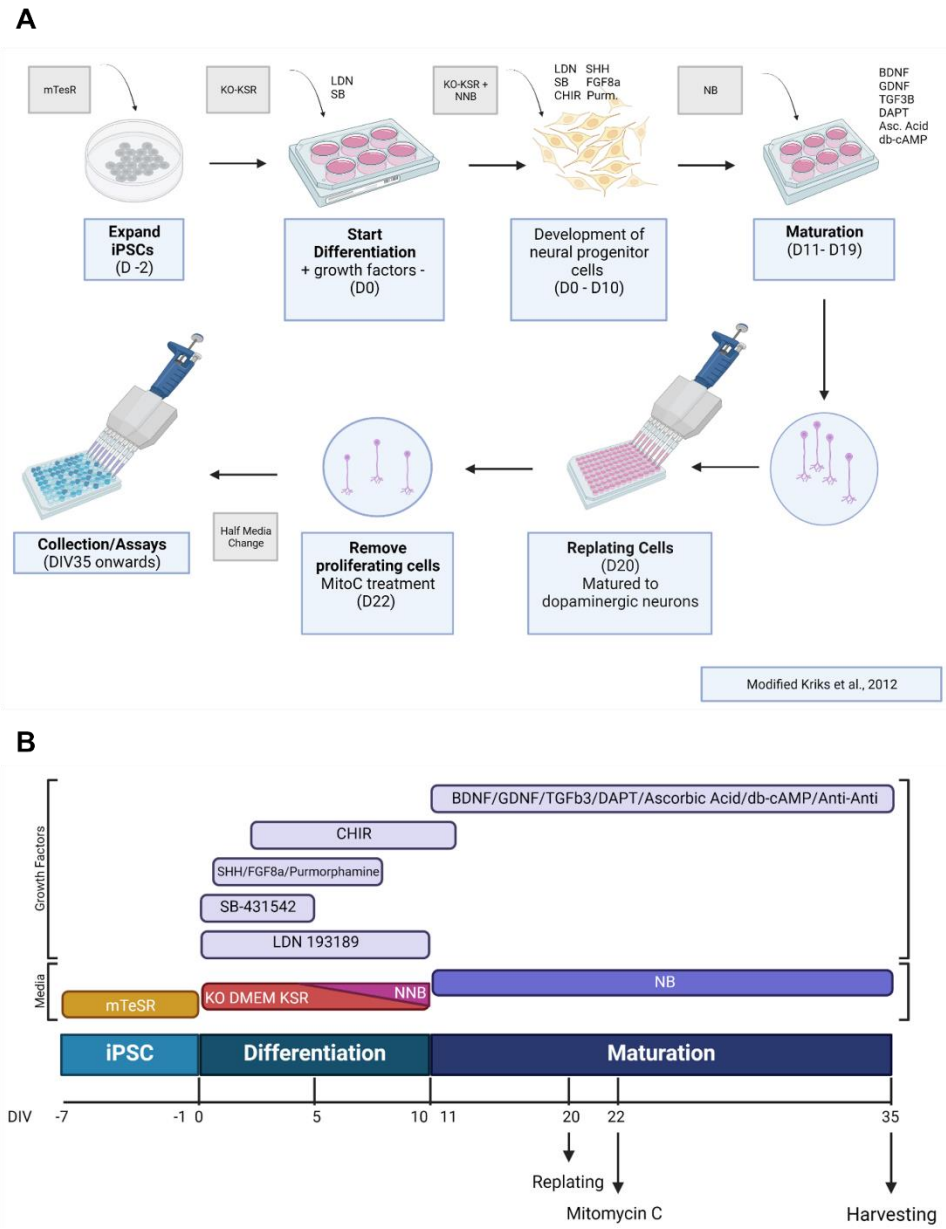

Figure 3.16 – iPSC Differentiation protocol for dopaminergic neurons and culture strategy. **(A)** Schematic representation of the protocol for iPSC-DAn culture differentiation used throughout this study and **(B)** detailed information for growth factors and media used (Kriks et al. 2011).

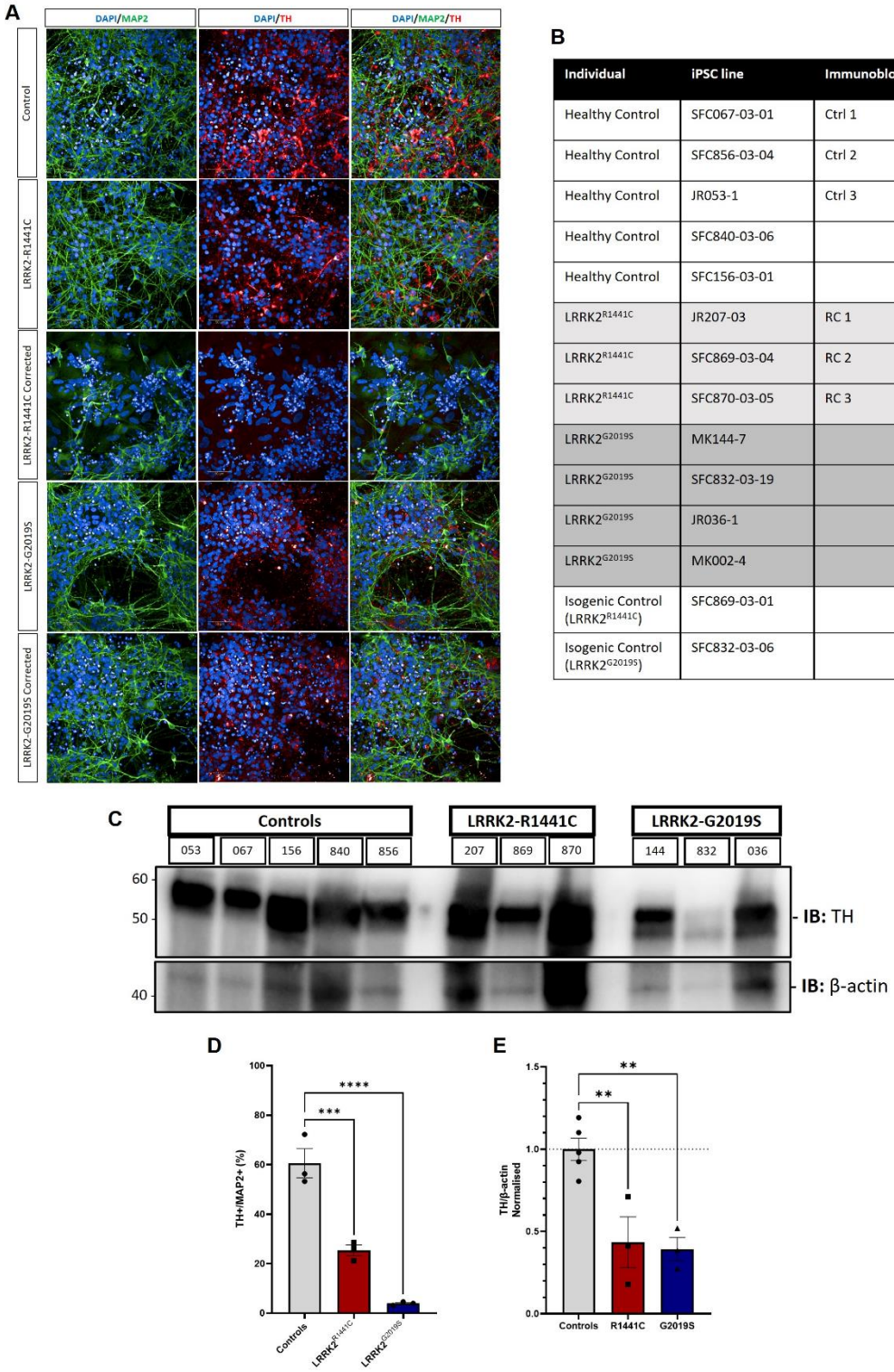

Individual	iPSC line	Immunoblot Code
Healthy Control	SFC067-03-01	Ctrl 1
Healthy Control	SFC856-03-04	Ctrl 2
Healthy Control	JR053-1	Ctrl 3
Healthy Control	SFC840-03-06	
Healthy Control	SFC156-03-01	
$LRRK2^{R1441C}$	JR207-03	RC 1
$LRRK2^{R1441C}$	SFC869-03-04	RC 2
$LRRK2^{R1441C}$	SFC870-03-05	RC 3
$LRRK2^{G2019S}$	MK144-7	
$LRRK2^{G2019S}$	SFC832-03-19	
$LRRK2^{G2019S}$	JR036-1	
$LRRK2^{G2019S}$	MK002-4	
Isogenic Control ($LRRK2^{R1441C}$)	SFC869-03-01	
Isogenic Control ($LRRK2^{G2019S}$)	SFC832-03-06	

Figure 3.17 – iPSC-derived Dopaminergic culture characterisation. **(A)** Representative images of iPSC-derived dopaminergic neurons from Control, *LRRK2-R1441C*, *LRRK2-G2019S* and respective isogenic control lines used throughout this study immunostained for MAP2, TH and DAPI. Scale bar represents 50 µm. Quantification of the percentage of cells positive for TH within the MAP2+ population, compared between Controls and patient lines **(D)**. **(B)** Table describing patient and control lines used in the study. **(C)**

Immunoblotting of iPSC-DAn lysates using anti-TH antibody to assess TH expression, quantified as the ratio of TH/β-actin, compared between genotypes **(E)**. Data points represent genotype lines, averaged by number of differentiations. IB: immunoblot. Bars, mean ± SEM from two/three independent differentiations (N = 3; ∗P <0.05; ∗∗∗P <0.01; ∗∗∗P<0.001 ;∗∗∗∗P<0.0001; non-significant (ns); Ordinary one-way ANOVA).

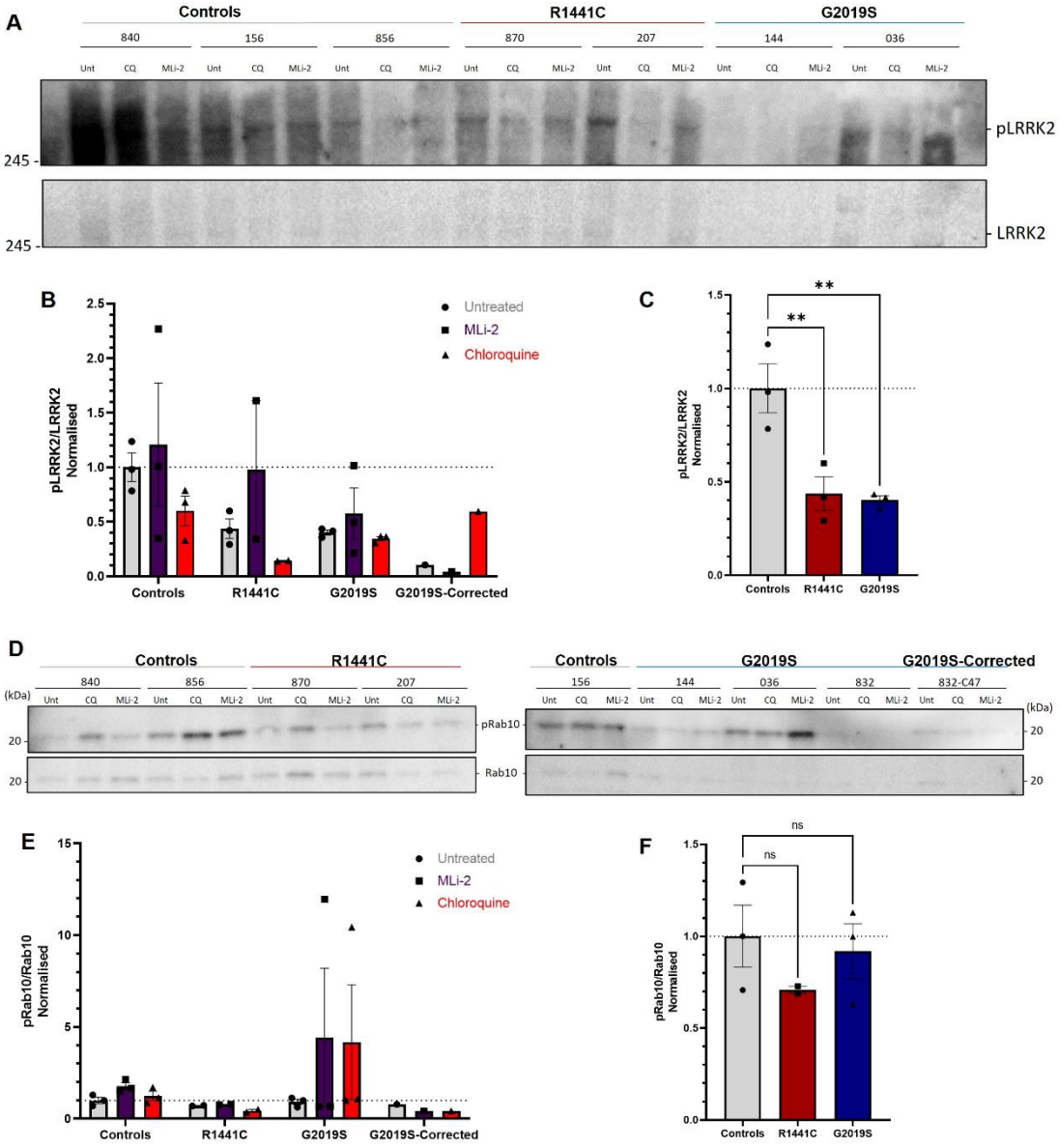

Figure 3.18 – LRRK2 kinase activity and MLi-2 treatment in iPSC-DA cultures. **(A)** To assess LRRK2 kinase inhibition, iPSC-derived dopaminergic cultures from Controls and *LRRK2-R1441C* patient lines were generated and treated with MLi-2 (50nM) for 48 h. **(B)** Western blots for LRRK2 phosphorylation substrate Rab12 (phospho S106) were used to assess kinase activity by normalising phosphorylated Rab12 to total Rab12 expression. (ns: non-significant; ∗P <0.05; Unpaired t test). **(C)** The effect of LRRK2 kinase inhibitor MLi-2

was quantified by western blot for pRab12 and Rab12 expression to assess pRab12/Rab12 fold change from basal (DMSO) in response to treatment with 50 nM MLi-2 for 48 h. Data points represent genotype lines, averaged by number of differentiations. **(D, G)** iPSC-derived dopaminergic neurons from Control, *LRRK2-R1441C*, *LRRK2-G2019S* and respective isogenic control lines were treated with Chloroquine (50nM for 24 h) or MLi-2 (50nM for 48 h) prior to lysate collection. LRRK2 kinase activity was measured as the ratio of immunoblotted of phosphorylated LRRK2 (Ser935) over LRRK2 **(E, F)**, or as the ratio of immunoblotted of phosphorylated Rab10 (phospho T73) over Rab10 **(H, I)**. Bars, mean ± SEM from two independent differentiations (ns: non-significant or not represented; ∗P <0.05; ∗∗P <0.01; Ordinary one-way ANOVA, Two way ANOVA).

To understand the effects of *LRRK2* mutations on vATPase-a1 subunit subcellular localisation in dopaminergic neurons, cultures were immunostained and immunoblotted in various experimental set ups. First, expression levels of LRRK2, vATPAse-a1 and vATPase-A1 subunit assessed by Western Blot showed no difference in *LRRK2* iPSC-DAn when compared to healthy Controls (Fig. 3.19). Then, co-localisation of v0a1 with calnexin, a marker for Endoplasmic Reticulum, was calculated as a percentage of total ER area by immunostaining LRRK2 iPSC-DA neuronal cultures and compare to healthy controls (Fig. 3.20). There was a slight decrease in v0a1 spots co-localised with ER spots in *LRRK2-R1441C* iPSC-DA but no significant differences were observed in *LRRK2* cultures (Fig. 3.20 B). Using the same immunostaining technique, no significant differences were found in v0a1 co-localisation with Golgi-Apparatus marker 58-k Golgi, or lysosomal marker LAMP1, in *LRRK2* iPSC-DA neuronal cultures, compared to healthy controls (Fig. 3.21, Fig. 3.22). These results would suggest LRRK2 does not alter vATPase-a1 subunit subcellular localisation in dopaminergic cultures.

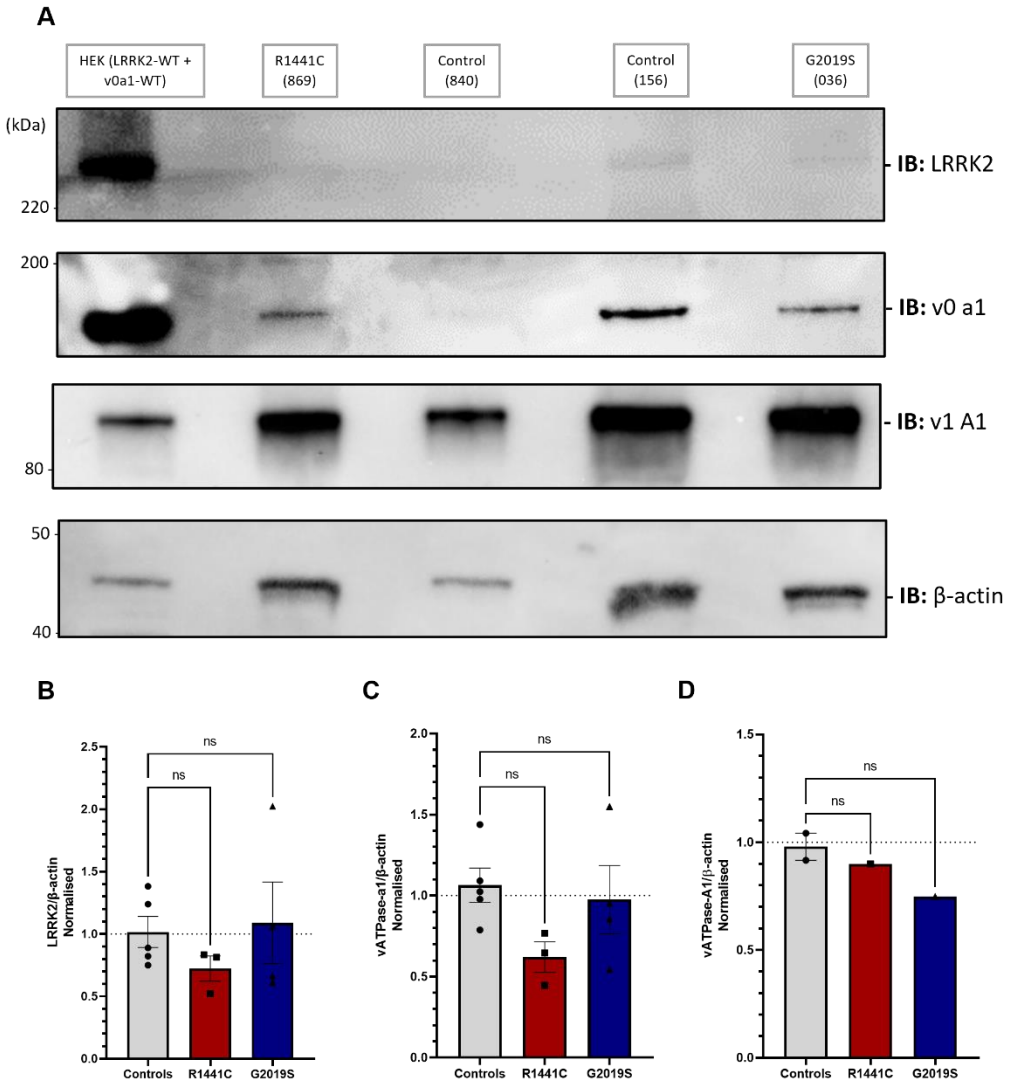

Figure 3.19 – Endogenous vATPase-a1 and LRRK2 expression in iPSC-DAn cultures. **(A)** iPSC-derived dopaminergic cultures from Controls and LRRK2 patient lines were generated and immunoblotted to assess endogenous expression of LRRK2, vATPase-a1 and vATPase-A1. Protein expression was quantified as the ratio of LRRK2/β-actin **(B)**, v0a1/β-actin **(C)** and v0A1/β-actin **(D)**, then compared between genotypes. Data points represent genotype lines, averaged by number of differentiations. IB: immunoblot. Bars, mean ± SEM from at least two independent differentiations (∗P <0.05; non-significant (ns); Ordinary one-way ANOVA).

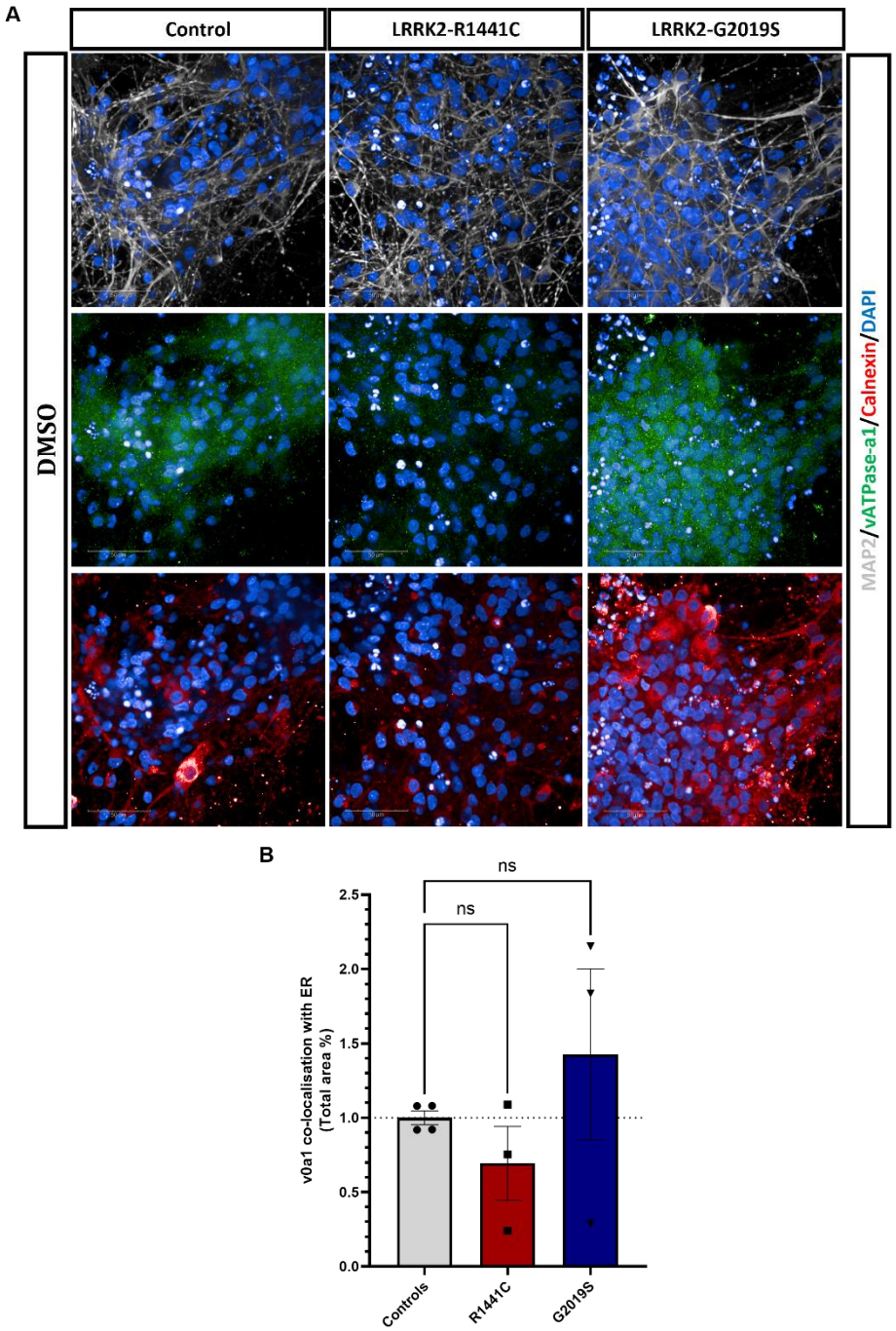

Figure 3.20 – Endoplasmic Reticulum vATPase-a1 expression in LRRK2 mutant iPSC-Dan cultures. **(A)** Representative images of iPSC-derived dopaminergic neurons from Control, *LRRK2-R1441C* and *LRRK2-G2019S* lines used throughout this study immunostained for MAP2, vATPase-a1 (v0a1), Calnexin and DAPI. Scale bar represents 50 µm. **(B)** vATPase-a1 spots co-localised with endoplasmic reticulum marker Calnexin (puncta area as a percentage of total v0a1 puncta) were measured in MAP2+ cells, normalised to average of controls and compared between Controls and patient lines. Data points represent genotype lines, averaged by number of differentiations. Bars, mean ± SEM

from two independent differentiations (∗P <0.05; non-significant (ns); Ordinary one-way ANOVA).

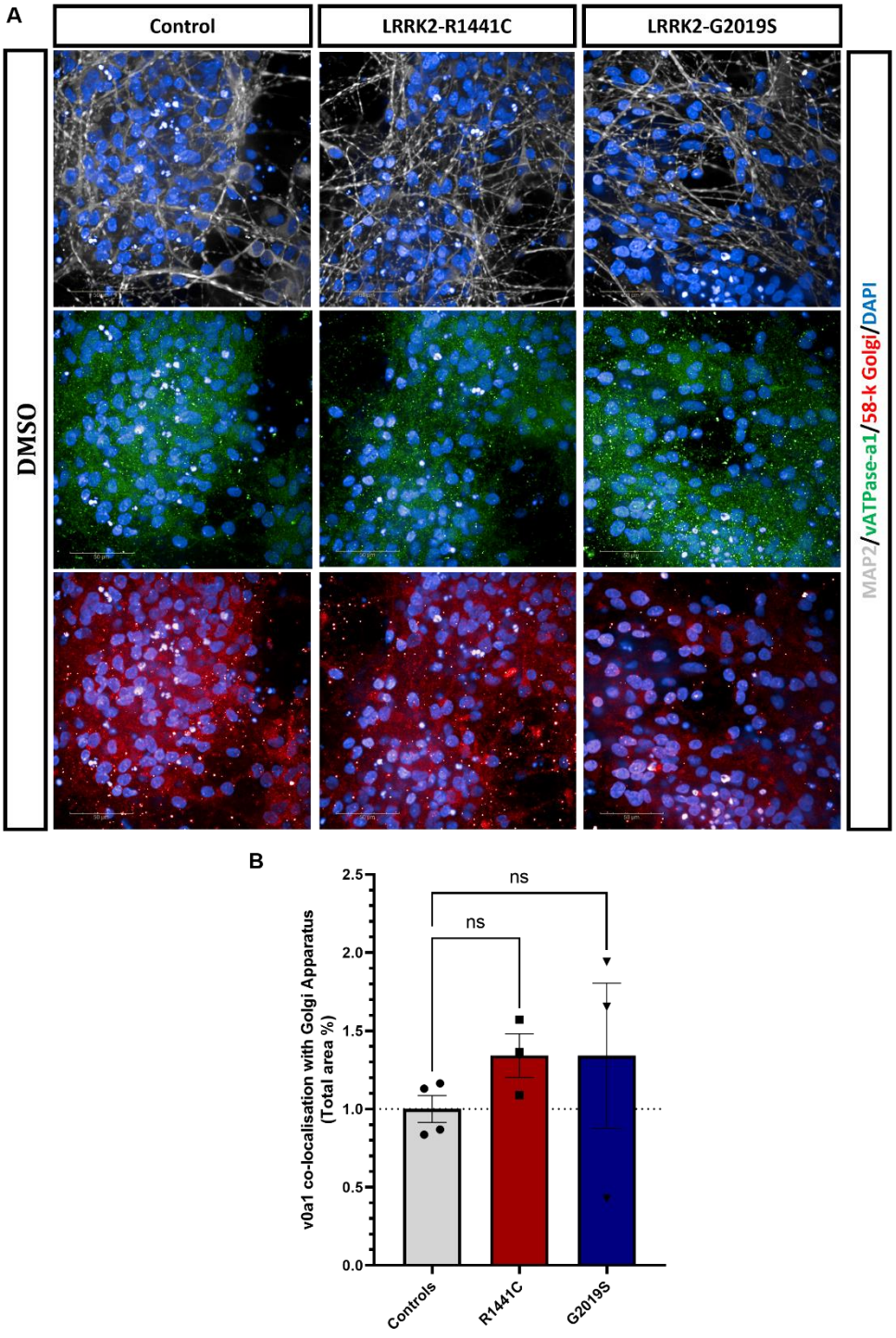

Figure 3.21 – Golgi Apparatus v0a1 expression in LRRK2 mutant iPSC-Dan cultures. **(A)** Representative images of iPSC-derived dopaminergic neurons from Control, *LRRK2-R1441C* and *LRRK2-G2019S* lines used throughout this study immunostained for MAP2,

vATPase-a1 (v0a1), 58-k Golgi and DAPI. Scale bar represents 50 µm. **(B)** vATPase-a1 spots co-localised with Golgi Apparatus marker 58-k Golgi (puncta area as a percentage of total v0a1 puncta) were measured in MAP2+ cells, normalised to average of controls and compared between Controls and patient lines. Data points represent genotype lines, averaged by number of differentiations. Bars, mean ± SEM from two independent differentiations (∗P <0.05; non-significant (ns); Ordinary one-way ANOVA).

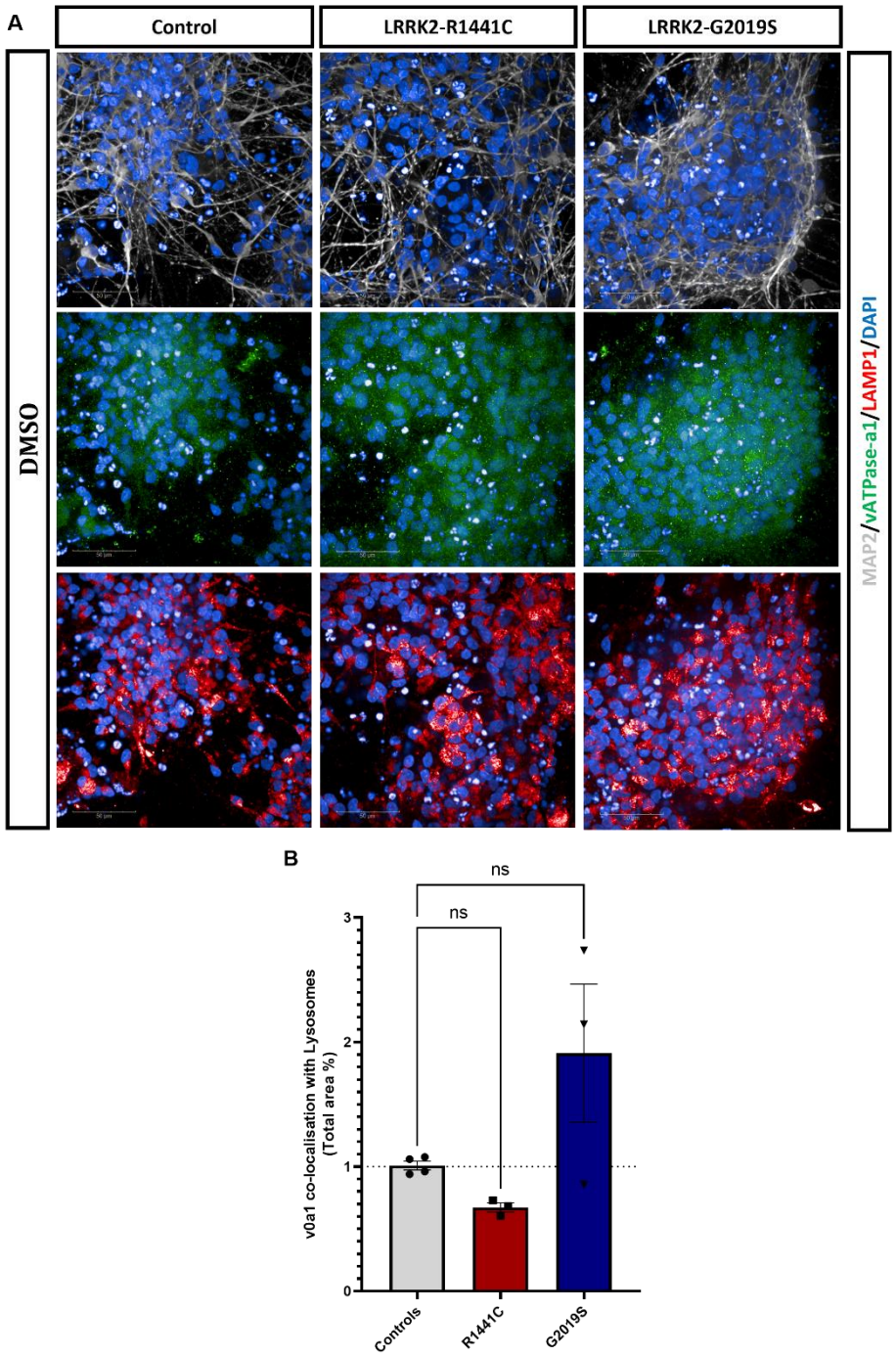

Figure 3.22 – Lysosomal v0a1 expression in LRRK2 mutant iPSC-DAn cultures. **(A)** Representative images of iPSC-derived dopaminergic neurons from Control, *LRRK2-R1441C* and *LRRK2-G2019S* lines used throughout this study immunostained for MAP2, vATPase-a1 (v0a1), LAMP1 and DAPI. Scale bar represents 50 µm. **(B)** vATPase-a1 spots co-localised with lysosomal marker LAMP1 (puncta area as a percentage of total v0a1 puncta) were measured in MAP2+ cells, normalised to average of controls and compared between Controls and patient lines. Data points represent genotype lines, averaged by number of differentiations. Bars, mean ± SEM from two independent differentiations (∗P <0.05; non-significant (ns); Ordinary one-way ANOVA).

Given LRRK2/v0a1 interaction was first reported in *LRRK2* primary cortical cultures (Wallings, Connor-Robson, and Wade-Martins 2019) and established in the present experimental work to also occur in co-transfected HEK cells, it is important to confirm whether this interaction also occurs in *LRRK2* human iPSC-derived dopaminergic cultures. To address this, *LRRK2* iPSC-DA neuronal cultures were immunostained for endogenous LRRK2 and v0a1, and their co-localisation was investigated. LRRK2 spots localised with v0a1 spots in iPSC-DA healthy controls, with LRRK2/voa1 spots also co-localising in *LRRK2* iPSC-DAn with no significant changes (Fig. 3.23 A-B). Since LRRK2/v0a1 interaction was reported to be abolished in LRRK2-R1441C cortical cultures, the interaction between LRRK2 and a1 subunit was also assessed using co-immunoprecipitation in *LRRK2-G2019S* and healthy control iPSC-DA neuronal cultures (Fig. 3.23 C). LRRK2 was immunoprecipitated with anti-LRRK2 antibody and pulled-down v0a1 subunit was detected by immunoblotting. A band for LRRK2 and a band for a1 was visible in the co-immunoprecipitated samples for healthy control and *LRRK2-G2019S* iPSC-DAn lysates, which reflects the presence of both protein complexes, confirming the LRRK2/v0a1 interaction also occurs in *LRRK2-WT* and *LRRK2-G2019S* human dopaminergic cultures, with no significant differences between genotypes (Fig. 3.23 C-D).

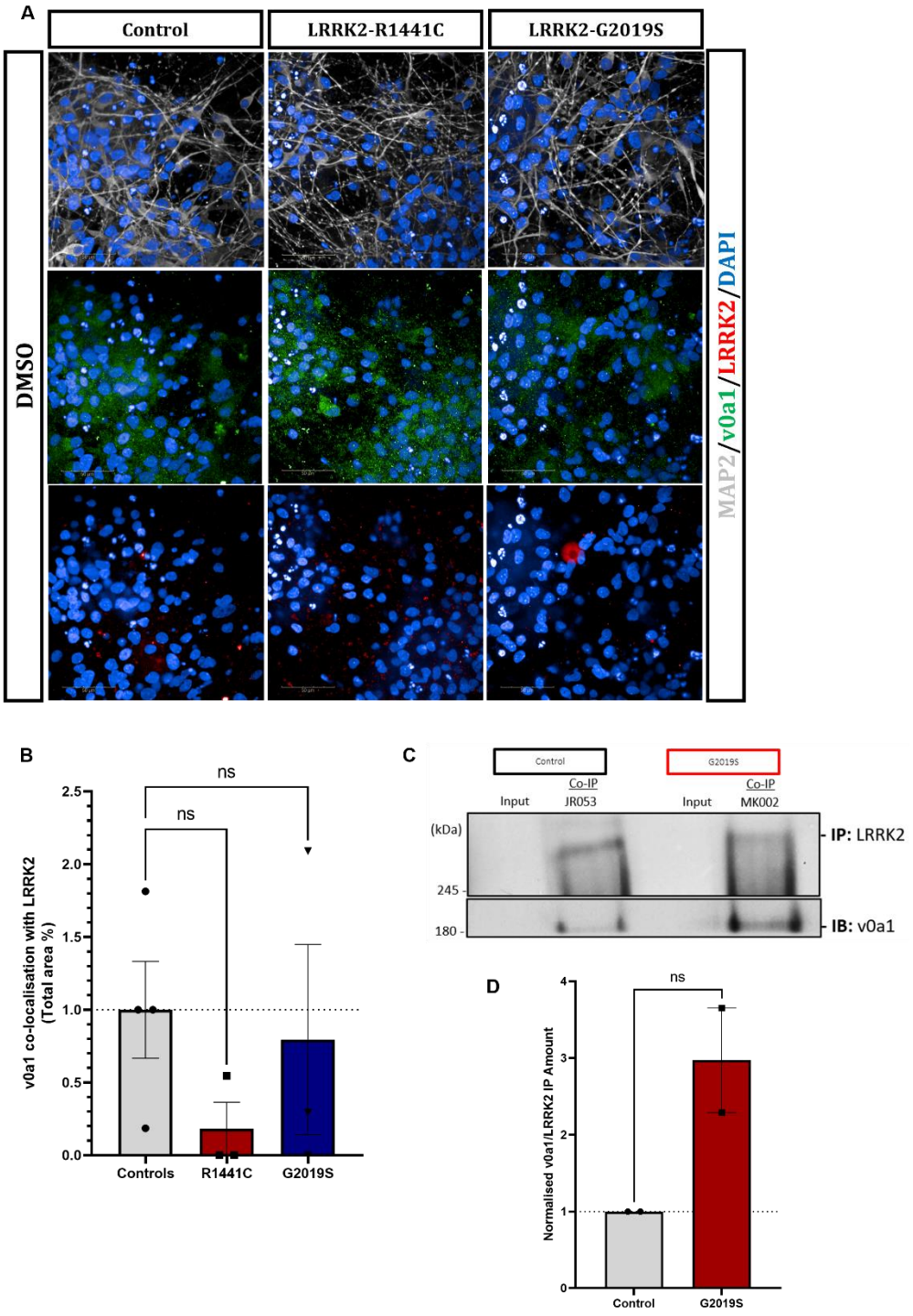

Figure 3.23 – LRRK2 and vATPase-a1 interaction in LRRK2 mutant iPSC-Dan cultures. **(A)** Representative images of iPSC-derived dopaminergic neurons from Control, *LRRK2-R1441C* and *LRRK2-G2019S* lines used throughout this study immunostained for MAP2, LRRK2, vATPase-a1 (v0a1) and DAPI. Scale bar represents 50 µm. **(B)** vATPase-a1 spots co-localised with LRRK2 (puncta area as a percentage of total v0a1 puncta) were measured in MAP2+ cells, normalised to average of controls and compared between

Controls and patient lines. **(C)** Co-immunoprecipitation of LRRK2 and vATPase-a1 under basal conditions from LRRK2-G2019S and control iPSC-derived dopaminergic cultures. Lysates were immunoprecipitated with LRRK2 and v0a1/LRRK2 protein expression observed. For quantification, the intensity of v0a1 band is divided by the total LRRK2 intensity, expressed as a fraction of the mean of Control iPSC-DA cultures **(D)**. IP: Immunoprecipitate; IB: immunoblot. Bars, mean ± SEM from two experimental repeats (∗P <0.05; non-significant (ns); Ordinary one-way ANOVA).

To summarise, these data suggest LRRK2/v0a1 novel interaction also occurs in human LRRK2-G2019S iPSC-DA neuronal cultures and healthy controls. However, *LRRK2* mutations did not appear to have an effect in the subcellular localisation of vATPase-a1 subunit within the ER, Golgi and lysosomal organelles.

3.3. Conclusions

The main conclusions highlighted in this chapter are:

1. LRRK2 interaction with vATPase-a1, previously reported using rat primary cultures, also occurs in the context of human cellular models.
2. Interaction of LRRK2 with the a1 subunit of vATPase occurs within human cell models at the ROC domain of LRRK2.
3. *LRRK2-R1441C* mutation does not seem to alter cellular localisation of vATPase-a1 subunit in rat primary cortical or iPSC-derived dopaminergic neuronal cultures.

Chapter 4 – LRRK2 and Autophagy

4.1. Introduction and aims

As mentioned previously (section 1.5), LRRK2 mutations affect the autophagy-lysosomal pathway (Madureira, Connor-Robson, and Wade-Martins 2020). Previous work demonstrated that primary cortical neuronal cultures of BAC transgenic rats expressing the *LRRK2-R1441C* mutation exhibit decreased autophagy-lysosomal fusion, altered lysosomal pH and decreased lysosomal protein degradation, deficits not found in *LRRK2-WT* or *LRRK2-G2019S* transgenic neurons (Wallings, Connor-Robson, and Wade-Martins 2019). Since *LRRK2-R1441C* rat cortical primary neuronal cultures displayed autophagy defects, we aimed to characterise the autophagy pathway in human *LRRK2* iPSC-DAn models. Utilising LRRK2 patient iPSC dopaminergic neuronal cultures presents a highly physiological model of PD, since neuropathology is characterised by progressive loss of dopaminergic neurons in the SNpc.

Chapter aims:

- To investigate autophagy flux in LRRK2 rat primary cortical cultures.
- To characterise autophagy markers and autophagy flux in LRRK2 iPSC-derived dopaminergic neuronal cultures.

4.2. Results

4.2.1. Autophagy flux in LRRK2 rat primary cortical cultures.

Previous work published by our group extensively characterised the autophagy-lysosomal pathway in *LRRK2* rat cortical primary cultures and showed autophagy defects in *LRRK2-R1441C* but not in *LRRK2-WT* or *LRRK2-G2019S* (Wallings, Connor-Robson, and Wade-Martins 2019). As it is important to confirm these autophagy phenotypes, we aimed to investigate autophagy flux in the presently established model of rat cortical primary cultures (Fig. 3.13).

Primary cortical neuronal cultures were generated from *LRRK2* BAC transgenic rat pups (P1-P5) expressing the human *LRRK2-WT*, *LRRK2-G2019S* or *LRRK2-R1441C* transgene, and non-transgenic (nTG) littermates (Sloan et al. 2016; Wallings, Connor-Robson, and Wade-Martins 2019). Then, lysosomal proteolysis was measured in neuronal cells using the fluorogenic substrate for proteases DQ Red BSA in neuronal cells stained with neuronal probe NeuO. Briefly, the self-quenched DQ Red BSA is cleaved by proteases in acidic compartments, such as lysosomes, resulting in fluorescence dequenching and

consequently increased fluorescence intensity at λ_{ex} = 590 nm and λ_{em} = 620 nm (Frost et al. 2017). Increased fluorescence directly correlates with lysosomal proteolytic activity. Results were expressed as DQ-BSA Index (DQ-BSA number of spots multiplied by relative spot intensity and spot area) in NeuO-positive cells, normalised to non-transgenic littermates treated with DMSO (Fig. 4.1 A-B). Treatment with chloroquine, used to inhibit lysosomal degradation and macroautophagy/autophagy through blocked autophagosome fusion with lysosomes (Mauthe et al. 2018), showed consistent significant decrease in DQ-BSA Index in *LRRK2-WT*, *LRRK2-G2019S* and respective nTG primary cultures, validating assay specificity (Fig. 4.1 B-C). Under basal conditions, *LRRK2-R1441C* cortical neuronal cultures show a 1.5-fold increase in DQ-BSA Index compared to nTG littermates, but no significant differences were found in *LRRK2-WT* or *LRRK2-G2019S* neuronal cortical cultures (Fig. 4.1 D-F). Interestingly, chloroquine-treated LRRK2-R1441C cortical neurons showed a non-significant decrease in DQ BSA Index, suggesting an intrinsic impairment of autolysosomal fusion (Fig. 4.1 B-C). Furthermore, the effect of clioquinol was investigated and showed no significant differences between genotypes nor treatment groups (Fig. 4.1 G). Taken together, these results show autophagy-lysosomal flux is impaired *LRRK2-R1441C* rat cortical cultures, but not *LRRK2-WT* or *LRRK2-G2019S*. Additionally, this impairment could not be rescued with clioquinol.

In agreement with previous reports of decreased lysosomal activity in *LRRK2-R1441C* rat cortical cultures (Wallings, Connor-Robson, and Wade-Martins 2019), a lack of chloroquine-induced decrease in DQ-BSA Index would suggest impaired autophagosome fusion with lysosomes in *LRRK2-R1441C*. However, this impairment could not be rescued with clioquinol, suggesting the vATPase pump is not sufficient to regulate autophagy-lysosomal pathway in this experimental setup.

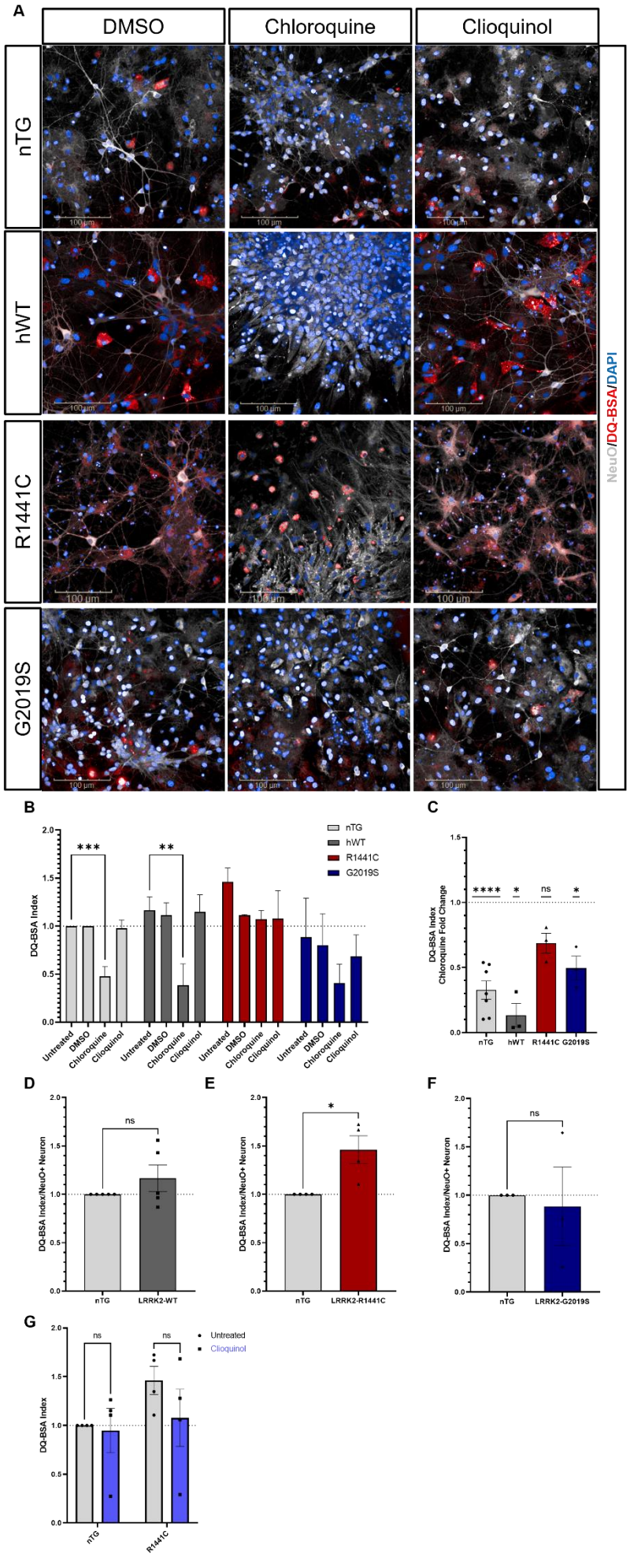
A
DMSO
Chloroquine
Clioquinol
nTG
hWT
R1441C
G2019S
NeuO/DQ-BSA/DAPI
100 µm
B
nTG
hWT
R1441C
G2019S
DQ-BSA Index
***
**
Untreated
DMSO
Chloroquine
Clioquinol
C
DQ-BSA Index Chloroquine Fold Change
****
*
ns
*
nTG
hWT
R1441C
G2019S
D
DQ-BSA Index/NeuO+ Neuron
ns
nTG
LRRK2-WT
E
DQ-BSA Index/NeuO+ Neuron
*
nTG
LRRK2-R1441C
F
DQ-BSA Index/NeuO+ Neuron
ns
nTG
LRRK2-G2019S
G
DQ-BSA Index
ns
ns
Untreated
Clioquinol
nTG
R1441C

Figure 4.1 – Lysosomal activity in LRRK2 mutant primary cortical cultures. Primary cortical neuronal cultures were generated from P1-P5 pups and assays at DIV 14. Primary cortical cultures were treated with Chloroquine (50 nM, 24h) or Clioquinol (100 nM, 48h), then incubated with 30 µg/ml of DQ Red BSA and NeuroFluor™ NeuO (0.1 µM) for 1 hour, prior to assay. **(A)** Cells were imaged and lysosomal activity was measured as DQ-BSA puncta spots multiplied by relative intensity in NeuO+ cells (DQ-BSA Index), normalised to non-transgenic littermates and compared to each genotypes DMSO **(B)**. Effect of Chloroquine was assessed as the fold change to Untreated. Data represents different LRRK2 transgenic litters and respective littermates (Bars represent mean +/- SEM; (N = 3; ns or not represented: non-significant; ∗P <0.05; ∗∗P <0.01; ∗∗∗P <0.001; ∗∗∗∗P <0.0001; Two-way ANOVA, One sample t test, Mann-Whitney non-parametric test). Scale bar = 100 µm).

4.2.2. Autophagy flux in LRRK2 iPSC-derived dopaminergic neuronal cultures.

Given the altered lysosomal degradation observed in *LRRK2-R1441C* rat cortical neuronal cultures, we assessed if this dysfunction was present in iPSC-derived dopaminergic (DA) neuronal cultures from Parkinson's patients with *LRRK2* mutations, as an independent model of PD. iPSCs derived from three patients with PD carrying the *LRRK2-R1441C* mutation, four patients with PD carrying the *LRRK2-G2019S* mutation, five healthy Controls, one isogenic Control for *LRRK2-R1441C* and one for *LRRK2-G2019S*, were differentiated to midbrain dopaminergic neurons. TH percentage was calculated in MAP2+ cells using immunostainings and LRRK2 phosphorylation was measured using immunoblottings (Fig. 3.17, Fig. 3.18 A-C).

To characterise the autophagy-lysosomal pathway in Control and *LRRK2* iPSC-derived dopaminergic neurons, cultures were treated with chloroquine or clioquinol and incubated with neuronal marker NeuO and DQ Red BSA to measure lysosomal proteolysis (Fig. 4.2 A). Results were expressed as DQ-BSA Index (DQ-BSA number of spots multiplied by relative spot intensity and spot area) in NeuO-positive cells, normalised to average of Control DMSO (Fig. 4.2 B). Treatment with chloroquine, used to inhibit autolysosome fusion, showed consistent significant ~80% decrease in DQ-BSA Index in *LRRK2-R1441C*, *LRRK2-G2019S* and Control iPSC-derived dopaminergic cultures, validating assay specificity (Fig. 4.2 B-C). Under basal conditions measured DQ-BSA Index in *LRRK2-R1441C* or *LRRK2-G2019S* neuronal dopaminergic cultures was slightly increased, but there were no significant differences found compared to Control lines (Fig. 4.2 D). Furthermore, corrected iPSC-derived isogenic lines for *LRRK2-R1441C* and *LRRK2-*

G2019S were compared to *LRRK2-R1441C* and *LRRK2-G2019S* respectively, and there were no significant differences in DQ-BSA Index (Fig. 4.2 E-F).

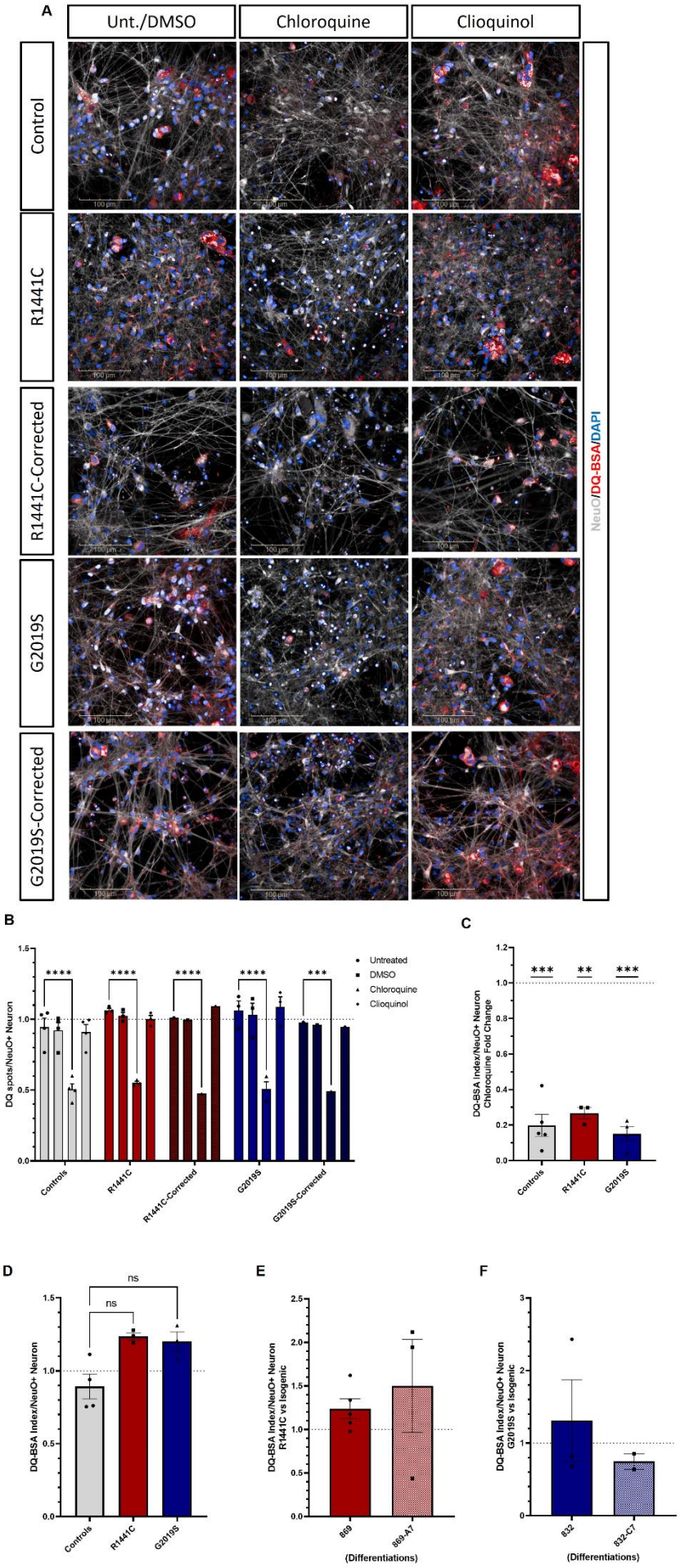
A
Unt./DMSO
Chloroquine
Clioquinol
Control
R1441C
R1441C-Corrected
G2019S
G2019S-Corrected
NeuO/DQ-BSA/DAPI
B
DQ spots/NeuO+ Neuron
Untreated
DMSO
Chloroquine
Clioquinol
Controls
R1441C
R1441C-Corrected
G2019S
G2019S-Corrected
C
DQ-BSA Index/NeuO+ Neuron
Chloroquine Fold Change
Controls
R1441C
G2019S
D
DQ-BSA Index/NeuO+ Neuron
ns
Controls
R1441C
G2019S
E
DQ-BSA Index/NeuO+ Neuron
R1441C vs Isogenic
869
869-A7
(Differentiations)
F
DQ-BSA Index/NeuO+ Neuron
G2019S vs Isogenic
832
832-C7
(Differentiations)

Figure 4.2 – Lysosomal activity in LRRK2 mutant primary cortical cultures. iPSC-derived dopaminergic cultures from LRRK2 patient and control lines were generated and treated with Chloroquine (50 nM, 24h) or Clioquinol (100 nM, 48h), then incubated with 30 µg/ml of DQ Red BSA and NeuroFluor™ NeuO (0.1 µM) for 1 hour, prior to assay at DIV 35. **(A)** Cells were imaged and lysosomal activity was measured as DQ-BSA puncta spots multiplied by relative intensity in NeuO+ cells (DQ-BSA Index), normalised to average of controls and compared to each genotypes DMSO **(B)**. Effect of Chloroquine was assessed as the fold change to Untreated. Data points represent genotype lines, averaged by number of differentiations. Bars, mean ± SEM from two independent differentiations (ns or not represented: non-significant; ∗P <0.05; ∗∗P <0.01; ∗∗∗P <0.001; ∗∗∗∗P <0.0001; Two-way ANOVA, one sample t test, Mann-Whitney non-parametric test). Scale bar = 100 µm).

4.2.3. Autophagy pathway characterisation in LRRK2 iPSC-DA neuronal cultures.

Given that lysosomal degradation was altered in *LRRK2-R1441C* rat cortical neuronal cultures, but no differences were observed in *LRRK2-R1441C* iPSC-DAn, the autophagy-lysosomal pathway was further characterised in Control and *LRRK2* iPSC-derived dopaminergic neurons. Cultures were immunostained for autophagosome marker LC3B, lysosomal marker LAMP1 and neuronal marker MAP2 (Fig. 4.3 A). Treatment with autophagy inhibitor chloroquine showed consistent decrease in LAMP1 spot number and increase in LC3B spot number, in Control iPSC-DA $MAP2^+$ neurons (Fig. 4.3 A, B, D). Furthermore, LAMP1 spots showed a significant decrease in chloroquine fold change, whereas LAMP1 spots co-localised with LC3B spots corresponding to autolysosomes showed a significant increase in chloroquine fold change in Control iPSC-DA $MAP2^+$ neurons (Fig. 4.3 A, C, E). These chloroquine-induced effects are reflective of decreased lysosomal degradation and accumulation of autophagosomes through blocked autolysosome fusion, thereby confirming assay specificity. When comparing autophagosome ($LC3B^+$ spots), lysosomal ($LAMP1^+$ spots) and autolysosome ($LC3B^+/LAMP1^+$ spots) marker expression with immunostaining, there were no differences between *LRRK2-R1441C* or *LRRK2-G2019S* iPSC-DA neuronal cultures and Control lines (Fig. 4.3 F-H, respectively). LC3-II is closely correlated with the number of autophagosomes, serving as a good indicator of autophagosome formation. Since LC3B detects endogenous levels of total LC3B protein, SDS-PAGE and immunoblotting was performed in iPSC-DA neuronal lysates in the presence and absence of chloroquine to resolve two bands, one representing LC3-I (cytosolic), and the other representing LC3-II,

which is conjugated with phosphatidylethanolamine (PE). Blocking autophagy with chloroquine treatment showed significant increase in LC3-II expression in Control and *LRRK2-G2019S* iPSC-DA neurons, reflecting autophagosome accumulation (Fig. 4.4 A, B, C). *LRRK2-R1441C* iPSC-DA neuronal cultures showed a chloroquine-induced increase, albeit non-significant (Fig. 4.4 C). Lysates were also treated with clioquinol, which showed no differences between treatments or genotypes (immunoblot data not shown). When using LC3-II as an indicator of autophagy with immunoblotting there was a decrease in autophagosome formation in *LRRK2-R1441C* iPSC-DA neuronal cultures compared to Controls (Fig. 4.4 D). There were no differences between Controls and *LRRK2-G2019S* iPSC-DA neuronal cultures or *LRRK2-G2019S* iPSC-DA neuronal cultures and the isogenic Control line (Fig. 4.4 D and E, respectively).

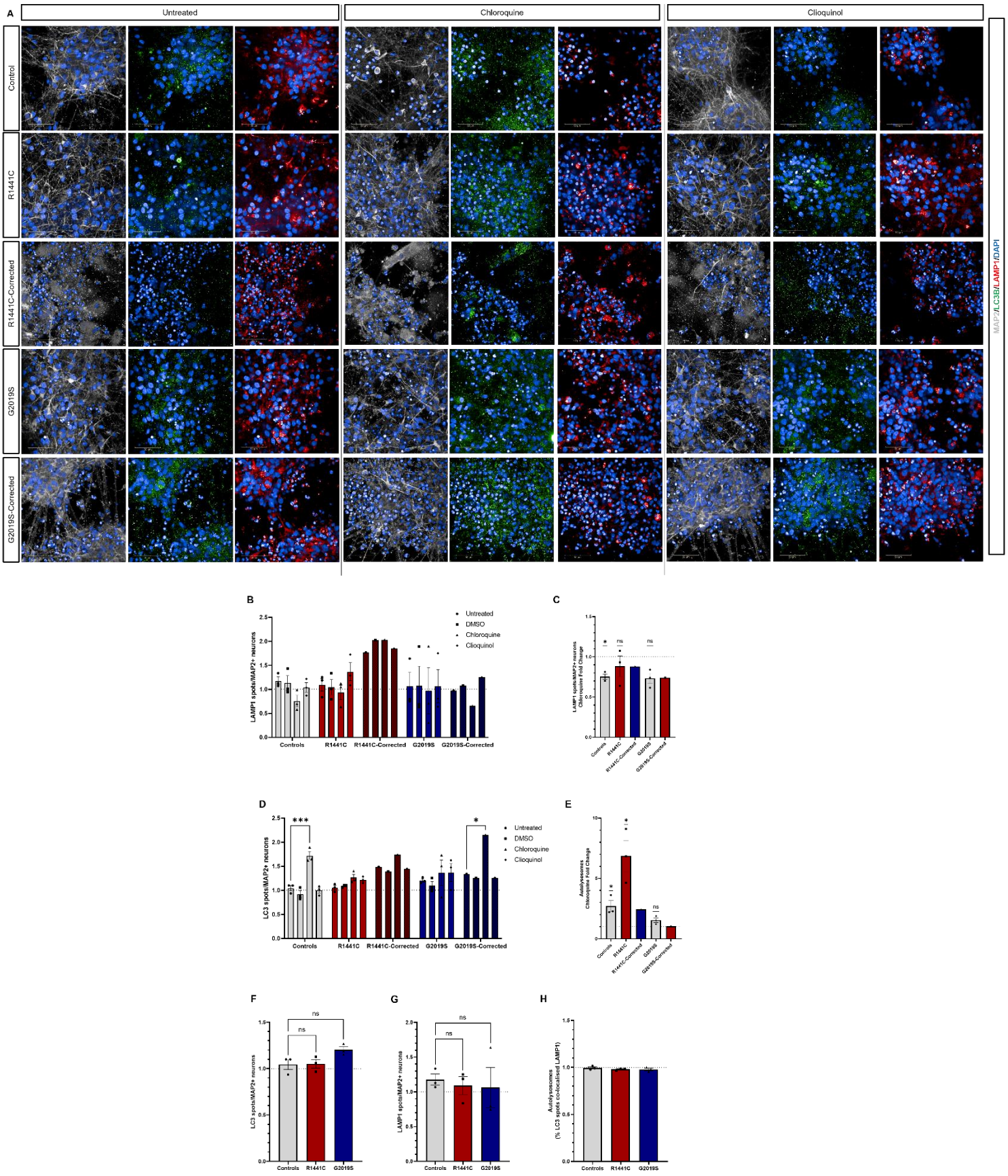
A
Untreated
Chloroquine
Clioquinol
Control
R1441C
R1441C-Corrected
G2019S
G2019S-Corrected
MAP2/LC3B/LAMP1/DAPI
B
Untreated
DMSO
Chloroquine
Clioquinol
LAMP1 spots/MAP2+ neurons
Controls
R1441C
R1441C-Corrected
G2019S
G2019S-Corrected
C
LAMP1 spots/MAP2+ neurons Chloroquine Fold Change
ns
D
LC3 spots/MAP2+ neurons
***
*
E
Autolysosomes Chloroquine Fold Change
F
LC3 spots/MAP2+ neurons
G
LAMP1 spots/MAP2+ neurons
H
Autolysosomes (% LC3 spots co-localised LAMP1)

Figure 4.3 – Lysosomal markers in LRRK2 iPSC-derived dopaminergic cultures. iPSC-derived dopaminergic cultures from LRRK2 patient control and isogenic lines were generated and treated with Chloroquine (50 nM, 24h) or Clioquinol (100 nM, 48h), then fixed at DIV 35 and immunostained with LC3B, LAMP1, MAP2 and DAPI **(A)**. LAMP1 spots **(B)** and LC3B spots **(D)** located in treated MAP2+ neurons were quantified and compared between genotypes **(F** and **G**, respectively**)**. Effects of Chloroquine treatment in LAMP1 **(C)** and LC3B **(E)** spots was assessed as the fold change to Untreated. Data points represent genotype lines, averaged by number of differentiations. Bars, mean ± SEM from two independent differentiations (∗P <0.05; non-significant (ns or not represented); One sample t test). Scale bar = 100 µm). **(H)** Autolysosomes were measured as LC3B spots co-localised with lysosomal marker LAMP1 (puncta area as a percentage of total v0a1 puncta) were measured in MAP2+ cells, normalised to average of controls and compared between Controls and patient lines. Data points represent genotype lines, averaged by number of differentiations. Bars, mean ± SEM from two independent differentiations (ns or not represented: non-significant; ∗P <0.05; ∗∗P <0.01; ∗∗∗P <0.001; Ordinary one-way ANOVA, Dunnett's multiple comparisons test Two-way ANOVA).

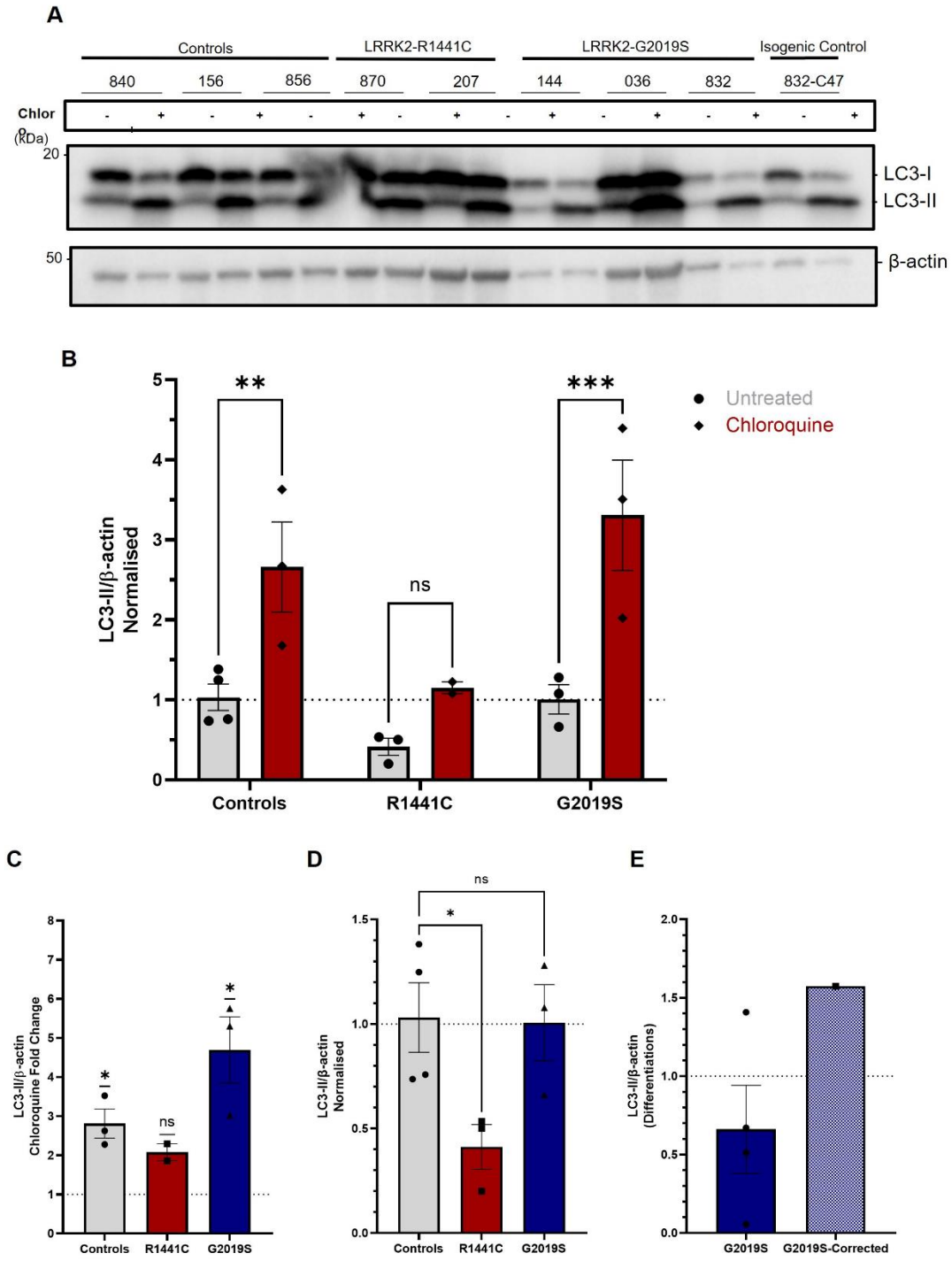

Figure 4.4 – Measuring LC3 expression levels in LRRK2 iPSC-derived dopaminergic cultures. **(A)** iPSC-derived dopaminergic cultures from LRRK2 patient control and isogenic lines were generated and treated with Chloroquine (50 nM, 24h), then fixed at DIV 35 and immunoblotted for LC3 and β-actin. **(B)** LC3-II was normalised to β-actin and compared between treatments. **(C)** Effects of Chloroquine treatment in LC3-II was assessed as the fold change to Untreated. Data points represent genotype lines, averaged by number of

differentiations. Bars, mean ± SEM from two independent differentiations (∗P <0.05; non-significant (ns or not represented); One sample t test). Scale bar = 100 μm). LC3-II basal expression was compared between patient lines and average of controls **(D)** and patient line to respective isogenic control **(E)**. Data points represent genotype lines, averaged by number of differentiations. Bars, mean ± SEM from two independent differentiations (ns or not represented: non-significant; ∗P <0.05; ∗∗P <0.01; ∗∗∗P <0.001; Dunnett's multiple comparisons test Two-way ANOVA, One sample t test, Ordinary one-way ANOVA).

To further investigate these results, immunoblotting of autophagy-lysosomal markers was performed in iPSC-DA neuronal lysates treated with LRRK2 kinase inhibitor MLi-2, clioquinol and chloroquine (Fig. 4.5 A-B). The effect of MLi-2 and clioquinol showed no significant differences in LAMP1 expression between genotypes nor treatment groups (Fig. 4.5 B). Consistent with immunostaining, there is a significant chloroquine-induced fold change decrease in LAMP1 expression (Fig. 4.5 C), confirming assay specificity. When comparing lysosomal marker expression, there were no differences between *LRRK2-R1441C* or *LRRK2-G2019S* iPSC-DA neuronal cultures and Control lines (Fig. 4.5 D). Expression of lysosomal H^+-pump subunit vATPase-a1 was assessed by immunoblotting iPSC-DA neuronal lysates and showed no significant differences between MLi-2, clioquinol and chloroquine treatment (Fig. 4.5 E) and no differences between *LRRK2* iPSC-DA lines or Controls (Fig. 4.5 F). One caveat of this experimental set up was that MLi-2 treatment at 50nM for 48 h was not sufficient to inhibit LRRK2 kinase activity in iPSC-DA cultures (Fig. 3.18) and it is likely to not be sufficient to exert any effects in other proteins, such as LRRK2 phosphorylation substrates Rab family of proteins.

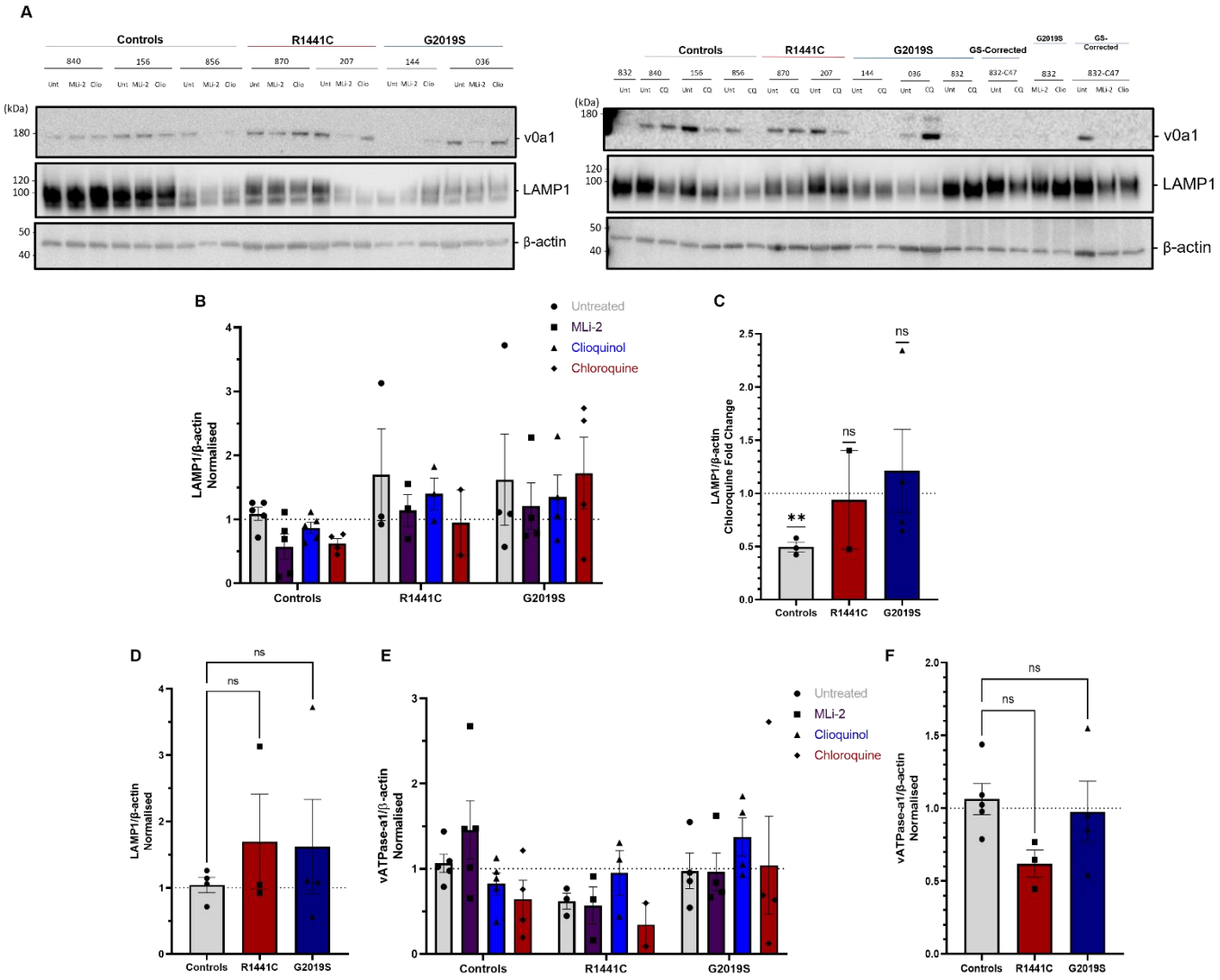

Figure 4.5 – Measuring LAMP1 expression levels in LRRK2 iPSC-derived dopaminergic cultures. **(A)** iPSC-derived dopaminergic cultures from LRRK2 patient control and isogenic lines were generated and treated with Chloroquine (50 nM, 24h), MLi-2 (50 nM, 48h) or Clioquinol (100 nM, 48h), then fixed at DIV 35 and immunoblotted for LAMP1, vATPase-a1 and β-actin. LAMP1 **(B)** and vATPase-a1 **(E)** were normalised to β-actin and compared between treatments. **(C)** Effects of Chloroquine treatment in LAMP1 was assessed as the fold change to Untreated. LAMP1 **(D)** and vATPase-a1 **(F)** basal expression in patient lines was compared to average of controls. Data points represent genotype lines, averaged by number of differentiations. Bars, mean ± SEM from two independent differentiations (ns or not represented: non-significant; ∗P <0.05; ∗∗P <0.01; ∗∗∗P <0.001; Dunnett's multiple comparisons test Two-way ANOVA, One sample t test, Ordinary one-way ANOVA).

In summary, measuring proteolytic degradation in rat cortical cultures using DQ-BSA showed increased levels in *LRRK2-R1441C* but no differences in *LRRK2-G2019S* or *LRRK2-WT*, compared to respective nTG littermates (Fig. 4.1). However, proteolytic degradation showed no differences between *LRRK2* patient iPSC-derived dopaminergic cultures compared to controls (Fig. 4.2). Further investigation of autophagy markers of lysosomes and autophagosomes (LAMP1 and LC3, respectively) showed no differences between *LRRK2* patient iPSC-derived dopaminergic cultures compared to controls measured by immunostaining (Fig. 4.3). Measuring LC3-II using immunoblotting showed a 50% decrease in *LRRK2-R1441C*, but not *LRRK2-G2019S* iPSC-DA cultures, compared to healthy controls (Fig. 4.4), and showed no differences in LAMP1 or vATPase-a1 expression levels (Fig. 4.5).

4.3. Conclusions

The main conclusions highlighted in this chapter are:

1. Proteolytic degradation in rat cortical cultures showed increased levels in *LRRK2-R1441C*, but no differences in *LRRK2-G2019S* or *LRRK2-WT*, compared to respective nTG littermates.
2. There were no differences in proteolytic degradation in iPSC-derived *LRRK2-G2019S* or *LRRK2-R1441C* dopaminergic cultures.
3. Assessing autophagy markers LAMP1 and LC3B showed no changes when comparing iPSC-derived *LRRK2-G2019S* or *LRRK2-R1441C* dopaminergic cultures to healthy controls.

Chapter 5 – LRRK2 and Mitochondria

5.1. Introduction and aims

As mentioned previously (section 1.6), LRRK2 mutations affect the mitochondrial network. Previous work demonstrated that primary cortical neuronal cultures of BAC transgenic rats expressing the *LRRK2-R1441C* mutation exhibit decreased autophagy-lysosomal fusion, altered lysosomal pH and decreased lysosomal protein degradation, deficits not found in *LRRK2-WT* or *LRRK2-G2019S* transgenic neurons (Wallings, Connor-Robson, and Wade-Martins 2019). Although *LRRK2-R1441C* cortical primary neuronal cultures displayed autophagy defects, mitochondrial health and mitophagy were not characterised in these models.

Chapter aims:

- To characterise mitochondrial health and mitophagy in LRRK2 rat primary cortical cultures.
- To investigate mitochondrial health and mitophagy markers in LRRK2 iPSC-derived dopaminergic neuronal cultures.
- To investigate molecular mechanisms for mitochondrial dysfunction in LRRK2 iPSC-derived dopaminergic neuronal cultures.

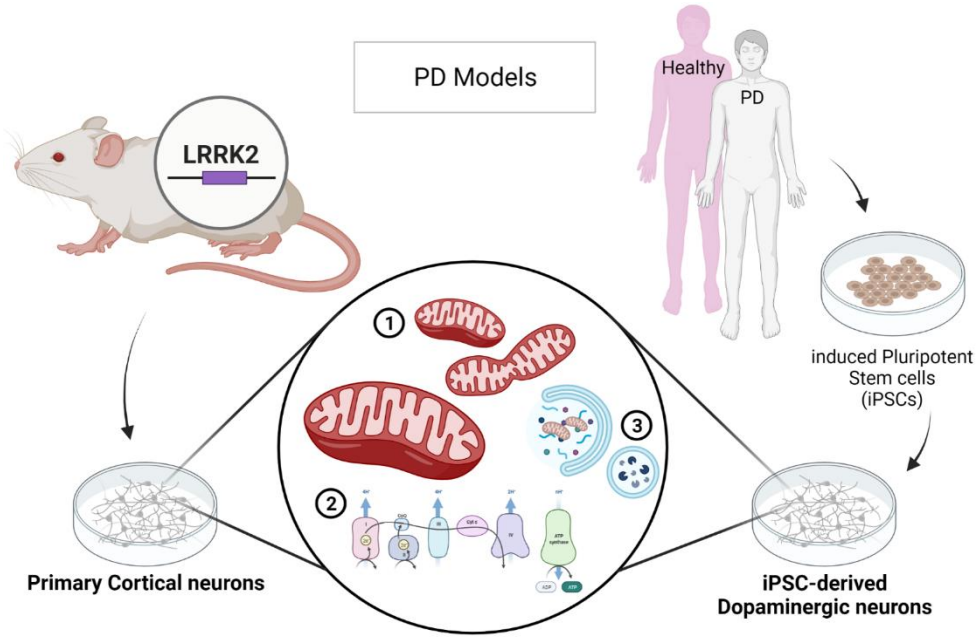

Figure 5.1 – Schematic representation of the models used to study mitochondrial homeostasis in LRRK2 Parkinson's disease. LRRK2 transgenic rat primary cortical cultures and induced pluripotent stem cell-derived dopaminergic neuronal cultures are used

to study (1) mitochondrial morphology, (2) mitochondrial health and function and (3) mitophagy.

5.2. Results

5.2.1. Primary rat LRRK2-R1441C cortical neuronal cultures exhibit mitochondrial damage and impaired mitophagy.

To investigate the role of PD-associated *LRRK2* mutations on mitochondrial structure and function, primary cortical neuronal cultures from *LRRK2* BAC transgenic rat pups (P1-P5) expressing the human *LRRK2-WT*, *LRRK2-G2019S* or *LRRK2-R1441C* transgene, and non-transgenic (nTG) littermates were generated (Sloan et al. 2016; Wallings, Connor-Robson, and Wade-Martins 2019). First, expression levels of electron transport chain (ETC) complexes I (NDUFB8), II (SDHB), III (UQCRC2), IV (MTCO1) and V (ATP5A) were measured and normalised to mitochondrial marker Hsp60. Under basal conditions, *LRRK2* cortical neuronal cultures show no significant difference in ETC protein expression levels, compared to nTG littermates (Fig. 5.2 A). In the presence of clioquinol, *LRRK2-WT* cortical neuronal cultures show a significant increase in UQCRC2 (Complex III) protein expression levels, compared to nTG littermates (Two-way ANOVA, P = 0.0019), but no other differences were observed (Fig. 5.2 D). To investigate mitochondrial respiratory function in *LRRK2* cortical neuronal cultures, cellular oxygen consumption and glycolysis was measured. Basal oxygen consumption rates (OCR), proton leak, ATP-linked CO_2 consumption, maximal respiration and spare capacity were not significantly changed in *LRRK2-G2019S* cortical cultures, compared to *LRRK2-WT* (Supplementary Fig. 5.3). MLi-2 treatment significantly decreased proton leak (P = 0.0145) and increased ATP-linked CO_2 consumption (P = 0.0354) in *LRRK2-WT* cortical cultures, but not in *LRRK2-G2019S* (Fig. 5.3 C, Fig. 5.3 D). Measuring extracellular acidification rate (ECAR) to evaluate glycolysis showed no differences between genotypes (Fig. 5.4). Thus, assessing the ETC complexes expression levels and mitochondrial respiratory function, there were no significant differences found in *LRRK2-G2019S* cortical neuronal cultures compared to nTG littermates.

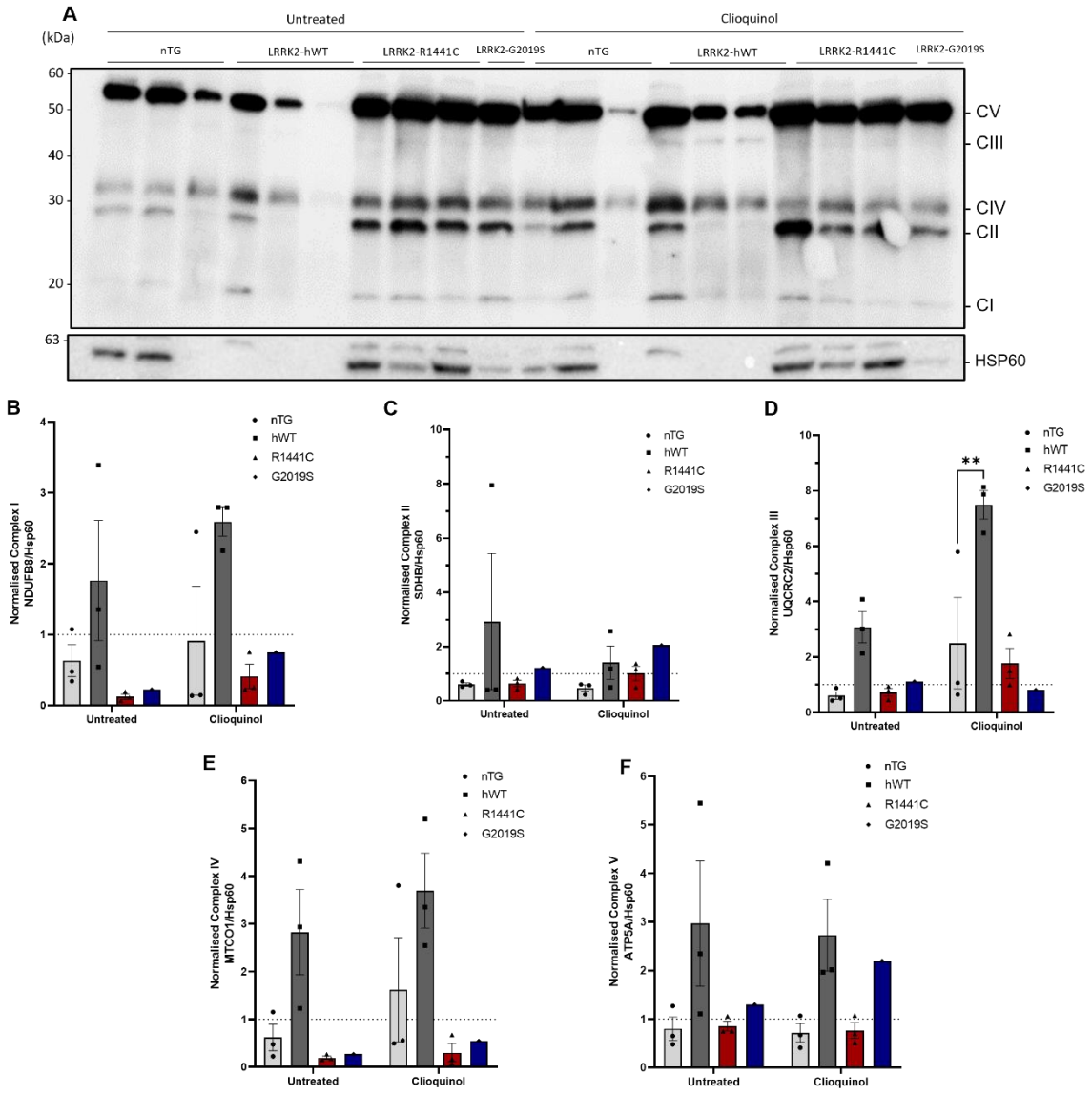

Figure 5.2 – Mitochondrial OxPhos complexes expression, in cortical cultures from mutant LRRK2-R1441C rats. Primary cortical neuronal cultures were generated from P1-P5 pups and assayed at DIV 14. Lysates were collected and immunoblotted using the OxPhos Rodent Western Blot Antibody Cocktail (ThermoFischer) for OxPhos **(B)** Complex I (NDUFB8), **(C)** Complex II (SDHB), **(D)** Complex III (UQCRC2), **(E)** Complex IV (MTCO1), **(F)** Complex V (ATP5A). Respective OxPhos band intensities were normalised to Hsp60, averaged to non-transgenic littermates and compared between genotypes. Data points represent averaged transgenic genotypes. Bars, mean ± SEM from four technical replicates (ns: non-significant; ∗P <0.05; ∗∗P <0.01; Ordinary one-way ANOVA).

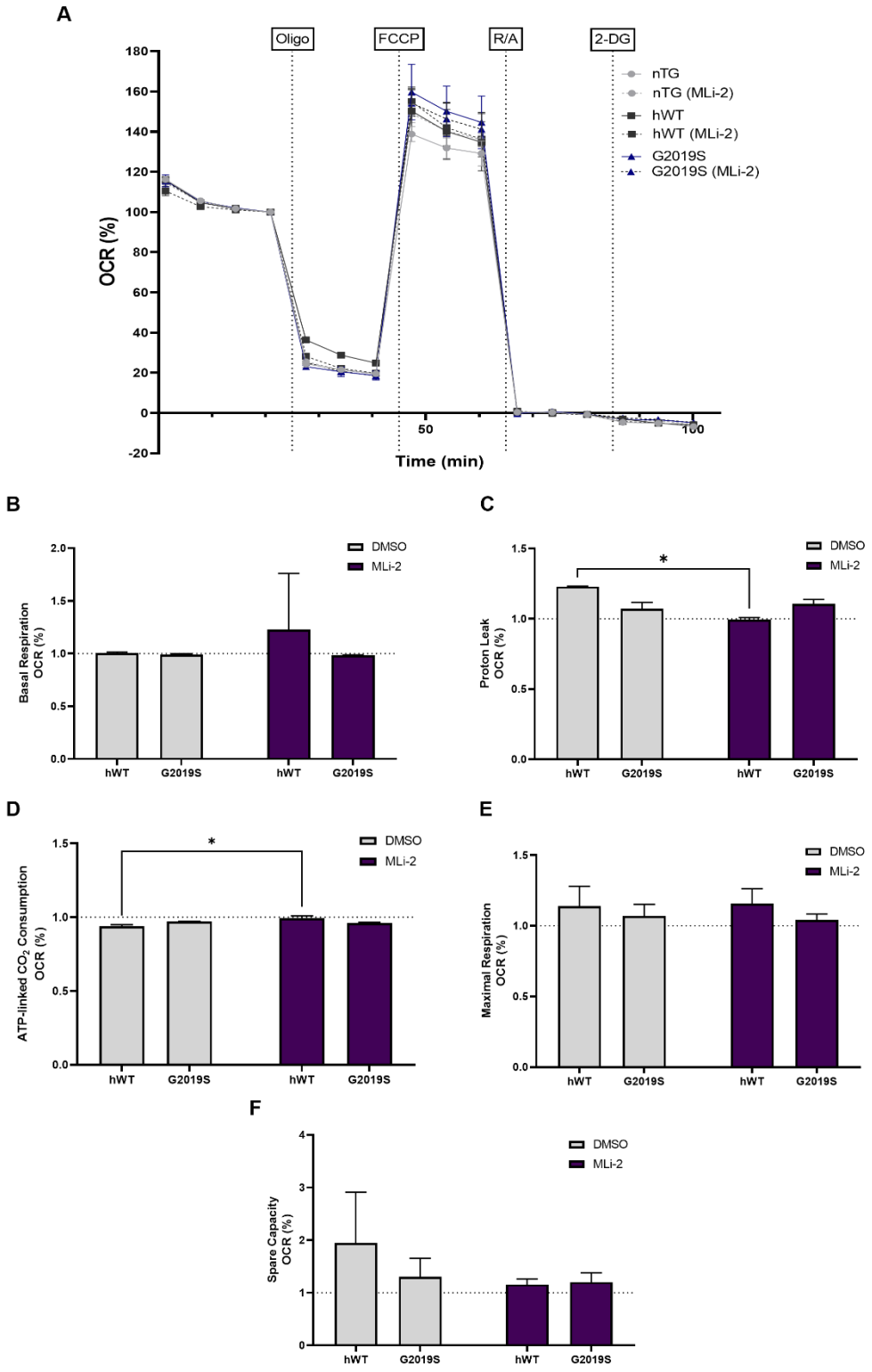

Figure 5.3 – Mitochondrial function in cortical cultures from transgenic LRRK2 rats. Primary cortical neuronal cultures were generated from P1-P5 pups and assayed at DIV 14. Oxygen consumption rates (OCRs) in cultures treated with DMSO or MLi-2 (100nM) for 48

h prior were measured on an XF24 Analyzer. **(A)** Normalised OCR profiles (% OCR to Basal OCR) from cultures for LRRK2-hWT, LRRK2-G2019S and non-transgenic littermates exposed sequentially to oligomycin (8 µM) (Oligo), FCCP (1 µM), rotenone (5 µM) plus antimycin A (5 µM) (R/A) and 2-Deoxyglucose (90 mg/ml) (2-DG). **(B)** Basal respiration was calculated as measurements before oligomycin injection (pmol O2/min/µg protein). After normalisation to % of Basal OCR, Proton leak, ATP linked to oxygen consumption, maximal respiration and spare capacity were calculated and fold change from basal was quantified to assess MLi-2 effect. **(C)** Proton leak was calculated as the measurements after oligomycin injection **(D)** ATP production linked to oxygen consumption was calculated as the measurements after oligomycin injection and measurement of basal respiration. **(E)** Maximal Respiration was calculated as measurements after FCCP injection, normalised from OCR %. **(F)** Spare Capacity was calculated as the difference between Maximal and Basal respiration, normalised from OCR %. Data points represent averaged litters per each genotype. Bars, mean ± SEM from at least three independent litters (ns: non-significant; $*P < 0.05$; Unpaired t test).

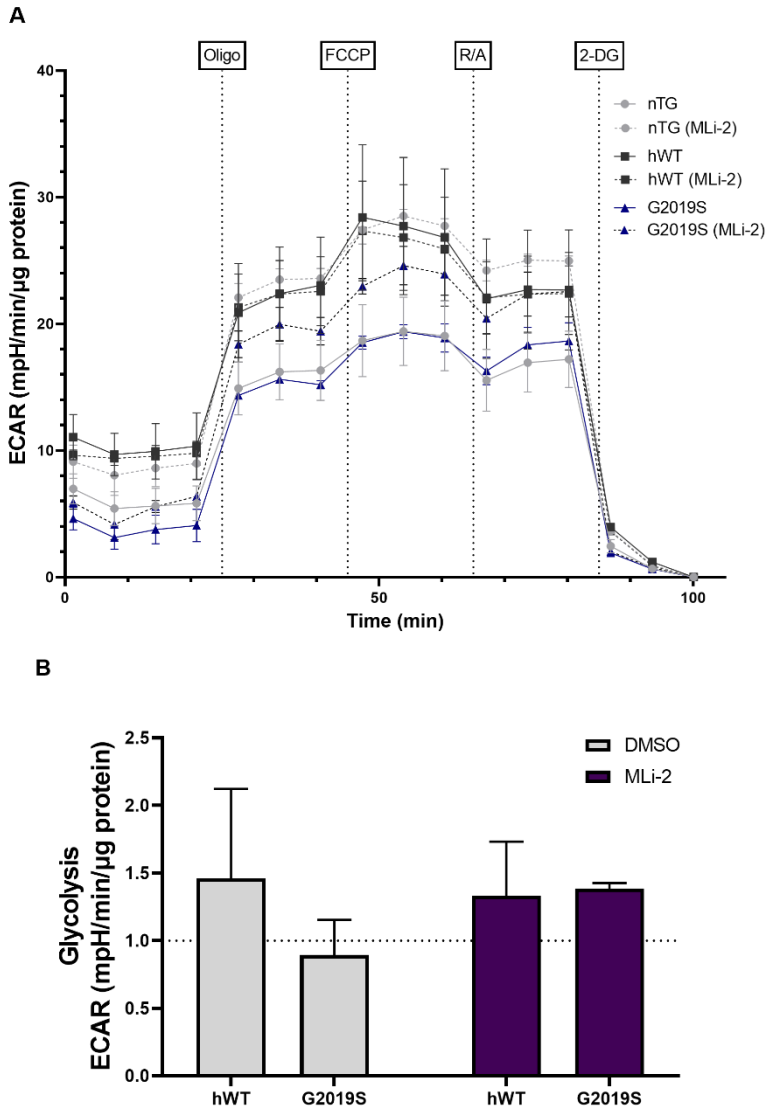

***Figure 5.4 – Measuring Extracellular Acidification Rates in cortical cultures from transgenic LRRK2 rats*.** Primary cortical neuronal cultures were generated from P1-P5 pups, treated with MLi-2 (100nM) for 48 h and assayed at DIV 14. Extracellular acidification rates (ECARs) in cortical cultures were measured on an XF24 Analyzer. **(A)** Normalised extracellular acidification profiles (% ECAR to Basal ECAR) are represented for LRRK2-hWT, LRRK2-G2019S and non-transgenic littermates exposed sequentially to oligomycin (8 µM) (Oligo), FCCP (1 µM), rotenone (5 µM) plus antimycin A (5 µM) (R/A) and 2-Deoxyglucose (90 mg/ml) (2-DG). **(B)** Normalised ECAR was calculated for LRRK2-hWT and LRRK2-G2019S relative to respective non-transgenic littermates and fold change from basal was quantified to assess MLi-2 effect. Data points represent averaged litters per each genotype. Bars, mean ± SEM from at least three independent litters (ns: non-significant; ∗P <0.05; Unpaired t test).

To assess mitochondrial health in *LRRK2-R1441C*, mitochondrial membrane potential (ΔΨm) was measured using the potentiometric JC-10 dye. Under basal conditions, *LRRK2-R1441C* cortical neuronal cultures show a significant decrease in ΔΨm, compared to nTG littermates (P = 0.012, Mann-Whitney t test) (Fig. 5.5A). These changes in *LRRK2-R1441C* cultures were coupled with a significant, >1.5-fold, increase in mitochondrial ROS production, as assessed using MitoSox dye (P = 0.0166) (Fig. 5.5 C-D), but were independent of changes in cellular ATP levels and alterations in mitochondrial morphology (Fig. 5.5 B; Fig. 5.6 A-C). In parallel, mitochondrial function in *LRRK2-WT* and *LRRK2-G2019S* primary cortical neuronal cultures was also assessed and no differences in mitochondrial membrane potential, ATP levels, mitochondrial ROS or basal mitophagy flux, were observed in *LRRK2-WT* and *LRRK2-G2019S* compared to nTG littermates (Fig. 5.6 D-L).

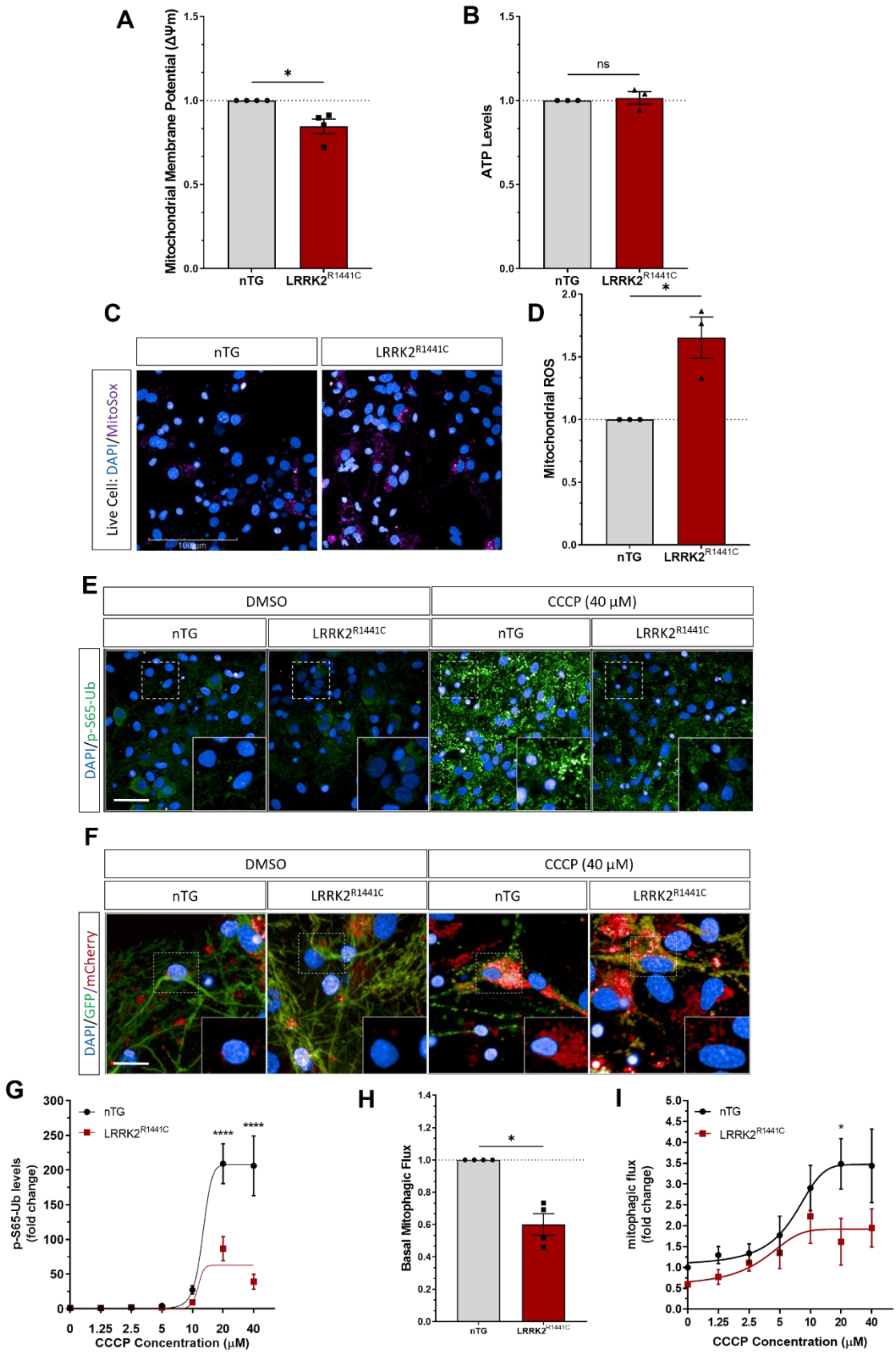

Figure 5.5 – Mitochondrial dysfunction and reduced mitophagy levels in primary cortical neuronal cultures from LRRK2-R1441C transgenic rats. Primary cortical

neuronal cultures were generated from P1-P5 pups and assayed at DIV 14 for **(A)** Mitochondrial membrane potential measured using JC-10 dye **(B)** ATP levels measured using a luminescent assay and **(C, D)** Mitochondrial ROS production using MitoSox changes measured in *LRRK2-R1441C* cortical cultures, normalised to non-transgenic littermate levels. Data points represent averaged transgenic genotypes. Bars, mean ± SEM from three independent litters (ns: non-significant; ∗P <0.05; Mann-Whitney Unpaired t test). **(E, G)** DIV 14 primary cortical cultures were treated CCCP for 8 h and pS65Ub was quantified in MAP2 and expressed as number of pS65Ub puncta per neuronal area was quantified. **(F)** DIV 14 primary cortical cultures were transduced with Mito-QC lentivirus reporter, treated with CCCP for 8 h. Mitophagic flux was assessed by quantifying mCherry puncta intensity and number in transfected cells under basal conditions **(H)** or after CCCP treatment **(I)**. Data points represent averaged litters per each genotype. Error bars: mean ± SEM from at least three independent litters (ns: non-significant; ∗P <0.05; ∗∗P <0.01; ∗∗∗P <0.001; ∗∗∗∗P <0.0001; Unpaired t test). Panels C, E, F, G and I were cultured and assayed by Dr. Matthew Williamson. Data from Panels A, B, D, G-I were analysed, and graphs generated by Marta Madureira.

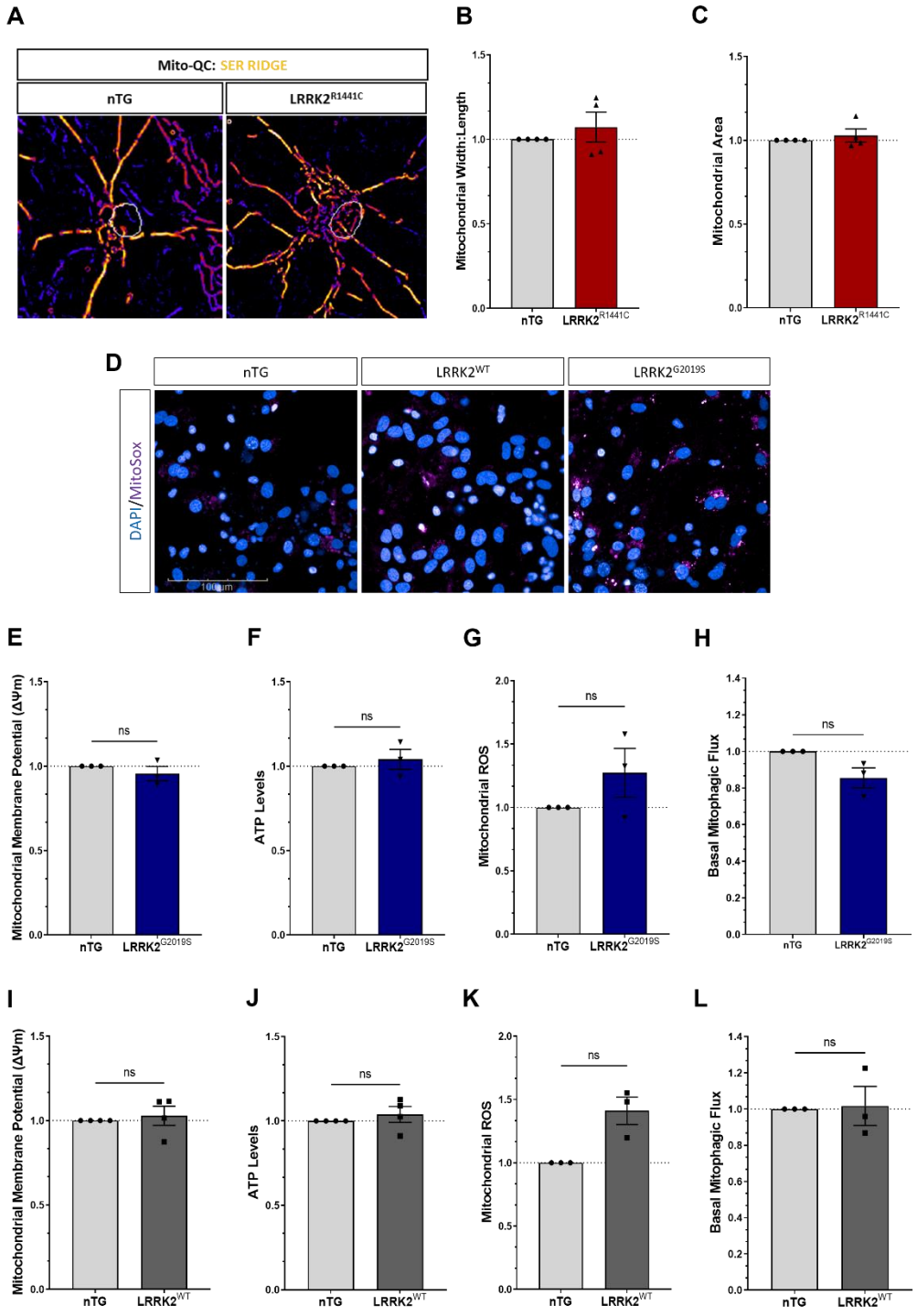

Figure 5.6 – Mitochondrial health and mitophagy levels in primary cortical neuronal cultures from LRRK2 transgenic rats. Primary cortical neuronal cultures were generated from P1-P5 pups and assayed at DIV 14. **(A)** Mitochondrial morphology was assessed using Mito-QC transduced cortical cultures, to calculate mitochondrial area (μm^2) **(B)** and mitochondrial width to length **(C)**, normalised to non-transgenic littermates. **(D)** The full dataset (from Fig. 1C) for mitochondrial ROS, measured using MitoSox live dye and compared between the genotypes. Mitochondrial health assessed in *LRRK2-G2019S* and

LRRK2-hWT cortical cultures using mitochondrial membrane potential changes measured with JC-10 live dye **(E, I)**, by ATP levels measured using a luminescent assay **(F, J**), and by mitochondrial ROS **(G, K)** normalised to non-transgenic littermate levels. Data points represent averaged transgenic genotypes. Error bars: mean ± SEM from 3-4 independent litters (ns: non-significant; ∗P <0.05; Mann-Whitney Unpaired t test). **(H, L)** Mitophagic flux was calculated as *mCherry*-only puncta for *Mito-QC* reporter transduced primary cortical cultures. Values were normalized to non-transgenic littermates and quantified to assess *mCherry* under basal conditions for *LRRK2-G2019S* and *LRRK2-hWT* genotypes. Error bars: mean ± SEM from three independent litters (ns: non-significant; ∗P <0.05; Mann-Whitney Unpaired t test). Panels A and D were performed and assayed by Dr. Matthew Williamson. Data from Panels B, C, E-L were analysed, and graphs generated by Marta Madureira.

Following these findings of impaired mitochondrial health in *LRRK2-R1441C* primary neurons, it was assessed if clearance of damaged mitochondria through mitophagy was altered in neuronal cultures. Given mitophagy levels have been reported to be altered under both basal and depolarised conditions in *LRRK2* models, an immunofluorescence staining of phosphorylated Ubiquitin (pS65Ub), a marker of PINK1-activation and mitophagy initiation was developed. In addition, the mitophagy reporter *Mito-QC* was used to assess mitophagy in primary neuronal cortical cultures (Fig. 5.5 E-F). CCCP-induced pS65Ub puncta number was significantly decreased in *LRRK2-R1441C* cells when compared to nTG cultures (P=<0.0001, Unpaired t test) (Fig. 5.5 E, Fig. 5.5 G). To confirm that decreased pS65Ub-induction resulted in impaired mitophagy, mitophagic flux was assessed in *LRRK2* primary cortical neuronal cultures transduced with *Mito-QC* reporter lentivirus (McWilliams et al. 2016; 2018). A 50% decrease in mitophagy was observed in *LRRK2-R1441C* neuronal cultures, as assessed by the number of mito-lysosomes (red puncta per cell) under basal conditions (P = 0.0286) (Fig. 5.5 F, Fig. 5.5 H). Additionally, depolarisation-induced mitophagy in *LRRK2-R1441C* primary neuronal cultures was also decreased compared to nTG (P=0.0409, two-way ANOVA) (Fig. 5.5 F, Fig. 5.5 I). Together, these data demonstrate impairments in mitochondrial function and PINK1-dependent (depolarisation-induced) mitophagy in *LRRK2-R1441C* primary cortical cultures.

Taken together, these data suggest that mitochondrial health is impaired in *LRRK2-R1441C* cortical neuronal cultures but not in *LRRK2-WT* and *LRRK2-G2019S* cells *in vitro*.

5.2.2. LRRK2-R1441C iPSC-DA neuronal cultures show mitochondrial alterations and dysfunction.

Given the mitochondrial dysfunction and impaired mitophagy observed in *LRRK2-R1441C* rat cortical neuronal cultures, it was assessed if this dysfunction was present in iPSC-derived dopaminergic (DA) neuronal cultures from Parkinson's patients with *LRRK2-R1441C* mutations, a highly physiological model of PD. iPSCs derived from three patients with PD carrying the *LRRK2-R1441C* mutation, and three healthy controls, were differentiated to midbrain dopaminergic neurons using the Expansion protocol (Williamson et al. 2023) to obtain higher neuronal density per differentiation (Materials and Methods 2.6.2.). The presence of mature neurons ($MAP2^+$) and the percentage of tyrosine hydroxylase-positive (TH^+) dopamine neurons was consistent across genotypes and multiple differentiations (Fig. 5.7). Endogenous LRRK2 expression levels and kinase activity, were similar between *LRRK2-R1441C* and control iPSC-DA neuronal cultures ($P = 0.7686$), as assessed by western blotting of LRRK2 and phosphorylation of the LRRK2 substrates Rab8A and Rab12 (Tasegian et al. 2021) ($P = 0.2358$ and 0.2462, respectively; Fig. 5.8).

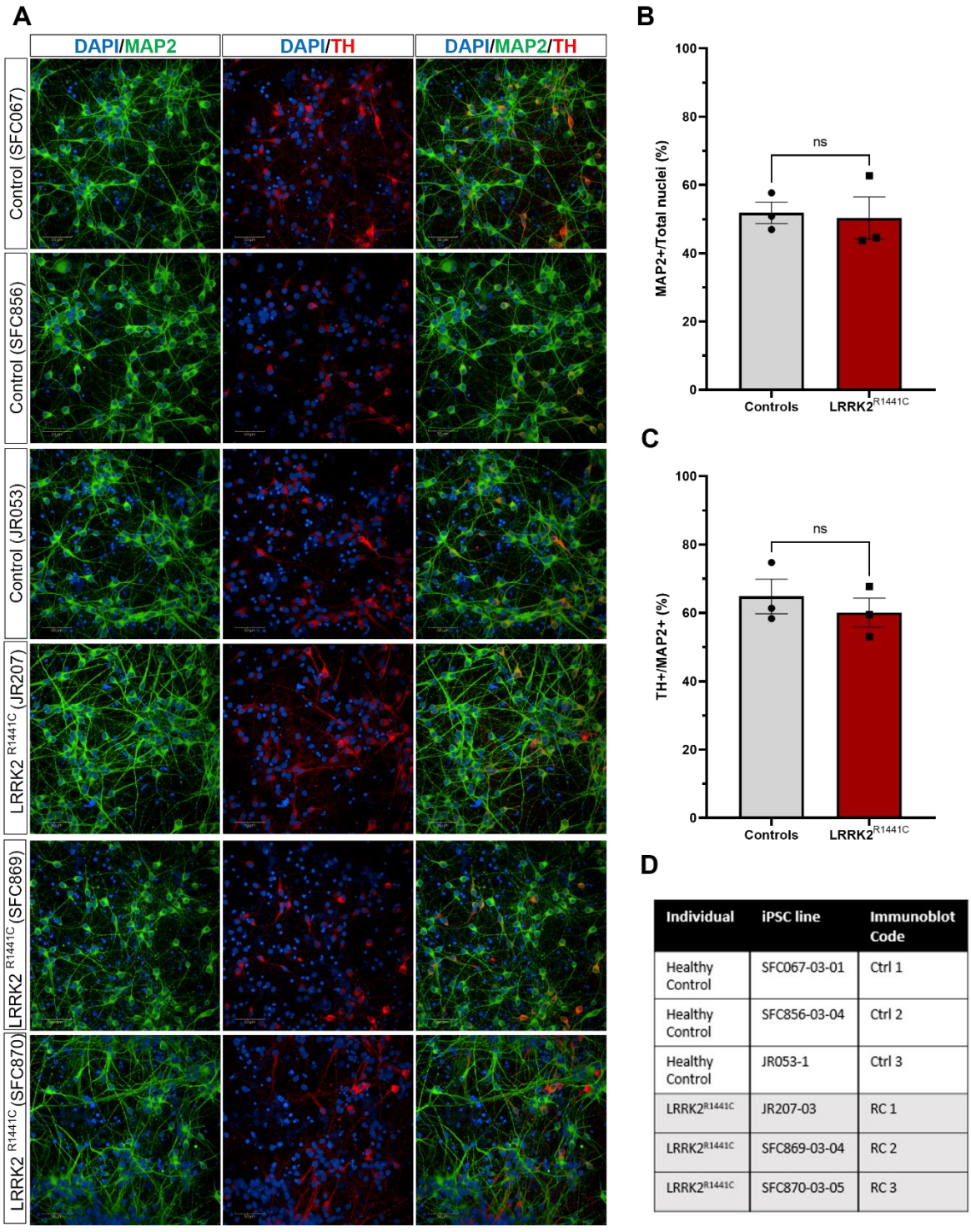

Individual	iPSC line	Immunoblot Code
Healthy Control	SFC067-03-01	Ctrl 1
Healthy Control	SFC856-03-04	Ctrl 2
Healthy Control	JR053-1	Ctrl 3
LRRK2^{R1441C}	JR207-03	RC 1
LRRK2^{R1441C}	SFC869-03-04	RC 2
LRRK2^{R1441C}	SFC870-03-05	RC 3

Fig. 5.7 – Characterisation of iPSC-DA neuronal cultures. **(A)** Representative images of control and *LRRK2-R1441C* iPSC-DA neuronal cultures used throughout this study stained for MAP2, TH and DAPI. Scale bar represents 50 µm. Quantification of the percentage of cells positive for MAP2^{+} within the total nuclei count **(B)** and percentage of cells positive for TH^{+} within the MAP2^{+} population **(C)**, compared between control and *LRRK2-R1441C* iPSC-DA neuronal cultures. Data points represent genotype lines, averaged by number of

differentiations. Error bars: mean ± SEM from three independent differentiations (ns: non-significant; ∗P <0.05; Unpaired t test). **(D)** Table describing patient and control lines used in the study.

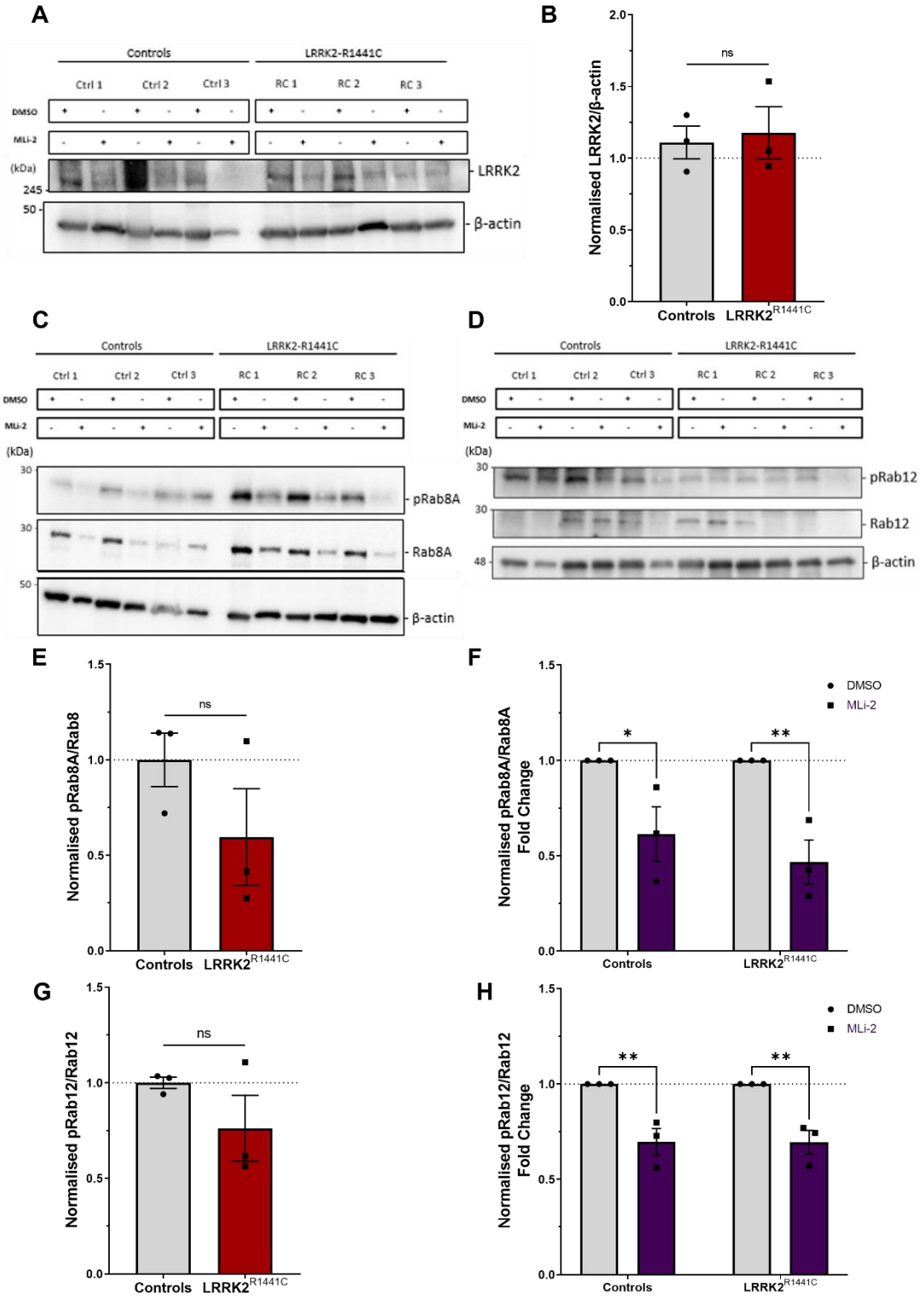

Fig. 5.8 – LRRK2 kinase activity and MLi-2 treatment in iPSC-DA neuronal cultures. To assess LRRK2 expression and kinase inhibition, iPSC-DA neuronal cultures from control and *LRRK2-R1441C* patient lines were treated with MLi-2 (100 nM) for 48 h. **(A, C, D)** Western blots were immunoblotted for LRRK2, Rab12 and Rab8A expression, quantified and normalised to average of controls and compared between genotypes. Western blots for **(B)** LRRK2 expression and LRRK2 phosphorylation substrates **(E)** Rab8A and **(G)** Rab12 were used to assess kinase activity by normalising phosphorylated Rab12 (or Rab8A) to total Rab12 (or Rab8A) expression (ns: non-significant; ∗P <0.05; Unpaired t test). **(F)** The effect of LRRK2 kinase inhibitor MLi-2 was quantified by western blot for pRab12 (phospho S106) and Rab12 expression to assess pRab12/Rab12 fold change from basal (DMSO) and **(H)** pRab8A (phospho ST72) and Rab8A, in response to treatment with 100 nM MLi-2 for 48 h. Data points represent genotype lines, averaged by number of differentiations. Error bars: mean ± SEM from two independent differentiations (ns: non-significant; ∗P <0.05; two-way ANOVA, Šídák's multiple comparisons test).

To understand the effects of the *LRRK2-R1441C* mutation on mitochondrial health in dopaminergic neurons, a number of assays of mitochondrial function were performed. Consistent with observations in primary cortical neuronal cultures, *LRRK2-R1441C* iPSC-DA neuronal cultures demonstrated lower mitochondrial membrane potential (ΔΨm) under basal conditions (P = 0.0490) (Fig. 5.9 A) with no change in basal ATP levels (Fig. 5.9 B). However, although iPSC-DA neuronal cultures derived from two lines demonstrated increased mitochondrial ROS production, as assessed by MitoSox, this effect was not significant in *LRRK2-R1441C* iPSC-DA neuronal cultures overall (Fig. 5.9 C-D). LRRK2 kinase inhibitors have been described to rescue mitochondrial alterations in PD models (Singh et al. 2021; Wauters et al. 2020; Bonello et al. 2019). First it was confirmed that LRRK2 kinase activity was efficiently inhibited by 100nM MLi-2 in iPSC-DA neuronal cultures after 48 h of treatment, as demonstrated by 40% reduction in the phosphorylation of LRRK2 substrate Rab8A and Rab12 (Fig. 5.8 C-D, F, H). However, treatment of *LRRK2-R1441C* or healthy control iPSC-DA neuronal cultures with MLi-2 had no effect on mitochondrial membrane potential under basal conditions (Fig. 5.10 A).

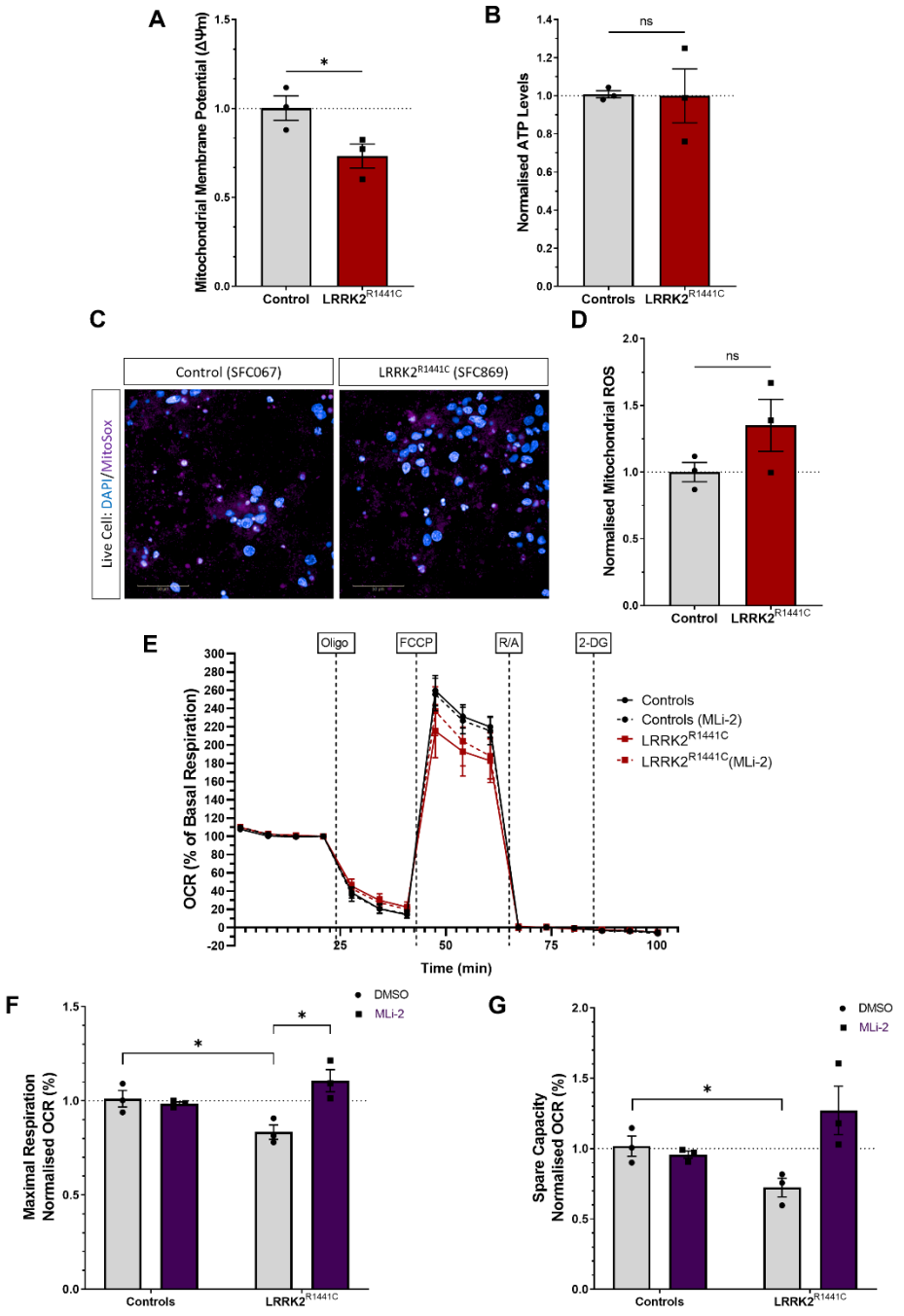

Figure 5.9 – Mitochondrial dysfunction in Parkinson's iPSC-DA neuronal cultures carrying the LRRK2-R1441C mutation. iPSC-DA neuronal cultures from controls and *LRRK2-R1441C* Parkinson's patient lines were generated to assess **(A)** mitochondrial membrane potential changes measured with JC-10 and **(B)** ATP Production measured using a luminescent assay and normalised to number of nuclei. Data points represent genotype lines, averaged by number of differentiations. Error bars: mean ± SEM from three independent differentiations (ns: non-significant; ∗P <0.05; Unpaired t test). **(C)** Oxidative stress was measured as abundance of mitochondrial ROS superoxide anion ($O_2^{\cdot-}$), as

revealed by MitoSox fluorescent puncta number per cell **(D).** Error bars, mean ± SEM from four independent differentiations. (ns: non-significant; Unpaired t test). **(E)** Oxygen consumption rates (OCRs) in iPSC- DA neuronal cultures treated with DMSO or MLi-2 (100 nM) for 48 h were measured on an XF24 Analyzer. Normalised OCR profiles (% OCR to Basal OCR) for control and *LRRK2-R1441C* iPSC-DA neuronal cultures. **(F)** Maximal Respiration was calculated as measurements after FCCP injection, normalised from OCR %, and fold change from DMSO treated controls was quantified to assess MLi-2 effect. **(G)** Spare Capacity was calculated as the difference between Maximal and Basal respiration, normalised from OCR %, and fold change from DMSO treated controls was quantified to assess MLi-2 effect. Data points represent genotype lines, averaged by number of differentiations. Error bars: mean ± SEM from three independent differentiations (ns: non-significant; ∗P <0.05; two-way ANOVA). Panel C was cultured and assayed by Dr. Matthew Williamson. Data from Panels A, B and D were analysed, and graphs generated by Marta Madureira. Panels E-G were performed by Marta Madureira.

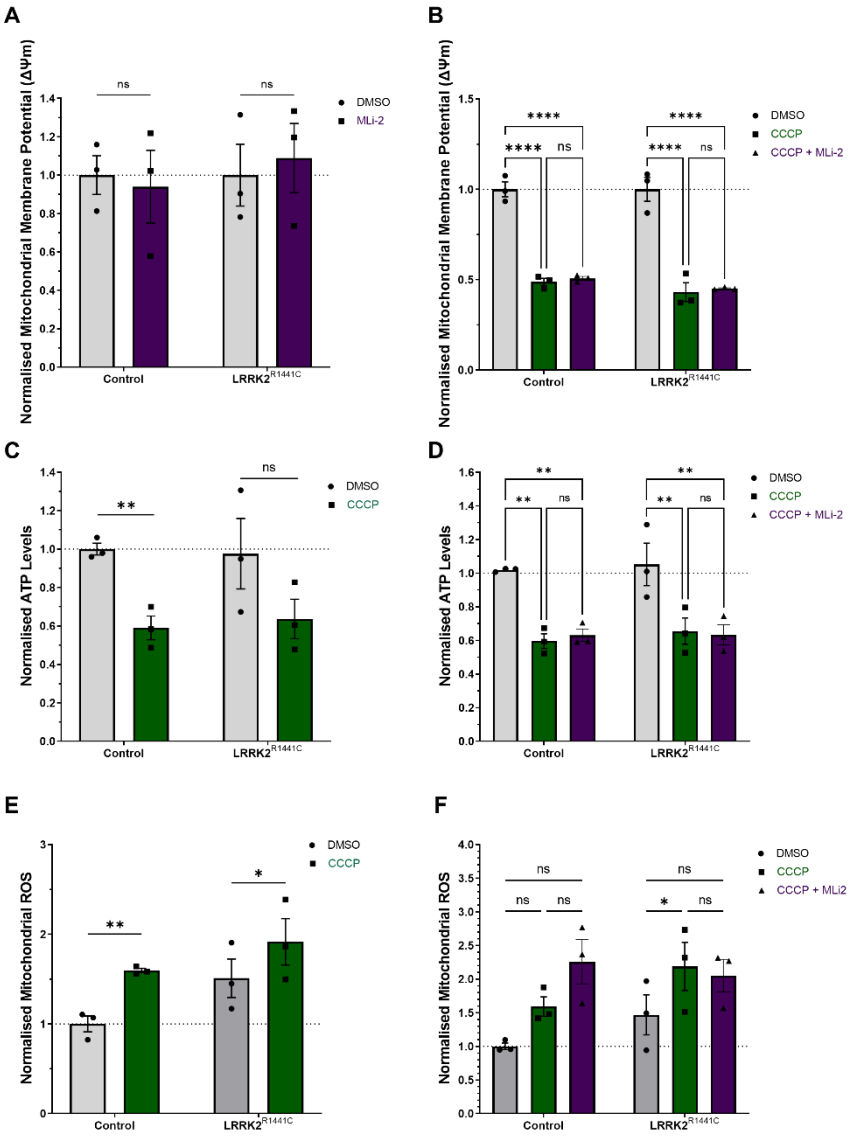

Figure 5.10 – Live cell mitochondrial assays in patient iPSC-DA neuronal cultures carrying the LRRK2-R1441C mutation. To assess the effects of LRRK2 kinase inhibition on mitochondrial membrane potential, iPSC-DA neuronal cultures from control and *LRRK2-R1441C* patient lines were treated with MLi-2 (100 nM) for 48 h prior to JC-10 assay **(A)** or treated with 10 µM CCCP for 6 hours and treated with MLi-2 (100 nM) for 48 h prior to JC-10 assay **(B)**. The fold change from the DMSO treatment of each genotype was quantified. Data points represent genotype lines, averaged by number of differentiations. Error bars: mean ± SEM from two and four independent differentiations, respectively (ns: non-significant; ∗P <0.05; ∗∗P <0.01; ∗∗∗P <0.001; ∗∗∗∗P <0.0001; Multiple t test, Bonferroni post hoc, two-way ANOVA). ATP production was measured using a luminescence assay and compared between control and *LRRK2-R1441C* patient iPSC-DA neuronal cultures, as fold change from basal (DMSO) after treatment with 10 µM CCCP for 6 hours **(C)** or with 10 µM CCCP for 6 hours MLi-2 (100 nM) for 48 h prior to assay **(D)**. Data points represent

genotype lines, averaged by number of differentiations. Error bars: mean ± SEM from three independent differentiations. (ns: non-significant; ∗P <0.05; Multiple t test, Bonferroni post hoc, two-way ANOVA). Oxidative stress was measured as abundance of mitochondrial ROS superoxide anion ($O_2^{\cdot-}$), as revealed by MitoSox fluorescent puncta fold change after treatment with 10 µM CCCP for 6 hours **(E)** or with 10 µM CCCP for 6 hours MLi-2 (100 nM) for 48 h prior to assay **(F)** prior to assay**.** Data points represent genotype lines, averaged by number of differentiations. Error bars: mean ± SEM from four and three independent differentiations, respectively. (ns: non-significant; ∗P <0.05; ∗∗P <0.01; Multiple t test, Bonferroni post hoc, two-way ANOVA). Cells cultured and assayed by Dr. Matthew Williamson. Data analysed and graphs generated by Marta Madureira.

To understand the effect of LRRK2 kinase activity on cellular response to mitochondrial stress, cultures were treated with the LRRK2 kinase inhibitor MLi-2 for 48 h, prior to depolarisation with CCCP. Both control and *LRRK2-R1441C* iPSC-DA neuronal cultures treated with CCCP for 6 h showed a significant decrease in mitochondrial membrane potential, as expected. Furthermore, MLi-2 treatment was not able to rescue mitochondrial membrane potential in control and *LRRK2-R1441C* iPSC-DA neuronal cultures after CCCP-induced depolarisation (Fig. 5.10 B). Similarly, LRRK2 kinase inhibition was unable to rescue CCCP-induced decreases in ATP levels (Fig. 5.10 C-D) or increased mitochondrial ROS production (Fig. 5.10 E-F), regardless of genotype. Thus, MLi-2 treatment was not able to rescue mitochondrial health in CCCP-induced depolarising conditions.

Next, it was investigated if the observed changes in mitochondrial membrane potential were associated with impaired cellular oxygen consumption and glycolysis in iPSC-DA neuronal cultures. Basal oxygen consumption rate (OCR) was not significantly changed in *LRRK2-R1441C* iPSC-DA neuronal cultures (P = 0.3084) (Fig. 5.11 A). To assess the relative changes in cellular oxygen consumption in each line, OCR rates were calculated relative to the basal respiration rates (Fig. 5.9 E, Fig. 5.11 B-C). Maximal respiration was decreased by approximately 20%, with spare capacity reduced by 25% in *LRRK2-R1441C* iPSC-DA neuronal cultures, when compared to control cells (P = 0.0333 and 0.0385, respectively) (Fig. 5.9 F, Fig. 5.9 G). MLi-2 treatment significantly increased maximal respiration (P = 0.0139) and showed a non-significant increase in spare capacity (P = 0.0619) in *LRRK2-R1441C* iPSC-DA neuronal cultures, which suggests a partial rescue of mitochondrial function (Fig. 5.9 F, Fig. 5.9 G). Measuring extracellular acidification rate (ECAR) to evaluate glycolysis showed no differences between genotypes (Fig. 5.11 D-F). Investigating mitochondrial health in *LRRK2-G2019S* iPSC-DA neuronal cultures showed no significant

differences in mitochondrial membrane potential (ΔΨm) under basal conditions (P = 0. 0.4017), with no change in basal ATP levels or mitochondrial ROS production (Fig. 5.12). Assay specificity was confirmed with CCCP-induced decreases in mitochondrial membrane potential and ATP levels in all cultures, compared to DMSO treated iPSC-DAn (Fig. 5.12 B-C).

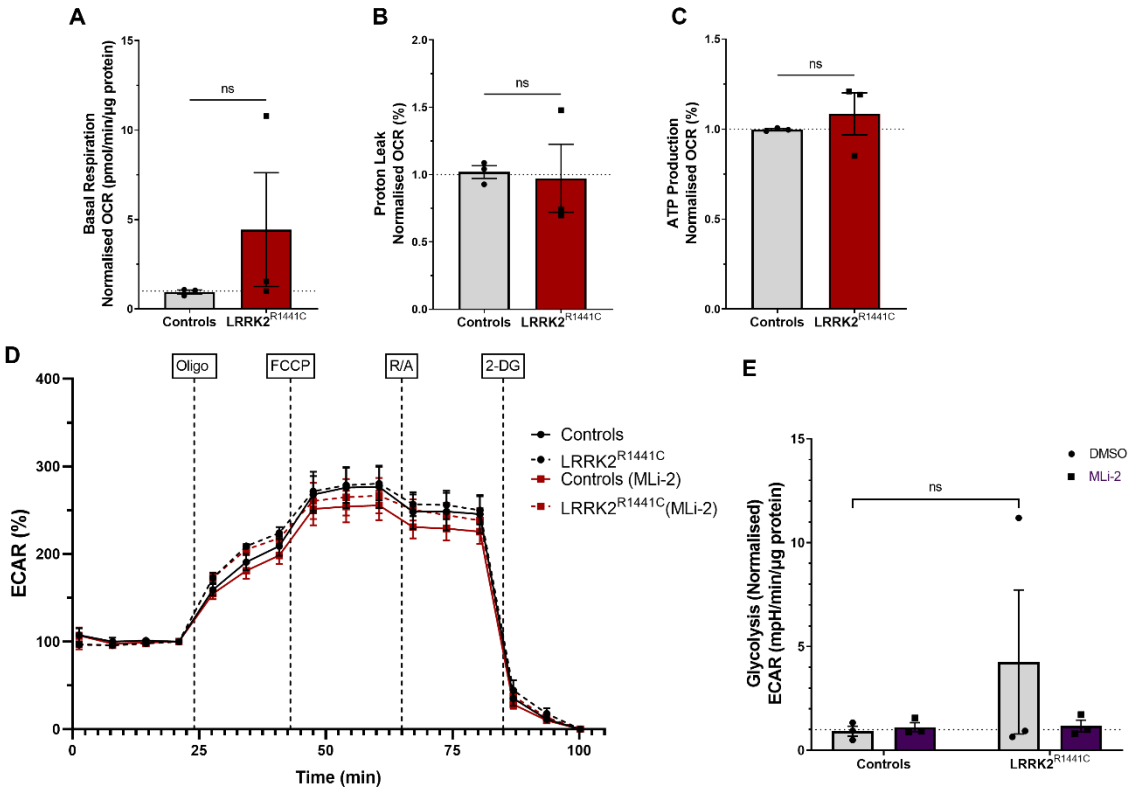

Figure 5.11 – Measuring oxygen consumption and extracellular acidification rates in iPSC-DA neuronal cultures. Oxygen consumption rates (OCRs) in iPSC-DA neuronal cultures were measured on an XF24 Analyzer. Oxygen consumption profiles (pmol O_2/min/µg of protein) are represented for controls and *LRRK2-R1441C* iPSC-DA neuronal cultures. **(A)** Basal respiration was calculated as measurements before oligomycin injection, for controls and *LRRK2-R1441C* iPSC-DA neuronal cultures (pmol O_2/min/µg protein). After normalisation to % of Basal OCR, Proton leak, ATP linked to oxygen consumption, maximal respiration and spare capacity were calculated. **(B)** Proton leak was calculated as the measurements after oligomycin injection **(C)** ATP production linked to oxygen consumption was calculated as the measurements after oligomycin injection and measurement of basal respiration. Data points represent genotype lines, averaged by number of differentiations. Bars, mean ± SEM from three independent differentiations (ns: non-significant; ∗P <0.05; Unpaired t test). **(D)** Extracellular acidification rates (ECARs) in iPSC-DA cultures were

measured on an XF24 Analyzer. Normalised Extracellular acidification profiles (% ECAR to Basal ECAR) are represented for control and *LRRK2-R1441C* iPSC-DA neuronal cultures. **(E)** Normalised ECAR was calculated for control and *LRRK2-R1441C* iPSC-DA cultures. Control and *LRRK2-R1441C* iPSC-DA neuronal cultures were treated with MLi-2 (100 nM) for 48 h and normalised ECAR were calculated. Data points represent genotype lines, averaged by number of differentiations. Error bars: mean ± SEM from two independent differentiations (ns: non-significant; ∗P <0.05; Unpaired t test).

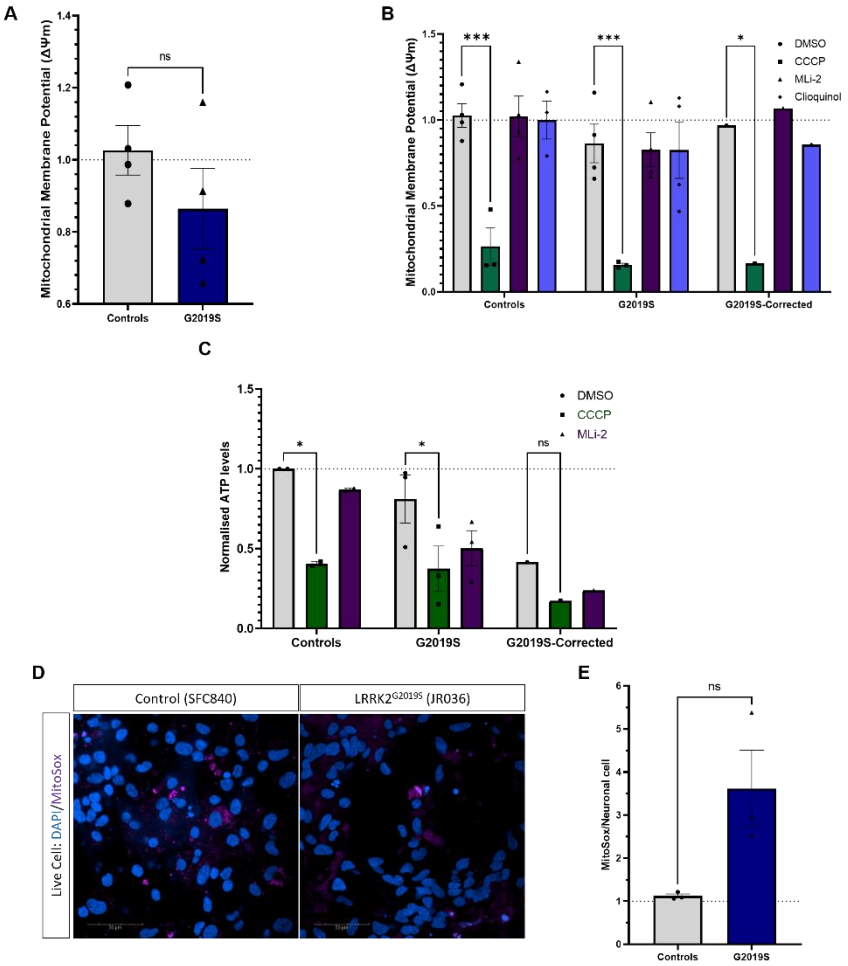

Figure 5.12 – Mitochondrial health assessment in LRRK2-G2019S iPSC-DA cultures. iPSC-derived dopaminergic cultures from Controls and *LRRK2-G2019S* patient lines were generated to assess **(A)** mitochondrial membrane potential changes measured with JC-10 and treatment with CCCP, MLi-2 and Clioquinol was assessed as fold change to DMSO **(B)**. **(C)** ATP Production measured using a luminescent assay and normalised to number of nuclei. Treatment with CCCP and MLi-2 was assessed as fold change to DMSO. **(D)** Oxidative stress was measured as abundance of mitochondrial ROS superoxide anion ($O_2^{\cdot -}$), as revealed by MitoSox fluorescent puncta number per cell **(E).** Data points represent genotype lines, averaged by number of differentiations. Bars, mean ± SEM from two

independent differentiations (ns: non-significant or not represented; ∗P <0.05; ∗∗P <0.01; ∗∗∗P <0.001; Unpaired t test).

Expression levels of electron transport chain (ETC) complexes I (NDUFB8), II (SDHB), III (UQCRC2), IV (COX II) and V (ATP5A) were measured in *LRRK2-R1441C* and *LRRK2-G2019S* and compared to controls iPSC-DA neuronal cultures. Consistently with the results obtained with LRRK2 transgenic primary cortical cultures, under basal conditions *LRRK2* dopaminergic neuronal cultures show no significant difference in ETC protein expression levels, compared to healthy controls (Fig. 5.13). Interestingly, clioquinol treatment induced a significant increase in UQCRC2 (Complex I) protein expression levels in *LRRK2-R1441C* iPSC-DAn as well as in COX II (Complex IV) and ATP5A (Complex V) levels in *LRRK2-G2019S* Corrected iPSC-DAn, compared to each genotypes untreated cultures (Fig. 5.13 B, Fig. 5.13 E-F). Using immunoblotting to assess expression of mitochondrial markers MFN2, OPA1, ubiquitinated OPA1 and TOM20 as well as initiation of autophagy marker p62 under basal conditions, there were no significant differences between *LRRK2* iPSC-derived dopaminergic neuronal cultures and healthy controls (Fig. 5.14). It is noteworthy to mention MFN2 expression levels in *LRRK2-R1441C* iPSC-DAn under basal conditions seem to be increased, albeit non-significantly, when compared to healthy controls. Thus, DMSO-, MLi-2- and clioquinol-induced effects were observed in these cultures, when compared to untreated *LRRK2-R1441C* iPSC derived dopaminergic cultures, but no differences were found when compared to genotype DMSO treated (Fig. 5.14 B).

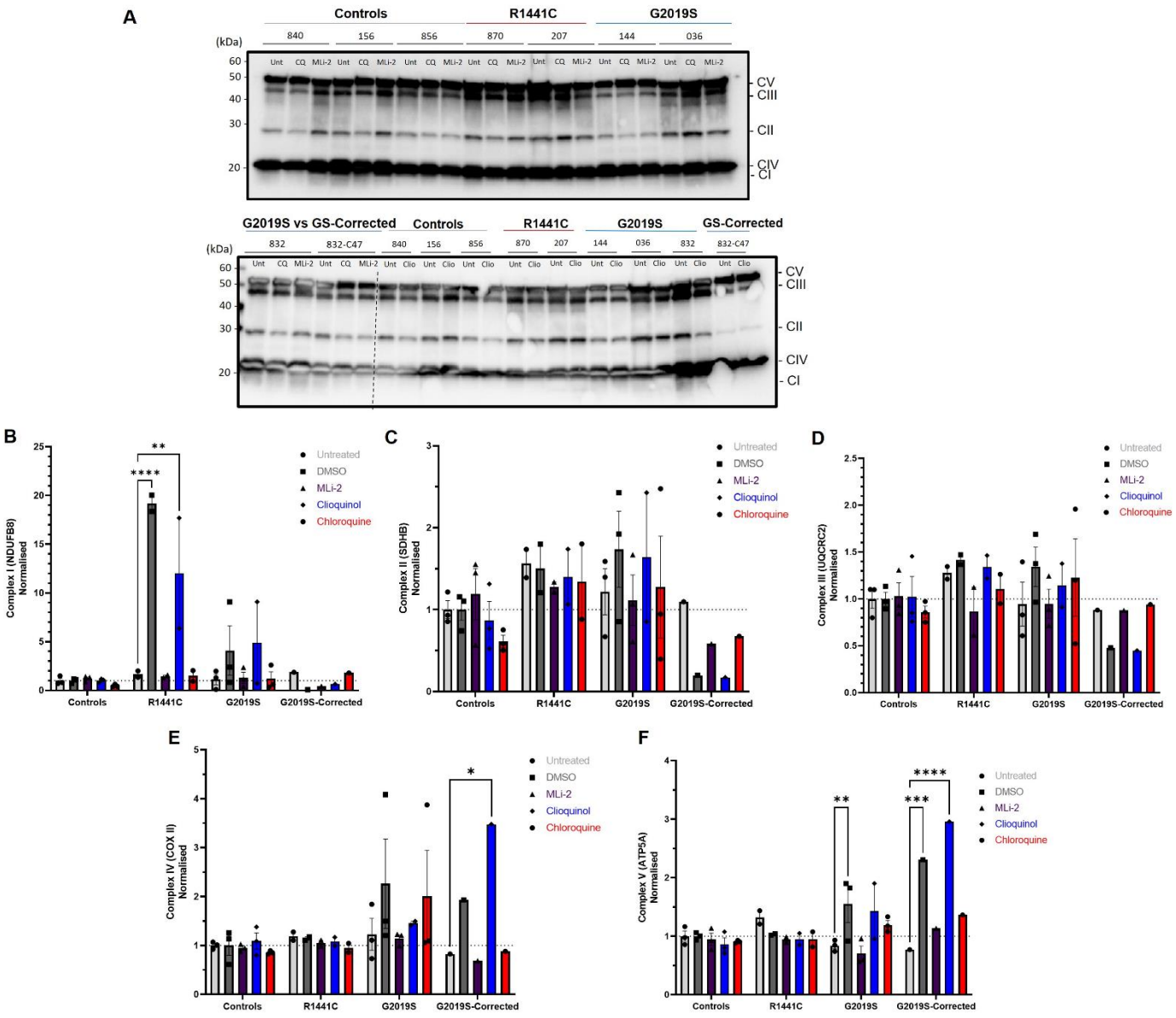

Figure 5.13 – Mitochondrial OxPhos complexes expression in LRRK2 iPSC-DA cultures. iPSC-derived dopaminergic cultures from Controls, *LRRK2-R1441C* and *LRRK2-G2019S* patient lines were generated, treated with Chloroquine (CQ), MLi-2 and Clioquinol (Clio) prior to assays at DIV 35. Lysates were collected and immunoblotted using the OxPhos Human Western Blot Antibody Cocktail (ThermoFischer) for OxPhos **(B)** Complex I (NDUFB8), **(C)** Complex II (SDHB), **(D)** Complex III (UQCRC2), **(E)** Complex IV (COX II), **(F)** Complex V (ATP5A). Chloroquine (CQ), MLi-2 and Clioquinol (Clio) effect was assessed as the fold change to either Untreated (Unt.) or DMSO measurements. Respective OxPhos band intensities were normalised to average of control lines and compared between genotypes. Data points represent genotype lines, averaged by number of differentiations.

Bars, mean ± SEM from two independent differentiations (ns: non-significant or not represented; ∗P <0.05; ∗∗P <0.01; ∗∗∗P <0.001; ∗∗∗∗P <0.0001; Unpaired t test).

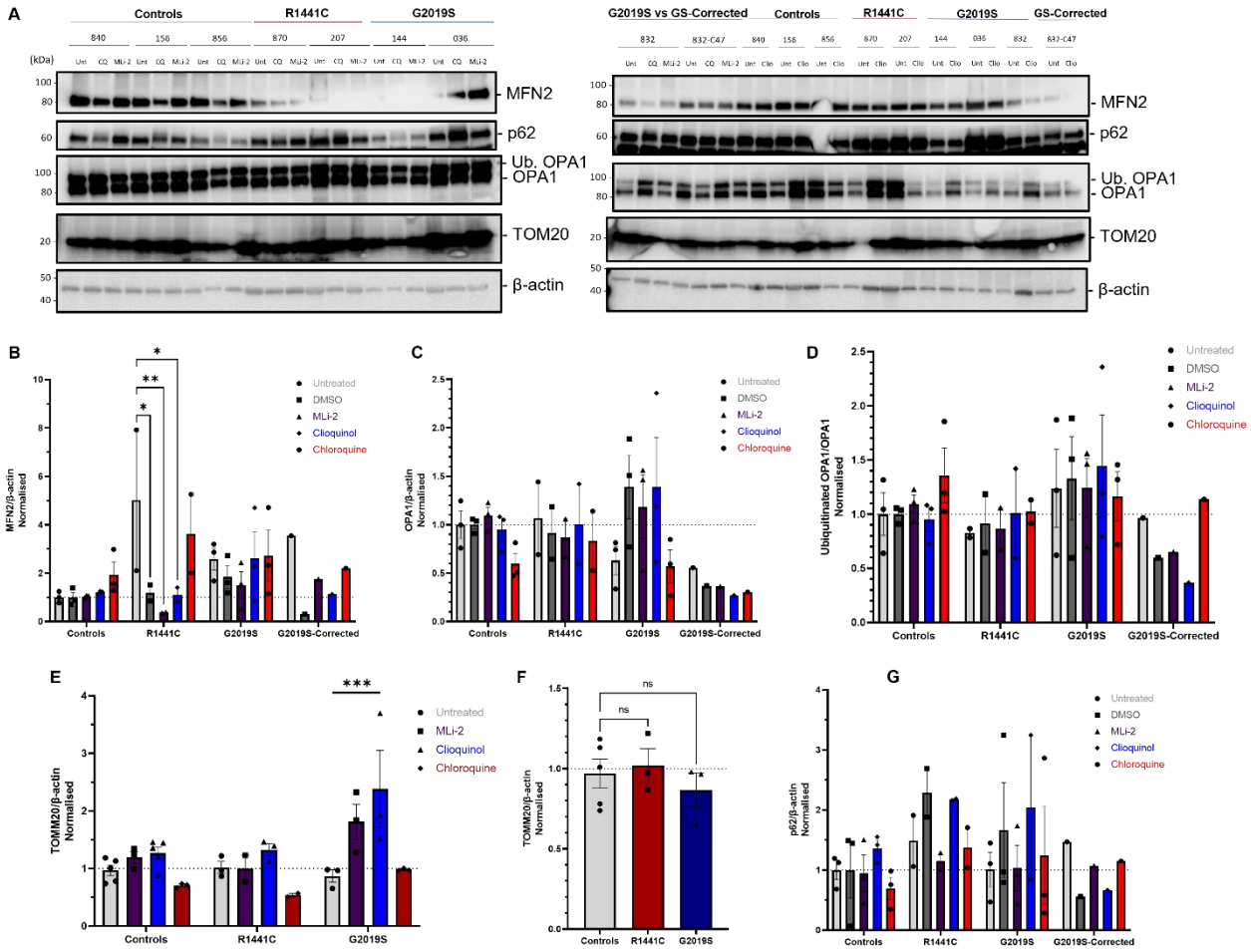

Figure 5.14 – Mitochondrial marker expression in iPSC-DA cultures. iPSC-derived dopaminergic cultures from Controls, *LRRK2-R1441C* and *LRRK2-G2019S* patient lines were generated, treated with Chloroquine (CQ), MLi-2 and Clioquinol (Clio) prior to assays at DIV 35. **(A)** Lysates were collected and immunoblotted for mitochondrial marker TOM20, mitochondrial fission and fusion markers Mitofusion (MFN2) and Optic Atrophy-1 (OPA1) and phagophore marker p62. Respective OxPhos band intensities were normalised to β-actin, averaged to controls and compared between genotypes. Chloroquine (CQ), MLi-2 and Clioquinol (Clio) effect was assessed as the fold change to either Untreated (Unt.) or DMSO measurements. Data points represent genotype lines, averaged by number of differentiations. Bars, mean ± SEM from two independent differentiations (ns: non-significant or not represented; ∗P <0.05; ∗∗P <0.01; ∗∗∗P <0.001; Unpaired t test).

Taken together, these results show subtle changes in the mitochondrial function in patient *LRRK2-R1441C* iPSC-derived DA neurons, including decreased mitochondrial membrane potential, decreased maximal respiration and mitochondrial spare capacity, but not in *LRRK2-G2019S* iPSC-derived dopaminergic cultures.

5.2.3. Levels of PINK1-dependent pS65Ub are decreased in LRRK2-R1441C iPSC-DA neuronal cultures.

To further investigate the effects of the *LRRK2-R1441C* mutation on mitochondria in iPSC-DA neurons and to understand the cell-type specific effects of the mutation, mitochondrial morphology in patient and control iPSC-DA neuronal cultures was assessed by immunostaining for the protein TOM20 under basal conditions. It was observed that mitochondria were significantly smaller, rounder and more fragmented in *LRRK2-R1441C* iPSC-DA neuronal cultures (Fig. 5.15 A-D). Furthermore, it was confirmed CCCP-induced fragmentation and depletion of the mitochondrial network in both control and *LRRK2-R1441C* iPSC-DA neuronal cultures (Fig. 5.16 A-C).

Given these observations of changes in mitochondrial morphology in patient *LRRK2-R1441C* iPSC-DA neuronal cultures, and our observations that *LRRK2-R1441C* primary cortical cultures demonstrated decreased mitophagy initiation through impaired PINK1-dependent pS65Ub levels upon mitochondrial depolarisation (Fig. 5.9), depolarisation-induced pS65Ub was assessed in iPSC-DA neuronal cultures from *LRRK2-R1441C* patients. Co-immunostaining of pS65Ub and TOM20 allowed us to assess the mitochondria labelled for mitophagy in *LRRK2-R1441C* and control iPSC-DA neuronal cultures following mitochondrial depolarisation (Fig. 5.15 E). Whilst CCCP induced a large increase in both the number of pS65Ub spots and pS65Ub spot area in iPSC-DA neuronal cultures (Controls: $P = 0.0002$ and $P < 0.0001$; *LRRK2-R1441C*: $P = 0.0025$ and $P = 0.0002$, for pS65Ub spot number and area respectively) (Fig. 5.15 F, Fig. 5.15 H), the fold induction of pS65Ub after depolarisation was decreased in *LRRK2-R1441C* iPSC-DA neuronal cultures ($P = 0.0132$ and $P = 0.0020$ for spot number and area, respectively) (Fig. 5.15 G, Fig. 5.15 I). These deficits in pS65Ub induction in *LRRK2-R1441C* neurons were not rescued by LRRK2 kinase inhibition by MLi-2 (Fig. 5.16 D-E). Consistent with our observations in primary cortical cultures, these data indicate that the activation of PINK1-dependent mitophagy marker pS65Ub is impaired in *LRRK2-R1441C* neurons, independent of LRRK2 kinase activity.

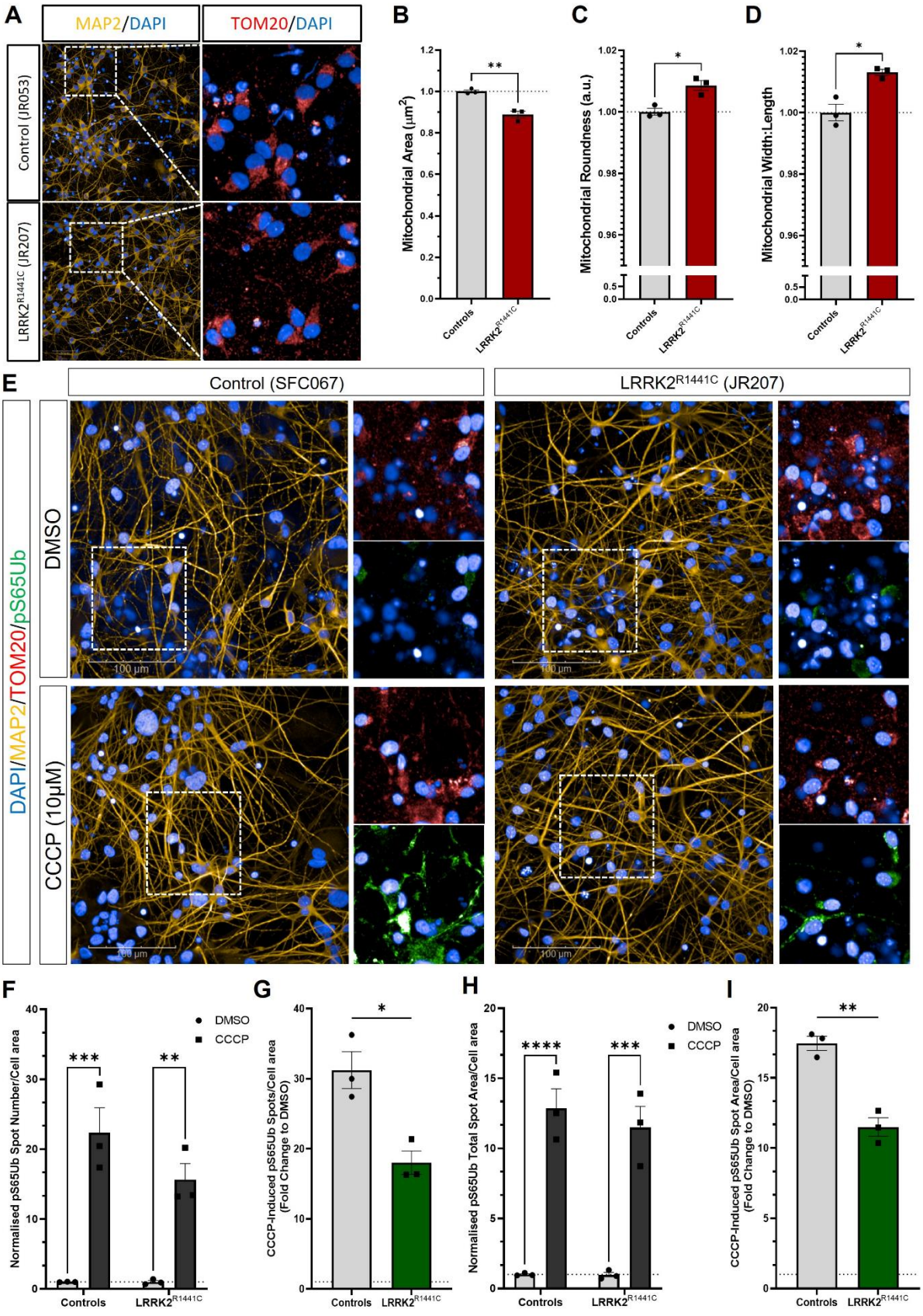

Figure 5.15 – PINK1-dependent pS65Ub formation is impaired in patient iPSC-DA neuronal cultures carrying the LRRK2-R1441C mutation. iPSC-DA neuronal cultures

from control and *LRRK2-R1441C* patient lines were fixed, stained for MAP2, pS65Ub and TOM20. **(A)** TOM20 puncta were identified per neuronal area (MAP2^{+}) and measured to assess mitochondrial morphology in control and *LRRK2-R1441C* iPSC-DA neuronal cultures. The measurements for mitochondrial area (μm^{2}) **(B)**, mitochondrial roundness **(C),** and mitochondrial width to length **(D)** were compared between genotypes. Data points represent genotype lines, averaged by number of differentiations. Error bars: mean ± SEM from five independent differentiations (ns: non-significant; ∗P <0.05; ∗∗P <0.01; Unpaired t test). **(E)** pS65Ub puncta were quantified as fold change from basal (DMSO) after treatment with 10 μM CCCP for 6 hours and total spot number **(F)**, and total spot area **(H)** were measured per neuronal area (MAP2^{+}) and compared between genotypes. (ns: non-significant; ∗P <0.05; ∗∗P <0.01; ∗∗∗P <0.001; ∗∗∗∗P <0.0001; two-way ANOVA). CCCP-induced pS65Ub total spot number **(G)** and total spot area **(I)** fold change to DMSO was measured and compared between genotypes. Data points represent genotype lines, averaged by number of differentiations. Bars, mean ± SEM from three independent differentiations (ns: non-significant; ∗P <0.05; Unpaired t test). Panels A and E were cultured and immunostained by Dr. Matthew Williamson, Rachel Heon-Roberts and Martha Lavelle. Images for Panels A and E composed by Marta Madureira. Data analysed, and all graphs generated by Marta Madureira.

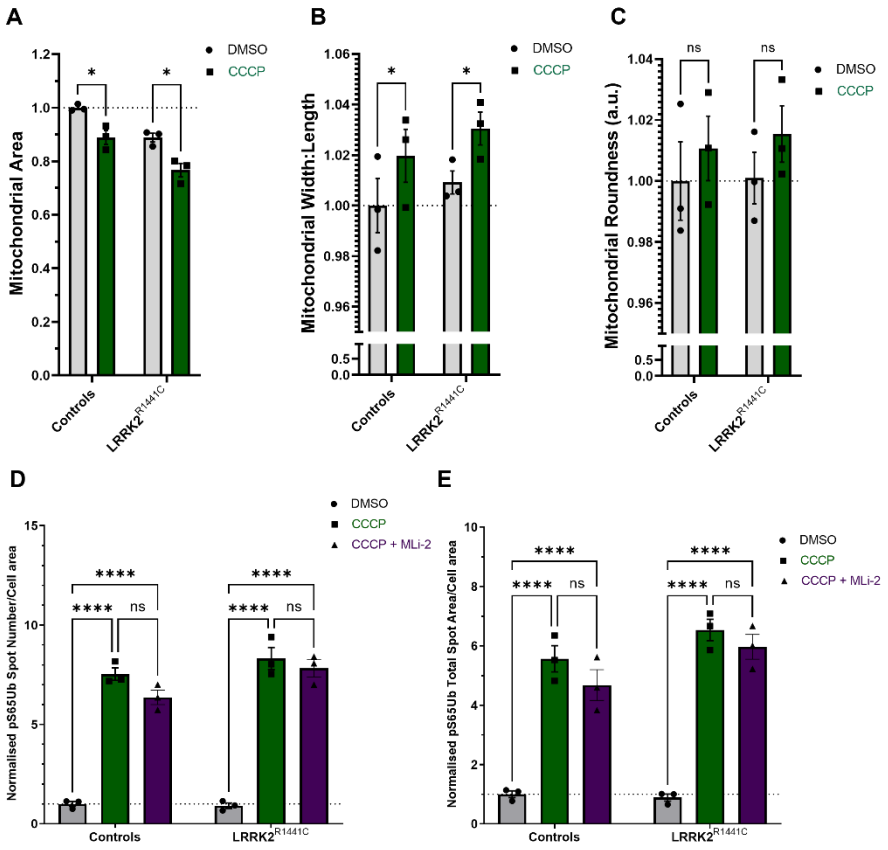

Fig. 5.16 – p65 Ubiquitination levels in iPSC-DA neuronal cultures. To confirm CCCP-induced depolarization effect, cells were fixed, stained for MAP2, pS65Ub and TOM20, and confocal microscopy images acquired. Mitochondrial morphology was assessed by calculating **(A)** mitochondrial area (μm^2), **(B)** roundness and **(C)** mitochondrial width to length, normalised to DMSO treated controls and compared between DMSO and CCCP treatment. To assess the effects of LRRK2 kinase inhibition, control and *LRRK2-R1441C* iPSC-DA neuronal cultures were treated with 10 µM CCCP for 6 hours and treated with MLi-2 (100 nM) for 48 h. Normalised pS65Ub puncta number (to average of controls) was quantified, and total spot number **(D)** and total spot area **(E)** was measured per neuronal area ($MAP2^+$) and compared between genotypes. Data points represent genotype lines, averaged by number of differentiations. Error bars, mean ± SEM from two independent differentiations (ns: non-significant; ∗P <0.05; ∗∗P <0.01; ∗∗∗P <0.001; ∗∗∗∗P <0.0001; two-way ANOVA). Cells used to obtain Panels A-E were cultured by William McGuinness, immunostained and imaged by Rachel Heon-Roberts and Martha Lavelle. Data from Panels A-E were analysed, and graphs generated by Marta Madureira.

5.2.4. MIRO1 degradation is impaired in LRRK2-R1441C iPSC-DA neuronal cultures.

As accumulation of the PINK1-substrate pS65Ub, an early event in mitophagy, was impaired in *LRRK2-R1441C* iPSC-DA neuronal cultures, the molecular mechanism behind this cellular phenotype was assessed. Several mechanisms have been proposed to link LRRK2 and regulation of mitophagy through the impaired degradation of MIRO1 and increased phosphorylation of Rab10 (Hsieh et al. 2016; Wauters et al. 2020). Consistent with the lack of altered kinase activity in *LRRK2-R1441C* iPSC-DA neuronal cultures, no difference in Rab10 phosphorylation was observed following mitochondrial depolarisation (Fig. 5.17). Given the observed impairment in early mitophagy initiation, the role of MIRO1 in depolarisation-induced mitophagy was investigated. This mitophagy regulatory mechanism has been described to rely on LRRK2 and MIRO1 forming a complex after mitochondrial depolarisation, which is independent of LRRK2 kinase-mediated phosphorylation (Hsieh et al. 2016). Under basal conditions, there is no difference in MIRO1 expression, comparing healthy, *LRRK2-R1441C* and *LRRK2-G2019S* iPSC-DA neuronal cultures (Fig. 5.18 A-B). Treatment with MLi-2 and clioquinol did not seem to have any effect, except a clioquinol-induced decrease in MIRO1 expression in *LRRK2-G2019S* iPSC-DA neuronal cultures, compared to untreated (Fig. 5.18 C).

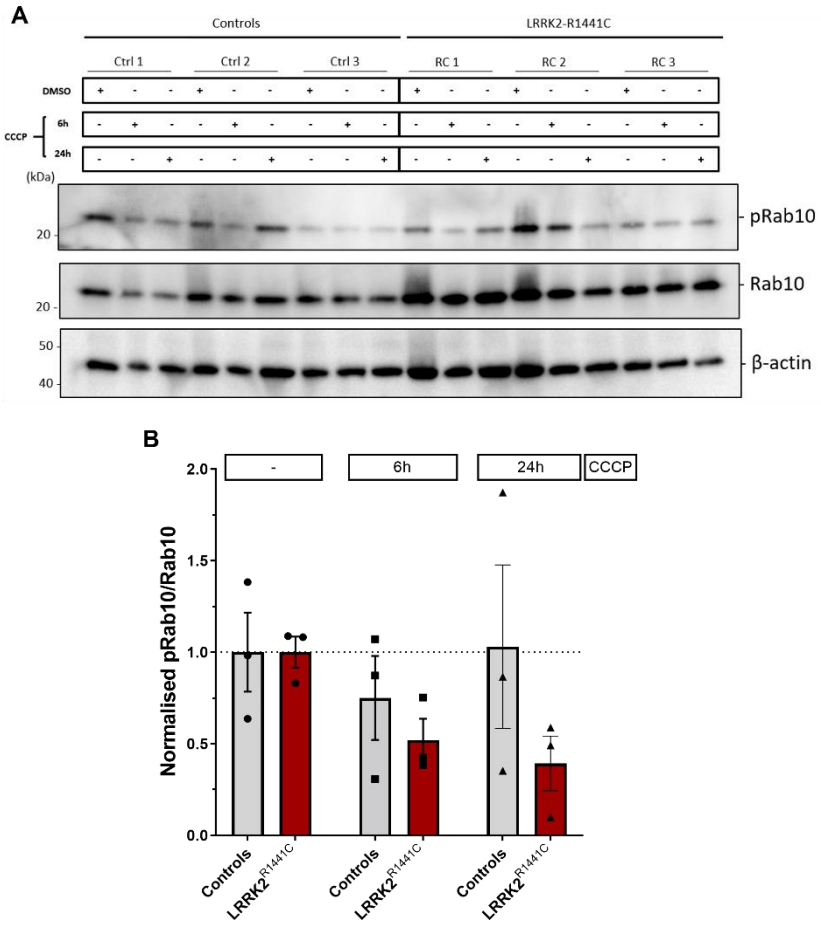

Figure 5.17 – Investigating Phosphorylated Rab10 LRRK2-regulated mitophagy mechanism using iPSC-DA neuronal cultures. Protein lysates were prepared from iPSC-DA neuronal cultures from control and *LRRK2-R1441C* patient lines. Western blots for phosphorylated Rab10 (phospho ST73) and Rab10 expression were quantified to assess pRab10/Rab10 fold change from basal (DMSO) in response to treatment with 10 μM CCCP for 6 h or 24 h **(A, B).** Data points represent genotype lines, averaged by number of differentiations. Bars, mean ± SEM from two independent differentiations (ns: non-significant; ∗P <0.05; ∗∗P <0.01; two-way ANOVA).

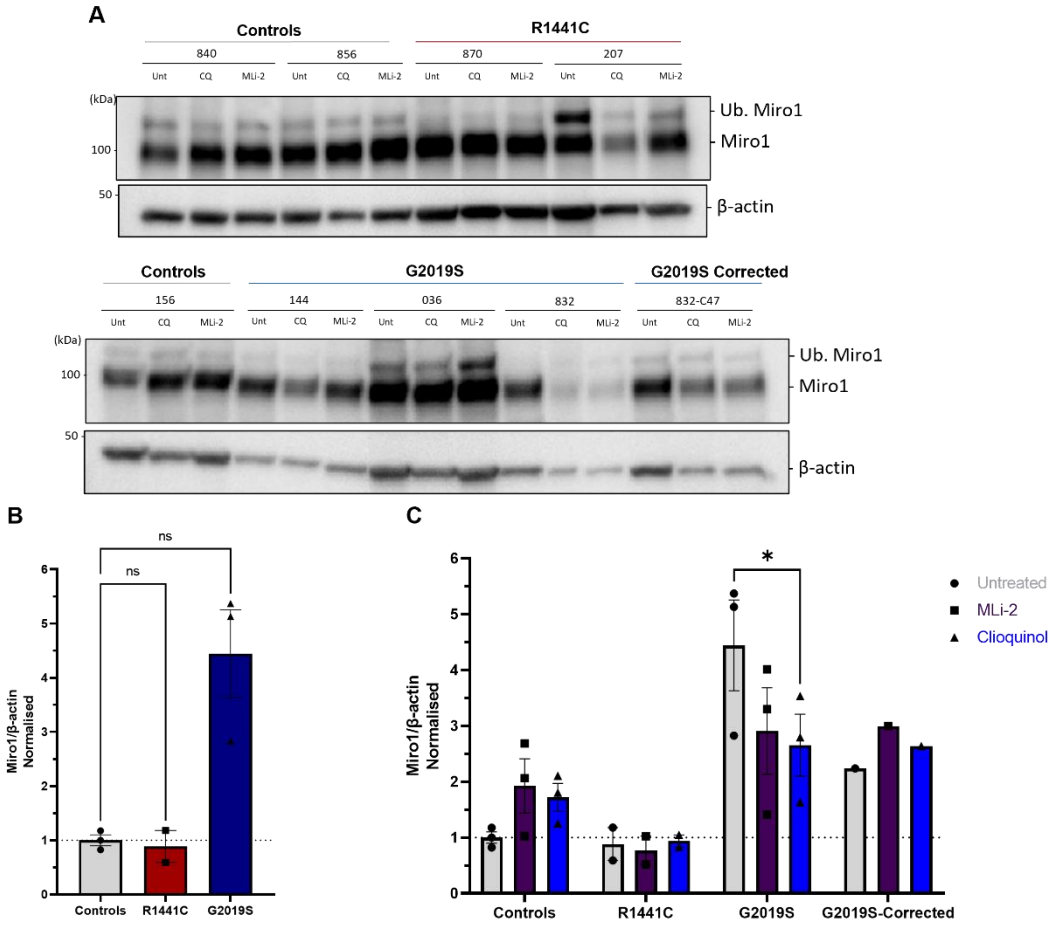

Figure 5.18 – Mitochondrial protein MIRO1 expression in iPSC-DA cultures. iPSC-derived dopaminergic cultures from Controls, *LRRK2-R1441C* and *LRRK2-G2019S* patient lines were generated, treated with Chloroquine (CQ) and LRRK2 kinase inhibitor MLi-2 prior to assays at DIV 35. **(A)** Lysates were collected and immunoblotted for outer mitochondrial membrane protein MIRO1. **(B)** Respective band intensities for MIRO1 were normalised to β-actin, averaged to controls and compared between genotypes. **(C)** Chloroquine (CQ) and MLi-2 effect was assessed as the fold change to Untreated (Unt.) measurements. Data points represent genotype lines, averaged by number of differentiations. Bars, mean ± SEM from two independent differentiations (ns: non-significant or not represented; ∗P <0.05; ∗∗P <0.01; ∗∗∗P <0.001; Unpaired t test).

Consistent with the literature, in the present iPSC-DA neuronal culture model LRRK2 and MIRO1 co-localise within mitochondrial network (TOM20 positive) regions, (Fig. 5.19 A, Fig. 5.20 A-E). However, the percentage of LRRK2-MIRO1 co-localised within mitochondrial regions was not significantly different in *LRRK2-R1441C* iPSC-DA neuronal cultures under basal or CCCP-induced conditions (Fig. 5.19 B), in contrast to previous findings which reported a decreased *LRRK2-G2019S* /MIRO1 interaction (Hsieh et al. 2016). As expected, there was a CCCP-dependent decrease in the number of mitochondria-localised MIRO1 events (spot number) by immunocytochemistry in both control and *LRRK2-R1441C* iPSC-DAn (Fig. 5.19 C-E). Importantly, no differences in MIRO1 spots not co-localised with mitochondrial marker TOM20 upon CCCP-induced depolarisation were observed (Fig. 5.20 A, F-G). Moreover, LRRK2 spots in mitochondria show no differences between genotypes or CCCP-treated conditions (Fig. 5.20 H-I).

To further understand the effect of *LRRK2-R1441C* on MIRO1 degradation, iPSC-DA neuronal cultures were treated with CCCP for 6 hours and 24 hours to induce mitochondrial depolarisation and assessed levels of MIRO1 and MIRO1 ubiquitination in iPSC-DA lysates. In agreement with our results from immunocytochemistry, control iPSC-DA neuronal cultures exhibited decreased levels of MIRO1 expression after 24 h of treatment (Fig. 5.19 F, Fig. 5.19 G). However, the decrease in MIRO1 expression was impaired in *LRRK2-R1441C* iPSC-DA neuronal cultures ($P = 0.0441$), demonstrating MIRO1 removal from depolarised mitochondria is impaired in mutant *LRRK2-R1441C* cells (Fig. 5.19 G). Moreover, as the ubiquitination of MIRO1 is necessary for its degradation (Safiulina et al., 2019), ubiquitinated MIRO1 was also quantified. Consistent with the impaired degradation of MIRO1, a decreased proportion of MIRO1 was found to be ubiquitinated in *LRRK2-R1441C* iPSC-DA neuronal cultures 24 h after CCCP treatment compared to control ($P = 0.0311$) (Fig. 5.19 H).

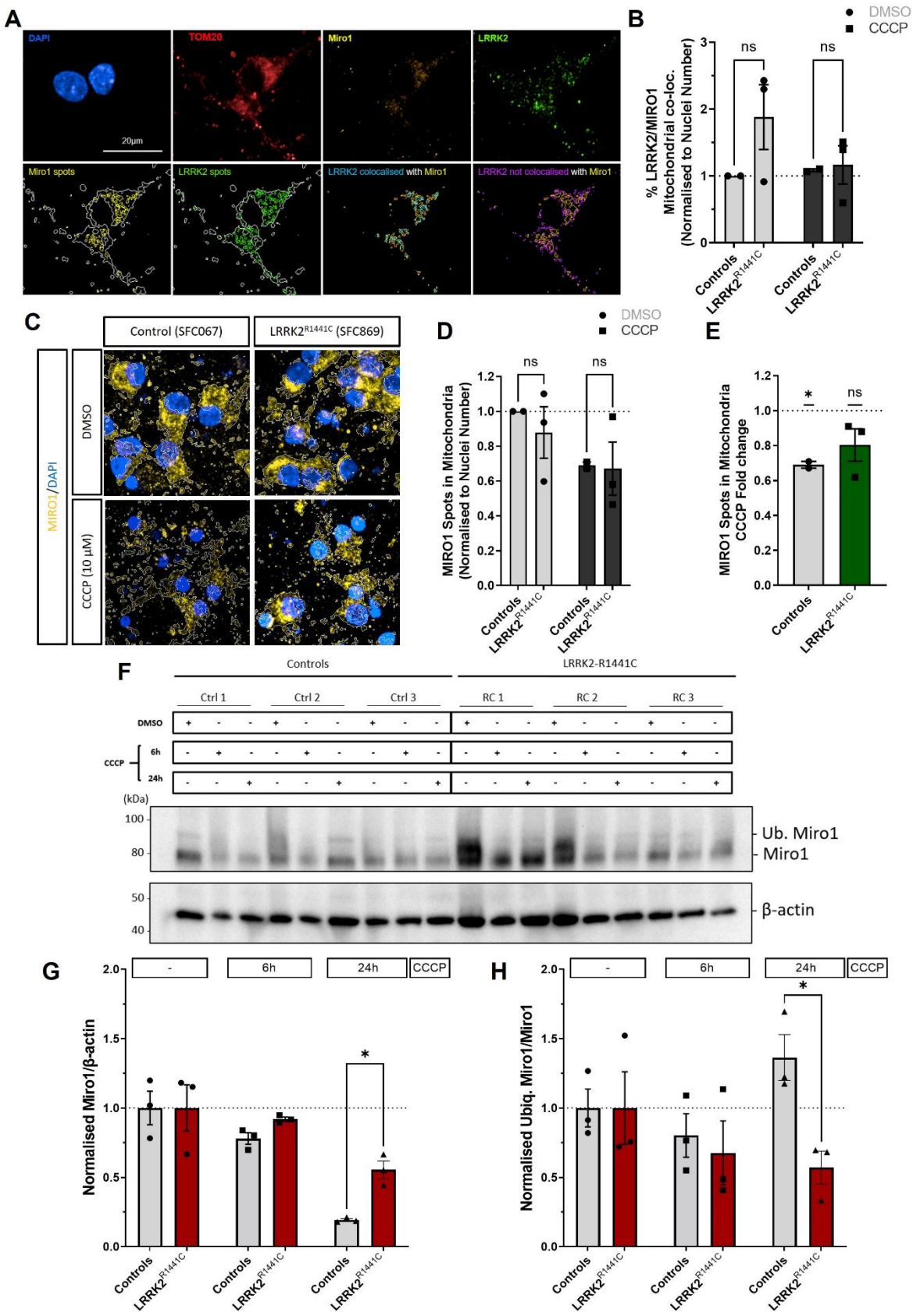

Figure 5.19 – The LRRK2-R1441C mutation impairs MIRO1 degradation. **(A)** To investigate interaction of LRRK2 and MIRO1 at mitochondria LRRK2 and MIRO1 were co-immunostained under basal conditions in *LRRK2-R1441C* and control iPSC-DA neuronal

cultures. An example from control iPSC-DA neurons (SFC067) illustrates MIRO1 and LRRK2 co-localisation within mitochondria (TOM20) and shows that the analysis pipeline identifies mitochondrial staining (TOM20) as the region of interest, then finds total MIRO1 spots within mitochondrial regions (yellow spots within white border), and total LRRK2 spots within mitochondrial regions (green spots within white border). Finally, the pipeline identifies all LRRK2 spots co-localised with MIRO1 within mitochondrial regions (cyan blue spots) and all the LRRK2 spots not co-localised with MIRO1 within mitochondrial regions (purple spots). **(B)** Quantification of the LRRK2 spots co-localised with MIRO1 within mitochondrial regions, as a percentage of all LRRK2 spots, normalised to the number of nuclei per well. **(C)** MIRO1 spots within mitochondrial regions, defined by TOM20 staining (yellow spots within white border) from *LRRK2-R1441C* and control iPSC-DA neuronal cultures. **(D)** Quantification of MIRO1 spots within mitochondria, with DMSO and CCCP treatment, normalised to the number of nuclei per well, compared to DMSO control levels. **(E)** CCCP-fold change compared between controls and *LRRK2-R1441C* iPSC-DA neuronal cultures. Protein lysates of iPSC-DA neuronal cultures from *LRRK2-R1441C* patient and control lines after 6 or 24 h treatment with 10 μM CCCP were quantified by western blot to assess changes in **(F, G)** MIRO1 and **(F, H)** ubiquitinated MIRO1 levels. Data points represent fold change in protein levels after CCCP treatment per line, averaged by number of differentiations. Error bars: mean ± SEM from two independent differentiations (ns: non-significant; ∗P <0.05; two-way ANOVA). Data points represent genotype lines, averaged by number of differentiations. Bars, mean ± SEM from two independent differentiations (ns: non-significant; ∗P <0.05; two-way ANOVA; Unpaired t test). Panels A and C were stained and assayed by Dr. Matthew Williamson and Rachael Heon-Roberts. Data from Panels B, D, E were analysed, and graphs generated by Marta Madureira. Panels F-H performed by Marta Madureira.

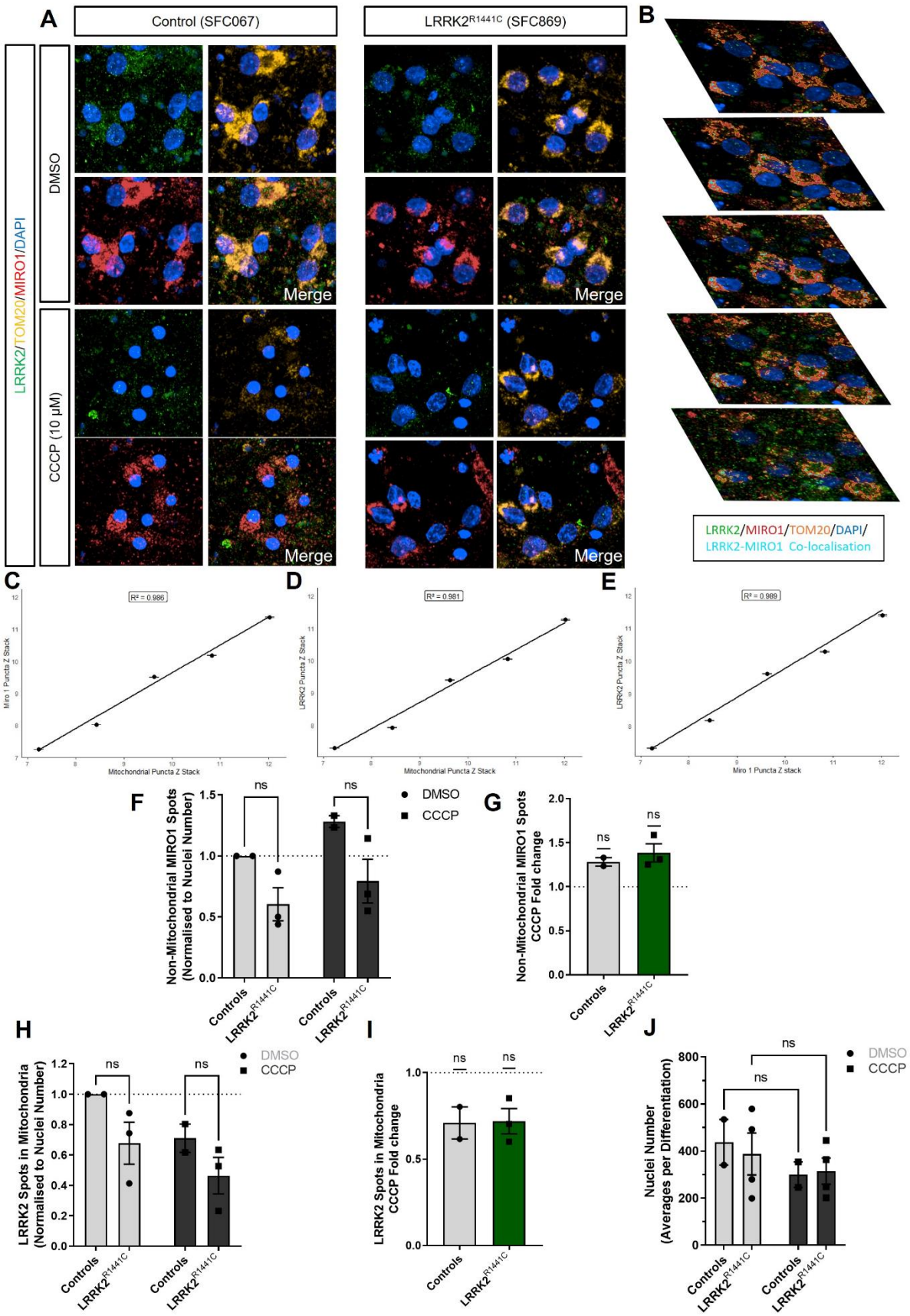

***Figure 5.20 – iPSC-DA neuronal culture expression of LRRK2/MIRO1 and TOM20*. (A)** iPSC-DA neuronal cultures from control and *LRRK2-R1441C* patient lines were treated with

DMSO or CCCP (24 h, 10 μM) then fixed, stained for LRRK2, TOM20 and MIRO1. **(B)** Example Z-stack profile of MIRO1-LRRK2-TOM20 co-localisation in control lines showing individual planes (LRRK2, green; MIRO1, red; co-localisation, cyan). **(C-E)** Correlation plot showing the brightest z-plane in co-immunofluorescence images for **(C)** MIRO1-TOM20, **(D)** LRRK2-TOM20 and **(E)** MIRO1-LRRK2. The plots demonstrate that the highest fluorescence intensity for each marker pair generally occur in the same plane. **(F)** Quantification of MIRO1 spots localised outside of mitochondrial regions, defined by TOM20 staining from *LRRK2-R1441C* and control iPSC-DA neuronal cultures, treated with DMSO and CCCP, normalised to each well nuclei number, compared to DMSO Control levels and **(G)** CCCP-fold change compared between controls and *LRRK2-R1441C* iPSC-DA neuronal cultures. **(H)** Quantification of LRRK2 spots within Mitochondria, with DMSO and CCCP treatment, normalised to each well nuclei number, compared to DMSO Control levels and **(I)** CCCP-fold change compared between controls and *LRRK2-R1441C* iPSC-DA neuronal cultures. **(J)** Nuclei number (DAPI), averaged per differentiation from *LRRK2-R1441C* and control iPSC-DA neuronal cultures, treated with DMSO and CCCP. Data points represent genotype lines, averaged by number of differentiations. Bars, mean ± SEM from two independent differentiations (ns: non-significant; two-way ANOVA; Unpaired t test). Panels A-E were cultured by William McGuinness, stained by Rachael Heon-Roberts, devised and assayed by Dr. Brent Ryan. Panels A-E composed by Dr. Brent Ryan. Panels F-J generated and analysed by Marta Madureira.

Overall, *LRRK2-R1441C* iPSC-DA neuronal cultures exhibit altered mitochondrial morphology and mitochondrial dysfunction. These deficits may be driven, in part, by impairments in the clearance of damaged mitochondria due to impaired PINK1-dependent pS65Ub accumulation and impaired degradation of MIRO1 found in a complex with LRRK2 after mitochondrial depolarisation.

5.2.5. Comparing LRRK2-R1441C patient lines reveals differences in mitochondrial health and mitophagy in iPSC-DA neuronal cultures.

iPSC-derived cellular models reflect the inherent variability between donors, making it essential to include lines from multiple patients in any study. To study the variability observed between iPSC-DA neuronal cultures derived from the three different *LRRK2-R1441C* patient lines in some assays of mitochondrial health and mitophagy, we calculated the corresponding Z-scores per patient line for the altered mitochondrial phenotypes observed (Fig. 5.21). Reassuringly, we found consistent observations across phenotypes *within* each patient line in addition to the consistent phenotypes within LRRK2 genotypes. For example, the iPSC-DA neuronal cultures from *LRRK2-R1441C* patient line SFC869 display the most fragmented mitochondria with the most decreased mitochondrial membrane potential, which corresponds to the highest mitochondrial ROS burden. Conversely, iPSC-DA neuronal cultures from *LRRK2-R1441C* patient JR207 present the least altered mitochondrial network, and the most decreased levels of mitophagy activation among *LRRK2-R1441C* patient lines.

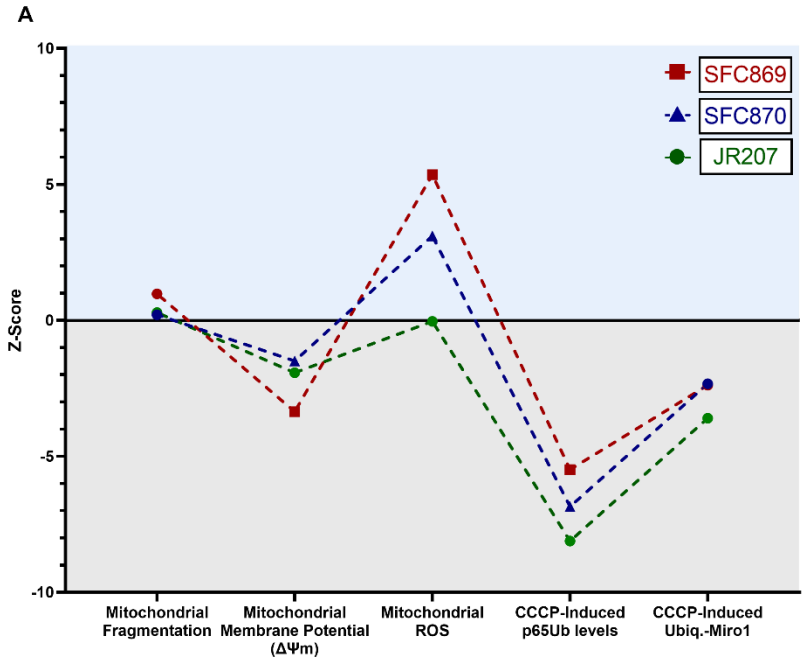

***Figure 5.21 – Heterogeneity in mitochondrial phenotypes among Parkinson's LRRK2-R1441C patient iPSC-DA neuronal cultures*. (A)** Z-scores were calculated for iPSC-DA neuronal cultures derived from each *LRRK2-R1441C* Parkinson's patient line plotted relative to control lines to assess inter-patient variation in mitochondrial membrane potential (ΔΨm), mitochondrial reactive oxygen species (ROS), pS65Ub levels (fold change in total pS65Ub spot area after CCCP treatment) and Ubiquitinated MIRO1 Induction (fold change

in Ubiq.-MIRO1 after CCCP treatment as assessed by immunoblot). Line SFC869 corresponds to patient line SFC869-03-04, SFC870 corresponds to patient line SFC870-03-05 and JR207 corresponds to patient line JR207-03. Panel A was devised by Dr. Brent Ryan, data analysed and composed by Marta Madureira.

5.3. Conclusions

The main conclusions highlighted in this chapter are:

1. *LRRK2-R1441C* primary cortical cultures show decreased mitochondrial membrane potential, increased ROS production and decreased mitophagy levels, but not *LRRK2-G2019S*.
2. *LRRK2-R1441C* iPSC-derived dopaminergic cultures show increased mitochondrial fragmentation, decreased mitochondrial membrane potential, decreased maximal respiration and spare capacity and decreased PINK-1 dependent phosphorylation of p65Ub, a marker of mitophagy initiation.
3. Treatment with LRRK2 kinase inhibitor MLi-2 did not correct mitochondrial phenotypes induced by *LRRK2-R1441C* in patient iPSC-DA.
4. Even though LRRK2 and MIRO1 proteins co-localise within mitochondria, the *LRRK2-R1441C* mutation results in no significant disruption of that interaction in iPSC-DA neuronal cultures.
5. Different *LRRK2-R1441C* patient lines displayed different phenotypic severities in iPSC-DA neuronal cultures.

Chapter 6 – Discussion

6.1. LRRK2 and vATPase-a1 interaction

Chapter 3 aimed to characterise the interaction between LRRK2 and vATPase-a1 in human models and investigate the hypothesis that LRRK2 could play a role in chaperoning a1 subunit within different subcellular compartments, such as ER, Golgi and lysosomes.

Co-transfection of each *LRRK2* construct individually with the *vATPase-a1-WT* construct and subsequent co-immunoprecipitation and western blot analysis revealed a bright band corresponding to a1 was present when pulling-down LRRK2-WT full length and LRRK2-ROC with magnetic beads conjugated to an *anti*-Myc antibody but not for LRR, RCK, COR, Kinase or WD-40 domains. The present data confirms the LRRK2 interaction with vATPase-a1 reported previously using rat primary cultures is not species-specific as it also occurs in the context of human cellular models (Wallings, Connor-Robson, and Wade-Martins 2019). Moreover, this suggests that interaction of LRRK2 with the a1 subunit of vATPase occurs within human cell models at the ROC domain (Fig. 3.6). This would support LRRK2/v0a1 interaction being severely decreased in *LRRK2-R1441C* cortical cultures, but not in *LRRK2-WT* or *LRRK2-G2019S*, since this mutation is located at the ROC domain (Wallings, Connor-Robson, and Wade-Martins 2019). However, vATPase-a1 was co-immunoprecipitated with LRRK2-R1441C, which indicates this mutation did not affect the interaction with vATPase-a1 in co-transfected HEK cells (Fig. 3.8). This difference could reflect a cell-type specific mechanism, characteristic of neuronal and glial cells, or an effect of LRRK2 overexpression in the rodent model. LRRK2/v0a1 interaction was also investigated in *LRRK2* patient iPSC-derived dopaminergic cultures, since this is a highly physiological model for PD. Immunostaining suggests co-localisation of v0a1 occurs with LRRK2 spots in *LRRK2-R1441C* and *LRRK2-G2019S* as well as healthy controls. Co-immunoprecipitation confirmed the interaction between LRRK2 and a1 also occurs in dopaminergic cultures, in both *LRRK2-G2019S* and healthy controls (Fig. 3.23). One caveat of the current experimental work was that the protein lysate obtained was insufficient to carry out the co-immunoprecipitation in *LRRK2-R1441C* iPSC-DA neuronal cultures, and therefore we were unable to confirm whether the LRRK2-R1441C would disrupt the interaction with vATPase-a1, as previously reported in LRRK2-R1441C primary cortical cultures (Wallings, Connor-Robson, and Wade-Martins 2019). This key question would be very interesting to follow up in future studies.

Additionally, there have been reports of co-immunoprecipitation protocols of vATPase-a1 with other proteins, such as PS-1 and VMA21, that are both suggested to be chaperones of a1, driving it from the ER to the lysosome to be fully assembled with V_1 domain (Esmail et al. 2018; Lee et al. 2010). Esmail and colleagues demonstrated the association of a1 subunit with the V-ATPase assembly chaperone VMA21 was dependent on the N-glycosylation of a1 at Asn495 (Esmail et al. 2018). Using immunostainings of transfected HEK cells, it was observed that vATPase-a1-Mut, which cannot be glycosylated at the N495Q site, accumulates in the Golgi and is less present in mitochondria, an organelle downstream of the protein transport pathway (Fig. 3.5). These data corroborate glycosylation of a1 subunit is necessary for the correct trafficking within subcellular locations (Esmail et al. 2018).

Since *LRRK2-R1441C* cortical cultures show abolished LRRK2/v0a1 interaction and correct cellular trafficking of v0a1 subunit is important to full vATPase assembly, it was hypothesised LRRK2 role could be chaperoning a1 subunit in a wider network within the cell, and pathogenic LRRK2 interacting with vATPase-a1 would alter its subcellular localisation. In a recent report, overexpression of *LRRK2-Y1699C*, another pathogenic LRRK2 mutation, in HEK cultures showed lysosomes become clustered in a perinuclear region, but intracellular positioning of early endosomes, ER, Golgi and mitochondria were not affected. Lysosomal localisation was altered in a kinase-dependent manner in overexpressing HEK but not SH-SY5Y cultures, suggesting that the mechanisms determining subcellular lysosomal location are cell type dependent (Ito et al. 2023). In agreement with this, at basal levels it was shown there were no differences in v0a1 spots within ER, Golgi-Apparatus or lysosomal regions in *LRRK2-R1441C* cortical cultures or *LRRK2* iPSC-derived dopaminergic cultures, when compared to respective controls (Fig. 3.13-15, Fig. 3.20-22). Ito and colleagues (2023) also reported increase in the phosphorylation of Rab12 by pathogenic increase of LRRK2-Y1699C kinase activity would compromise intracellular lysosomal transport, via the enhanced interaction of Rab12 with RILPL1. This would be consistent with co-immunoprecipitation of co-transfected HEK cells showing an increase of LRRK2/v0a1 interaction in the presence of kinase dead LRRK2 (Fig. 3.9) (Ito et al. 2023).

Clioquinol, a zinc ionophore used to rescue impaired lysosomal function phenotypes in *LRRK2-R1441C* cortical cultures (Wallings, Connor-Robson, and Wade-Martins 2019), did not show any effects in LRRK2/v0a1 interaction measured by co-immunoprecipitation (Fig. 3.8). Interestingly, clioquinol decreased the presence of vATPase-a1 spots in ER and Golgi-Apparatus regions in *LRRK2-R1441C* primary cortical neurons to levels of non-transgenic

littermates. This evidence could suggest that *LRRK2-R1441C* mutation, which affects the ROC domain of LRRK2, could alter cellular localisation and therefore cellular trafficking of a1 subunit in cortical primary cultures. Clioquinol treatment, which alters lysosome integrity and inhibits the proteasome, had no effect in v0a1 presence in lysosomes themselves, but significantly decreased v0a1 co-localisation in ER and Golgi spots. This perhaps would suggest lysosomes are not the principal destination for a1 subunit being chaperoned by LRRK2 within *LRRK2-R1441C* cortical neurons. Indeed, LRRK2 influences both retrograde and post-Golgi trafficking pathways in a manner dependent on its GTP binding and kinase activity, which was increased in primary astrocytes from *R1441C* knock-in animals compared WT littermates (Beilina et al. 2020). It could also suggest that if LRRK2 plays a role in chaperoning a1 subunit within cells, it would be involved in the earlier steps of a1 protein trafficking, during synthesis in the ER and post-translational modifications in the Golgi-Apparatus. Taken together, these data would suggest that LRRK2 could still be involved in chaperoning a1 subunit within subcellular compartments, and this mechanistic pathway could have other important players not investigated here, such as Rabs. Finally, these datasets would benefit from further experimental work to investigate the role of LRRK2 in cellular trafficking of a1 subunit, as well as further work to characterise a1 co-localisation with ER, Golgi-Apparatus and lysosomal organelles in *LRRK2-WT* and *LRRK2-G2019S* models.

6.2. LRRK2 and Autophagy

This chapter focused on investigating autophagy-lysosomal pathway in LRRK2 models of PD. Measuring proteolytic degradation in rat cortical cultures using DQ-BSA showed increased levels in *LRRK2-R1441C* but no differences in *LRRK2-G2019S* or *LRRK2-WT*, compared to respective nTG littermates. Chloroquine treatment did not sufficiently decrease proteolytic degradation in *LRRK2-R1441C* primary cortical cultures, also indicating a surplus autophagic flux in these cultures (Fig. 4.1). Contrastingly, Wallings and colleagues thoroughly characterised the autophagy and lysosomal pathway in *LRRK2* BAC transgenic rat cortical cultures and reported opposing effects, showing a decrease in lysosomal degradation in *LRRK2-R1441C* but not in *LRRK2-G2019S* or *LRRK2-WT*, compared to respective nTG littermates (Wallings, Connor-Robson, and Wade-Martins 2019). These disparaging results could be due to different assay sensitivities since proteolytic degradation was measured using DQ-BSA assay in the present study whereas Wallings and colleagues used a radiolabelled pulse-chase assay. Furthermore, it had previously been reported that autophagic flux is decreased in *LRRK2-R1441C* human fibroblasts (Manzoni et al. 2013).

However, measuring proteolytic degradation in *LRRK2-R1441C* and *LRRK2-G2019S* iPSC-derived dopaminergic cultures using DQ-BSA assay showed no differences when compared to healthy controls (Fig. 4.2) which points to a cell-specific LRRK2 role in autophagy-lysosomal pathway (Madureira, Connor-Robson, and Wade-Martins 2020). Lysosomal marker LAMP1 expression measured by immunostaining and immunoblotting showed no differences in *LRRK2* iPSC-DA cultures (Fig. 4.3, Fig. 4.5). However, LC3-II expression measured by immunoblotting showed a decrease in *LRRK2-R1441C* iPSC-derived dopaminergic cultures (Fig. 4.4). Despite a decrease in LC3-II at basal levels in *LRRK2-R1441C* iPSC-DA cultures, the amount of LC3-II is higher in the presence of the autophagosome-lysosome fusion inhibitor chloroquine, which is indicative of autophagic flux occurring in these cultures. Additionally, co-localisation of LC3B and LAMP1 spots measured by immunostaining showed no differences between *LRRK2* iPSC-derived dopaminergic cultures and healthy controls, suggesting there were no alterations in autolysosomes at basal levels (Fig. 4.3 H). Therefore, it is unlikely this significant change in LC3-II is affecting lysosomal degradation downstream of autophagosome formation in dopaminergic cultures. Thorough characterisation of autophagic markers in *LRRK2-G2019S* iPSC-derived astrocyte cultures showed decreased autophagic flux (di Domenico et al. 2019), but the present data suggests there are no changes in *LRRK2-G2019S* iPSC-derived dopaminergic cultures, highlighting once again cell-specific differences in LRRK2-regulated autophagy. Results presented in this experimental setup would benefit from further validation using other autophagy lysosomal markers, such as fluorescently tagged-LC3 or endogenous LC3, unfortunately not carried out due to time restraints. There have been many reports of LRRK2 impairing autophagy-lysosomal pathways, using different techniques to measure this dynamic pathway. In the future, it is important to achieve a level of consistency between different methodologies that would make the comparisons of different models more biologically relevant. To this effect, thorough guidelines for carrying out and interpreting autophagy assays have been updated and published in 2021 (Klionsky et al. 2021).

DQ-Red BSA is a robust technique to measure proteolytic degradation. A potential caveat to this technique is due to the fact DQ-BSA is internalised into cells *via* the endocytic pathway, which shows alterations in aged striatal rat *LRRK2-G2019S* and *LRRK2-R1441C* (Connor-Robson et al. 2019). Additionally, Connor-Robson and colleagues reported that RAB5B, RAB7A and RAB10 proteins, which are localized to the early and maturing endosome, were reduced in *LRRK2* iPSC-derived dopaminergic neurons and increased in striatal tissue of mutant *LRRK2* BAC transgenic rats, compared to respective controls. In this case, iPSC-derived dopaminergic neurons, as well as cortical *LRRK2* transgenic

cultures from young rats, likely represent a very early stage of PD pathogenesis, whereas the aged BAC transgenic rats represent an intermediate phase. This indicates age of PD models is crucial to capture pathophysiological events and it must be recognised *LRRK2* BAC transgenic rat cortical cultures, collected from pups and assessed at DIV14, might not recapitulate autophagy and endo-lysosomal impairments previously characterised in disease models corresponding to more advanced stages of PD. In parallel, it is important to consider the morphological and functional differences between cortical, striatal and dopaminergic neurons, as PD-related endo-lysosomal alterations could be cell type-specific.

6.3. LRRK2 and Mitochondria

Here we have characterised mitochondrial health in two independent neuronal models of *LRRK2-R1441C* and demonstrated mitochondrial dysfunction and impaired mitophagy activation. First using transgenic primary cortical neuronal cultures, we observed that the *LRRK2-R1441C* mutation decreases mitochondrial membrane potential and increases ROS production. This mitochondrial dysregulation is linked to a functional impairment of mitophagy, both under basal and depolarising conditions. Interestingly, no significant changes were found in *LRRK2-G2019S* cortical neuronal cultures, suggesting divergent pathology of *LRRK2* mutations (Fig. 5.5). Second, similar perturbations in mitochondrial function were demonstrated in human *LRRK2-R1441C* iPSC-DA neuronal cultures, revealing decreased mitochondrial membrane potential, decreased maximal respiration and spare capacity in *LRRK2-R1441C*. In parallel, we observed reduced pS65Ub levels in *LRRK2-R1441C* iPSC-DA neuronal cultures. Interestingly, all *LRRK2-R1441C* phenotypic alterations were shown to be independent of LRRK2 kinase activity. We have investigated previously reported mechanisms by which LRRK2 regulates mitophagy, including altered interaction of mutant LRRK2 with MIRO1, altered Drp1 and exacerbated phosphorylation of Rab10 (Bonello et al. 2019; Hsieh et al. 2016; Wauters et al. 2020). We demonstrate here that LRRK2 and MIRO1 proteins co-localise within mitochondria and that the *LRRK2-R1441C* mutation results in no significant disruption of that interaction.

The dopaminergic neurons of the SNpc, which are affected in PD, project to the dorsal striatum. Therefore, mitochondrial morphology was investigated in dorsal striatal brain tissue from aged (21-22 months old) *LRRK2* BAC transgenic rats and nTG littermates. Striatal tissue sections were imaged using electron microscopy (EM) to analyse mitochondrial morphology (Fig. 6.1 A). Mitochondrial area and mitochondrial roundness were calculated and compared between animals expressing *LRRK2* wild-type and mutant

proteins. It was observed that mitochondrial area was not changed in *LRRK2-R1441C* and *LRRK2-G2019S* aged striatum (P = 0.2683 and 0.3388, respectively) (Fig. 6.1 B). However, mitochondrial roundness was altered in *LRRK2-G2019S* animals when compared to non-transgenic littermates (P = 0.0197), but not altered in *LRRK2-R1441C* and *LRRK2-WT* (Fig. 6.1 C). Striatal tissue sections from aged *LRRK2-G2019S* rats exhibited rounder

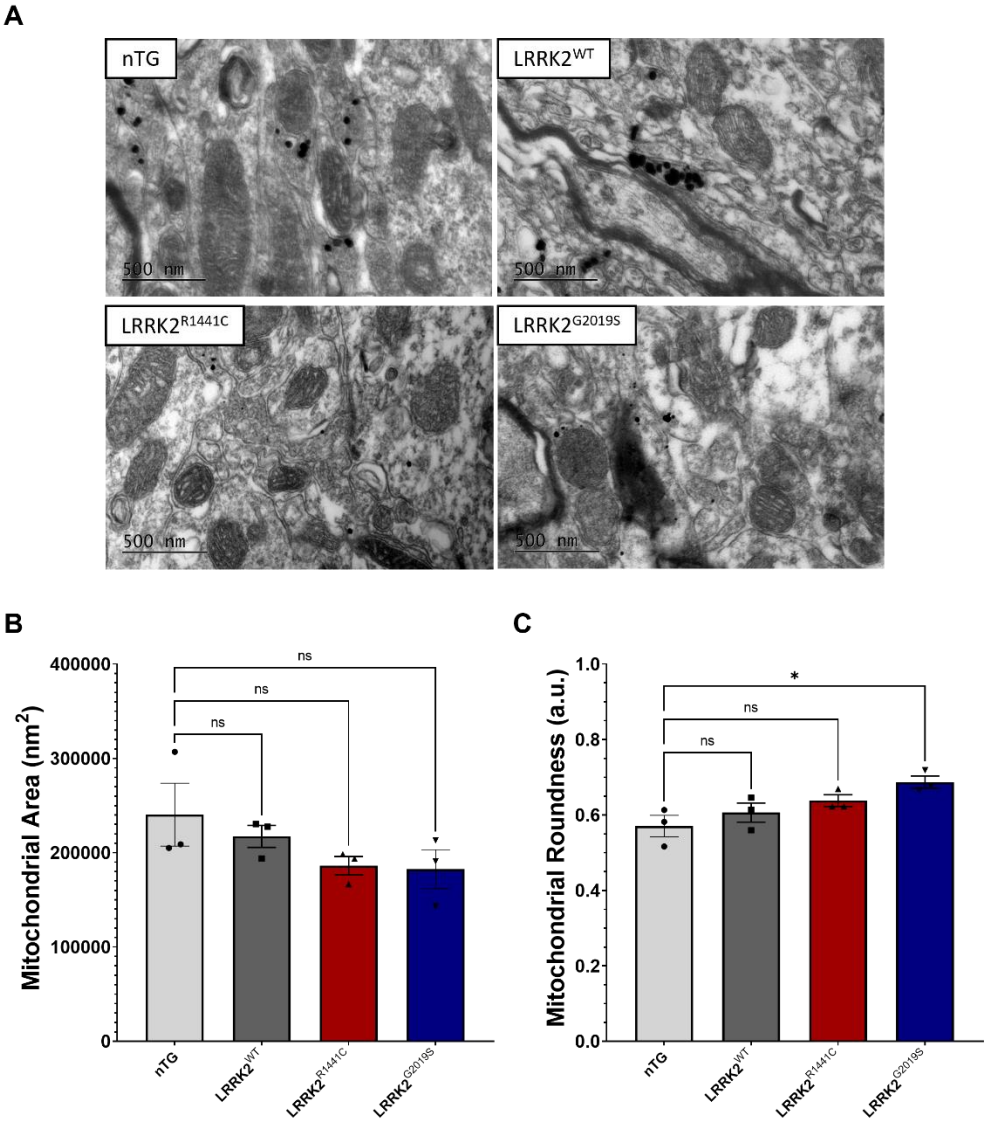

mitochondria, which could indicate a perturbed mitochondrial network, although no change in mitochondrial function was seen in *LRRK2-G2019S* primary cortical neurons *in vitro*.

Figure 6.1 – Mitochondrial morphology in striatal tissue from aged LRRK2 rats. **(A)** Representative immunogold labelled dopaminergic terminals, scale bar represents 500 nm. Mitochondrial morphology of the dorsal striatum of 21-22 months old *LRRK2* BAC transgenic rats was assessed by calculating **(B)** mitochondrial area (μm^2) and **(C)** mitochondrial roundness using ImageJ software. Data points represent values averaged from each animal. Scale bars correspond to 500 nm. Bars, mean ± SEM from three independent litters (ns: non-significant; ∗P <0.05; Kruskal–Wallis non-parametric ANOVA).

Data points represent averaged measures per animal analysed for each genotype. Bars, mean ± SEM from three independent litters (ns: non-significant; ∗P <0.05; Kruskal–Wallis non-parametric ANOVA). Panel A was performed, stained and assayed by Dr. Natalie Connor-Robson and Dr. Matthew Williamson.

Mitochondrial dysfunction has been thoroughly described in *LRRK2-G2019S* PD models to date, with the more penetrant but less frequent *LRRK2-R1441C* mutation less explored. Here we show *LRRK2-R1441C* iPSC-DA neuronal cultures display decreased mitochondrial membrane potential, reduced maximal respiration and spare capacity, indicating mitochondria are less efficient when compared to control iPSC-DA neuronal cultures (Fig. 5.10). We observed specific changes in membrane potential and OXPHOS function in *LRRK2-R1441C* iPSC-DA neuronal cultures although there was no gross energetic deficit. However, ATP levels in *LRRK2-R1441C* iPSC-DA neuronal cultures were unchanged, suggesting compensation by other pathways. It has been previously reported that mitochondrial uncoupling proteins are altered in *LRRK2-G2019S* models and similar mechanisms may also be operative in R1441C neurons (Papkovskaia et al. 2012).

Furthermore, calculating *LRRK2-R1441C* patient line Z-scores for the different assays in our study revealed that DA neuronal cultures derived from the *LRRK2-R1441C* iPSC line SFC869 presented with the worst Z-score for mitochondrial morphology, mitochondrial membrane potential and mitochondrial ROS, while presenting the highest score for mitophagy activation of all the patient lines. Overall, it is clear the *LRRK2-R1441C* patient line SFC869 displayed more severe phenotypical alterations than iPSC-DA neurons derived from patient lines SFC870 and JR207 (Fig. 5.21). Although the present study does not establish causality between mitochondria damage and mitophagy, our work demonstrates how mitochondrial networks are intricately balanced and highlights inter-patient variability between *LRRK2-R1441C* mutation carriers. The link between iPSC-DA neuronal mitochondrial phenotypes and patient clinical phenotypes will be interesting to understand in large iPSC collections from well-characterised patient cohorts (Marek et al., 2011). However, the lack of correction of *LRRK2-R1441C* phenotypes in patient iPSC-DA cultures reported here suggests mechanisms independent of kinase activity.

We also observe changes in mitochondrial morphology in *LRRK2-R1441C* iPSC-dopaminergic cultures. Specifically, mitochondria are smaller, rounder and have an increased width to length ratio, which indicates mitochondria are fragmented. Our results suggest damaged mitochondria are accumulating in iPSC-DA neuronal cultures (Fig. 5.16). Moreover, we report *LRRK2-R1441C* iPSC-DA neuronal cultures exhibit altered OXPHOS

complex activity, confirming that mitochondrial morphology alterations are associated with mitochondrial dysfunction. When analysing mitochondrial morphology in primary cortical cultures and in aged striatal tissue, there were no differences in *LRRK2-R1441C* compared to nTG littermates, suggesting that PD-related mitochondrial morphology alterations could be cell type-specific.

Taken together, our work illustrates mitochondria are damaged and less efficient in *LRRK2-R1441C* neuronal cultures. Removal of damaged mitochondria by mitophagy is a key step in limiting the pool of damaged mitochondria and failure of this process is linked to PD (Malpartida et al. 2021). We have shown that *LRRK2-R1441C* primary cortical neurons exhibit decreased mitophagy levels under steady state and CCCP-induced depolarising conditions, in line with previous reports from *LRRK2-G2019S* models (Singh et al. 2021; McWilliams et al. 2018). We also confirm decreased levels of pS65Ub, which is induced by PINK1 activation, after mitochondrial depolarisation in *LRRK2-R1441C* iPSC-DA neuronal cultures. Importantly, the mechanism of decreased pS65Ub levels in *LRRK2-R1441C* mutants could involve altered PINK1 activation or increased activity of ubiquitin phosphatases such as PPEF2 or PTEN-L (Wall et al. 2019; Wang et al. 2018). Therefore, decreased mitophagy could further exacerbate perturbations on mitochondrial homeostasis, since damaged mitochondria are not being degraded and could disturb the mitochondrial network, contributing to molecular pathology in PD.

Investigating the mechanisms of LRRK2-mediated regulation of mitophagy, we were able to partially confirm the findings described by Hsieh and colleagues (2016), whereby the interaction of LRRK2 with MIRO1 promotes MIRO1 degradation and removal from the OMM, leading to mitophagy initiation (Hsieh et al. 2016). In the present study, we demonstrate MIRO1 depletion induced by mitochondrial damage is impaired in *LRRK2-R1441C* iPSC-DA neuronal cultures. Importantly, we show that LRRK2-MIRO1 co-localisation occurs within mitochondrial structures in iPSC-DA neuronal cultures but, contrary to the mechanism demonstrated for LRRK2-G2019S/MIRO1 interaction, we do not observe a significant disruption of LRRK2-R1441C/MIRO1 co-localisation compared to control (Fig. 5.20). Additionally, MIRO1 expression at basal levels was increased, but not significantly, in *LRRK2-G2019S* iPSC-derived dopaminergic cultures when compared to healthy controls and there was a significant clioquinol-induced increase in MIRO1 levels in *LRRK2-G2019S* dopaminergic cultures. Since clioquinol can alter lysosome integrity and inhibits the proteasome, it is plausible this affects MIRO1 degradation in *LRRK2-G2019S* neurons, leading to an abnormal accumulation of this protein, similarly to the observations reported by Hsieh and colleagues (2016) (Hsieh et al. 2016; Grossmann et al. 2020). Although more experiments would be necessary to confirm these observations, this

evidence adds to the ongoing hypothesis that the underlying pathophysiology of the *LRRK2-G2019S* and *LRRK2-R1441C* mutations have distinct mechanisms impacting neuronal cell health. These observations are interesting when considering the multi-factored susceptibility of dopaminergic neurons of the SNpc.

Conversely, in iPSC-DA *LRRK2-R1441C* neuronal cultures we did not observe the increased phosphorylation of Rab10 found in *LRRK2-G2019S* mutant primary fibroblasts. The differing results highlight the complex cell-type and mutation specificity of LRRK2-PD pathology. In a recent study, Hsieh and colleagues (2019) demonstrated small molecule modulators promoting MIRO1 degradation increased mitophagy levels in *LRRK2-G2019S* iPSC-derived cultures (Hsieh et al. 2019) which may also be relevant in *LRRK2-R1441C* models.

Overall, this study determined that *LRRK2-R1441C* iPSC-DA neuronal cultures exhibited mitochondrial dysfunction and impaired mitophagy. We found that the LRRK2 kinase inhibitor MLi-2 did not fully restore OXPHOS function, mitochondrial membrane potential or CCCP-induced mitophagy activation defects in *LRRK2-R1441C* iPSC-DA neuronal cultures (Fig. 6.2). Importantly, different *LRRK2-R1441C* patient iPSC-DA neuronal cultures displayed different phenotypic severities at the molecular level, reflecting a need for patient stratification in the treatment of LRRK2-related PD.

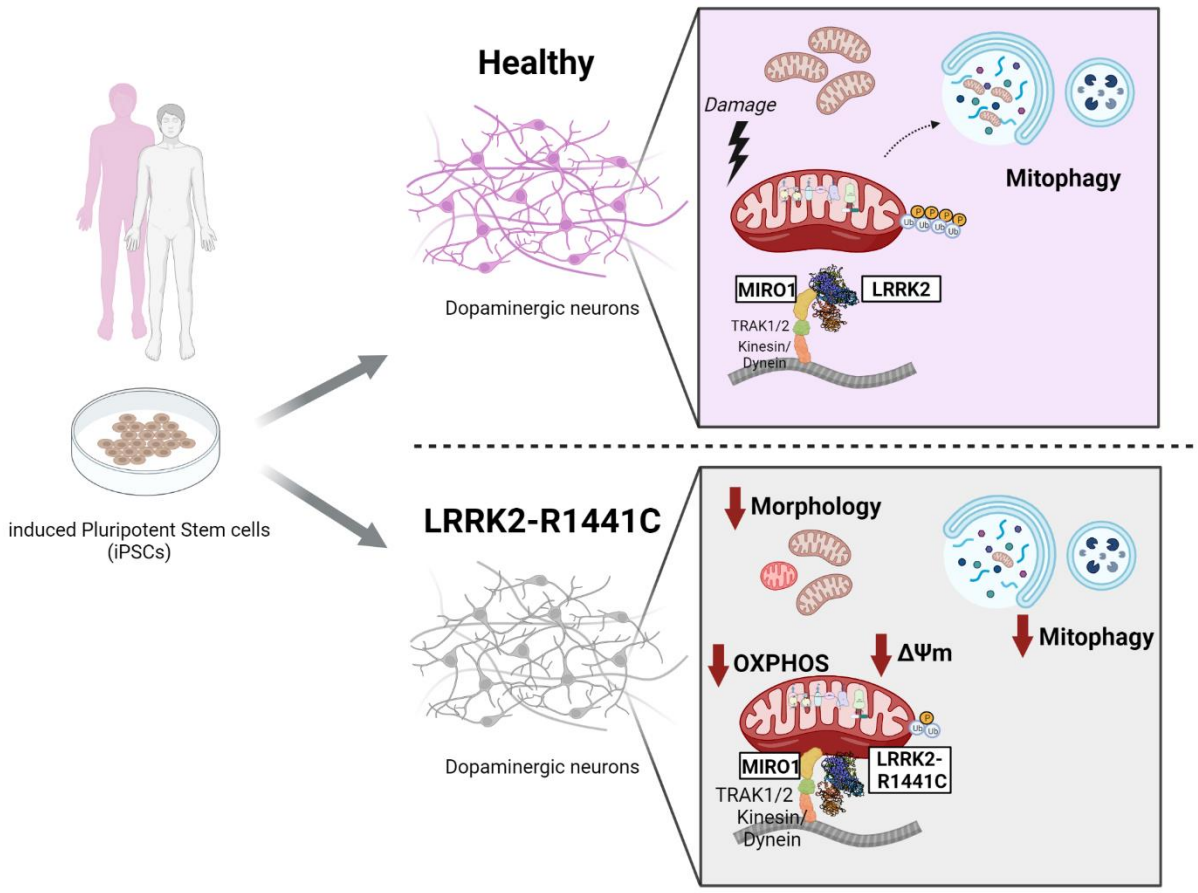

Figure 6.2 – Schematic representation of mitochondrial alterations in LRRK2-R1441C PD. *LRRK2-R1441C* induced pluripotent stem cell-derived dopaminergic neuronal cultures (iPSC-DAn) exhibit altered mitochondrial morphology and membrane potential, which is linked to mitochondrial dysfunction of OxPhos complexes. Damaged mitochondria undergo decreased PINK1-dependent activation of mitophagy. Disrupted LRRK2 regulation of mitophagy is caused by loss of interaction between LRRK2-R1441C and outer mitochondrial membrane MIRO1. This leads to impaired degradation of MIRO1, anchoring damaged mitochondria to microtubules.

6.4. General conclusions and future studies

The present body of work contributes to further the understanding of LRRK2-related mechanisms of action in PD, by investigating the novel interaction of LRRK2 with vATPase-a1 subunit of the vATPase proton pump complex (Chapter 3), autophagy-lysosomal pathways (Chapter 4) and mitochondrial function and mitophagy (Chapter 5) in relevant LRRK2 disease models.

In previous literature, disease pathways involving autophagy-lysosomal pathway and mitochondrial function have been suggested to be cell-type specific (Panicker et al. 2021).

Thus, it is important to focus on studying these cellular functions in dopaminergic neurons, a physiologically relevant disease model for PD. In the present study, dopaminergic neuronal cultures were derived using iPSC from healthy controls and *LRRK2-R1441C* patients to assess autophagy. Using immunoblotting to measure expression of autophagy markers showed a decrease in LC3-II levels in *LRRK2-R1441C* iPSC-derived dopaminergic cultures (Fig. 4.4), but no change in LAMP1 levels (Fig. 4.3, Fig. 4.5). This could suggest a defect in the early stages of autophagy, relating to generation and packaging of autophagosomes, which does not seem to be accompanied by defects in lysosomal organelles. Furthermore, proteolytic degradation levels were not changed in *LRRK2-R1441C* iPSC-derived dopaminergic cultures compared to healthy controls (Fig. 4.2; Fig. 6.3). Since the autophagy-lysosomal pathway is a dynamic cellular function critical to maintain neuronal health, it would be important to further investigate this mechanism in *live* cell models of LRRK2 dopaminergic neurons. Equally as important, it would be essential to study this pathway in more complex models that capture neuronal and glial contributions, such as brain organoids. Recently, Jarazo and colleagues showed decreased autophagy and mitophagy levels in *PINK1* (p.I368N) patient-derived cells in midbrain organoids, compared to healthy controls (Jarazo et al. 2022). A similar study using *LRRK2-R1441C* patient-derived cells in midbrain organoids would be crucial to understand LRRK2 contribution to molecular pathways and its role in PD.

Since bioenergetics are important to maintain neuronal health, dopaminergic neuronal cultures were derived using iPSC from healthy controls and *LRRK2-R1441C* patients to assess mitochondrial function and mitophagy. It was demonstrated that mitochondrial function is decreased in the OxPhos complexes, since there was decreased maximal respiration and spare capacity, mitochondrial are more fragmented, there is decreased mitochondrial membrane potential and decreased PINK1-dependent activation of mitophagy in *LRRK2-R1441C* iPSC-derived dopaminergic cultures and primary cortical cultures, but not *LRRK2-G2019S* neuronal models (Fig. 6.2, Fig. 6.3). A recent clinical trial was terminated at Phase 2, using MitoQ (Mitoquinone) to treat early onset of PD (NCT00329056). This mitochondria-targeted antioxidant was used as a protecting agent against mitochondrial redox stress *in vitro* using human skin fibroblasts (Koopman et al. 2005). Surprisingly, there are no clinical trials for mitochondrial-targetted drugs in PD currently (Source: clinicaltrials.gov, accessed 26-06-2023). The data presented in this study highlights an interesting mitochondrial phenotypic difference between the two most common LRRK2 mutations in PD patients, and suggests mitochondrial-targeted drugs could soon bring very exciting prospects into the pharmacological space for neurodegeneration.

Furthermore, two important interacting partners of LRRK2 have been investigated. Firstly, LRRK2 seems to interact with vATPase-a1 subunit of proton pumps in human cellular models, but does not seem to be crucial for maintaining lysosomal activity in iPSC-derived dopaminergic cultures. Secondly, LRRK2 interacts with MIRO1 to promote MIRO1 degradation and removal from the OMM, leading to mitophagy initiation, which is impaired in *LRRK2-R1441C* iPSC derived dopaminergic cultures. Additionally, LRRK2 kinase inhibitor MLi-2 and zync-ionophore Clioquinol did not rescue any of the mitochondrial or autophagic impairments, respectively. Hence, it will be important to take into consideration LRRK2 kinase inhibitors currently undergoing clinical trials, such as DNL-151 in Phase 3 (NCT05418673) and NEU-723 in Phase 1 (NCT05633745) could have better effects in *LRRK2-G2019S* PD patients than in *LRRK2-R1441C*, highlighting patient stratification in complex neurodegenerative disorders. It is important to highlight another LRRK2 targetting therapy, ION-859, a LRRK2 antisense oligonucleotide therapy targetting *LRRK2* mRNA to inhibit the *LRRK2* gene (Phase 2 clinical trial, NCT03976349). Future investigation into key players of PD molecular disruption such as LRRK2 and GBA, and the respective cellular mechanism they regulate such as autophagy and mitochondrial health in relevant disease models, will prove most useful to inform drug tractability for PD patients.

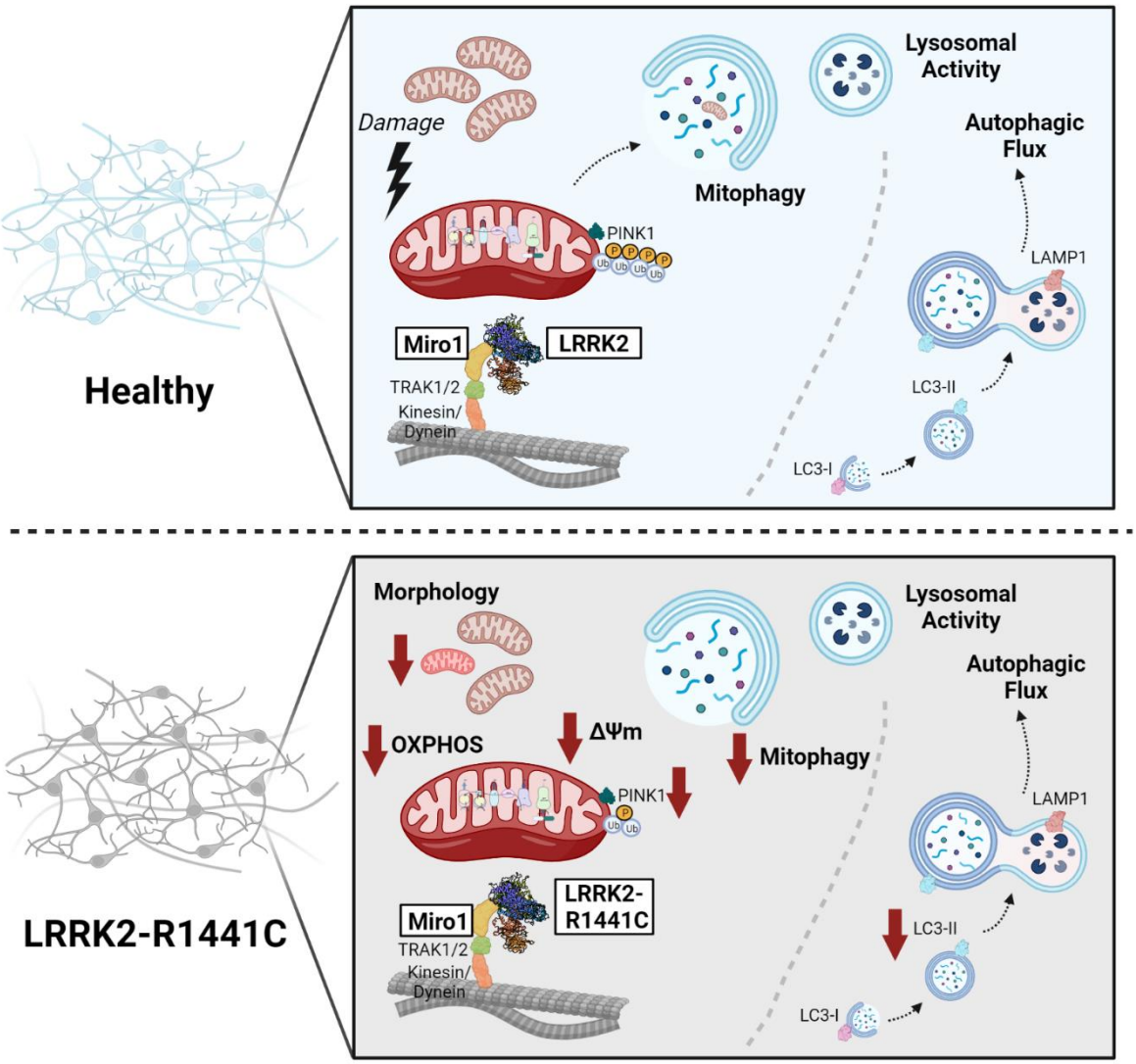

Figure 6.3 – Mitochondrial and autophagy-lysosomal alterations in LRRK2-R1441C iPSC-derived DA cultures. *LRRK2-R1441C* induced pluripotent stem cell-derived dopaminergic neuronal cultures (iPSC-DAn) showed decreased LC3-II expression, despite showing no changes in autophagy-lysosomal marker LAMP1 or autophagic flux. In parallel, *LRRK2-R1441C* iPSC-DAn exhibit altered mitochondrial morphology and membrane potential, which is linked to mitochondrial dysfunction of OxPhos complexes. Damaged mitochondria undergo decreased PINK1-dependent activation of mitophagy. Disrupted LRRK2 regulation of phosphorylated ubiquitin affects mitophagy in *LRRK2-R1441C,* while still interacting with outer mitochondrial membrane MIRO1. This leads to impaired degradation of MIRO1, anchoring damaged mitochondria to microtubules.

Chapter 7 - References

Abbas, Yazan M., Di Wu, Stephanie A. Bueler, Carol V. Robinson, and John L. Rubinstein. 2020. “Structure of V-ATPase from the Mammalian Brain.” *Science* 367 (6483): 1240–46. https://doi.org/10.1126/science.aaz2924.

Ahmed, Ishrat, Yideng Liang, Sabitha Schools, Valina L Dawson, Ted M Dawson, and Joseph M Savitt. 2012. “Development and Characterization of a New Parkinson ’ s Disease Model Resulting from Impaired Autophagy” 32 (46): 16503–9. https://doi.org/10.1523/JNEUROSCI.0209-12.2012.

Alcalay, Roy N., Oren A. Levy, Cheryl C. Waters, Stanley Fahn, Blair Ford, Sheng Han Kuo, Pietro Mazzoni, et al. 2015. “Glucocerebrosidase Activity in Parkinson’s Disease with and without GBA Mutations.” *Brain* 138 (9): 2648–58. https://doi.org/10.1093/brain/awv179.

Alegre-Abarrategui, Javier, Helen Christian, Michele M.P. Lufino, Ruxandra Mutihac, Lara Lourenço Venda, Olaf Ansorge, and Richard Wade-Martins. 2009. “LRRK2 Regulates Autophagic Activity and Localizes to Specific Membrane Microdomains in a Novel Human Genomic Reporter Cellular Model.” *Human Molecular Genetics* 18 (21): 4022–34. https://doi.org/10.1093/hmg/ddp346.

Alegre-Abarrategui, Javier, and Richard Wade-Martins. 2009. “Parkinson Disease, LRRK2 and the Endocytic-Autophagic Pathway.” *Autophagy* 5 (8): 1208–10. https://doi.org/10.4161/auto.5.8.9894.

Alers, S., A. S. Loffler, S. Wesselborg, and B. Stork. 2012. “Role of AMPK-MTOR-Ulk1/2 in the Regulation of Autophagy: Cross Talk, Shortcuts, and Feedbacks.” *Molecular and Cellular Biology* 32 (1): 2–11. https://doi.org/10.1128/mcb.06159-11.

Alonso-Cánovas, Araceli, José Luis López-Sendón, Javier Buisán, Alicia DeFelipe-Mimbrera, Marta Guillán, Nuria García-Barragán, Iñigo Corral, et al. 2014. “Sonography for Diagnosis of Parkinson Disease—From Theory to Practice.” *Journal of Ultrasound in Medicine* 33 (12): 2069–74. https://doi.org/10.7863/ULTRA.33.12.2069.

Antony, Paul M.A., Nico J. Diederich, Rejko Krüger, and Rudi Balling. 2013. “The Hallmarks of Parkinson’s Disease.” *FEBS Journal* 280 (23): 5981–93. https://doi.org/10.1111/febs.12335.

Appel-Cresswell, Silke, Carles Vilarino-Guell, Mary Encarnacion, Holly Sherman, Irene Yu, Brinda Shah, David Weir, et al. 2013. “Alpha-Synuclein p.H50Q, a Novel Pathogenic Mutation for Parkinson’s Disease.” *Movement Disorders : Official Journal of the Movement Disorder Society* 28 (6): 811–13. https://doi.org/10.1002/MDS.25421.

Armstrong, Melissa J., and Michael S. Okun. 2020. “Diagnosis and Treatment of Parkinson Disease: A Review.” *JAMA - Journal of the American Medical Association* 323 (6): 548–60. https://doi.org/10.1001/jama.2019.22360.

Atashrazm, Farzaneh, and Nicolas Dzamko. 2016. “LRRK2 Inhibitors and Their Potential in the Treatment of Parkinson’s Disease: Current Perspectives.” *Clinical Pharmacology: Advances and Applications* 8: 177–89. https://doi.org/10.2147/CPAA.S102191.

Bae, Eun Jin, Dong Kyu Kim, Changyoun Kim, Michael Mante, Anthony Adame, Edward Rockenstein, Ayse Ulusoy, et al. 2018. “LRRK2 Kinase Regulates α-Synuclein Propagation via RAB35 Phosphorylation.” *Nature Communications* 9 (1). https://doi.org/10.1038/s41467-018-05958-z.

Bahmad, Hisham, Ola Hadadeh, Farah Chamaa, Katia Cheaito, and Batoul Darwish. 2017. “Modeling Human Neurological and Neurodegenerative Diseases : From Induced Pluripotent Stem Cells to Neuronal Differentiation and Its Applications in Neurotrauma” 10 (February). https://doi.org/10.3389/fnmol.2017.00050.

Bandyopadhyay, U., S. Kaushik, L. Varticovski, and A. M. Cuervo. 2008. “The Chaperone-Mediated Autophagy Receptor Organizes in Dynamic Protein Complexes at the Lysosomal Membrane.” *Molecular and Cellular Biology* 28 (18): 5747–63. https://doi.org/10.1128/mcb.02070-07.

Bang, Yeojin, Kwang Soo Kim, Wongi Seol, and Hyun Jin Choi. 2016. “LRRK2 Interferes with Aggresome Formation for Autophagic Clearance.” *Molecular and Cellular Neuroscience* 75: 71–80. https://doi.org/10.1016/j.mcn.2016.06.007.

Baptista, Marco A.S., Kuldip D. Dave, Mark A. Frasier, Todd B. Sherer, Melanie Greeley, Melissa J. Beck, Julie S. Varsho, et al. 2013. “Loss of Leucine-Rich Repeat Kinase 2 (LRRK2) in Rats Leads to Progressive Abnormal Phenotypes in Peripheral Organs.” *PLoS ONE* 8 (11): 1–16. https://doi.org/10.1371/journal.pone.0080705.

Beavan, Michelle S., and Anthony H.V. Schapira. 2013. “Glucocerebrosidase Mutations and the Pathogenesis of Parkinson Disease.” *Annals of Medicine*. Taylor & Francis. https://doi.org/10.3109/07853890.2013.849003.

Behrends, Christian, Mathew E. Sowa, Steven P. Gygi, and J. Wade Harper. 2010. “Network Organization of the Human Autophagy System.” *Nature* 466 (7302): 68–76. https://doi.org/10.1038/nature09204.

Beilina, Alexandra, Luis Bonet-Ponce, Ravindran Kumaran, Juan S Bonifacino, Darren J Moore, Mark R Cookson Correspondence, Jennifer J Kordich, et al. 2020. “The Parkinson’s Disease Protein LRRK2 Interacts with the GARP Complex to Promote Retrograde Transport to the Trans-Golgi Network.” https://doi.org/10.1016/j.celrep.2020.107614.

Beilina, Alexandria, Iakov N. Rudenko, Alice Kaganovich, Laura Civiero, Hien Chau, Suneil K. Kalia, Lorraine V. Kalia, et al. 2014. “Unbiased Screen for Interactors of Leucine-Rich Repeat Kinase 2 Supports a Common Pathway for Sporadic and Familial Parkinson Disease.” *Proceedings of the National Academy of Sciences of the United States of America* 111 (7): 2626–31. https://doi.org/10.1073/pnas.1318306111.

Bender, Andreas, Kim J. Krishnan, Christopher M. Morris, Geoffrey A. Taylor, Amy K. Reeve, Robert H. Perry, Evelyn Jaros, et al. 2006. “High Levels of Mitochondrial DNA Deletions in Substantia Nigra Neurons in Aging and Parkinson Disease.” *Nature Genetics* 38 (5): 515–17. https://doi.org/10.1038/NG1769.

Bengoa-Vergniory, Nora, Rosalind F. Roberts, Richard Wade-Martins, and Javier Alegre-Abarrategui. 2017. “Alpha-Synuclein Oligomers: A New Hope.” *Acta Neuropathologica* 134 (6): 819–38. https://doi.org/10.1007/S00401-017-1755-1.

Berwick, Daniel C., George R. Heaton, Sonia Azeggagh, and Kirsten Harvey. 2019. "LRRK2 Biology from Structure to Dysfunction: Research Progresses, but the Themes Remain the Same." *Molecular Neurodegeneration* 14 (1): 1–22. https://doi.org/10.1186/s13024-019-0344-2.

Blauwendraat, Cornelis, Xylena Reed, Lynne Krohn, Karl Heilbron, Sara Bandres-Ciga, Manuela Tan, J. Raphael Gibbs, et al. 2020. "Genetic Modifiers of Risk and Age at Onset in GBA Associated Parkinson's Disease and Lewy Body Dementia." *Brain* 143 (1): 234–48. https://doi.org/10.1093/brain/awz350.

Bliek, Alexander M. Van Der, Margaret M. Sedensky, and Phil G. Morgan. 2017. "Cell Biology of the Mitochondrion." *Genetics* 207 (3): 843–71. https://doi.org/10.1534/GENETICS.117.300262.

Bloem, Bastiaan R., Michael S. Okun, and Christine Klein. 2021. "Parkinson's Disease." *Lancet (London, England)* 397 (10291): 2284–2303. https://doi.org/10.1016/S0140-6736(21)00218-X.

Bodzęta, Anna, Martin Kahms, and Jürgen Klingauf. 2017. "The Presynaptic V-ATPase Reversibly Disassembles and Thereby Modulates Exocytosis but Is Not Part of the Fusion Machinery." *Cell Reports* 20 (6): 1348–59. https://doi.org/10.1016/J.CELREP.2017.07.040.

Bonello, Fiona, Sidi Mohamed Hassoun, François Mouton-Liger, Yea Seul Shin, Adeline Muscat, Christelle Tesson, Suzanne Lesage, et al. 2019. "LRRK2 Impairs PINK1/Parkin-Dependent Mitophagy via Its Kinase Activity: Pathologic Insights into Parkinson's Disease." *Human Molecular Genetics* 28 (10): 1645–60. https://doi.org/10.1093/hmg/ddz004.

Braak, Heiko, Kelly Del Tredici, Udo Rüb, Rob A.I. De Vos, Ernst N.H. Jansen Steur, and Eva Braak. 2003. "Staging of Brain Pathology Related to Sporadic Parkinson's Disease." *Neurobiology of Aging* 24 (2): 197–211. https://doi.org/10.1016/S0197-4580(02)00065-9.

Bragoszewski, Piotr, Michal Turek, and Agnieszka Chacinska. 2017. "Control of Mitochondrial Biogenesis and Function by the Ubiquitin-Proteasome System." *Open Biology* 7 (4). https://doi.org/10.1098/RSOB.170007.

Bräuer, Philipp, Joanne L. Parker, Andreas Gerondopoulos, Iwan Zimmermann, Markus A. Seeger, Francis A. Barr, and Simon Newstead. 2019. "Structural Basis for PH-Dependent Retrieval of ER Proteins from the Golgi by the KDEL Receptor." *Science (New York, N.Y.)* 363 (6431): 1103–7. https://doi.org/10.1126/SCIENCE.AAW2859.

Bravo-San Pedro, José M., Mireia Niso-Santano, Rubén Gómez-Sánchez, Elisa Pizarro-Estrella, Ana Aiastui-Pujana, Ana Gorostidi, Vicente Climent, et al. 2013. "The LRRK2 G2019S Mutant Exacerbates Basal Autophagy through Activation of the MEK/ERK Pathway." *Cellular and Molecular Life Sciences* 70 (1): 121–36. https://doi.org/10.1007/s00018-012-1061-y.

Bury, Alexander G., Angela Pyle, Joanna L. Elson, Laura Greaves, Christopher M. Morris, Gavin Hudson, and Ilse S. Pienaar. 2017. "Mitochondrial DNA Changes in Pedunculopontine Cholinergic Neurons in Parkinson Disease." *Annals of Neurology* 82 (6): 1016–21. https://doi.org/10.1002/ANA.25099.

Caesar, M., S. Felk, J. O. Aasly, and F. Gillardon. 2015. “Changes in Actin Dynamics and F-Actin Structure Both in Synaptoneurosomes of LRRK2(R1441G) Mutant Mice and in Primary Human Fibroblasts of LRRK2(G2019S) Mutation Carriers.” *Neuroscience* 284 (January): 311–24. https://doi.org/10.1016/j.neuroscience.2014.09.070.

Calabresi, Paolo, Massimiliano Di Filippo, Veronica Ghiglieri, Nicola Tambasco, and Barbara Picconi. 2010. “Levodopa-Induced Dyskinesias in Patients with Parkinson’s Disease: Filling the Bench-to-Bedside Gap.” *The Lancet Neurology* 9 (11): 1106–17. https://doi.org/10.1016/S1474-4422(10)70218-0.

Cannon, Jason R., Kindiya D. Geghman, Victor Tapias, Thomas Sew, Michelle K. Dail, Chenjian Li, and J. Timothy Greenamyre. 2013. “Expression of Human E46K-Mutated α-Synuclein in BAC-Transgenic Rats Replicates Early-Stage Parkinson’s Disease Features and Enhances Vulnerability to Mitochondrial Impairment.” *Experimental Neurology* 240 (1): 44–56. https://doi.org/10.1016/J.EXPNEUROL.2012.11.007.

Carling, Phillippa J., Heather Mortiboys, Claire Green, Simeon Mihaylov, Cynthia Sandor, Aurelie Schwartzentruber, Rosie Taylor, et al. 2020. “Deep Phenotyping of Peripheral Tissue Facilitates Mechanistic Disease Stratification in Sporadic Parkinson’s Disease.” *Progress in Neurobiology* 187 (April). https://doi.org/10.1016/J.PNEUROBIO.2020.101772.

Chan, Edmond Y W, Serkan Kir, and Sharon A Tooze. 2007. “SiRNA Screening of the Kinome Identifies ULK1 as a Multidomain Modulator of Autophagy * □ S.” https://doi.org/10.1074/jbc.M703663200.

Chang, Diana, Mike A. Nalls, Ingileif B. Hallgrímsdóttir, Julie Hunkapiller, Marcel van der Brug, Fang Cai, Geoffrey A. Kerchner, et al. 2017. “A Meta-Analysis of Genome-Wide Association Studies Identifies 17 New Parkinson’s Disease Risk Loci.” *Nature Genetics* 49 (10): 1511–16. https://doi.org/10.1038/ng.3955.

Chen, C. Y., Y. H. Weng, K. Y. Chien, K. J. Lin, T. H. Yeh, Y. P. Cheng, C. S. Lu, and H. L. Wang. 2012. “(G2019S) LRRK2 Activates MKK4-JNK Pathway and Causes Degeneration of SN Dopaminergic Neurons in a Transgenic Mouse Model of PD.” *Cell Death and Differentiation* 19 (10): 1623–33. https://doi.org/10.1038/CDD.2012.42.

Chen, Meng Ling, and Ruey Meei Wu. 2018. “LRRK 2 Gene Mutations in the Pathophysiology of the ROCO Domain and Therapeutic Targets for Parkinson’s Disease: A Review Julie Y.H. Chan.” *Journal of Biomedical Science* 25 (1): 1–11. https://doi.org/10.1186/s12929-018-0454-0.

Cherubini, Marta, and Richard Wade-Martins. 2018. “Convergent Pathways in Parkinson’s Disease.” *Cell and Tissue Research* 373 (1): 79–90. https://doi.org/10.1007/s00441-017-2700-2.

Chinta, Shankar J., Jyothi K. Mallajosyula, Anand Rane, and Julie K. Andersen. 2010. “Mitochondrial α-Synuclein Accumulation Impairs Complex I Function in Dopaminergic Neurons and Results in Increased Mitophagy in Vivo.” *Neuroscience Letters* 486 (3): 235–39. https://doi.org/10.1016/J.NEULET.2010.09.061.

Chlebanowska, Paula, Anna Tejchman, Maciej Sułkowski, Klaudia Skrzypek, and Marcin Majka. 2020. “Use of 3D Organoids as a Model to Study Idiopathic Form of

Parkinson's Disease." *International Journal of Molecular Sciences* 21 (3). https://doi.org/10.3390/IJMS21030694.

Cho, Hyun Jin, Jia Yu, Chengsong Xie, Parvathi Rudrabhatla, Xi Chen, Junbing Wu, Loukia Parisiadou, et al. 2014. " Leucine-rich Repeat Kinase 2 Regulates Sec16A at ER Exit Sites to Allow ER –Golgi Export ." *The EMBO Journal* 33 (20): 2314–31. https://doi.org/10.15252/embj.201487807.

Chou, Jun Shiao, Chu Yu Chen, Ying Ling Chen, Yi Hsin Weng, Tu Hsueh Yeh, Chin Song Lu, Ya Ming Chang, and Hung Li Wang. 2014. "(G2019S) LRRK2 Causes Early-Phase Dysfunction of SNpc Dopaminergic Neurons and Impairment of Corticostriatal Long-Term Depression in the PD Transgenic Mouse." *Neurobiology of Disease* 68 (August): 190–99. https://doi.org/10.1016/J.NBD.2014.04.021.

Chu, Charleen T. 2006. "Autophagic Stress in Neuronal Injury and Disease." *Journal of Neuropathology and Experimental Neurology* 65 (5): 423–32. https://doi.org/10.1097/01.jnen.0000229233.75253.be.

Chu, Yaping, Hemraj Dodiya, Patrick Aebischer, C. Warren Olanow, and Jeffrey H. Kordower. 2009. "Alterations in Lysosomal and Proteasomal Markers in Parkinson's Disease: Relationship to Alpha-Synuclein Inclusions." *Neurobiology of Disease* 35 (3): 385–98. https://doi.org/10.1016/j.nbd.2009.05.023.

Chung, Chee Yeun, Vikram Khurana, Pavan K. Auluck, Daniel F. Tardiff, Joseph R. Mazzulli, Frank Soldner, Valeriya Baru, et al. 2013. "Identification and Rescue of α-Synuclein Toxicity in Parkinson Patient-Derived Neurons." *Science* 342 (6161): 983–87. https://doi.org/10.1126/science.1245296.

Colla, Emanuela, Poul H. Jensen, Olga Pletnikova, Juan C. Troncoso, Charles Glabe, and Michael K. Lee. 2012. "Accumulation of Toxic α-Synuclein Oligomer within Endoplasmic Reticulum Occurs in α-Synucleinopathy in Vivo." *Journal of Neuroscience* 32 (10): 3301–5. https://doi.org/10.1523/JNEUROSCI.5368-11.2012.

Collins, Michael P., and Michael Forgac. 2020. "Regulation and Function of V-ATPases in Physiology and Disease." *Biochimica et Biophysica Acta (BBA) - Biomembranes* 1862 (12): 183341. https://doi.org/10.1016/J.BBAMEM.2020.183341.

Colosimo, C., A. J. Hughes, L. Kilford, and A. J. Lees. 2003. "Lewy Body Cortical Involvement May Not Always Predict Dementia in Parkinson's Disease." *Journal of Neurology, Neurosurgery & Psychiatry* 74 (7): 852–56. https://doi.org/10.1136/JNNP.74.7.852.

Connor-Robson, Natalie, Heather Booth, Jeffrey G. Martin, Benbo Gao, Kejie Li, Natalie Doig, Jane Vowles, et al. 2019. "An Integrated Transcriptomics and Proteomics Analysis Reveals Functional Endocytic Dysregulation Caused by Mutations in LRRK2." *Neurobiology of Disease* 127: 512–26. https://doi.org/10.1016/j.nbd.2019.04.005.

Cook, D. A., G. T. Kannarkat, A. F. Cintron, Laura M. Butkovich, Kyle B. Fraser, J. Chang, N. Grigoryan, et al. 2017. "LRRK2 Levels in Immune Cells Are Increased in Parkinson's Disease." *Npj Parkinson's Disease* 3 (1): 1–11. https://doi.org/10.1038/s41531-017-0010-8.

Cookson, Mark R. 2016. “Cellular Functions of LRRK2 Implicate Vesicular Trafficking Pathways in Parkinson’s Disease.” *Biochemical Society Transactions* 44 (6): 1603–10. https://doi.org/10.1042/BST20160228.

Cookson, Mark R. 2017. “Mechanisms of Mutant LRRK2 Neurodegeneration.” In *Advances in Neurobiology*, 14:227–39. Springer New York LLC. https://doi.org/10.1007/978-3-319-49969-7_12.

Court, Felipe A., and Michael P. Coleman. 2012. “Mitochondria as a Central Sensor for Axonal Degenerative Stimuli.” *Trends in Neurosciences* 35 (6): 364–72. https://doi.org/10.1016/J.TINS.2012.04.001.

Coutinho, Maria Francisca, Maria João Prata, and Sandra Alves. 2012. “Mannose-6-Phosphate Pathway: A Review on Its Role in Lysosomal Function and Dysfunction.” *Molecular Genetics and Metabolism* 105 (4): 542–50. https://doi.org/10.1016/J.YMGME.2011.12.012.

Coxhead, Jonathan, Marzena Kurzawa-Akanbi, Rafiqul Hussain, Angela Pyle, Patrick Chinnery, and Gavin Hudson. 2016. “Somatic MtDNA Variation Is an Important Component of Parkinson’s Disease.” *Neurobiology of Aging* 38 (August): 217.e1-217.e6. https://doi.org/10.1016/J.NEUROBIOLAGING.2015.10.036.

Cuervo, Ana Maria, Leonidas Stafanis, Ross Fredenburg, Peter T. Lansbury, and David Sulzer. 2004. “Impaired Degradation of Mutant α-Synuclein by Chaperone-Mediated Autophagy.” *Science* 305 (5688): 1292–95. https://doi.org/10.1126/science.1101738.

Dawson, Ted M, Han Seok Ko, and Valina L Dawson. 2010. “Review Genetic Animal Models of Parkinson’s Disease.” https://doi.org/10.1016/j.neuron.2010.04.034.

Deng, Hao, Wei Dong Le, Anthony L. Davidson, Wen Jie Xie, and Joseph Jankovic. 2006. “The LRRK2 I2012T, G2019S and I2020T Mutations Are Not Common in Patients with Essential Tremor.” *Neuroscience Letters* 407 (2): 97–100. https://doi.org/10.1016/J.NEULET.2006.08.012.

Deretic, Vojo. 2011. “Autophagy in Immunity and Cell-Autonomous Defense against Intracellular Microbes.” *Immunological Reviews* 240 (1): 92–104. https://doi.org/10.1111/j.1600-065X.2010.00995.x.

Desai, Varsha G., Ritchie J. Feuers, Ronald W. Hart, and Syed F. Ali. 1996. “MPP(+)-Induced Neurotoxicity in Mouse Is Age-Dependent: Evidenced by the Selective Inhibition of Complexes of Electron Transport.” *Brain Research* 715 (1–2): 1–8. https://doi.org/10.1016/0006-8993(95)01255-9.

Detmer, Scott A., and David C. Chan. 2007. “Complementation between Mouse Mfn1 and Mfn2 Protects Mitochondrial Fusion Defects Caused by CMT2A Disease Mutations.” *The Journal of Cell Biology* 176 (4): 405–14. https://doi.org/10.1083/JCB.200611080.

Dikic, Ivan, and Zvulun Elazar. 2018. “Mechanism and Medical Implications of Mammalian Autophagy.” *Nature Reviews Molecular Cell Biology* 19 (6): 349–64. https://doi.org/10.1038/s41580-018-0003-4.

Dodson, Mark W., Lok K. Leung, Mohiddin Lone, Michael A. Lizzio, and Ming Guo. 2014. “Novel Ethyl Methanesulfonate (EMS)-Induced Null Alleles of the Drosophila Homolog of LRRK2 Reveal a Crucial Role in Endolysosomal Functions and Autophagy in Vivo.” *DMM Disease Models and Mechanisms* 7 (12): 1351–63. https://doi.org/10.1242/dmm.017020.

Dodson, Mark W., Ting Zhang, Changan Jiang, Shengdi Chen, and Ming Guo. 2012. "Roles of the Drosophila LRRK2 Homolog in Rab7-Dependent Lysosomal Positioning." *Human Molecular Genetics* 21 (6): 1350–63. https://doi.org/10.1093/hmg/ddr573.

Doherty, Karen M., and John Hardy. 2013. "Parkin Disease and the Lewy Body Conundrum." *Movement Disorders : Official Journal of the Movement Disorder Society* 28 (6): 702–4. https://doi.org/10.1002/MDS.25486.

Dölle, Christian, Irene Flønes, Gonzalo S. Nido, Hrvoje Miletic, Nelson Osuagwu, Stine Kristoffersen, Peer K. Lilleng, et al. 2016. "Defective Mitochondrial DNA Homeostasis in the Substantia Nigra in Parkinson Disease." *Nature Communications* 7 (November). https://doi.org/10.1038/NCOMMS13548.

Domenico, Angelique di, Giulia Carola, Carles Calatayud, Meritxell Pons-Espinal, Juan Pablo Muñoz, Yvonne Richaud-Patin, Irene Fernandez-Carasa, et al. 2019. "Patient-Specific IPSC-Derived Astrocytes Contribute to Non-Cell-Autonomous Neurodegeneration in Parkinson's Disease." *Stem Cell Reports* 12 (2): 213–29. https://doi.org/10.1016/j.stemcr.2018.12.011.

Dorsey, E. R., R. Constantinescu, J. P. Thompson, K. M. Biglan, R. G. Holloway, K. Kieburtz, F. J. Marshall, et al. 2007. "Projected Number of People with Parkinson Disease in the Most Populous Nations, 2005 through 2030." *Neurology* 68 (5): 384–86. https://doi.org/10.1212/01.wnl.0000247740.47667.03.

Dutheil, Fabien, Philippe Beaune, Christophe Tzourio, Marie Anne Loriot, and Alexis Elbaz. 2010. "Interaction Between ABCB1 and Professional Exposure to Organochlorine Insecticides in Parkinson Disease." *Archives of Neurology* 67 (6): 739–45. https://doi.org/10.1001/ARCHNEUROL.2010.101.

Edmondson, Dale E., Claudia Binda, and Andrea Mattevi. 2007. "Structural Insights into the Mechanism of Amine Oxidation by Monoamine Oxidases A and B." *Archives of Biochemistry and Biophysics* 464 (2): 269–76. https://doi.org/10.1016/j.abb.2007.05.006.

Eguchi, Tomoya, Tomoki Kuwahara, Maria Sakurai, Tadayuki Komori, Tetta Fujimoto, Genta Ito, Shin Ichiro Yoshimura, et al. 2018. "LRRK2 and Its Substrate Rab GTPases Are Sequentially Targeted onto Stressed Lysosomes and Maintain Their Homeostasis." *Proceedings of the National Academy of Sciences of the United States of America* 115 (39): E9115–24. https://doi.org/10.1073/pnas.1812196115.

Ehringer, H., and O. Hornykiewicz. 1960. "[Distribution of Noradrenaline and Dopamine (3-Hydroxytyramine) in the Human Brain and Their Behavior in Diseases of the Extrapyramidal System]." *Klinische Wochenschrift* 38 (24): 1236–39. https://doi.org/10.1007/BF01485901.

Ellis, J. Michael, and Matthew J. Fell. 2017. "Current Approaches to the Treatment of Parkinson's Disease." *Bioorganic and Medicinal Chemistry Letters* 27 (18): 4247–55. https://doi.org/10.1016/j.bmcl.2017.07.075.

Erb, Madalynn L., and Darren J. Moore. 2020. "LRRK2 and the Endolysosomal System in Parkinson's Disease." *Journal of Parkinson's Disease* 10 (4): 1271–91. https://doi.org/10.3233/JPD-202138.

Esmail, Sally, Norbert Kartner, Yeqi Yao, Joo Wan Kim, Reinhart A.F. Reithmeier, and Morris F. Manolson. 2018. “N-Linked Glycosylation of a Subunit Isoforms Is Critical for Vertebrate Vacuolar H+-ATPase (V-ATPase) Biosynthesis.” *Journal of Cellular Biochemistry* 119 (1): 861–75. https://doi.org/10.1002/jcb.26250.

Farré, Jean Claude, and Suresh Subramani. 2004. “Peroxisome Turnover by Micropexophagy: An Autophagy-Related Process.” *Trends in Cell Biology* 14 (9): 515–23. https://doi.org/10.1016/j.tcb.2004.07.014.

Fernandes, Hugo J.R., Elizabeth M. Hartfield, Helen C. Christian, Evangelia Emmanoulidou, Ying Zheng, Heather Booth, Helle Bogetofte, et al. 2016. “ER Stress and Autophagic Perturbations Lead to Elevated Extracellular α-Synuclein in GBA-N370S Parkinson’s IPSC-Derived Dopamine Neurons.” *Stem Cell Reports* 6 (3): 342–56. https://doi.org/10.1016/j.stemcr.2016.01.013.

Fiesel, Fabienne C, Maya Ando, Roman Hudec, Anneliese R Hill, Monica Castanedes-Casey, Thomas R Caulfield, Elisabeth L Moussaud-Lamodière, et al. 2015. “(Patho-)Physiological Relevance of PINK1-Dependent Ubiquitin Phosphorylation.” *EMBO Reports* 16 (9): 1114–30. https://doi.org/10.15252/EMBR.201540514.

Fonzo, Alessio Di, Yah Huei Wu-Chou, Chin Song Lu, Marina Van Doeselaar, Erik J. Simons, Christan F. Rohé, Hsiu Chen Chang, et al. 2006. “A Common Missense Variant in the LRRK2 Gene, Gly2385Arg, Associated with Parkinson’s Disease Risk in Taiwan.” *Neurogenetics* 7 (3): 133–38. https://doi.org/10.1007/S10048-006-0041-5/METRICS.

Frattini, Annalisa, Paul J. Orchard, Cristina Sobacchi, Silvia Giliani, Mario Abinun, Jan P. Mattsson, David J. Keeling, et al. 2000. “Defects in TCIRG1 Subunit of the Vacuolar Proton Pump Are Responsible for a Subset of Human Autosomal Recessive Osteopetrosis.” *Nature Genetics* 25 (3): 343–46. https://doi.org/10.1038/77131.

Friedman, Lauren G, M Lenard Lachenmayer, Jing Wang, Liqiang He, Shibu M Poulose, Masaaki Komatsu, Gay R Holstein, and Zhenyu Yue. 2012. “Disrupted Autophagy Leads to Dopaminergic Axon and Dendrite Degeneration and Promotes Presynaptic Accumulation of ␣-Synuclein and LRRK2 in the Brain” 32 (22): 7585–93. https://doi.org/10.1523/JNEUROSCI.5809-11.2012.

Frost, L. S., A. Dhingra, J. Reyes-Reveles, and K. Boesze-Battaglia. 2017. “The Use of DQ-BSA to Monitor the Turnover of Autophagy-Associated Cargo.” *Methods in Enzymology* 587: 43–54. https://doi.org/10.1016/BS.MIE.2016.09.052.

Funayama, Manabu, Kazuko Hasegawa, Hisayuki Kowa, Masaaki Saito, Shoji Tsuji, and Fumiya Obata. 2002. “A New Locus for Parkinson’s Disease (PARK8) Maps to Chromosome 12p11.2–Q13.1.” *Annals of Neurology* 51 (3): 296–301. https://doi.org/10.1002/ANA.10113.

Funayama, Manabu, Kenji Ohe, Taku Amo, Norihiko Furuya, Junji Yamaguchi, Shinji Saiki, Yuanzhe Li, et al. 2015. “CHCHD2 Mutations in Autosomal Dominant Late-Onset Parkinson’s Disease: A Genome-Wide Linkage and Sequencing Study.” *The Lancet. Neurology* 14 (3): 274–82. https://doi.org/10.1016/S1474-4422(14)70266-2.

Futerman, Anthony H., Joel L. Sussman, Mia Horowitz, Israel Silman, and Ari Zimran. 2004. “New Directions in the Treatment of Gaucher Disease.” *Trends in Pharmacological Sciences* 25 (3): 147–51. https://doi.org/10.1016/j.tips.2004.01.004.

Gaig, Carles, María José Martí, Mario Ezquerra, Maria Jesús Rey, Adriana Cardozo, and Eduardo Tolosa. 2007. “G2019S LRRK2 Mutation Causing Parkinson’s Disease without Lewy Bodies.” *Journal of Neurology, Neurosurgery, and Psychiatry* 78 (6): 626. https://doi.org/10.1136/JNNP.2006.107904.

Galluzzi, Lorenzo, Eric H Baehrecke, Andrea Ballabio, Patricia Boya, José Manuel Bravo-San Pedro, Francesco Cecconi, Augustine M Choi, et al. 2017. “Molecular Definitions of Autophagy and Related Processes.” *The EMBO Journal* 36 (13): 1811–36. https://doi.org/10.15252/EMBJ.201796697.

Galter, Dagmar, Marie Westerlund, Andrea Carmine, Eva Lindqvist, Olof Sydow, and Lars Olson. 2006. “LRRK2 Expression Linked to Dopamine-Innervated Areas.” *Annals of Neurology* 59 (4): 714–19. https://doi.org/10.1002/ana.20808.

Gan-Or, Ziv, Patrick A. Dion, and Guy A. Rouleau. 2015. “Genetic Perspective on the Role of the Autophagy-Lysosome Pathway in Parkinson Disease.” *Autophagy* 11 (9): 1443–57. https://doi.org/10.1080/15548627.2015.1067364.

Gasser, Thomas. 2015. “Usefulness of Genetic Testing in PD and PD Trials: A Balanced Review.” *Journal of Parkinson’s Disease* 5 (2): 209–15. https://doi.org/10.3233/JPD-140507.

Ghislat, Ghita, and Erwin Knecht. 2013. “Ca^{2+}-Sensor Proteins in the Autophagic and Endocytic Traffic.” *Current Protein & Peptide Science* 14 (2): 97–110. http://www.pubmedcentral.nih.gov/articlerender.fcgi?artid=3664516&tool=pmcentrez&rendertype=abstract.

Giaime, Emilie, Youren Tong, Lisa K. Wagner, Yang Yuan, Guodong Huang, and Jie Shen. 2017. “Age-Dependent Dopaminergic Neurodegeneration and Impairment of the Autophagy-Lysosomal Pathway in LRRK-Deficient Mice.” *Neuron* 96 (4): 796-807.e6. https://doi.org/10.1016/j.neuron.2017.09.036.

Giesert, Florian, Andreas Hofmann, Alexander Bürger, Julia Zerle, Karina Kloos, Ulrich Hafen, Luise Ernst, Jingzhong Zhang, Daniela Maria Vogt-Weisenhorn, and Wolfgang Wurst. 2013. “Expression Analysis of Lrrk1, Lrrk2 and Lrrk2 Splice Variants in Mice.” *PLoS ONE* 8 (5). https://doi.org/10.1371/journal.pone.0063778.

Gillardon, F., R. Schmid, and H. Draheim. 2012. “Parkinson’s Disease-Linked Leucine-Rich Repeat Kinase 2(R1441G) Mutation Increases Proinflammatory Cytokine Release from Activated Primary Microglial Cells and Resultant Neurotoxicity.” *Neuroscience* 208: 41–48. https://doi.org/10.1016/j.neuroscience.2012.02.001.

Giménez-Xavier, Pol, Roser Francisco, Francesca Platini, Ricardo Pérez, and Santiago Ambrosio. 2008. “LC3-I Conversion to LC3-II Does Not Necessarily Result in Complete Autophagy.” *International Journal of Molecular Medicine* 22 (6): 781–85. https://doi.org/10.3892/ijmm_00000085.

Gladkova, Christina, Sarah L. Maslen, J. Mark Skehel, and David Komander. 2018. “Mechanism of Parkin Activation by PINK1.” *Nature* 559 (7714): 410–14. https://doi.org/10.1038/S41586-018-0224-X.

Godena, Vinay K., Nicholas Brookes-Hocking, Annekathrin Moller, Gary Shaw, Matthew Oswald, Rosa M. Sancho, Christopher C.J. Miller, Alexander J. Whitworth, and Kurt J. De Vos. 2014. “Increasing Microtubule Acetylation Rescues Axonal Transport and

Locomotor Deficits Caused by LRRK2 Roc-COR Domain Mutations." *Nature Communications* 5. https://doi.org/10.1038/ncomms6245.

Gómez-Suaga, Patricia, Berta Luzón-Toro, Dev Churamani, Ling Zhang, Duncan Bloor-Young, Sandip Patel, Philip G. Woodman, Grant C. Churchill, and Sabine Hilfiker. 2012. "Leucine-Rich Repeat Kinase 2 Regulates Autophagy through a Calcium-Dependent Pathway Involving NAADP." *Human Molecular Genetics* 21 (3): 511–25. https://doi.org/10.1093/hmg/ddr481.

Grossmann, Dajana, Clara Berenguer-Escuder, Axel Chemla, Giuseppe Arena, and Rejko Krüger. 2020. "The Emerging Role of RHOT1/Miro1 in the Pathogenesis of Parkinson's Disease." *Frontiers in Neurology* 11 (September). https://doi.org/10.3389/FNEUR.2020.00587.

Guaitoli, Giambattista, Bernd K. Gilsbach, Francesco Raimondi, and Christian Johannes Gloeckner. 2016. "First Model of Dimeric LRRK2: The Challenge of Unrevealing the Structure of a Multidomain Parkinson's-Associated Protein." *Biochemical Society Transactions* 44 (6): 1635–41. https://doi.org/10.1042/BST20160226.

Han, Jung Min, Seung Jae Jeong, Min Chul Park, Gyuyoup Kim, Nam Hoon Kwon, Hoi Kyoung Kim, Sang Hoon Ha, Sung Ho Ryu, and Sunghoon Kim. 2012. "Leucyl-TRNA Synthetase Is an Intracellular Leucine Sensor for the MTORC1-Signaling Pathway." *Cell* 149 (2): 410–24. https://doi.org/10.1016/j.cell.2012.02.044.

Hardy, John. 2010. "Genetic Analysis of Pathways to Parkinson Disease." *Neuron* 68 (2): 201–6. https://doi.org/10.1016/j.neuron.2010.10.014.

Härtlova, Anetta, Susanne Herbst, Julien Peltier, Angela Rodgers, Orsolya Bilkei-Gorzo, Antony Fearns, Brian D Dill, et al. 2018. " LRRK2 Is a Negative Regulator of Mycobacterium Tuberculosis Phagosome Maturation in Macrophages ." *The EMBO Journal* 37 (12): 1–17. https://doi.org/10.15252/embj.201798694.

Healy, Daniel G., Mario Falchi, Sean S. O'Sullivan, Vincenzo Bonifati, Alexandra Durr, Susan Bressman, Alexis Brice, et al. 2008. "Phenotype, Genotype, and Worldwide Genetic Penetrance of LRRK2-Associated Parkinson's Disease: A Case-Control Study." *The Lancet Neurology* 7 (7): 583–90. https://doi.org/10.1016/S1474-4422(08)70117-0.

Healy, Daniel G., Nicholas W. Wood, and Anthony H.V. Schapira. 2008. "Test for LRRK2 Mutations in Patients with Parkinson's Disease." *Practical Neurology* 8 (6): 381–85. https://doi.org/10.1136/jnnp.2008.162420.

Heikkila, Richard E., Lawrence Manzino, Felicitas S. Cabbat, and Roger C. Duvoisin. 1984. "Protection against the Dopaminergic Neurotoxicity of 1-Methyl-4-Phenyl-1,2,5,6-Tetrahydropyridine by Monoamine Oxidase Inhibitors." *Nature* 311 (5985): 467–69. https://doi.org/10.1038/311467A0.

Helwig, Michael, Michael Klinkenberg, Raffaella Rusconi, Ruth E. Musgrove, Nour K. Majbour, Omar M.A. El-Agnaf, Ayse Ulusoy, and Donato A. Di Monte. 2016. "Brain Propagation of Transduced α-Synuclein Involves Non-Fibrillar Protein Species and Is Enhanced in α-Synuclein Null Mice." *Brain* 139 (3): 856–70. https://doi.org/10.1093/BRAIN/AWV376.

Henderson, Michael X., Medha Sengupta, Ian McGeary, Bin Zhang, Modupe F. Olufemi, Hannah Brown, John Q. Trojanowski, and Virginia M. Y. Lee. 2019. "LRRK2

Inhibition Does Not Impart Protection from α-Synuclein Pathology and Neuron Death in Non-Transgenic Mice." *Acta Neuropathologica Communications* 7 (1): 1–12. https://doi.org/10.1186/s40478-019-0679-5.

Henry, Anastasia G., Soheil Aghamohammadzadeh, Harry Samaroo, Yi Chen, Kewa Mou, Elie Needle, and Warren D. Hirst. 2015. "Pathogenic LRRK2 Mutations, through Increased Kinase Activity, Produce Enlarged Lysosomes with Reduced Degradative Capacity and Increase ATP13A2 Expression." *Human Molecular Genetics* 24 (21): 6013–28. https://doi.org/10.1093/hmg/ddv314.

Higashi, Shinji, Darren J. Moore, Ryoko Yamamoto, Michiko Minegishi, Kiyoshi Sato, Takashi Togo, Omi Katsuse, et al. 2009. "Abnormal Localization of Leucine-Rich Repeat Kinase 2 to the Endosomal-Lysosomal Compartment in Lewy Body Disease." *Journal of Neuropathology and Experimental Neurology* 68 (9): 994–1005. https://doi.org/10.1097/NEN.0b013e3181b44ed8.

Hnasko, Thomas S., and Robert H. Edwards. 2012. "Neurotransmitter Corelease: Mechanism and Physiological Role." *Annual Review of Physiology* 74: 225–43. https://doi.org/10.1146/ANNUREV-PHYSIOL-020911-153315.

Ho, Dong Hwan, A. Reum Je, Haejin Lee, Ilhong Son, Hee Seok Kweon, Hyung Gun Kim, and Wongi Seol. 2018. "LRRK2 Kinase Activity Induces Mitochondrial Fission in Microglia via Drp1 and Modulates Neuroinflammation." *Experimental Neurobiology* 27 (3): 171–80. https://doi.org/10.5607/en.2018.27.3.171.

Ho, Dong Hwan, Hyejung Kim, Daleum Nam, Hyuna Sim, Janghwan Kim, Hyung Gun Kim, Ilhong Son, and Wongi Seol. 2018. "LRRK2 Impairs Autophagy by Mediating Phosphorylation of Leucyl-TRNA Synthetase." *Cell Biochemistry and Function* 36 (8): 431–42. https://doi.org/10.1002/cbf.3364.

Ho, Philip Wing Lok, Chi Ting Leung, Huifang Liu, Shirley Yin Yu Pang, Colin Siu Chi Lam, Jiawen Xian, Lingfei Li, Michelle Hiu Wai Kung, David Boyer Ramsden, and Shu Leong Ho. 2019. "Age-Dependent Accumulation of Oligomeric SNCA/α-Synuclein from Impaired Degradation in Mutant LRRK2 Knockin Mouse Model of Parkinson Disease: Role for Therapeutic Activation of Chaperone-Mediated Autophagy (CMA)." *Autophagy* 0 (0): 1–24. https://doi.org/10.1080/15548627.2019.1603545.

Hockey, L. N., B. S. Kilpatrick, Emily R. Eden, Yaping Lin-Moshier, G. Cristina Brailoiu, Eugen Brailoiu, Clare E. Futter, Anthony H. Schapira, Jonathan S. Marchant, and Sandip Patel. 2015. "Dysregulation of Lysosomal Morphology by Pathogenic LRRK2 Is Corrected by TPC2 Inhibition." *Journal of Cell Science* 128 (2): 232–38. https://doi.org/10.1242/jcs.164152.

Hou, Xu, Fabienne C. Fiesel, Dominika Truban, Monica Castanedes Casey, Wen lang Lin, Alexandra I. Soto, Pawel Tacik, et al. 2018. "Age- and Disease-Dependent Increase of the Mitophagy Marker Phospho-Ubiquitin in Normal Aging and Lewy Body Disease." *Autophagy* 14 (8): 1404–18. https://doi.org/10.1080/15548627.2018.1461294.

Hsieh, Chung Han, Li Li, Roeland Vanhauwaert, Kong T. Nguyen, Mary D. Davis, Guojun Bu, Zbigniew K. Wszolek, and Xinnan Wang. 2019. "Miro1 Marks Parkinson's Disease Subset and Miro1 Reducer Rescues Neuron Loss in Parkinson's Models." *Cell Metabolism* 30 (6): 1131-1140.e7. https://doi.org/10.1016/J.CMET.2019.08.023.

Hsieh, Chung Han, Atossa Shaltouki, Ashley E. Gonzalez, Alexandre Bettencourt da Cruz, Lena F. Burbulla, Erica St. Lawrence, Birgitt Schüle, Dimitri Krainc, Theo D. Palmer, and Xinnan Wang. 2016. “Functional Impairment in Miro Degradation and Mitophagy Is a Shared Feature in Familial and Sporadic Parkinson’s Disease.” *Cell Stem Cell* 19 (6): 709–24. https://doi.org/10.1016/j.stem.2016.08.002.

Hu, D., Jian-Yi Niu, Jing Xiong, Shu-Ke Nie, Fei Zeng, and Zhao-Hui Zhang. 2018. “LRRK2 G2019S Mutation Inhibits Degradation of α-Synuclein in an In Vitro Model of Parkinson’s Disease.” *Current Medical Science* 38 (6): 1012–17. https://doi.org/10.1007/s11596-018-1977-z.

Hu, Yong Bo, Eric B. Dammer, Ru Jing Ren, and Gang Wang. 2015. “The Endosomal-Lysosomal System: From Acidification and Cargo Sorting to Neurodegeneration.” *Translational Neurodegeneration* 4 (1): 1–10. https://doi.org/10.1186/s40035-015-0041-1.

Huang, Chi Hsien, Chi Wei Lin, Yi Che Lee, Chih Yuan Huang, Ru Yi Huang, Yi Cheng Tai, Kuo Wei Wang, San Nan Yang, Yuan Ting Sun, and Hao Kuang Wang. 2018. “Is Traumatic Brain Injury a Risk Factor for Neurodegeneration? A Meta-Analysis of Population-Based Studies.” *BMC Neurology* 18 (1). https://doi.org/10.1186/S12883-018-1187-0.

Ikeda, Aya, Kenya Nishioka, Hongrui Meng, Masashi Takanashi, Iwao Hasegawa, Tsuyoshi Inoshita, Kahori Shiba-Fukushima, et al. 2019. “Mutations in CHCHD2 Cause α-Synuclein Aggregation.” *Human Molecular Genetics* 28 (23): 3895–3911. https://doi.org/10.1093/HMG/DDZ241.

Ishizawa, Takashi, Petri Mattila, Peter Davies, Dengshun Wang, and Dennis W. Dickson. 2003. “Colocalization of Tau and Alpha-Synuclein Epitopes in Lewy Bodies.” *Journal of Neuropathology & Experimental Neurology* 62 (4): 389–97. https://doi.org/10.1093/JNEN/62.4.389.

Ito, Kyohei, Miho Araki, Yuta Katai, Yuki Nishimura, Sota Imotani, Haruki Inoue, Genta Ito, and Taisuke Tomita. 2023. “Pathogenic LRRK2 Compromises the Subcellular Distribution of Lysosomes in a Rab12-RILPL1-Dependent Manner.” *The FASEB Journal* 37 (5): e22930. https://doi.org/10.1096/FJ.202200780RR.

Janezic, Stephanie, Sarah Threlfell, Paul D. Dodson, Megan J. Dowie, Tonya N. Taylor, Dawid Potgieter, Laura Parkkinen, et al. 2013. “Deficits in Dopaminergic Transmission Precede Neuron Loss and Dysfunction in a New Parkinson Model.” *Proceedings of the National Academy of Sciences of the United States of America* 110 (42). https://doi.org/10.1073/PNAS.1309143110/SUPPL_FILE/SM02.MPG.

Jankovic, Joseph, and Eng King Tan. 2020. “Parkinson’s Disease: Etiopathogenesis and Treatment.” *Journal of Neurology, Neurosurgery, and Psychiatry* 91 (8): 795–808. https://doi.org/10.1136/JNNP-2019-322338.

Jarazo, Javier, Kyriaki Barmpa, Jennifer Modamio, Cláudia Saraiva, Sònia Sabaté-Soler, Isabel Rosety, Anne Griesbeck, et al. 2022. “Parkinson’s Disease Phenotypes in Patient Neuronal Cultures and Brain Organoids Improved by 2-Hydroxypropyl-β-Cyclodextrin Treatment.” *Movement Disorders* 37 (1): 80–94. https://doi.org/10.1002/MDS.28810.

Jin, Seok Min, and Richard J. Youle. 2013. “The Accumulation of Misfolded Proteins in the Mitochondrial Matrix Is Sensed by PINK1 to Induce PARK2/Parkin-Mediated

Mitophagy of Polarized Mitochondria." *Autophagy* 9 (11): 1750–57. https://doi.org/10.4161/AUTO.26122.

Jodko-Piorecka, Katarzyna, and Grzegorz Litwinienko. 2013. "First Experimental Evidence of Dopamine Interactions with Negatively Charged Model Biomembranes." https://doi.org/10.1021/cn4000633.

Johnson, Michaela E., Benjamin Stecher, Viviane Labrie, Lena Brundin, and Patrik Brundin. 2019. "Triggers, Facilitators, and Aggravators: Redefining Parkinson's Disease Pathogenesis." *Trends in Neurosciences* 42 (1): 4–13. https://doi.org/10.1016/j.tins.2018.09.007.

Juárez-Flores, Diana Luz, Ingrid González-Casacuberta, Mario Ezquerra, María Bañó, Francesc Carmona-Pontaque, Marc Catalán-García, Mariona Guitart-Mampel, et al. 2018. "Exhaustion of Mitochondrial and Autophagic Reserve May Contribute to the Development of LRRK2 G2019S -Parkinson's Disease." *Journal of Translational Medicine* 16 (1): 1–13. https://doi.org/10.1186/s12967-018-1526-3.

Kachergus, Jennifer, Ignacio F Mata, Mary Hulihan, Julie P Taylor, Sarah Lincoln, Jan Aasly, J Mark Gibson, et al. 2005. "Identification of a Novel LRRK2 Mutation Linked to Autosomal Dominant Parkinsonism: Evidence of a Common Founder across European Populations." *Am. J. Hum. Genet* 76: 672–80.

Kalia, Lorraine V., and Anthony E. Lang. 2015. "Parkinson's Disease." *Lancet (London, England)* 386 (9996): 896–912. https://doi.org/10.1016/S0140-6736(14)61393-3.

Kalia, Raghav, Ray Yu Ruei Wang, Ali Yusuf, Paul V. Thomas, David A. Agard, Janet M. Shaw, and Adam Frost. 2018. "Structural Basis of Mitochondrial Receptor Binding and Constriction by DRP1." *Nature* 558 (7710): 401–5. https://doi.org/10.1038/S41586-018-0211-2.

Kalogeropulou, Alexia F., Jing Zhao, Marc F. Bolliger, Anna Memou, Shreya Narasimha, Tyler P. Molitor, William H. Wilson, Hardy J. Rideout, and R. Jeremy Nichols. 2018. "P62/SQSTM1 Is a Novel Leucine-Rich Repeat Kinase 2 (LRRK2) Substrate That Enhances Neuronal Toxicity." *Biochemical Journal* 475 (7): 1271–93. https://doi.org/10.1042/BCJ20170699.

Kamada, Yoshiaki, Tomoko Funakoshi, Takahiro Shintani, Kazuya Nagano, Mariko Ohsumi, and Yoshinori Ohsumi. 2000. "Tor-Mediated Induction of Autophagy via an Apg1 Protein Kinase Complex." *Journal of Cell Biology* 150 (6): 1507–13. https://doi.org/10.1083/jcb.150.6.1507.

Kandimalla, Ramesh, and P. Hemachandra Reddy. 2016. "Multiple Faces of Dynamin-Related Protein 1 and Its Role in Alzheimer's Disease Pathogenesis." *Biochimica et Biophysica Acta (BBA) - Molecular Basis of Disease* 1862 (4): 814–28. https://doi.org/10.1016/J.BBADIS.2015.12.018.

Karet, Fiona E., Karin E. Finberg, Raoul D. Nelson, Ahmet Nayir, Hilal Mocan, Sami A. Sanjad, Juan Rodriguez-Soriano, et al. 1999. "Mutations in the Gene Encoding B1 Subunit of H+-ATPase Cause Renal Tubular Acidosis with Sensorineural Deafness." *Nature Genetics* 21 (1): 84–90. https://doi.org/10.1038/5022.

Karuppagounder, Senthilkumar S., Yulan Xiong, Yunjong Lee, Maeve C. Lawless, Donghyun Kim, Emily Nordquist, Ian Martin, et al. 2016. "LRRK2 G2019S Transgenic Mice Display Increased Susceptibility to 1-Methyl-4-Phenyl-1,2,3,6-

Tetrahydropyridine (MPTP)-Mediated Neurotoxicity." *Journal of Chemical Neuroanatomy* 76 (October): 90–97. https://doi.org/10.1016/j.jchemneu.2016.01.007.

Kawamoto, Yasuhiro, Ichiro Akiguchi, Shinichi Nakamura, Yasuyuki Honjyo, Hiroshi Shibasaki, and Herbert Budka. 2002. "14-3-3 Proteins in Lewy Bodies in Parkinson Disease and Diffuse Lewy Body Disease Brains." *Journal of Neuropathology & Experimental Neurology* 61 (3): 245–53. https://doi.org/10.1093/JNEN/61.3.245.

Kett, Lauren R., and William T. Dauer. 2012. "Leucine-Rich Repeat Kinase 2 for Beginners: Six Key Questions." *Cold Spring Harbor Perspectives in Medicine* 2 (3). https://doi.org/10.1101/CSHPERSPECT.A009407.

Khalaf, Ossama, Bruno Fauvet, Abid Oueslati, Igor Dikiy, Anne Laure Mahul-Mellier, Francesco Simone Ruggeri, Martial K. Mbefo, et al. 2014. "The H50Q Mutation Enhances α-Synuclein Aggregation, Secretion, and Toxicity." *The Journal of Biological Chemistry* 289 (32): 21856–76. https://doi.org/10.1074/JBC.M114.553297.

Kim, Hongwon, Hyeok Ju Park, Hwan Choi, Yujung Chang, Hanseul Park, Jaein Shin, Junyeop Kim, Christopher J. Lengner, Yong Kyu Lee, and Jongpil Kim. 2019. "Modeling G2019S-LRRK2 Sporadic Parkinson's Disease in 3D Midbrain Organoids." *Stem Cell Reports* 12 (3): 518–31. https://doi.org/10.1016/j.stemcr.2019.01.020.

Kimura, Tomonori, Ashish Jain, Seong Won Choi, Michael A. Mandell, Kate Schroder, Terje Johansen, and Vojo Deretic. 2015. "TRIM-Mediated Precision Autophagy Targets Cytoplasmic Regulators of Innate Immunity." *Journal of Cell Biology* 210 (6): 973–89. https://doi.org/10.1083/jcb.201503023.

Kitada, Tohru, Shuichi Asakawa, Nobutaka Hattori, Hiroto Matsumine, Yasuhiro Yamamura, Shinsei Minoshima, Masayuki Yokochi, Yoshikuni Mizuno, and Nobuyoshi Shimizu. 1998. "Mutations in the Parkin Gene Cause Autosomal Recessive Juvenile Parkinsonism." *Nature* 392 (6676): 605–8. https://doi.org/10.1038/33416.

Klein, C., and A. Westenberger. 2012. "Genetics of Parkinson's Disease." *Cold Spring Harbor Perspectives in Medicine* 2 (1): a008888–a008888. https://doi.org/10.1101/cshperspect.a008888.

Klionsky, Daniel J., Amal Kamal Abdel-Aziz, Sara Abdelfatah, Mahmoud Abdellatif, Asghar Abdoli, Steffen Abel, Hagai Abeliovich, et al. 2021. "Guidelines for the Use and Interpretation of Assays for Monitoring Autophagy (4th Edition)1." *Autophagy* 17 (1): 1–382. https://doi.org/10.1080/15548627.2020.1797280.

Klionsky, Daniel J., Kotb Abdelmohsen, Akihisa Abe, Md Joynal Abedin, Hagai Abeliovich, Abraham Acevedo Arozena, Hiroaki Adachi, et al. 2016. "Guidelines for the Use and Interpretation of Assays for Monitoring Autophagy (3rd Edition)." *Autophagy* 12 (1): 1–222. https://doi.org/10.1080/15548627.2015.1100356.

Kluss, Jillian H., Adamantios Mamais, and Mark R. Cookson. 2019. "LRRK2 Links Genetic and Sporadic Parkinson's Disease." *Biochemical Society Transactions* 47 (2): 651–61. https://doi.org/10.1042/BST20180462.

Kojima, Waka, Yuki Kujuro, Kei Okatsu, Queliconi Bruno, Fumika Koyano, Mayumi Kimura, Koji Yamano, Keiji Tanaka, and Noriyuki Matsuda. 2016. "Unexpected Mitochondrial Matrix Localization of Parkinson's Disease-Related DJ-1 Mutants but

Not Wild-Type DJ-1." *Genes to Cells : Devoted to Molecular & Cellular Mechanisms* 21 (7): 772–88. https://doi.org/10.1111/GTC.12382.

Koopman, Werner J.H., Sjoerd Verkaart, Henk Jan Visch, Francois H. Van Der Westhuizen, Michael P. Murphy, Lambertus W.P.J. Van Den Heuvel, Jan A.M. Smeitink, and Peter H.G.M. Willems. 2005. "Inhibition of Complex I of the Electron Transport Chain Causes O2-. -Mediated Mitochondrial Outgrowth." *American Journal of Physiology. Cell Physiology* 288 (6). https://doi.org/10.1152/AJPCELL.00607.2004.

Kordower, Jeffrey H., Yaping Chu, Robert A. Hauser, Thomas B. Freeman, and C. Warren Olanow. 2008a. "Lewy Body-like Pathology in Long-Term Embryonic Nigral Transplants in Parkinson's Disease." *Nature Medicine* 14 (5): 504–6. https://doi.org/10.1038/NM1747.

Kordower, Jeffrey H., Yaping Chu, Robert A. Hauser, C. Warren Olanow, and Thomas B. Freeman. 2008b. "Transplanted Dopaminergic Neurons Develop PD Pathologic Changes: A Second Case Report." *Movement Disorders : Official Journal of the Movement Disorder Society* 23 (16): 2303–6. https://doi.org/10.1002/MDS.22369.

Korecka, Joanna A., Ria Thomas, Dan P. Christensen, Anthony J. Hinrich, Eliza J. Ferrari, Simon A. Levy, Michelle L. Hastings, Penelope J. Hallett, and Ole Isacson. 2019. "Mitochondrial Clearance and Maturation of Autophagosomes Are Compromised in LRRK2 G2019S Familial Parkinson's Disease Patient Fibroblasts." *Human Molecular Genetics* 28 (19): 3232–43. https://doi.org/10.1093/hmg/ddz126.

Kornak, Uwe, Ellen Reynders, Aikaterini Dimopoulou, Jeroen Van Reeuwijk, Bjoern Fischer, Anna Rajab, Birgit Budde, et al. 2008. "Impaired Glycosylation and Cutis Laxa Caused by Mutations in the Vesicular H+-ATPase Subunit ATP6V0A2." *Nature Genetics* 40 (1): 32–34. https://doi.org/10.1038/NG.2007.45.

Korvatska, Olena, Nicholas S. Strand, Jason D. Berndt, Tim Strovas, Dong Hui Chen, James B. Leverenz, Konstantin Kiianitsa, et al. 2013. "Altered Splicing of ATP6AP2 Causes X-Linked Parkinsonism with Spasticity (XPDS)." *Human Molecular Genetics* 22 (16): 3259–68. https://doi.org/10.1093/HMG/DDT180.

Kriks, Sonja, Jae Won Shim, Jinghua Piao, Yosif M. Ganat, Dustin R. Wakeman, Zhong Xie, Luis Carrillo-Reid, et al. 2011. "Dopamine Neurons Derived from Human ES Cells Efficiently Engraft in Animal Models of Parkinson's Disease." *Nature* 480 (7378): 547–51. https://doi.org/10.1038/NATURE10648.

Lang, Charmaine, Kieran R. Campbell, Brent J. Ryan, Phillippa Carling, Moustafa Attar, Jane Vowles, Olga V. Perestenko, et al. 2019. "Single-Cell Sequencing of IPSC-Dopamine Neurons Reconstructs Disease Progression and Identifies HDAC4 as a Regulator of Parkinson Cell Phenotypes." *Cell Stem Cell* 24 (1): 93-106.e6. https://doi.org/10.1016/J.STEM.2018.10.023.

Langston, J. William, Ian Irwin, Elizabeth B. Langston, and Lysia S. Forno. 1984. "1-Methyl-4-Phenylpyridinium Ion (MPP+): Identification of a Metabolite of MPTP, a Toxin Selective to the Substantia Nigra." *Neuroscience Letters* 48 (1): 87–92. https://doi.org/10.1016/0304-3940(84)90293-3.

Lee, He Jin, Eun Duk Cho, Kyung Won Lee, Jung Hyun Kim, Ssang Goo Cho, and Seung Jae Lee. 2013. "Autophagic Failure Promotes the Exocytosis and Intercellular Transfer of α-Synuclein." *Experimental and Molecular Medicine* 45 (5): 1–9. https://doi.org/10.1038/emm.2013.45.

Lee, Heyne, William S. James, and Sally A. Cowley. 2017. “LRRK2 in Peripheral and Central Nervous System Innate Immunity: Its Link to Parkinson’s Disease.” *Biochemical Society Transactions* 45 (1): 131–39. https://doi.org/10.1042/BST20160262.

Lee, Jang Won, and Jason R. Cannon. 2015. “LRRK2 Mutations and Neurotoxicant Susceptibility.” *Experimental Biology and Medicine (Maywood, N.J.)* 240 (6): 752–59. https://doi.org/10.1177/1535370215579162.

Lee, Jang Won, Victor Tapias, Roberto Di Maio, J. Timothy Greenamyre, and Jason R. Cannon. 2015. “Behavioral, Neurochemical, and Pathological Alterations in BAC Transgenic G2019S LRRK2 Rats.” *Neurobiology of Aging* 36 (1): 505. https://doi.org/10.1016/J.NEUROBIOLAGING.2014.07.011.

Lee, Ju Hyun, W. Haung Yu, Asok Kumar, Sooyeon Lee, Panaiyur S. Mohan, Corrinne M. Peterhoff, Devin M. Wolfe, et al. 2010. “Lysosomal Proteolysis and Autophagy Require Presenilin 1 and Are Disrupted by Alzheimer-Related PS1 Mutations.” *Cell* 141 (7): 1146–58. https://doi.org/10.1016/J.CELL.2010.05.008.

Leverenz, James B., Imran Umar, Qing Wang, Thomas J. Montine, Pamela J. McMillan, Debby W. Tsuang, Jinghua Jin, et al. 2007. “Proteomic Identification of Novel Proteins in Cortical Lewy Bodies.” *Brain Pathology* 17 (2): 139–45. https://doi.org/10.1111/J.1750-3639.2007.00048.X.

Lewis, Patrick A., Elisa Greggio, Alexandra Beilina, Shushant Jain, Acacia Baker, and Mark R. Cookson. 2007. “The R1441C Mutation of LRRK2 Disrupts GTP Hydrolysis.” *Biochemical and Biophysical Research Communications* 357 (3): 668–71. https://doi.org/10.1016/j.bbrc.2007.04.006.

Lewitt, Peter A. 2015. “Levodopa Therapy for Parkinson’s Disease: Pharmacokinetics and Pharmacodynamics.” *Movement Disorders* 30 (1): 64–72. https://doi.org/10.1002/mds.26082.

Li, Guoliang, Jingyi Yang, Chunyuan Yang, Minglu Zhu, Yan Jin, Michael A. McNutt, and Yuxin Yin. 2018. “PTENα Regulates Mitophagy and Maintains Mitochondrial Quality Control.” *Autophagy* 14 (10): 1742–60. https://doi.org/10.1080/15548627.2018.1489477.

Li, Hongyu, Ahrom Ham, Thong Chi Ma, Sheng Han Kuo, Ellen Kanter, Donghoon Kim, Han Seok Ko, et al. 2019. “Mitochondrial Dysfunction and Mitophagy Defect Triggered by Heterozygous GBA Mutations.” *Autophagy* 15 (1): 113–30. https://doi.org/10.1080/15548627.2018.1509818.

Li, Jia Yi, Elisabet Englund, Janice L. Holton, Denis Soulet, Peter Hagell, Andrew J. Lees, Tammaryn Lashley, et al. 2008. “Lewy Bodies in Grafted Neurons in Subjects with Parkinson’s Disease Suggest Host-to-Graft Disease Propagation.” *Nature Medicine* 14 (5): 501–3. https://doi.org/10.1038/NM1746.

Li, Minghui, Wei K. Zhang, Nicole M. Benvin, Xiaoyuan Zhou, Deyuan Su, Huan Li, Shu Wang, et al. 2017. “Structural Basis of Dual Ca 2+ /PH Regulation of the Endolysosomal TRPML1 Channel.” *Nature Structural and Molecular Biology* 24 (3): 205–13. https://doi.org/10.1038/nsmb.3362.

Li, Xianting, Jyoti C. Patel, Jing Wang, Marat V. Avshalumov, Charles Nicholson, Joseph D. Buxbaum, Gregory A. Elder, Margaret E. Rice, and Zhenyu Yue. 2010. “Enhanced

Striatal Dopamine Transmission and Motor Performance with LRRK2 Overexpression in Mice Is Eliminated by Familial Parkinson's Disease Mutation G2019S." *Journal of Neuroscience* 30 (5): 1788–97. https://doi.org/10.1523/JNEUROSCI.5604-09.2010.

Li, Yanping, Wencheng Liu, Tinmarla F. Oo, Lei Wang, Yi Tang, Vernice Jackson-Lewis, Chun Zhou, et al. 2009. "Mutant LRRK2R1441G BAC Transgenic Mice Recapitulate Cardinal Features of Parkinson's Disease." *Nature Neuroscience* 12 (7): 826–28. https://doi.org/10.1038/nn.2349.

Liu, Huifang, Philip Wing Lok Ho, Chi Ting Leung, Shirley Yin Yu Pang, Eunice Eun Seo Chang, Zoe Yuen Kiu Choi, Michelle Hiu Wai Kung, David Boyer Ramsden, and Shu Leong Ho. 2021. "Aberrant Mitochondrial Morphology and Function Associated with Impaired Mitophagy and DNM1L-MAPK/ERK Signaling Are Found in Aged Mutant Parkinsonian LRRK2 R1441G Mice." *Autophagy* 17 (10): 3196–3220. https://doi.org/10.1080/15548627.2020.1850008.

Liu, Wei Jing, Lin Ye, Wei Fang Huang, Lin Jie Guo, Zi Gan Xu, Hong Luan Wu, Chen Yang, and Hua Feng Liu. 2016. "P62 Links the Autophagy Pathway and the Ubiqutin-Proteasome System Upon Ubiquitinated Protein Degradation." *Cellular and Molecular Biology Letters* 21 (1): 1–14. https://doi.org/10.1186/s11658-016-0031-z.

Liu, Yi Ting, Xiaoping Huang, Diana Nguyen, Mario K. Shammas, Beverly P. Wu, Eszter Dombi, Danielle A. Springer, Joanna Poulton, Shiori Sekine, and Derek P. Narendra. 2020. "Loss of CHCHD2 and CHCHD10 Activates OMA1 Peptidase to Disrupt Mitochondrial Cristae Phenocopying Patient Mutations." *Human Molecular Genetics* 29 (9): 1547–67. https://doi.org/10.1093/HMG/DDAA077.

Lu, Jiahong, Mingyue Wu, and Zhenyu Yue. 2020. "Autophagy and Parkinson's Disease." *Advances in Experimental Medicine and Biology* 1207: 21–51. https://doi.org/10.1007/978-981-15-4272-5_2.

MacLeod, David A., Herve Rhinn, Tomoki Kuwahara, Ari Zolin, Gilbert Di Paolo, Brian D. MacCabe, Karen S. Marder, et al. 2013. "RAB7L1 Interacts with LRRK2 to Modify Intraneuronal Protein Sorting and Parkinson's Disease Risk." *Neuron* 77 (3): 425–39. https://doi.org/10.1016/j.neuron.2012.11.033.

MacLeod, David, Julia Dowman, Rachel Hammond, Thomas Leete, Keiichi Inoue, and Asa Abeliovich. 2006. "The Familial Parkinsonism Gene LRRK2 Regulates Neurite Process Morphology." *Neuron* 52 (4): 587–93. https://doi.org/10.1016/j.neuron.2006.10.008.

Madureira, Marta, Natalie Connor-Robson, and Richard Wade-Martins. 2020. "'LRRK2: Autophagy and Lysosomal Activity.'" *Frontiers in Neuroscience* 14 (May). https://doi.org/10.3389/FNINS.2020.00498.

Majumdar, Amitabha, Estibaliz Capetillo-Zarate, Dana Cruz, Gunnar K. Gouras, and Frederick R. Maxfield. 2011. "Degradation of Alzheimer's Amyloid Fibrils by Microglia Requires Delivery of ClC-7 to Lysosomes." *Molecular Biology of the Cell* 22 (10): 1664–76. https://doi.org/10.1091/MBC.E10-09-0745.

Malpartida, Ana Belen, Matthew Williamson, Derek P. Narendra, Richard Wade-Martins, and Brent J. Ryan. 2021. "Mitochondrial Dysfunction and Mitophagy in Parkinson's Disease: From Mechanism to Therapy." *Trends in Biochemical Sciences* 46 (4): 329–43. https://doi.org/10.1016/j.tibs.2020.11.007.

Mamais, Adamantios, Claudia Manzoni, Iqra Nazish, Charles Arber, Berkiye Sonustun, Selina Wray, Thomas T. Warner, Mark R. Cookson, Patrick A. Lewis, and Rina Bandopadhyay. 2018. “Analysis of Macroautophagy Related Proteins in G2019S LRRK2 Parkinson’s Disease Brains with Lewy Body Pathology.” *Brain Research* 1701: 75–84. https://doi.org/10.1016/j.brainres.2018.07.023.

Mantri, S., James F. Morley, and Andrew D. Siderowf. 2019. “The Importance of Preclinical Diagnostics in Parkinson Disease.” *Parkinsonism & Related Disorders* 64 (July): 20–28. https://doi.org/10.1016/J.PARKRELDIS.2018.09.011.

Manzoni, Claudia. 2017. “The LRRK2-Macroautophagy Axis and Its Relevance to Parkinson’s Disease.” *Biochemical Society Transactions* 45 (1): 155–62. https://doi.org/10.1042/BST20160265.

Manzoni, Claudia, and Patrick Lewis. 2017. “LRRK2 and Autophagy.” In *Leucine-Rich Repeat 2 (LRRK2)*, edited by Hardy J. Rideout, 14:89–105. Springer International Publishing AG. https://doi.org/10.1007/978-3-319-49969-7_5.

Manzoni, Claudia, Adamantios Mamais, Sybille Dihanich, Rosella Abeti, Marc P.M. Soutar, Helene Plun-Favreau, Paola Giunti, Sharon A. Tooze, Rina Bandopadhyay, and Patrick A. Lewis. 2013. “Inhibition of LRRK2 Kinase Activity Stimulates Macroautophagy.” *Biochimica et Biophysica Acta - Molecular Cell Research* 1833 (12): 2900–2910. https://doi.org/10.1016/j.bbamcr.2013.07.020.

Manzoni, Claudia, Adamantios Mamais, Sybille Dihanich, Phillip McGoldrick, Michael J. Devine, Julia Zerle, Eleanna Kara, et al. 2013. “Pathogenic Parkinson’s Disease Mutations across the Functional Domains of LRRK2 Alter the Autophagic/Lysosomal Response to Starvation.” *Biochemical and Biophysical Research Communications* 441 (4): 862–66. https://doi.org/10.1016/j.bbrc.2013.10.159.

Manzoni, Claudia, Adamantios Mamais, Sybille Dihanich, Marc P.M. Soutar, Helene Plun-Favreau, Rina Bandopadhyay, Rosella Abeti, et al. 2018. “MTOR Independent Alteration in ULK1 Ser758 Phosphorylation Following Chronic LRRK2 Kinase Inhibition.” *Bioscience Reports* 38 (2): 1–10. https://doi.org/10.1042/BSR20171669.

Manzoni, Claudia, Adamantios Mamais, Dorien A. Roosen, Sybille Dihanich, Marc P.M. Soutar, Helene Plun-Favreau, Rina Bandopadhyay, et al. 2016. “MTOR Independent Regulation of Macroautophagy by Leucine Rich Repeat Kinase 2 via Beclin-1.” *Scientific Reports* 6 (October): 1–10. https://doi.org/10.1038/srep35106.

Marek K., et al. “The Parkinson progression marker initiative (PPMI) Prog”. Neurobiol. 2011;95:629–635. doi: 10.1016/j.pneurobio.2011.09.005

Markesbery, William R., Gregory A. Jicha, Huaichen Liu, and Frederick A. Schmitt. 2009. “Lewy Body Pathology in Normal Elderly Subjects.” *Journal of Neuropathology & Experimental Neurology* 68 (7): 816–22. https://doi.org/10.1097/NEN.0B013E3181AC10A7.

Marras, Connie, and Anthony Lang. 2013. “Parkinson’s Disease Subtypes: Lost in Translation?” *Journal of Neurology, Neurosurgery, and Psychiatry* 84 (4): 409–15. https://doi.org/10.1136/JNNP-2012-303455.

Mauthe, Mario, Idil Orhon, Cecilia Rocchi, Xingdong Zhou, Morten Luhr, Kerst Jan Hijlkema, Robert P. Coppes, Nikolai Engedal, Muriel Mari, and Fulvio Reggiori. 2018. “Chloroquine Inhibits Autophagic Flux by Decreasing Autophagosome-Lysosome

Fusion." *Autophagy* 14 (8): 1435–55. https://doi.org/10.1080/15548627.2018.1474314.

McGlinchey, Ryan P, and Jennifer C Lee. 2015. "Cysteine Cathepsins Are Essential in Lysosomal Degradation of α-Synuclein." *Proceedings of the National Academy of Sciences of the United States of America* 112 (30): 9322–27. https://doi.org/10.1073/pnas.1500937112.

McWilliams, Thomas G., Alan R. Prescott, George F.G. Allen, Jevgenia Tamjar, Michael J. Munson, Calum Thomson, Miratul M.K. Muqit, and Ian G. Ganley. 2016. "Mito-QC Illuminates Mitophagy and Mitochondrial Architecture in Vivo." *Journal of Cell Biology* 214 (3): 333–45. https://doi.org/10.1083/JCB.201603039/VIDEO-3.

McWilliams, Thomas G., Alan R. Prescott, Lambert Montava-Garriga, Graeme Ball, François Singh, Erica Barini, Miratul M.K. Muqit, Simon P. Brooks, and Ian G. Ganley. 2018. "Basal Mitophagy Occurs Independently of PINK1 in Mouse Tissues of High Metabolic Demand." *Cell Metabolism* 27 (2): 439-449.e5. https://doi.org/10.1016/J.CMET.2017.12.008.

Meeusen, Shelly, Rachel DeVay, Jennifer Block, Ann Cassidy-Stone, Sarah Wayson, J. Michael McCaffery, and Jodi Nunnari. 2006. "Mitochondrial Inner-Membrane Fusion and Crista Maintenance Requires the Dynamin-Related GTPase Mgm1." *Cell* 127 (2): 383–95. https://doi.org/10.1016/j.cell.2006.09.021.

Mehra, Surabhi, Shruti Sahay, and Samir K. Maji. 2019. "α-Synuclein Misfolding and Aggregation: Implications in Parkinson's Disease Pathogenesis." *Biochimica et Biophysica Acta. Proteins and Proteomics* 1867 (10): 890–908. https://doi.org/10.1016/J.BBAPAP.2019.03.001.

Meley, Daniel, Chantal Bauvy, Judith H P M Houben-Weerts, Peter F Dubbelhuis, Mariette T J Helmond, Patrice Codogno, and Alfred J Meijer. 2006. "AMP-Activated Protein Kinase and the Regulation of Autophagic Proteolysis *." https://doi.org/10.1074/jbc.M605488200.

Meng, Hongrui, Chikara Yamashita, Kahori Shiba-Fukushima, Tsuyoshi Inoshita, Manabu Funayama, Shigeto Sato, Tomohisa Hatta, et al. 2017. "Loss of Parkinson's Disease-Associated Protein CHCHD2 Affects Mitochondrial Crista Structure and Destabilizes Cytochrome c." *Nature Communications* 8 (June). https://doi.org/10.1038/NCOMMS15500.

Miklossy, Judith, Tetsuaki Arai, Jian Ping Guo, Andis Klegeris, Sheng Yu, Edith G. McGeer, and Patrick L. McGeer. 2006. "LRRK2 Expression in Normal and Pathologic Human Brain and in Human Cell Lines." *Journal of Neuropathology and Experimental Neurology* 65 (10): 953–63. https://doi.org/10.1097/01.jnen.0000235121.98052.54.

Mindell, Joseph A. 2012. "Lysosomal Acidification Mechanisms." *Annual Review of Physiology* 74 (1): 69–86. https://doi.org/10.1146/annurev-physiol-012110-142317.

Mishra, Prashant, and David C. Chan. 2014. "Mitochondrial Dynamics and Inheritance during Cell Division, Development and Disease." *Nature Reviews. Molecular Cell Biology* 15 (10): 634–46. https://doi.org/10.1038/NRM3877.

Mizushima, Noboru, Yoshinori Ohsumi, and Tamotsu Yoshimori. 2002. "Autophagosome Formation in Mammalian Cells." *Cell Structure and Function* 27 (6): 421–29. https://doi.org/10.1247/csf.27.421.

Mizushima, Noboru, and Tamotsu Yoshimori. 2007. “How to Interpret LC3 Immunoblotting.” *Autophagy* 3 (6): 542–45. https://doi.org/10.4161/auto.4600.

Moehle, Mark S, Philip J Webber, Tonia Tse, Nour Sukar, David G Standaert, Tara M Desilva, Rita M Cowell, and Andrew B West. 2012. “LRRK2 Inhibition Attenuates Microglial Inflammatory Responses” 32 (5): 1602–11. https://doi.org/10.1523/JNEUROSCI.5601-11.2012.

Monte, Donato A. Di, Mitra Lavasani, and Amy B. Manning-Bog. 2002. “Environmental Factors in Parkinson’s Disease.” *NeuroToxicology* 23 (4–5): 487–502. https://doi.org/10.1016/S0161-813X(02)00099-2.

Mortiboys, Heather, Krisztina K. Johansen, Jan O. Aasly, and Oliver Bandmann. 2010. “Mitochondrial Impairment in Patients with Parkinson Disease with the G2019S Mutation in LRRK2.” *Neurology* 75 (22): 2017–20. https://doi.org/10.1212/WNL.0b013e3181ff9685.

Mukherjee, Anindita, Bindi Patel, Hiroshi Koga, Ana Maria Cuervo, and Andreas Jenny. 2016. “Selective Endosomal Microautophagy Is Starvation-Inducible in Drosophila.” *Autophagy* 12 (11): 1984–99. https://doi.org/10.1080/15548627.2016.1208887/SUPPL_FILE/KAUP_A_1208887_SM3062.ZIP.

Muller, Florian L., Yuhong Liu, and Holly Van Remmen. 2004. “Complex III Releases Superoxide to Both Sides of the Inner Mitochondrial Membrane.” *Journal of Biological Chemistry* 279 (47): 49064–73. https://doi.org/10.1074/jbc.M407715200.

Murphy, Michael P. 2009. “How Mitochondria Produce Reactive Oxygen Species.” *Biochemical Journal* 417 (1): 1–13. https://doi.org/10.1042/BJ20081386.

Myasnikov, Alexander, Hanwen Zhu, Patricia Hixson, Boer Xie, Kaiwen Yu, Aaron Pitre, Junmin Peng, and Ji Sun. 2021. “Structural Analysis of the Full-Length Human LRRK2.” *Cell* 184 (13): 3519-3527.e10. https://doi.org/10.1016/j.cell.2021.05.004.

Nalls, Mike A., Nathan Pankratz, Christina M. Lill, Chuong B. Do, Dena G. Hernandez, Mohamad Saad, Anita L. Destefano, et al. 2014. “Large-Scale Meta-Analysis of Genome-Wide Association Data Identifies Six New Risk Loci for Parkinson’s Disease.” *Nature Genetics* 46 (9): 989–93. https://doi.org/10.1038/ng.3043.

Narendra, Derek P., Seok Min Jin, Atsushi Tanaka, Der Fen Suen, Clement A. Gautier, Jie Shen, Mark R. Cookson, and Richard J. Youle. 2010. “PINK1 Is Selectively Stabilized on Impaired Mitochondria to Activate Parkin.” *PLoS Biology* 8 (1). https://doi.org/10.1371/JOURNAL.PBIO.1000298.

Naslavsky, Naava, and Steve Caplan. 2018. “The Enigmatic Endosome - Sorting the Ins and Outs of Endocytic Trafficking.” *Journal of Cell Science* 131 (13). https://doi.org/10.1242/JCS.216499.

Näsström, Thomas, Susana Gonçalves, Charlotte Sahlin, Eva Nordström, Valentina Screpanti Sundquist, Lars Lannfelt, Joakim Bergström, Tiago F. Outeiro, and Martin Ingelsson. 2011. “Antibodies against Alpha-Synuclein Reduce Oligomerization in Living Cells.” *PLOS ONE* 6 (10): e27230. https://doi.org/10.1371/JOURNAL.PONE.0027230.

Ness, Daniel, Zhao Ren, Shyra Gardai, Douglas Sharpnack, Victor J. Johnson, Richard J. Brennan, Elizabeth F. Brigham, and Andrew J. Olaharski. 2013. “Leucine-Rich

Repeat Kinase 2 (LRRK2)-Deficient Rats Exhibit Renal Tubule Injury and Perturbations in Metabolic and Immunological Homeostasis." *PloS One* 8 (6). https://doi.org/10.1371/JOURNAL.PONE.0066164.

Neupert, Walter, and Johannes M. Herrmann. 2007. "Translocation of Proteins into Mitochondria." *Https://Doi.Org/10.1146/Annurev.Biochem.76.052705.163409* 76 (June): 723–49. https://doi.org/10.1146/ANNUREV.BIOCHEM.76.052705.163409.

Nguyen, An Phu Tran, Elpida Tsika, Kaela Kelly, Nathan Levine, Xi Chen, Andrew B. West, Sylviane Boularand, Pascal Barneoud, and Darren J. Moore. 2020. "Dopaminergic Neurodegeneration Induced by Parkinson's Disease-Linked G2019S LRRK2 Is Dependent on Kinase and GTPase Activity." *Proceedings of the National Academy of Sciences of the United States of America* 117 (29): 17296–307. https://doi.org/10.1073/PNAS.1922184117.

Nguyen, Maria, Yvette C. Wong, Daniel Ysselstein, Alex Severino, and Dimitri Krainc. 2019. "Synaptic, Mitochondrial, and Lysosomal Dysfunction in Parkinson's Disease." *Trends in Neurosciences* 42 (2): 140–49. https://doi.org/10.1016/J.TINS.2018.11.001.

Nichols, R Jeremy, Nicolas Dzamko, Nicholas A Morrice, David G Campbell, Maria Deak, Alban Ordureau, Thomas Macartney, et al. 2010. "14-3-3 Binding to LRRK2 Is Disrupted by Multiple Parkinson ' s Disease-Associated Mutations and Regulates Cytoplasmic Localization" 404: 393–404. https://doi.org/10.1042/BJ20100483.

Nichols, William C., Nathan Pankratz, Dena Hernandez, Coro Paisán-Ruíz, Shushant Jain, Cheryl A. Halter, Veronika E. Michaels, et al. 2005. "Genetic Screening for a Single Common LRRK2 Mutation in Familial Parkinson's Disease." *Lancet* 365 (9457): 410–12. https://doi.org/10.1016/S0140-6736(05)17828-3.

Nido, Gonzalo S., Christian Dölle, Irene Flønes, Helen A. Tuppen, Guido Alves, Ole Bjørn Tysnes, Kristoffer Haugarvoll, and Charalampos Tzoulis. 2018. "Ultradeep Mapping of Neuronal Mitochondrial Deletions in Parkinson's Disease." *Neurobiology of Aging* 63 (March): 120–27. https://doi.org/10.1016/J.NEUROBIOLAGING.2017.10.024.

Noda, Takeshi, and Yoshinori Ohsumi. 1998. "Tor, a Phosphatidylinositol Kinase Homologue, Controls Autophagy in Yeast." *Journal of Biological Chemistry* 273 (7): 3963–66. https://doi.org/10.1074/jbc.273.7.3963.

Nunnari, Jodi, and Anu Suomalainen. 2012. "Mitochondria: In Sickness and in Health." *Cell* 148 (6): 1145–59. https://doi.org/10.1016/J.CELL.2012.02.035.

Obergasteiger, Julia, Giulia Frapporti, Giulia Lamonaca, Sara Pizzi, Anne Picard, Alexandros A. Lavdas, Francesca Pischedda, et al. 2020. "Kinase Inhibition of G2019S-LRRK2 Enhances Autolysosome Formation and Function to Reduce Endogenous Alpha-Synuclein Intracellular Inclusions." *Cell Death Discovery* 6 (1). https://doi.org/10.1038/s41420-020-0279-y.

Obergasteiger, Julia, Giulia Frapporti, Peter P. Pramstaller, Andrew A. Hicks, and Mattia Volta. 2018. "A New Hypothesis for Parkinson's Disease Pathogenesis: GTPase-P38 MAPK Signaling and Autophagy as Convergence Points of Etiology and Genomics." *Molecular Neurodegeneration* 13 (1): 1–17. https://doi.org/10.1186/s13024-018-0273-5.

Olanow, C. Warren, Jose A. Obeso, and Fabrizio Stocchi. 2006. “Continuous Dopamine-Receptor Treatment of Parkinson’s Disease: Scientific Rationale and Clinical Implications.” *Lancet Neurology*. Elsevier. https://doi.org/10.1016/S1474-4422(06)70521-X.

Orenstein, Samantha J., Sheng Han Kuo, Inmaculada Tasset, Esperanza Arias, Hiroshi Koga, Irene Fernandez-Carasa, Etty Cortes, et al. 2013. “Interplay of LRRK2 with Chaperone-Mediated Autophagy.” *Nature Neuroscience* 16 (4): 394–406. https://doi.org/10.1038/nn.3350.

Oster, K. A., and S. Z. Sorkin. 1942. “Effects of Intravenous Injections of L-Dopa upon Blood Pressure.” *Experimental Biology and Medicine* 51 (1): 67–70. https://doi.org/10.3181/00379727-51-13831.

Outeiro, Tiago Fleming, Kirsten Harvey, Antonio Dominguez-Meijide, and Ellen Gerhardt. 2019. “LRRK2, Alpha-Synuclein, and Tau: Partners in Crime or Unfortunate Bystanders?” *Biochemical Society Transactions* 47 (3): 827–38. https://doi.org/10.1042/bst20180466.

Paisán-Ruíz, Coro, Shushant Jain, E. Whitney Evans, William P. Gilks, Javier Simón, Marcel Van Der Brug, Adolfo López De Munain, et al. 2004. “Cloning of the Gene Containing Mutations That Cause PARK8-Linked Parkinson’s Disease.” *Neuron* 44 (4): 595–600. https://doi.org/10.1016/j.neuron.2004.10.023.

Palikaras, Konstantinos, Eirini Lionaki, and Nektarios Tavernarakis. 2018. “Mechanisms of Mitophagy in Cellular Homeostasis, Physiology and Pathology.” *Nature Cell Biology* 20 (9): 1013–22. https://doi.org/10.1038/S41556-018-0176-2.

Palmer, Catherine S., Laura D. Osellame, David Laine, Olga S. Koutsopoulos, Ann E. Frazier, and Michael T. Ryan. 2011. “MiD49 and MiD51, New Components of the Mitochondrial Fission Machinery.” *EMBO Reports* 12 (6): 565–73. https://doi.org/10.1038/EMBOR.2011.54.

Pan, Lina, Lanxia Meng, Mingyang He, and Zhentao Zhang. 2021. “Tau in the Pathophysiology of Parkinson’s Disease.” *Journal of Molecular Neuroscience : MN* 71 (11): 2179–91. https://doi.org/10.1007/S12031-020-01776-5.

Pan, Ping Yue, Xianting Li, Jing Wang, James Powell, Qian Wang, Yuanxi Zhang, Zhaoyu Chen, et al. 2017. “Parkinson’s Disease-Associated LRRK2 Hyperactive Kinase Mutant Disrupts Synaptic Vesicle Trafficking in Ventral Midbrain Neurons.” *Journal of Neuroscience* 37 (47): 11366–76. https://doi.org/10.1523/JNEUROSCI.0964-17.2017.

Panicker, Nikhil, Preston Ge, Valina L. Dawson, and Ted M. Dawson. 2021. “The Cell Biology of Parkinson’s Disease.” *The Journal of Cell Biology* 220 (4). https://doi.org/10.1083/JCB.202012095.

Papkovskaia, Tatiana D., Kai Yin Chau, Francisco Inesta-vaquera, Dmitri B. Papkovsky, Daniel G. Healy, Koji Nishio, James Staddon, et al. 2012. “G2019S Leucine-Rich Repeat Kinase 2 Causes Uncoupling Protein-Mediated Mitochondrial Depolarization.” *Human Molecular Genetics* 21 (19): 4201–13. https://doi.org/10.1093/HMG/DDS244.

Parisiadou, Loukia, Jia Yu, Carmelo Sgobio, Chengsong Xie, Guoxiang Liu, Lixin Sun, Xing Long Gu, et al. 2014. “LRRK2 Regulates Synaptogenesis and Dopamine

Receptor Activation through Modulation of PKA Activity." *Nature Neuroscience* 17 (3): 367–76. https://doi.org/10.1038/nn.3636.

Park, Sangwook, Seulki Han, Insup Choi, Beomsue Kim, Seung Pyo Park, Eun Hye Joe, and Young Ho Suh. 2016. "Interplay between Leucine-Rich Repeat Kinase 2 (LRRK2) and P62/SQSTM-1 in Selective Autophagy." *PLoS ONE* 11 (9): 1–14. https://doi.org/10.1371/journal.pone.0163029.

Parkinson, James. 1817. "An Essay on the Shaking Palsy." *London: Whittingham and Rowland for Sherwood, Neely and Jones*.

Parkkinen, Laura, Tuula Pirttilä, and Irina Alafuzoff. 2008. "Applicability of Current Staging/Categorization of α-Synuclein Pathology and Their Clinical Relevance." *Acta Neuropathologica* 115 (4): 399–407. https://doi.org/10.1007/S00401-008-0346-6/TABLES/4.

Pepper, Joshua, Ludvic Zrinzo, Bilal Mirza, Thomas Foltynie, Patricia Limousin, and Marwan Hariz. 2013. "The Risk of Hardware Infection in Deep Brain Stimulation Surgery Is Greater at Impulse Generator Replacement than at the Primary Procedure." *Stereotactic and Functional Neurosurgery* 91 (1): 56–65. https://doi.org/10.1159/000343202.

Pimenta De Castro, I., A. C. Costa, D. Lam, R. Tufi, V. Fedele, N. Moisoi, D. Dinsdale, E. Deas, S. H.Y. Loh, and L. M. Martins. 2012. "Genetic Analysis of Mitochondrial Protein Misfolding in Drosophila Melanogaster." *Cell Death and Differentiation* 19 (8): 1308–16. https://doi.org/10.1038/CDD.2012.5.

Pissadaki, Eleftheria Kyriaki, and J. Paul Bolam. 2013. "The Energy Cost of Action Potential Propagation in Dopamine Neurons: Clues to Susceptibility in Parkinson's Disease." *Frontiers in Computational Neuroscience* 7 (FEB). https://doi.org/10.3389/FNCOM.2013.00013.

Plowey, Edward D., Salvatore J. Cherra, Yong Jian Liu, and Charleen T. Chu. 2008. "Role of Autophagy in G2019S-LRRK2-Associated Neurite Shortening in Differentiated SH-SY5Y Cells." *Journal of Neurochemistry* 105 (3): 1048–56. https://doi.org/10.1111/j.1471-4159.2008.05217.x.

Polymeropoulos, Mihael H., Christian Lavedan, Elisabeth Leroy, Susan E. Ide, Anindya Dehejia, Amalia Dutra, Brian Pike, et al. 1997. "Mutation in the α-Synuclein Gene Identified in Families with Parkinson's Disease." *Science* 276 (5321): 2045–47. https://doi.org/10.1126/science.276.5321.2045.

Pupyshev, Alexander B., Tatiana A. Korolenko, Anna A. Akopyan, Tamara G. Amstislavskaya, and Maria A. Tikhonova. 2018. "Suppression of Autophagy in the Brain of Transgenic Mice with Overexpression of A53T-Mutant α-Synuclein as an Early Event at Synucleinopathy Progression." *Neuroscience Letters* 672 (December 2017): 140–44. https://doi.org/10.1016/j.neulet.2017.12.001.

Ramirez, Alfredo, André Heimbach, Jan Gründemann, Barbara Stiller, Dan Hampshire, L. Pablo Cid, Ingrid Goebel, et al. 2006. "Hereditary Parkinsonism with Dementia Is Caused by Mutations in ATP13A2, Encoding a Lysosomal Type 5 P-Type ATPase." *Nature Genetics* 38 (10): 1184–91. https://doi.org/10.1038/ng1884.

Ramonet, David, João Paulo L. Daher, Brian M. Lin, Klodjan Stafa, Jaekwang Kim, Rebecca Banerjee, Marie Westerlund, et al. 2011. "Dopaminergic Neuronal Loss,

Reduced Neurite Complexity and Autophagic Abnormalities in Transgenic Mice Expressing G2019S Mutant LRRK2." *PLoS ONE* 6 (4): 13–19. https://doi.org/10.1371/journal.pone.0018568.

Reddy, P. Hemachandra, Tejaswini P. Reddy, Maria Manczak, Marcus J. Calkins, Ulziibat Shirendeb, and Peizhong Mao. 2011. "Dynamin-Related Protein 1 and Mitochondrial Fragmentation in Neurodegenerative Diseases." *Brain Research Reviews* 67 (1–2): 103–18. https://doi.org/10.1016/J.BRAINRESREV.2010.11.004.

Reeve, Amy K., Kim J. Krishnan, Joanna L. Elson, Christopher M. Morris, Andreas Bender, Robert N. Lightowlers, and Douglass M. Turnbull. 2008. "Nature of Mitochondrial DNA Deletions in Substantia Nigra Neurons." *American Journal of Human Genetics* 82 (1): 228–35. https://doi.org/10.1016/J.AJHG.2007.09.018.

Reinhardt, Peter, Benjamin Schmid, Lena F. Burbulla, David C. Schöndorf, Lydia Wagner, Michael Glatza, Susanne Höing, et al. 2013. "Genetic Correction of a LRRK2 Mutation in Human IPSCs Links Parkinsonian Neurodegeneration to ERK-Dependent Changes in Gene Expression." *Cell Stem Cell* 12 (3): 354–67. https://doi.org/10.1016/J.STEM.2013.01.008.

Ren, Guiqi, Shengchang Xin, Song Li, Hanbing Zhong, and Shuo Lin. 2011. "Disruption of LRRK2 Does Not Cause Specific Loss of Dopaminergic Neurons in Zebrafish." *PloS One* 6 (6). https://doi.org/10.1371/JOURNAL.PONE.0020630.

Rivero-Ríos, Pilar, Jesús Madero-Pérez, Belén Fernández, and Sabine Hilfiker. 2016. "Targeting the Autophagy/Lysosomal Degradation Pathway in Parkinsons Disease." *Current Neuropharmacology* 14 (3): 238–49. https://doi.org/10.2174/1570159x13666151030103027.

Roberts, Rosalind F., Nora Bengoa-Vergniory, and Javier Alegre-Abarrategui. 2019. "Alpha-Synuclein Proximity Ligation Assay (AS-PLA) in Brain Sections to Probe for Alpha-Synuclein Oligomers." *Methods in Molecular Biology* 1948: 69–76. https://doi.org/10.1007/978-1-4939-9124-2_7.

Roberts, Rosalind F., Richard Wade-Martins, and Javier Alegre-Abarrategui. 2015. "Direct Visualization of Alpha-Synuclein Oligomers Reveals Previously Undetected Pathology in Parkinson's Disease Brain." *Brain* 138 (6): 1642–57. https://doi.org/10.1093/BRAIN/AWV040.

Roh, Soung Hun, Nicholas J. Stam, Corey F. Hryc, Sergio Couoh-Cardel, Grigore Pintilie, Wah Chiu, and Stephan Wilkens. 2018. "The 3.5-Å CryoEM Structure of Nanodisc-Reconstituted Yeast Vacuolar ATPase Vo Proton Channel." *Molecular Cell* 69 (6): 993-1004.e3. https://doi.org/10.1016/J.MOLCEL.2018.02.006.

Ross, Owen A., Yih Ru Wu, Mei Ching Lee, Manabu Funayama, Meng Ling Chen, Alexandra I. Soto, Ignacio F. Mata, et al. 2008. "Analysis of Lrrk2 R1628P as a Risk Factor for Parkinson's Disease." *Annals of Neurology* 64 (1): 88–92. https://doi.org/10.1002/ANA.21405.

Rossmann, Marlies P., Sonia M. Dubois, Suneet Agarwal, and Leonard I. Zon. 2021. "Mitochondrial Function in Development and Disease." *Disease Models & Mechanisms* 14 (6). https://doi.org/10.1242/DMM.048912.

Roy, Madhuparna, P. Hemachandra Reddy, Miho Iijima, and Hiromi Sesaki. 2015. "Mitochondrial Division and Fusion in Metabolism." *Current Opinion in Cell Biology* 33 (April): 111–18. https://doi.org/10.1016/J.CEB.2015.02.001.

Ryan, Brent J., Selim Hoek, Edward A. Fon, and Richard Wade-Martins. 2015. "Mitochondrial Dysfunction and Mitophagy in Parkinson's: From Familial to Sporadic Disease." *Trends in Biochemical Sciences* 40 (4): 200–210. https://doi.org/10.1016/J.TIBS.2015.02.003.

Ryan, Scott D., Nima Dolatabadi, Shing Fai Chan, Xiaofei Zhang, Mohd Waseem Akhtar, James Parker, Frank Soldner, et al. 2013. "Isogenic Human IPSC Parkinson's Model Shows Nitrosative Stress-Induced Dysfunction in MEF2-PGC1α Transcription." *Cell* 155 (6): 1351. https://doi.org/10.1016/j.cell.2013.11.009.

Saez-Atienzar, S., L. Bonet-Ponce, J. R. Blesa, F. J. Romero, M. P. Murphy, J. Jordan, and M. F. Galindo. 2014. "The LRRK2 Inhibitor GSK2578215A Induces Protective Autophagy in SH-SY5Y Cells: Involvement of Drp-1-Mediated Mitochondrial Fission and Mitochondrial-Derived ROS Signaling." *Cell Death and Disease* 5 (8): 1–10. https://doi.org/10.1038/cddis.2014.320.

Saha, Anirban R., Josephine Hill, Michelle A. Utton, Ayodeji A. Asuni, Steven Ackerley, Andrew J. Grierson, Christopher C. Miller, et al. 2004. "Parkinson's Disease Alpha-Synuclein Mutations Exhibit Defective Axonal Transport in Cultured Neurons." *Journal of Cell Science* 117 (Pt 7): 1017–24. https://doi.org/10.1242/JCS.00967.

Saha, Shamol, Peter E.A. Ash, Vivek Gowda, Liqun Liu, Orian Shirihai, and Benjamin Wolozin. 2015. "Mutations in LRRK2 Potentiate Age-Related Impairment of Autophagic Flux." *Molecular Neurodegeneration* 10 (1). https://doi.org/10.1186/s13024-015-0022-y.

Saha, Shamol, Maria D. Guillily, Andrew Ferree, Joel Lanceta, Diane Chan, Joy Ghosh, Cindy H. Hsu, et al. 2009. "LRRK2 Modulates Vulnerability to Mitochondrial Dysfunction in Caenorhabditis Elegans." *The Journal of Neuroscience : The Official Journal of the Society for Neuroscience* 29 (29): 9210–18. https://doi.org/10.1523/JNEUROSCI.2281-09.2009.

Sahu, Ranjit, Susmita Kaushik, Cristina C Clement, Elvira S Cannizzo, Brian Scharf, Antonia Follenzi, Ilaria Potolicchio, Edward Nieves, Ana Maria Cuervo, and Laura Santambrogio. 2011. "Developmental Cell Microautophagy of Cytosolic Proteins by Late Endosomes." *DEVCEL* 20: 131–39. https://doi.org/10.1016/j.devcel.2010.12.003.

Sánchez-Danés, Adriana, Yvonne Richaud-Patin, Iria Carballo-Carbajal, Senda Jiménez-Delgado, Carles Caig, Sergio Mora, Claudia Di Guglielmo, et al. 2012. "Disease-Specific Phenotypes in Dopamine Neurons from Human IPS-Based Models of Genetic and Sporadic Parkinson's Disease." *EMBO Molecular Medicine* 4 (5): 380–95. https://doi.org/10.1002/emmm.201200215.

Sanders, Laurie H., Jennifer McCoy, Xiaoping Hu, Pier G. Mastroberardino, Bryan C. Dickinson, Christopher J. Chang, Charleen T. Chu, Bennett Van Houten, and J. T. Greenamyre. 2014. "Mitochondrial DNA Damage: Molecular Marker of Vulnerable Nigral Neurons in Parkinson's Disease." *Neurobiology of Disease* 70: 214–23. https://doi.org/10.1016/J.NBD.2014.06.014.

Sanyal, Anwesha, Mark P. DeAndrade, Hailey S. Novis, Steven Lin, Jianjun Chang, Nathalie Lengacher, Julianna J. Tomlinson, Malú G. Tansey, and Matthew J. LaVoie. 2020. “Lysosome and Inflammatory Defects in *GBA1* -Mutant Astrocytes Are Normalized by LRRK2 Inhibition.” *Movement Disorders*, February, mds.27994. https://doi.org/10.1002/mds.27994.

Schapansky, Khasnavis, DeAndrade, Nardozzi, Falkson, Boyd, Sanderson, Bartels, Melrose, and LaVoie. 2018. “Familial Knockin Mutation of LRRK2 Causes Lysosomal Dysfunction and Accumulation of Endogenous Insoluble α-Synuclein in Neurons.” *Neurobiology of Disease* 111 (March): 26–35. https://doi.org/10.1016/j.nbd.2017.12.005.

Schapansky, Nardozzi, Felizia, and LaVoie. 2014. “Membrane Recruitment of Endogenous LRRK2 Precedes Its Potent Regulation of Autophagy.” *Human Molecular Genetics* 23 (16): 4201–14. https://doi.org/10.1093/hmg/ddu138.

Schapansky, Nardozzi, and Lavoie. 2015. “The Complex Relationships between Microglia, Alpha-Synuclein, and LRRK2 in Parkinson’s Disease.” *Neuroscience* 302: 74–88. https://doi.org/10.1016/j.neuroscience.2014.09.049.

Schapira, A. H.V., J. M. Cooper, D. Dexter, P. Jenner, J. B. Clark, and C. D. Marsden. 1989. “Mitochondrial Complex I Deficiency in Parkinson’s Disease.” *Lancet (London, England)* 1 (8649): 1269. https://doi.org/10.1016/S0140-6736(89)92366-0.

Schneider, Susanne A., and Roy N. Alcalay. 2017. “Neuropathology of Genetic Synucleinopathies with Parkinsonism: Review of the Literature.” *Movement Disorders* 32 (11): 1504–23. https://doi.org/10.1002/mds.27193.

Schöndorf, David C., Dina Ivanyuk, Pascale Baden, Alvaro Sanchez-Martinez, Silvia De Cicco, Cong Yu, Ivana Giunta, et al. 2018. “The NAD+ Precursor Nicotinamide Riboside Rescues Mitochondrial Defects and Neuronal Loss in IPSC and Fly Models of Parkinson’s Disease.” *Cell Reports* 23 (10): 2976–88. https://doi.org/10.1016/J.CELREP.2018.05.009.

Schoonderwoert, Vincent Th G., Joost C.M. Holthuis, Shigeyasu Tanaka, Sharon A. Tooze, and Gerard J.M. Martens. 2000. “Inhibition of the Vacuolar H+-ATPase Perturbs the Transport, Sorting, Processing and Release of Regulated Secretory Proteins.” *European Journal of Biochemistry* 267 (17): 5646–54. https://doi.org/10.1046/J.1432-1327.2000.01648.X.

Schuepbach, W.M.M., J. Rau, K. Knudsen, J. Volkmann, P. Krack, L. Timmermann, T.D. Hälbig, et al. 2013. “Neurostimulation for Parkinson’s Disease with Early Motor Complications.” *Https://Doi.Org/10.1056/NEJMoa1205158* 368 (7): 610–22. https://doi.org/10.1056/NEJMOA1205158.

Shaikh, Komal T., Alvin Yang, Ekaterina Youshin, and Susanne Schmid. 2015. “Transgenic LRRK2 (R1441G) Rats-a Model for Parkinson Disease?” *PeerJ* 3 (5). https://doi.org/10.7717/PEERJ.945.

Shani, Vered, Hazem Safory, Raymonde Szargel, Ninghan Wang, Tsipora Cohen, Fatimah Abd Elghani, Haya Hamza, et al. 2019. “Physiological and Pathological Roles of LRRK2 in the Nuclear Envelope Integrity.” *Human Molecular Genetics* 28 (23): 3982–96. https://doi.org/10.1093/hmg/ddz245.

Sheng, Donglai, Dianbo Qu, Ken Hon Hung Kwok, Seok Shin Ng, Adrian Yin Ming Lim, Sharon Siqi Aw, Charlie Wah Heng Lee, et al. 2010. “Deletion of the WD40 Domain of LRRK2 in Zebrafish Causes Parkinsonism-like Loss of Neurons and Locomotive Defect.” *PLoS Genetics* 6 (4). https://doi.org/10.1371/JOURNAL.PGEN.1000914.

Sheng, Zu Hang, and Qian Cai. 2012. “Mitochondrial Transport in Neurons: Impact on Synaptic Homeostasis and Neurodegeneration.” *Nature Reviews. Neuroscience* 13 (2): 77–93. https://doi.org/10.1038/NRN3156.

Shulman, Joshua M., Philip L. De Jager, and Mel B. Feany. 2011. “Parkinson’s Disease: Genetics and Pathogenesis.” *Https://Doi.Org/10.1146/Annurev-Pathol-011110-130242* 6 (January): 193–222. https://doi.org/10.1146/ANNUREV-PATHOL-011110-130242.

Singh, Francois, and Ian G. Ganley. 2021. “Parkinson’s Disease and Mitophagy: An Emerging Role for LRRK2.” *Biochemical Society Transactions* 49 (2): 551–62. https://doi.org/10.1042/BST20190236.

Singh, Francois, Alan R. Prescott, Philippa Rosewell, Graeme Ball, Alastair D. Reith, and Ian G. Ganley. 2021. “Pharmacological Rescue of Impaired Mitophagy in Parkinson’s Disease-Related LRRK2 G2019S Knock-in Mice.” *ELife* 10: 1–26. https://doi.org/10.7554/ELIFE.67604.

Singh, Pawan Kishor, and Miratul M.K. Muqit. 2020. “Parkinson’s: A Disease of Aberrant Vesicle Trafficking.” *Annual Review of Cell and Developmental Biology* 36 (October): 237–64. https://doi.org/10.1146/ANNUREV-CELLBIO-100818-125512.

Singleton, Andrew B., Matthew J. Farrer, and Vincenzo Bonifati. 2013. “The Genetics of Parkinson’s Disease: Progress and Therapeutic Implications.” *Movement Disorders* 28 (1): 14–23. https://doi.org/10.1002/mds.25249.

Sloan, Max, Javier Alegre-Abarrategui, Dawid Potgieter, Anna Kristin Kaufmann, Richard Exley, Thierry Deltheil, Sarah Threlfell, et al. 2016. “LRRK2 BAC Transgenic Rats Develop Progressive, L-DOPA-Responsive Motor Impairment, and Deficits in Dopamine Circuit Function.” *Human Molecular Genetics* 25 (5): 951–63. https://doi.org/10.1093/hmg/ddv628.

Smith, Annabel N., Jennifer Skaug, Keith A. Choate, Ahmet Nayir, Aysin Bakkaloglu, Seza Ozen, Sally A. Hulton, et al. 2000. “Mutations in ATP6N1B, Encoding a New Kidney Vacuolar Proton Pump 116-KD Subunit, Cause Recessive Distal Renal Tubular Acidosis with Preserved Hearing.” *Nature Genetics* 26 (1): 71–75. https://doi.org/10.1038/79208.

Smith, Wanli W., Haibing Jiang, Zhong Pei, Yuji Tanaka, Hokuto Morita, Akira Sawa, Valina L. Dawson, Ted M. Dawson, and Christopher A. Ross. 2005. “Endoplasmic Reticulum Stress and Mitochondrial Cell Death Pathways Mediate A53T Mutant Alpha-Synuclein-Induced Toxicity.” *Human Molecular Genetics* 14 (24): 3801–11. https://doi.org/10.1093/hmg/ddi396.

Song, Zhiyin, Mariam Ghochani, J. Michael McCaffery, Terrence G. Frey, and David C. Chan. 2009. “Mitofusins and OPA1 Mediate Sequential Steps in Mitochondrial Membrane Fusion.” *Molecular Biology of the Cell* 20 (15): 3525–32. https://doi.org/10.1091/MBC.E09-03-0252/ASSET/IMAGES/LARGE/ZMK0150991310007.JPEG.

Spillantini, M. G., M. L. Schmidt, John Q. Trojanowski, R. Jakes, and Michel Goedert. 1997. “A -Synuclein in Lewy Bodies.” *Nature* 388: 839–40.

Steger, Martin, Francesca Tonelli, Genta Ito, Paul Davies, Matthias Trost, Melanie Vetter, Stefanie Wachter, et al. 2016. “Phosphoproteomics Reveals That Parkinson’s Disease Kinase LRRK2 Regulates a Subset of Rab GTPases.” *ELife* 5 (JANUARY2016): 1–28. https://doi.org/10.7554/eLife.12813.001.

Stowe, Rebecca, Natalie Ives, Carl E. Clarke, Kelly Handley, Alexandra Furmston, Katherine Deane, J. J. van Hilten, Keith Wheatley, and Richard Gray. 2011. “Meta-Analysis of the Comparative Efficacy and Safety of Adjuvant Treatment to Levodopa in Later Parkinson’s Disease.” *Movement Disorders* 26 (4): 587–98. https://doi.org/10.1002/MDS.23517.

Stransky, Laura, Kristina Cotter, and Michael Forgac. 2016. “The Function of V-ATPases in Cancer.” *Physiological Reviews* 96 (3): 1071–91. https://doi.org/10.1152/PHYSREV.00035.2015.

Strobbe, Daniela, Alexis A. Robinson, Kirsten Harvey, Lara Rossi, Caterina Ferraina, Valerio De Biase, Carlo Rodolfo, Robert J. Harvey, and Michelangelo Campanella. 2018. “Distinct Mechanisms of Pathogenic DJ-1 Mutations in Mitochondrial Quality Control.” *Frontiers in Molecular Neuroscience* 11 (March). https://doi.org/10.3389/FNMOL.2018.00068.

Su, Yu Chin, Xing Guo, and Xin Qi. 2015. “Threonine 56 Phosphorylation of Bcl-2 Is Required for LRRK2 G2019S-Induced Mitochondrial Depolarization and Autophagy.” *Biochimica et Biophysica Acta - Molecular Basis of Disease* 1852 (1): 12–21. https://doi.org/10.1016/j.bbadis.2014.11.009.

Su, Yu Chin, and Xin Qi. 2013. “Inhibition of Excessive Mitochondrialfissionreduced Aberrant Autophagy and Neuronal Damage Caused by LRRK2 G2019S Mutation.” *Human Molecular Genetics* 22 (22): 4545–61. https://doi.org/10.1093/hmg/ddt301.

Surmeier, D. James, Jaime N. Guzman, and Javier Sanchez-Padilla. 2010. “Calcium, Cellular Aging, and Selective Neuronal Vulnerability in Parkinson’s Disease.” *Cell Calcium* 47 (2): 175–82. https://doi.org/10.1016/J.CECA.2009.12.003.

Swatek, Kirby N., Joanne L. Usher, Anja F. Kueck, Christina Gladkova, Tycho E.T. Mevissen, Jonathan N. Pruneda, Tim Skern, and David Komander. 2019. “Insights into Ubiquitin Chain Architecture Using Ub-Clipping.” *Nature* 572 (7770): 533–37. https://doi.org/10.1038/S41586-019-1482-Y.

Taguchi, Yumiko V., Jun Liu, Jiapeng Ruan, Joshua Pacheco, Xiaokui Zhang, Justin Abbasi, Joan Keutzer, Pramod K. Mistry, and Sreeganga S. Chandra. 2017. “Glucosylsphingosine Promotes α-Synuclein Pathology in Mutant GBA-Associated Parkinson’s Disease.” *Journal of Neuroscience* 37 (40): 9617–31. https://doi.org/10.1523/JNEUROSCI.1525-17.2017.

Takahashi, Kazutoshi, and Shinya Yamanaka. 2006. “Induction of Pluripotent Stem Cells from Mouse Embryonic and Adult Fibroblast Cultures by Defined Factors.” *Cell* 126 (4): 663–76. https://doi.org/10.1016/J.CELL.2006.07.024.

Takashimizu, Y., & Iiyoshi, M. (2016). New parameter of roundness R: circularity corrected by aspect ratio. Progress in Earth and Planetary Science, 3(1). https://doi.org/10.1186/s40645-015-0078-x

Tanaka, Atsushi, Megan M. Cleland, Shan Xu, Derek P. Narendra, Der Fen Suen, Mariusz Karbowski, and Richard J. Youle. 2010. “Proteasome and P97 Mediate Mitophagy and Degradation of Mitofusins Induced by Parkin.” *The Journal of Cell Biology* 191 (7): 1367–80. https://doi.org/10.1083/JCB.201007013.

Tasegian, Anna, Francois Singh, Ian G. Ganley, Alastair D. Reith, and Dario R. Alessi. 2021. “Impact of Type II LRRK2 Inhibitors on Signaling and Mitophagy.” *The Biochemical Journal* 478 (19): 3555–73. https://doi.org/10.1042/BCJ20210375.

Tofaris, George K., Azam Razzaq, Bernardino Ghetti, Kathryn S. Lilley, and Maria Grazia Spillantini. 2003. “Ubiquitination of α-Synuclein in Lewy Bodies Is a Pathological Event Not Associated with Impairment of Proteasome Function.” *Journal of Biological Chemistry* 278 (45): 44405–11. https://doi.org/10.1074/jbc.M308041200.

Tong, Youren, Emilie Giaime, Hiroo Yamaguchi, Takaharu Ichimura, Yumin Liu, Huiqing Si, Huaibin Cai, Joseph V. Bonventre, and Jie Shen. 2012. “Loss of Leucine-Rich Repeat Kinase 2 Causes Age-Dependent Bi-Phasic Alterations of the Autophagy Pathway.” *Molecular Neurodegeneration* 7 (1): 1–16. https://doi.org/10.1186/1750-1326-7-222230652.

Tong, Youren, Hiroo Yamaguchi, Emilie Giaime, Scott Boyle, Raphael Kopan, Raymond J. Kelleher, and Jie Shen. 2010. “Loss of Leucine-Rich Repeat Kinase 2 Causes Impairment of Protein Degradation Pathways, Accumulation of α-Synuclein, and Apoptotic Cell Death in Aged Mice.” *Proceedings of the National Academy of Sciences of the United States of America* 107 (21): 9879–84. https://doi.org/10.1073/pnas.1004676107.

Toyofuku, Toshihiko, Yuki Okamoto, Takako Ishikawa, Shigemi Sasawatari, and Atsushi Kumanogoh. 2020. “LRRK2 Regulates Endoplasmic Reticulum-Mitochondrial Tethering through the PERK-Mediated Ubiquitination Pathway.” *The EMBO Journal* 39 (2). https://doi.org/10.15252/EMBJ.2018100875.

Trabzuni, Daniah, Mina Ryten, Warren Emmett, Adaikalavan Ramasamy, Karl J. Lackner, Tanja Zeller, Robert Walker, et al. 2013. “Fine-Mapping, Gene Expression and Splicing Analysis of the Disease Associated LRRK2 Locus.” *PLoS ONE* 8 (8). https://doi.org/10.1371/journal.pone.0070724.

Trist, Benjamin G., Dominic J. Hare, and Kay L. Double. 2019. “Oxidative Stress in the Aging Substantia Nigra and the Etiology of Parkinson’s Disease.” *Aging Cell* 18 (6). https://doi.org/10.1111/ACEL.13031.

Tsika, Elpida, Meghna Kannan, Caroline Shi Yan Foo, Dustin Dikeman, Liliane Glauser, Sandra Gellhaar, Dagmar Galter, et al. 2014. “Conditional Expression of Parkinson’s Disease-Related R1441C LRRK2 in Midbrain Dopaminergic Neurons of Mice Causes Nuclear Abnormalities without Neurodegeneration.” *Neurobiology of Disease* 71 (1): 345–58. https://doi.org/10.1016/j.nbd.2014.08.027.

Tsika, Elpida, An Phu Tran Nguyen, Julien Dusonchet, Philippe Colin, Bernard L. Schneider, and Darren J. Moore. 2015. “Adenoviral-Mediated Expression of G2019S LRRK2 Induces Striatal Pathology in a Kinase-Dependent Manner in a Rat Model of Parkinson’s Disease.” *Neurobiology of Disease* 77 (May): 49–61. https://doi.org/10.1016/J.NBD.2015.02.019.

Usmani, Ahsan, Farbod Shavarebi, and Annie Hiniker. 2021. “The Cell Biology of LRRK2 in Parkinson’s Disease.” *Molecular and Cellular Biology* 41 (5). https://doi.org/10.1128/mcb.00660-20.

Uytterhoeven, Valerie, Elsa Lauwers, Ine Maes, Katarzyna Miskiewicz, Manuel N Melo, Jef Swerts, Sabine Kuenen, et al. 2015. “Hsc70-4 Deforms Membranes to Promote Synaptic Protein Turnover by Endosomal Microautophagy.” *Neuron* 88: 735–48. https://doi.org/10.1016/j.neuron.2015.10.012.

Valente, Enza Maria, Anna Rita Bentivoglio, Peter H. Dixon, Alessandro Ferraris, Tamara Lalongo, Marina Frontali, Alberto Albanese, and Nicholas W. Wood. 2001. “Localization of a Novel Locus for Autosomal Recessive Early-Onset Parkinsonism, PARK6, on Human Chromosome 1p35-P36.” *American Journal of Human Genetics* 68 (4): 895–900. https://doi.org/10.1086/319522.

Vasanthakumar, Thamiya, and John L. Rubinstein. 2020. “Structure and Roles of V-Type ATPases.” *Trends in Biochemical Sciences* 45 (4): 295–307. https://doi.org/10.1016/J.TIBS.2019.12.007.

Vives-Bauza, Cristofol, Chun Zhou, Yong Huang, Mei Cui, Rosa L.A. De Vries, Jiho Kim, Jessica May, et al. 2010. “PINK1-Dependent Recruitment of Parkin to Mitochondria in Mitophagy.” *Proceedings of the National Academy of Sciences of the United States of America* 107 (1): 378–83. https://doi.org/10.1073/pnas.0911187107.

Vogiatzi, Tereza, Maria Xilouri, Kostas Vekrellis, and Leonidas Stefanis. 2008. “Wild Type α-Synuclein Is Degraded by Chaperone-Mediated Autophagy and Macroautophagy in Neuronal Cells.” *Journal of Biological Chemistry* 283 (35): 23542–56. https://doi.org/10.1074/jbc.M801992200.

Volpicelli-Daley, Laura A., Hisham Abdelmotilib, Zhiyong Liu, Lindsay Stoyka, João Paulo Lima Daher, Austen J. Milnerwood, Vivek K. Unni, et al. 2016. “G2019s-LRRK2 Expression Augments α-Synuclein Sequestration into Inclusions in Neurons.” *Journal of Neuroscience* 36 (28): 7415–27. https://doi.org/10.1523/JNEUROSCI.3642-15.2016.

Walker, Matthew D., Mattia Volta, Stefano Cataldi, Katherine Dinelle, Dayne Beccano-Kelly, Lise Munsie, Rick Kornelsen, et al. 2014. “Behavioral Deficits and Striatal DA Signaling in LRRK2 p.G2019S Transgenic Rats: A Multimodal Investigation Including PET Neuroimaging.” *Journal of Parkinson’s Disease* 4 (3): 483–98. https://doi.org/10.3233/JPD-140344.

Wall, Christopher E., Christopher M. Rose, Max Adrian, Yi J. Zeng, Donald S. Kirkpatrick, and Baris Bingol. 2019. “PPEF2 Opposes PINK1-Mediated Mitochondrial Quality Control by Dephosphorylating Ubiquitin.” *Cell Reports* 29 (10): 3280-3292.e7. https://doi.org/10.1016/J.CELREP.2019.10.130.

Wallings, Rebecca, Natalie Connor-Robson, and Richard Wade-Martins. 2019. “LRRK2 Interacts with the Vacuolar-Type H+-ATPase Pump A1 Subunit to Regulate Lysosomal Function.” *Human Molecular Genetics* 28 (16): 2696–2710. https://doi.org/10.1093/hmg/ddz088.

Wallings, Rebecca L., and Malú G. Tansey. 2019. “LRRK2 Regulation of Immune-Pathways and Inflammatory Disease.” *Biochemical Society Transactions* 47 (6): 1581–95. https://doi.org/10.1042/BST20180463.

Wallings, Rebecca, Claudia Manzoni, and Rina Bandopadhyay. 2015. “Cellular Processes Associated with LRRK2 Function and Dysfunction.” *FEBS Journal* 282 (15): 2806–26. https://doi.org/10.1111/febs.13305.

Walter, Jonas, Silvia Bolognin, Paul M.A. Antony, Sarah L. Nickels, Suresh K. Poovathingal, Luis Salamanca, Stefano Magni, et al. 2019. “Neural Stem Cells of Parkinson’s Disease Patients Exhibit Aberrant Mitochondrial Morphology and Functionality.” *Stem Cell Reports* 12 (5): 878–89. https://doi.org/10.1016/j.stemcr.2019.03.004.

Wang, Liming, Yik Lam Cho, Yancheng Tang, Jigang Wang, Jung Eun Park, Yajun Wu, Chunxin Wang, et al. 2018. “PTEN-L Is a Novel Protein Phosphatase for Ubiquitin Dephosphorylation to Inhibit PINK1-Parkin-Mediated Mitophagy.” *Cell Research* 28 (8): 787–802. https://doi.org/10.1038/S41422-018-0056-0.

Wang, Longfei, Di Wu, Carol V. Robinson, Hao Wu, and Tian Min Fu. 2020. “Structures of a Complete Human V-ATPase Reveal Mechanisms of Its Assembly.” *Molecular Cell* 80 (3): 501-511.e3. https://doi.org/10.1016/J.MOLCEL.2020.09.029.

Wang, Rong, Tao Long, Abdirahman Hassan, Jin Wang, Yingyuan Sun, Xiao Song Xie, and Xiaochun Li. 2020. “Cryo-EM Structures of Intact V-ATPase from Bovine Brain.” *Nature Communications* 11 (1). https://doi.org/10.1038/S41467-020-17762-9.

Wang, Ting, and Jesse C. Hay. 2015. “Alpha-Synuclein Toxicity in the Early Secretory Pathway: How It Drives Neurodegeneration in Parkinsons Disease.” *Frontiers in Neuroscience* 9 (NOV): 1–8. https://doi.org/10.3389/fnins.2015.00433.

Wang, Wenzhang, Xinglong Wang, Hisashi Fujioka, Charles Hoppel, Alan L. Whone, Maeve A. Caldwell, Peter J. Cullen, Jun Liu, and Xiongwei Zhu. 2016. “Parkinson’s Disease-Associated Mutant VPS35 Causes Mitochondrial Dysfunction by Recycling DLP1 Complexes.” *Nature Medicine* 22 (1): 54–63. https://doi.org/10.1038/NM.3983.

Wang, Xinglong, Michael H Yan, Hisashi Fujioka, Jun Liu, Amy Wilson-Delfosse, Shu G Chen, George Perry, Gemma Casadesus, and Xiongwei Zhu. 2012. “LRRK2 Regulates Mitochondrial Dynamics and Function through Direct Interaction with DLP1.” *Human Molecular Genetics* 21 (9): 1931–44. https://doi.org/10.1093/hmg/dds003.

Wang, Xinnan. 2017. “Destructive Cellular Paths Underlying Familial and Sporadic Parkinson Disease Converge on Mitophagy.” *Autophagy* 13 (11): 1998–99. https://doi.org/10.1080/15548627.2017.1327511.

Wauer, Tobias, Michal Simicek, Alexander Schubert, and David Komander. 2015. “Mechanism of Phospho-Ubiquitin-Induced PARKIN Activation.” *Nature* 524 (7565): 370–74. https://doi.org/10.1038/NATURE14879.

Wauters, Fieke, Tom Cornelissen, Dorien Imberechts, Shaun Martin, Brianada Koentjoro, Carolyn Sue, Peter Vangheluwe, and Wim Vandenberghe. 2020. “LRRK2 Mutations Impair Depolarization-Induced Mitophagy through Inhibition of Mitochondrial Accumulation of RAB10.” *Autophagy* 16 (2): 203–22. https://doi.org/10.1080/15548627.2019.1603548.

Webb, Julie L, Brinda Ravikumar, Jane Atkins, Jeremy N Skepper, and David C Rubinsztein. 2003. “␣ -Synuclein Is Degraded by Both Autophagy and the Proteasome *” 278 (27): 25009–13. https://doi.org/10.1074/jbc.M300227200.

West, Andrew B., Rita M. Cowell, João P.L. Daher, Mark S. Moehle, Kelly M. Hinkle, Heather L. Melrose, David G. Standaert, and Laura A. Volpicelli-Daley. 2014. “Differential LRRK2 Expression in the Cortex, Striatum, and Substantia Nigra in Transgenic and Nontransgenic Rodents.” *Journal of Comparative Neurology* 522 (11): 2465–80. https://doi.org/10.1002/cne.23583.

West, Andrew B., Darren J. Moore, Saskia Biskup, Artem Bugayenko, Wanli W. Smith, Christopher A. Ross, Valina L. Dawson, and Ted M. Dawson. 2005. “Parkinson’s Disease-Associated Mutations in Leucine-Rich Repeat Kinase 2 Augment Kinase Activity.” *Proceedings of the National Academy of Sciences of the United States of America* 102 (46): 16842–47. https://doi.org/10.1073/pnas.0507360102.

White, Judith M., and Gary R. Whittaker. 2016. “Fusion of Enveloped Viruses in Endosomes.” *Traffic (Copenhagen, Denmark)* 17 (6): 593–614. https://doi.org/10.1111/TRA.12389.

William Langston, J., Philip Ballard, James W. Tetrud, and Ian Irwin. 1983. “Chronic Parkinsonism in Humans Due to a Product of Meperidine-Analog Synthesis.” *Science (New York, N.Y.)* 219 (4587): 979–80. https://doi.org/10.1126/SCIENCE.6823561.

Williamson, Matthew G, Marta Madureira, William McGuinness, Rachel Heon-Roberts, Elliot D Mock, Kalina Naidoo, Kaitlyn M L Cramb, et al. 2023. “Mitochondrial Dysfunction and Mitophagy Defects in LRRK2-R1441C Parkinson’s Disease Models.” *Human Molecular Genetics*, June. https://doi.org/10.1093/HMG/DDAD102.

Winner, Beate, Roberto Jappelli, Samir K. Maji, Paula A. Desplats, Leah Boyer, Stefan Aigner, Claudia Hetzer, et al. 2011. “In Vivo Demonstration That α-Synuclein Oligomers Are Toxic.” *Proceedings of the National Academy of Sciences of the United States of America* 108 (10): 4194–99. https://doi.org/10.1073/PNAS.1100976108/SUPPL_FILE/PNAS.201100976SI.PDF.

Xiao, Bin, Jian Yuan Goh, Lin Xiao, Hongxu Xian, Kah Leong Lim, and Yih Cherng Liou. 2017. “Reactive Oxygen Species Trigger Parkin/PINK1 Pathway-Dependent Mitophagy by Inducing Mitochondrial Recruitment of Parkin.” *The Journal of Biological Chemistry* 292 (40): 16697–708. https://doi.org/10.1074/JBC.M117.787739.

Xilouri, Maria, Oystein Rod Brekk, and Leonidas Stefanis. 2013. “α-Synuclein and Protein Degradation Systems: A Reciprocal Relationship.” *Molecular Neurobiology* 47 (2): 537–51. https://doi.org/10.1007/s12035-012-8341-2.

Xiong, Yulan, and Jianzhong Yu. 2018. “Modeling Parkinson’s Disease in Drosophila: What Have We Learned for Dominant Traits?” *Frontiers in Neurology* 9 (APR): 348880. https://doi.org/10.3389/FNEUR.2018.00228/BIBTEX.

Xiong, Yulan, Changqing Yuan, Rong Chen, Ted M. Dawson, and Valina L. Dawson. 2012. “ArfGAP1 Is a GTPase Activating Protein for LRRK2: Reciprocal Regulation of ArfGAP1 by LRRK2.” *The Journal of Neuroscience : The Official Journal of the Society for Neuroscience* 32 (11): 3877–86. https://doi.org/10.1523/JNEUROSCI.4566-11.2012.

Yahalom, Gilad, Lior Greenbaum, Simon Israeli-Korn, Tsvia Fay-Karmon, Vered Livneh, Jennifer A. Ruskey, Léanne Roncière, Armaghan Alam, Ziv Gan-Or, and Sharon Hassin-Baer. 2019. “Carriers of Both GBA and LRRK2 Mutations, Compared to Carriers of Either, in Parkinson’s Disease: Risk Estimates and Genotype-Phenotype

Correlations." *Parkinsonism and Related Disorders* 62 (May): 179–84. https://doi.org/10.1016/j.parkreldis.2018.12.014.

Yan, Dandan, Yunjian Zhang, Liegang Liu, Nian Shi, and Hong Yan. 2018. "Pesticide Exposure and Risk of Parkinson's Disease: Dose-Response Meta-Analysis of Observational Studies." *Regulatory Toxicology and Pharmacology : RTP* 96 (July): 57–63. https://doi.org/10.1016/J.YRTPH.2018.05.005.

Yao, Chen, Rabih El Khoury, Wen Wang, Tara A. Byrd, Elizabeth A. Pehek, Colin Thacker, Xiongwei Zhu, Mark A. Smith, Amy L. Wilson-Delfosse, and Shu G. Chen. 2010. "LRRK2-Mediated Neurodegeneration and Dysfunction of Dopaminergic Neurons in a Caenorhabditis Elegans Model of Parkinson's Disease." *Neurobiology of Disease* 40 (1): 73–81. https://doi.org/10.1016/J.NBD.2010.04.002.

Yoshii, Saori R., and Noboru Mizushima. 2017. "Monitoring and Measuring Autophagy." *International Journal of Molecular Sciences* 18 (9): 1–13. https://doi.org/10.3390/ijms18091865.

Ysselstein D., Nguyen M., Young T. J., Severino A., Schwake M., Merchant K., Krainc D. "LRRK2 kinase activity regulates lysosomal glucocerebrosidase in neurons derived from Parkinson's disease patients". Nat Commun. 2019 Dec 5;10(1):5570. doi: 10.1038/s41467-019-13413-w. PMID: 31804465; PMCID: PMC6895201.

Yuan, Yiyuan, Pengxiu Cao, Mark A. Smith, Kristopher Kramp, Ying Huang, Naoki Hisamoto, Kunihiro Matsumoto, Maria Hatzoglou, Hui Jin, and Zhaoyang Feng. 2011. "Dysregulated LRRK2 Signaling in Response to Endoplasmic Reticulum Stress Leads to Dopaminergic Neuron Degeneration in C. Elegans." *PloS One* 6 (8). https://doi.org/10.1371/JOURNAL.PONE.0022354.

Yue, M., K. M. Hinkle, P. Davies, E. Trushina, F. C. Fiesel, T. A. Christenson, A. S. Schroeder, et al. 2015. "Progressive Dopaminergic Alterations and Mitochondrial Abnormalities in LRRK2 G2019S Knock-in Mice." *Neurobiology of Disease* 78: 172–95. https://doi.org/10.1016/j.nbd.2015.02.031.

Yun, Hye Jin, Hyejung Kim, Inhwa Ga, Hakjin Oh, Dong Hwan Ho, Jiyoung Kim, Hyemyung Seo, Ilhong Son, and Wongi Seol. 2015. "An Early Endosome Regulator, Rab5b, Is an LRRK2 Kinase Substrate." *Journal of Biochemistry* 157 (6): 485–95. https://doi.org/10.1093/jb/mvv005.

Zambon, Federico, Marta Cherubini, Hugo J.R. Fernandes, Charmaine Lang, Brent J. Ryan, Viola Volpato, Nora Bengoa-Vergniory, et al. 2019. "Cellular α-Synuclein Pathology Is Associated with Bioenergetic Dysfunction in Parkinson's IPSC-Derived Dopamine Neurons." *Human Molecular Genetics* 28 (12): 2001–13. https://doi.org/10.1093/HMG/DDZ038.

Zavodszky, Eszter, Matthew N.J. Seaman, Kevin Moreau, Maria Jimenez-Sanchez, Sophia Y. Breusegem, Michael E. Harbour, and David C. Rubinsztein. 2014. "Mutation in VPS35 Associated with Parkinson's Disease Impairs WASH Complex Association and Inhibits Autophagy." *Nature Communications* 5 (May): 1–16. https://doi.org/10.1038/ncomms4828.

Zeng, Xian Si, Wen Shuo Geng, Jin Jing Jia, Lei Chen, and Peng Peng Zhang. 2018. "Cellular and Molecular Basis of Neurodegeneration in Parkinson Disease." *Frontiers in Aging Neuroscience* 10 (APR): 1–16. https://doi.org/10.3389/fnagi.2018.00109.

Zhou, Hongxia, Cao Huang, Jianbin Tong, Weimin C. Hong, Yong Jian Liu, and Xu Gang Xia. 2011. “Temporal Expression of Mutant LRRK2 in Adult Rats Impairs Dopamine Reuptake.” *International Journal of Biological Sciences* 7 (6): 753–61. https://doi.org/10.7150/IJBS.7.753.

Zhou, You Fa, Qing Xia Wang, Hai Yan Zhou, and Gang Chen. 2016. “Autophagy Activation Prevents Sevoflurane-Induced Neurotoxicity in H4 Human Neuroglioma Cells.” *Acta Pharmacologica Sinica* 37 (5): 580–88. https://doi.org/10.1038/aps.2016.6.

Zimprich, Alexander, Saskia Biskup, Petra Leitner, Peter Lichtner, Matthew Farrer, Sarah Lincoln, Jennifer Kachergus, et al. 2004. “Mutations in LRRK2 Cause Autosomal-Dominant Parkinsonism with Pleomorphic Pathology.” *Neuron* 44 (4): 601–7. https://doi.org/10.1016/j.neuron.2004.11.005.